Moment-Rotation Behavior of “Pinned” Column Base-Plate Connections in Low-Rise Metal Buildings

A Dissertation

Presented to

the Faculty of the Department of Civil and Environmental Engineering

University of Houston

In Partial Fulfillment

Of the Requirements for the Degree

Doctor of Philosophy

In Civil Engineering

by

Florentia Kavoura

August 2016

Moment-Rotation Behavior of "Pinned" Column Base-Plate Connections in Low-Rise Metal Buildings

Florentia Kavoura

Approved:

Chair of the Committee
Bora Gencturk, Assistant Professor,
Civil and Environmental Engineering

Committee Members:

Kaspar J. Willam, Professor,
Civil and Environmental Engineering

Mina Dawood, Associate Professor,
Civil and Environmental Engineering

Qianmei (May) Feng, Associate Professor,
Industrial Engineering

Konstantinos Kostarelos, Associate Professor,
Petroleum Engineering

Suresh K. Khator, Associate Dean,
Cullen College of Engineering

Roberto Ballarini, Professor and Chair of Dept
in Civil and Environmental Engineering

ACKNOWLEDGMENTS

I would like to express my sincere gratitude to my advisor Dr. Bora Gencturk for his continuous encouragement and guidance, and for the dedication of his time and energy. It has been an honor to be one of his first Ph.D. students. Dr. Gencturk inspired me in the field of structural engineering and he helped me to improve myself, more so than just academically. The joy and enthusiasm he has as a supervisor and professor was contagious and motivational for me, even during the tough times of my Ph.D. pursuit. I really appreciate all his support to make my Ph.D. experience productive and stimulating.

Besides my advisor, I would like to thank Dr. Mina Dawood, who has contributed significantly to this research and guided me in many endeavors throughout my graduate studies. I would also like to share my gratitude with the rest of my committee members, Dr. Qianmei Feng, Dr. Konstantinos Kostarelos and Professor Kaspar J. Willam for their suggestions and guidance. The experimental programs of the research were funded by NCI Buidling Systems Inc. and Metal Building Manufacturers Association which are gratefully acknowledged. Financial support of this research was also provided by the teaching and research assistantship from the Civil and Environmental Engineering Department at the University of Houston which is acknowledged.

I would also like to thank the technicians, helpers and colleagues for the help, guidance and generous time provided in order to accomplish my experimental work. Special thanks go to Gerald Mc. Tigret, Bora Acun, Josue Navarro, David Ibague Gill, Antonio Cabrales Juan, Oscar Serna, Anna Milani, Alexy Idicula, Lucas Feitosa and Mauricio Bonisson. Special thanks also go to my good friends and fellow graduate students who shared the challenges that I faced during my research program including Arezou Attar, Farshid Hosseini, Mohammad Hanifzadeh, Qian Li, Giovanna Xotta, Botong Zheng, Cheng Shi, Hossein Karagah, Prakash Poudel, Reza Mousavi, Ibrahim Kaymaz, Kazi Hossain, Jeannot Ahossin. My sincere thanks also goes to Mr. Jerry Hatch and Mr. Ronald Mays for their continuous advice regarding the application of this research in the engineering industry. Also, I would like to thank Muhammed Gurbuz and Asfandyar Ahmad for their excellent collaboration and support with the experimental and analytical aspects of the research.

Last but not least I would like to thank my family for contributing the most in this research. The continuous support and love of my father Anastasios, my mother Chrysi and my sisters Antigoni and Anna gave me strength in order to cross the finish line. Special thanks also go to Vasili Samara for sharing my struggles and supporting me emotionally in my worst and best times.

To my family for their love and support.

Moment-Rotation Behavior of "Pinned" Column Base-Plate Connections in Low-Rise Metal Buildings

An Abstract

of a

Dissertation

Presented to

the Faculty of the Department of Civil and Environmental Engineering

University of Houston

In Partial Fulfillment

Of the Requirements for the Degree

Doctor of Philosophy

In Civil Engineering

by

Florentia Kavoura

August 2016

ABSTRACT

In the past few decades, the popularity of metal buildings has grown immensely and today, they are extensively used for low-rise constructions in United States. They account for approximately fifty percent of the total low-rise business construction market and are widely used in many sectors of the North American economy including house manufacturing facilities and warehouses, retail stores, shopping centers, schools, libraries and medical or athletic facilities (MBMA, 2015). Low-rise metal buildings are used in all geographic locations, including high seismic regions. In the design of low-rise metal building systems, column base connections are commonly modeled as pinned supports with no rotational stiffness for both serviceability and strength limit states. However, past studies have indicated that base connections, which are designed as pinned supports, exhibit a non-negligible level of rotational stiffness. Neglecting the rotational stiffness of the base connection may result in a significant overestimation of the lateral displacement of the frames. This additional displacement is addressed by increasing the flexural stiffness of the frame members thereby unnecessarily increasing the cost of low-rise metal buildings. However, there is a distinct lack of design guidelines and experimental data to support the use of rotational stiffness or moment capacity at the so-called pinned column bases.

To bridge this gap, this study investigated the moment-rotation behavior of nineteen “pinned” base-plate connections through an experimental program consisting of two phases and an analytical parametric study that included the simulation of over two hundred different base-plate connection configurations. The tests were performed on full-scale specimens subjected to horizontal cyclic displacements with increasing amplitude and a constant axial loading. The first phase of the experimental research involves testing of columns stubs from eight typical low-rise metal building designs in the United States on a steel foundation. In the second phase of the experimental research, eleven column stubs were tested on concrete foundations and a more systematic investigation was performed to study the influence of various parameters, including base-plate dimensions, number

of anchor rods, anchor rod diameter and gage distance on the connection behavior. All the tested specimens showed high deformation capacity and a considerable rotational stiffness.

The findings from the first phase of the experimental program were used for analysis of typical gabled frames, where the base connections were modeled as rotational springs with the same stiffness as measured in the tests. The results indicated that including the rotational stiffness of the pinned base connections reduces the frame deflections and the frame weight. The outcomes from the second phase of the experimental program indicated that the geometrical characteristics of the column base-plate connections have a significant impact on the overall behavior, rotational stiffness and moment capacity of the connections. For this reason, a parametric study was performed to evaluate the most influential parameters of the column base-plate connections on the rotational stiffness and moment capacity of the connections. Prior to the parametric study, the numerical models were validated using the experimental data from the second phase of testing. It was observed that the most influential parameters on the rotational stiffness and moment capacity of the connections are the base-plate thickness, anchor rod number and diameter and flange thicknesses. Finally, rotational stiffness and the moment capacity measured during the experimental study were compared with the calculated rotational stiffness and moment capacity based on the provisions of the American and European design codes. It was observed that the moment capacity of the connections calculated based on the American design codes was closer to the ones recorded during the experiments, compared with the ones calculated according to Eurocodes. It is expected that the results from this investigation adds knowledge that could later be used for revision of the metal building design codes and standards.

TABLE OF CONTENTS

LIST OF FIGURES

LIST OF TABLES

1. INTRODUCTION

1.1. Problem Statement

Low-rise metal building systems are widely used as complex production facilities and warehouses, retail stores, shopping centers, schools, libraries and medical or athletic facilities. They account for approximately 50% of the total non-residential low-rise construction in the United States (MBMA, 2015). The main advantages of low-rise metal buildings are cost effectiveness, easy fabrication and installation, and quick turnaround times. The buildings are typically made from built-up I-sections, commonly with tapered-webs [see Figure 1.1(a) as an example of a gabled-frame in a low-rise metal building and Figure 1.1(b) as an example of web-tapered column]. The base-plate connections are designed with the anchor rods placed inside the column flanges [see Figure 1.1(c)] which leads to the “pinned” connection assumption. Thus, the rotational stiffness they might provide is ignored in the design of metal buildings.

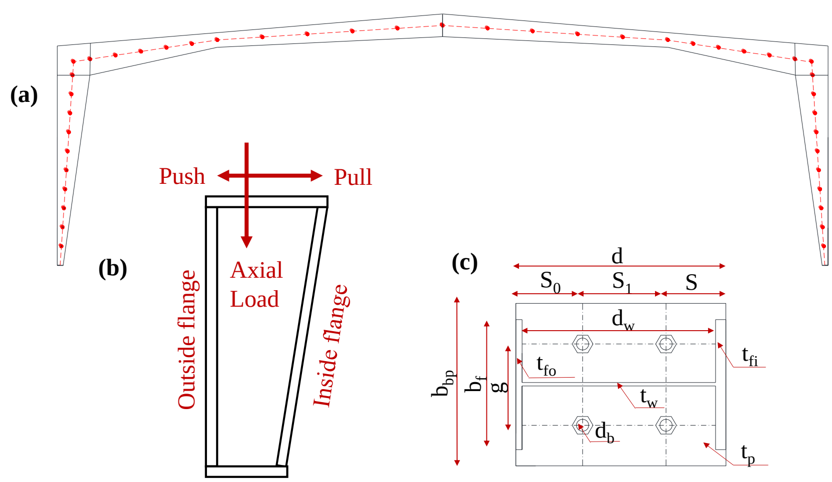

Figure 1.1. (a) An example gabled frame used in low-rise metal building construction, (b) elevation view of the column stub, (c) base-plate connection details.

The common practice in design of low-rise metal buildings, as mentioned earlier, is to assume zero rotational restraint for the column base-plate connections. Their behavior can be characterized for design purposes with the aid of the *M-θ* (moment-rotation) curves. These curves are generally taken directly from individual tests or the derivation by best-fit techniques from the results of multiple experiments. The stiffness, strength and ductility of the base-plate connections are directly affected by the synthesis of the connection's main characteristics. However, the lack of specifications and design guides for estimating the rotational stiffness or moment capacity of the column base-plate connections does not allow the engineers to accurately obtain this information and consider it in the design of the overall structure.

Prior research indicates that the use of "fully-restrained moment connections", "pinned connections" or "partially-restrained moment connections" at column-to-foundation connection may lead to a significant variation in the stiffness and strength of the frames (El-Khoraibie, 1978; Vernon et al., 1985; Robertson 1991; Astaneh et al, 1992; Jaspart et al, 1998; Eroz et al., 2009; Bajwa et al., 2010). Additionally, it has been observed that the assumption of zero rotational stiffness of the column base-plate connection results in a significant underestimation of the overall lateral stiffness of horizontally loaded moment frames leading to less economical designs (Eroz et al., 2009; Bajwa et al., 2010). For this reason, numerous studies have been performed in order to research the overall behavior of column base-plate connections and estimate their rotational stiffness and moment capacity. Column base-plate connections in metal buildings consist of a number of elements including anchor rods, base-plate, grout, and concrete foundation. All these variables affect the moment capacity and rotational stiffness of the connections (El-Khoraibie, 1978; DeWolf and Sarisley 1980; Picard et al., 1985; Thambiratnam and Paramasivam 1986; Sato, 1987; Hon et al., 1988; Melchers, 1992; Nakashima, 1992; Targowski et al., 1993; Jaspart et al., 1998; Stamatopoulos et al., 2011; Kanvinvde, 2012). This research aims to investigate how each of these parameters affects the overall behavior and performance of the base-plate connections. Thus, its main purpose is to advance the understanding of column base-plate connection behavior with a focus on "pinned" connections. It is expected that the knowledge gained through this research will lead to a more accurate representation of the moment capacity and rotational stiffness of the column base-plate connections and eventually give the opportunity to the designer to perform a more reliable and low-cost design of low-rise metal buildings.

1.2. Objectives and Scope

The objective of this research is to quantify the rotational stiffness and the moment capacity of column base-plate connections in low-rise metal building systems through testing of nineteen full-scale base-plate connections and over two hundred additional configurations through an analytical parametric study with varying base-plate dimensions, number of anchor rods, anchor rod diameters and gage distances, and flange thicknesses. In this study the rotational stiffness in defined in the elastic region. The experimental program is divided into two phases. The first phase included testing of eight full-scale column base-plate connections, which are selected from actual building designs that are representative of the typical metal buildings in the United States, on a steel foundation. This first phase was an exploratory study to investigate whether these pinned connections could provide any appreciable stiffness. The results warranted a second phase of testing on reinforced concrete foundations, which was more representative of the real building configurations. The second phase of the experimental program consisted of similar eleven full-scale tests on reinforced concrete foundations. As such, this two phase experimental program aims to provide component-level experimental data for use in the evaluation of the rotational stiffness and moment capacity of the “pinned” column base-plate connections and examine the effect of different parameters including the base-plate thickness, number of anchor rods, anchor rod diameter and gage distance, flange thicknesses and foundation material on the connection behavior. A piecewise nonlinear spring model was fitted to the test data to represent the rotational stiffness of the joints beyond the elastic range. The rotational stiffness of each of the connections was calculated in the elastic and inelastic range and compared to other base-plate configurations. The rotational stiffness of the column base-plate connections tested in the first phase of the experimental program was used to evaluate the reduction in the frame deflections under service loads and in the total weight of the gabled frames.

The parametric study included the development and calibration of analytical models using the experimental results from the second phase. Overall, the models were in a good agreement with the test data. Using the developed analytical models as a basis, a parametric study was performed to evaluate the most influential parameters of the column base-plate connections on the rotational stiffness and moment capacity of the connections. The main purpose of the parametric analysis was to evaluate the influence of the geometric characteristics of the connections in the overall behavior of the column base-plate connections, as well to provide additional information to develop design guidelines. The parametric study included connections with three different web-depths (12, 18, 22 inches) and the influence of eleven parameters on the rotational stiffness, moment capacity and overall behavior of the connections was investigated. These parameters are the flange width, web thickness, flange thickness, base-plate width, base-plate thickness, anchor rod diameter, number of anchor rods, gage, setback and pitch distances of the anchor rods and the applied axial load. In parallel, the combination of different base-plate thickness with different anchor rod diameters and applied axial loads was examined. It was observed that each of the geometric parameters considered has an impact on the rotational stiffness and moment capacity of the connections. The most influential parameters were found to be the base-plate thickness, the anchor rod diameter and the flange thicknesses.

Additionally, the rotational stiffness and moment capacity of the connections were measured during the second phase of the experimental program were compared with the rotational stiffness and moment capacity calculated according to the provisions of the American and European design standards. The moment capacity of the connections was computed based on the provisions of the American Institute of Steel Construction (AISC) Steel Constructional Manual (AISC, 2011), and the rotational stiffness is estimated using the component method presented in the Eurocode 3 (prEN1993-1-8). It was found that the design codes conservatively estimate the rotational stiffness and moment capacity of the column base-plate connections investigated in this research. However, due to the lack of design provisions for base-plate connections considered in this research (anchor rods inside the column flanges), some assumptions had to be made in order to estimate the base-plate rotational stiffness and moment capacity. These assumptions are explained in Section 5.4 and Section 5.5. The results of this study provide additional data on the base connection moment-rotation behavior and performance, and hence they could be a useful source for future revisions of codes and standards.

1.3. Organization of the Dissertation

The dissertation consists of six chapters. This first chapter presents the problem statement, main objectives and the scope of the research. The second chapter is a literature review of previous experimental research, analytical studies and code provisions on column-base-plate connections. A database consisting of 25 experimental studies from late 1970s to present day on exposed column base-plate connections was created and the most common parameters under investigation and their impact on the overall behavior of the base-plate connections was examined. Experimental studies were recorded for different connection configurations tested under different load combinations and a summary of the main findings is described. In addition, analytical studies on column base-plate connections are discussed. Finally, American, European and Japanese provisions for the design and the calculation of the rotational stiffness of column base-plate connections are presented.

The third chapter presents the first phase of the experimental program and provides the details of test setup, specimens, material properties, instrumentation, loading protocols and the main outcomes from the experiments. The results of the rotational stiffness of the eight column base-plate connections which were tested on steel foundations are presented. In parallel a semi-quantitative damage evaluation of the eight tested connections and their failure mechanism is discussed.

The fourth chapter presents the results of the second phase experimental program that consisted of eleven column base-plate connections tested on reinforced concrete foundations. The details of the test setup, specimens, material properties, instrumentation, loading protocols and the main outcomes from the experiments are presented. The effect of each of the parameters under investigation in the rotational stiffness and moment capacity of the connections is discussed in detail. A semi-quantitative damage evaluation was performed and the failure mechanism of the connections is provided.

The fifth chapter presents the analytical work performed building on the findings from the first and the second phase of the experimental program. The outcomes from the first phase of the experimental program are used in order to evaluate the savings on the frame design by considering the rigidity of the column base-plate connections. The frames were representative of typical metal buildings in U.S. and their base configurations were identical with the ones tested in the first phase of the experiments. Additionally, detailed analytical model analyses were conducted for the specimens of the second experimental program and the models were calibrated in order to reasonably agree with the experimental results. The developed numerical tools were utilized for a parametric study on three web-depth (12 inch, 18 inch, 22 inch) column base-plate connections with eleven different geometric parameters under investigation. The effect of each of the geometric parameters on the rotational stiffness and moment capacity is presented. Finally, the rotational stiffness and moment capacity of the connections were calculated according to the American and European design standards and a discussion of the results is provided.

The dissertation concludes with the sixth chapter which lists the main findings from each chapter and recommendations for future research. As a supplementary documentation, the test results from the nineteen column base-plate connections are archived in Appendix A and the corresponding frames investigated in the first phase of the experimental program are provided in Appendix B. Additionally, material experimental results are given in Appendix C and the values of the rotational stiffness calculated in the parametric study are provided in Appendix D.

.

2. LITERATURE REVIEW

2.1. Previous Experimental Investigations on Column-Base-Plate Connections

Column base-plate connections attracted less attention of researchers compared to other connections such as the column-beam connections. The literature review performed here identified 242 tests on exposed column base-plate connections that were compiled in a database. The first studies date back to late 1970s and the most recent study was performed 2012. In total, 24 studies have been used to create the database. The first two experimental studies on column base-plate connections were conducted by DeWolf and El-Khoraibie in 1978, and presented in two separate publications. After 1980s, the number of studies started to gradually increase. Eighty-nine percent of the experiments were conducted on concrete foundations while the 11% were performed on steel foundations.

The database provides an insight to the literature on column base-plate connection testing. A lower number of tests were performed on connections with anchor rods inside the column flanges. Figure 2.1(a) presents the percentage of experiments conducted with the anchor rods outside and inside the flanges. According to the Figure 2.1(a), 33% (62 tests) of all the specimens had anchor rods inside the flanges. It is noted that 80% of these tests (52 out of 62 tests) had a two-anchor rods configuration. Figure 2.1(b) is a comparison between the experiments conducted on steel and concrete foundations with the anchor rods inside and outside the flanges. These categories are steel foundation-anchor rod inside, steel foundation-anchor rod outside, concrete foundation-anchor rod inside, and concrete foundation-anchor rod outside. It is shown that 60% of all the experiments were conducted with the anchor rods outside the column flanges and on concrete foundations. Additionally, it is seen that only the 27% of the experiments were conducted on base-plate configurations with the anchor rods inside the flanges and on concrete foundations similar to the connections tested in this study. However, as mentioned earlier most of these experiments were conducted on connections with two anchor rods (48 out of 57 tests), which is a less common connection configuration in practice (a minimum of four anchor rods is usually used).

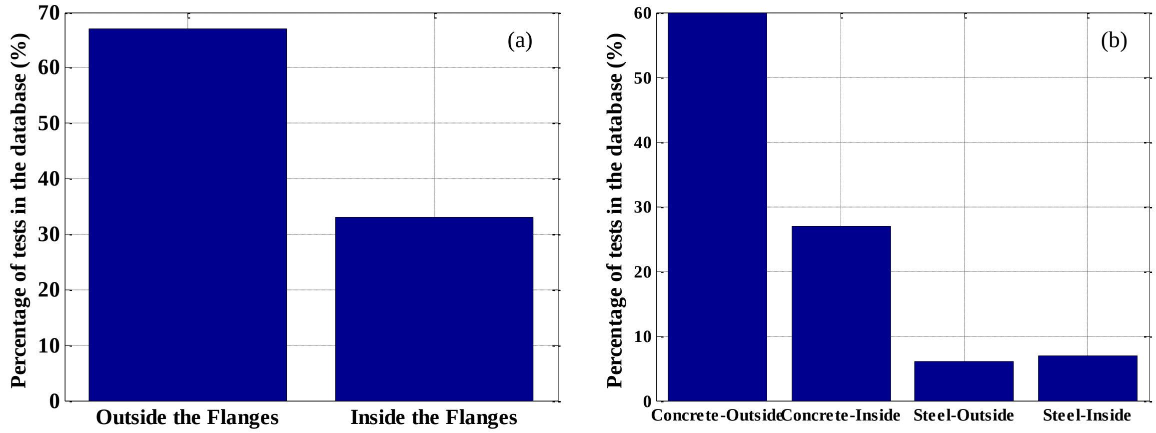

Figure 2.1. Percentage of tests in the database with different foundation type-anchor rod location combinations.

The base-plate thickness and anchor rod diameter have been identified by the majority of the experimental studies in the database as the most influential parameters on the overall behavior of the column base-plate connections. As shown in Figure 2.2(a) the base-plate thicknesses used in the column base-plate connection tests vary from 1/5 inch to more than 1 1/4 inches, while base-plate thicknesses between 3/4 inch and 1 inch were most commonly used. Fifty-four percent of the tests had anchor rods with diameters between 3/4 inch and 1 inch. Twenty-seven percent of the tests had anchor rods with diameters less than 3/4 inch. Figure 2.2(b) presents the distribution of the tests in the database with regards to the anchor rod diameter. Differences in the overall behavior of the base-plate connections was observed when these two parameters varied while keeping the rest of the parameters the same. The different base-plate connections behaviors observed in these tests are discussed in the next sections. The studies considered in the database are given in Table 2.1.

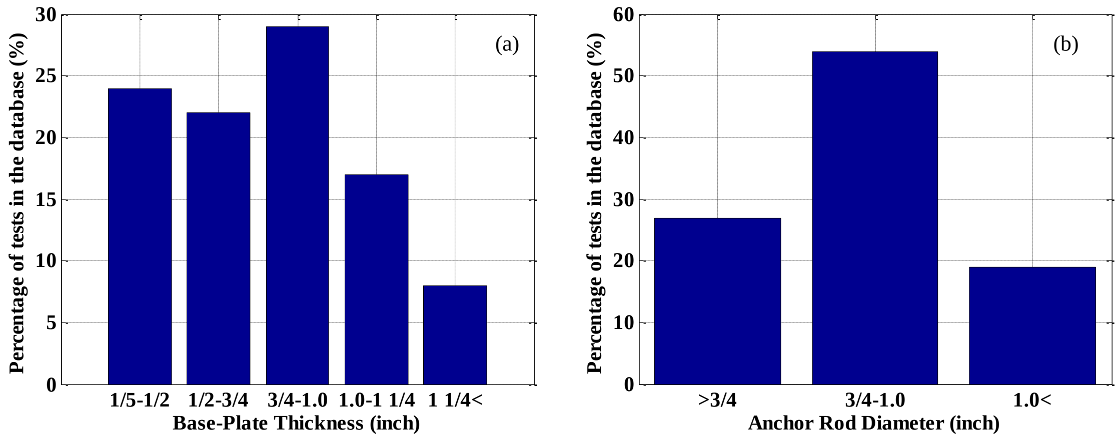

Figure 2.2. Percentage of tests in the database with (a) different base-plate thickness, and (b) anchor rod diameter.

Table 2.1. Studies Considered in the Database

Author	Year	Number of Tests
DeWolf	1978	19
El-Khoraibie	1978	6
DeWolf and Sarisley	1980	14
Murray	1983	2
Picard and Beaulieu	1985	15
Akijuma et al.	1985	25
Thambiratnam and Paramasivam	1986	12
Picard et al.	1987	14
Hon and Melchers	1987	26
Sato	1987	6
Melchers	1992	10
Astaneh et al.	1992	6
Nakashima	1992	14
Targowski et al.	1993	12
Kallolil and Chakrabarti	1997	3
Jaspart and Vandegans	1998	12
Li et al.	2001	7
Wong and Chung	2002	5
Tamakatsu	2002	2
Gomez et al.	2009	7
Myers et al.	2009	6
Adany et al.	2010	5
Stamatopoulos and Ermopoulos	2011	8
Kanvinde et al.	2012	6

2.1.1. Base-plate connections with anchor rods inside the column flanges

Few studies have been conducted to evaluate the rotational stiffness of base-plate connections with two or four anchor rods inside the column flanges, assumed to be pinned base-plate connection condition (Picard and Beaulieu, 1985; Picard et al., 1987; Hon and Melchers, 1988; Melchers, 1992; Jaspart and Vandegans, 1998). Examples of typical pinned base-plate connection configurations with two or four anchor rods positioned inside the flanges are shown in Figure 2.3. No study was reported on pinned base-plate connections with more than four anchor rods inside the column flanges.

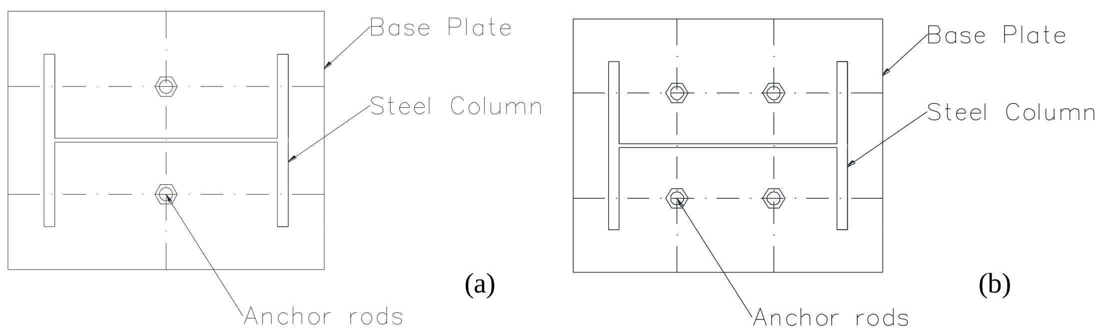

Figure 2.3. Examples of pinned typical base-plate configurations with (a) two or (b) four anchor rods positioned inside the flanges, tested in literature.

Picard and Beaulieu (1985) and Picard et al. (1987) stated that the purpose of their tests on two anchor rod connection configuration was to study the behavior and performance of the base-plate connection and to determine the influence of axial load on the base-plate connection rigidity. Their findings indicated the beneficial effect on the column and frame stability that the consideration of the base fixity can result in. Jaspart and Vandegans (1998) performed experiments in column base-plate connections with two anchor rods inside the column flanges. They examined the effect of the axial load, base-plate thickness and anchor rod diameter on the behavior of column base-plate connections. It was found that the base-plate connections that are considered "pinned" might exhibit a semi-rigid behavior. However, the regulations of the United States Occupational Safety and Health Administration (OSHA, 2011) – Safety Standards for Steel Erection (OSHA, 2011), effective on January 18, 2002, require a minimum of four anchor rods in column base-plate connections. This requirement was supported by the fact that the base-plate connections need to be designed for a specific bending moment in order to provide the necessary stability during the erection process.

Hon and Melchers (1988) and Melchers (1992) investigated the moment-rotation behavior of base-plate connections with two and four hold-down rods subjected to bending moment and compressive, tensile or no axial load. Their test setup is shown in Figure 2.4. The reinforced concrete block with two or four anchor rods was connected with the strong floor of the laboratory. In order to allow the anchor rods to be replaced after each tests without replacing the reinforced concrete block, each anchor rod was screwed into a sleeve which was anchored into the block by a high-tensile rod. A total of thirty six specimens were tested in two experimental programs and only four of them were conducted in base-plate connections with four anchor rods inside the column flanges. The studies stated that there is an important role of base-plate thickness and anchor rod size on the resulting moment resistance and stiffness of the connection. They concluded to two overall behaviors of the column base-plate connections according to their base-plate thickness. Specifically, they showed that the overall connection behavior consisting of thin base-plates was ductile due to the formation of a yield-line mechanism in the base-plate (see Figure 2.5). On the other hand, they showed that the overall behavior of thicker base-plates was dominated by the anchor rod dimensions and was characterized as brittle behavior. Additionally, it was found that the higher eccentricity of the loading led to greater bending stiffness. Hon and Melchers (1988) showed that connections with four anchor rods have about 100% increase in strength and 100-200% increase in the rotational stiffness compared with the connections with the two anchor rods.

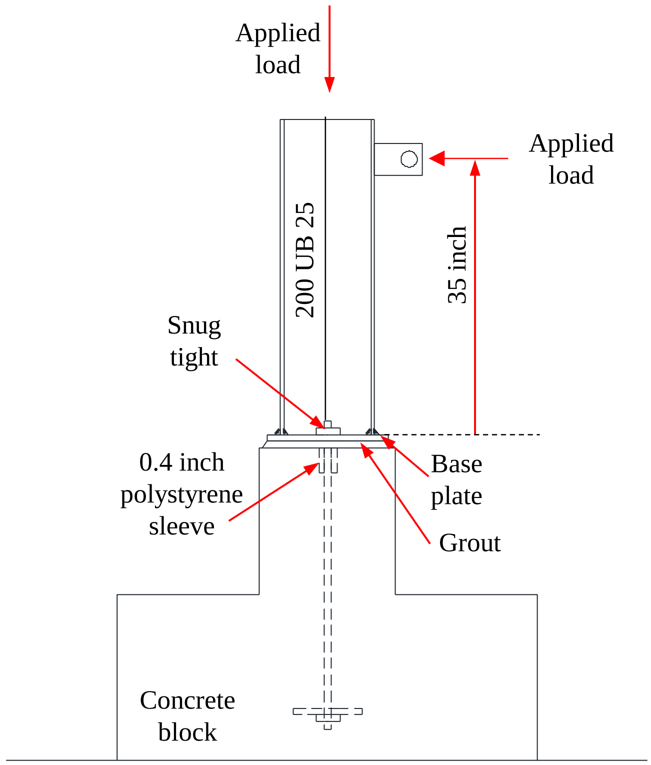

Figure 2.4. Elevation view of the specimens [Hon and Melchers (1988) and Melchers (1992)].

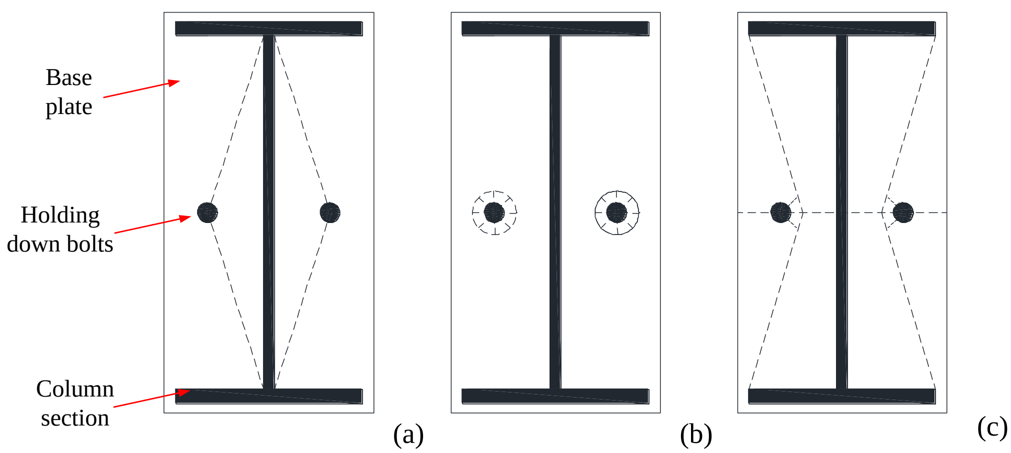

Figure 2.5. Baseplate yieldline mechanisms for thin base-plates [Hon and Melchers (1988)].

Three typical modes of failure were observed in the experiments mentioned above with the anchor rods positioned inside the column flanges. These are the failure of the anchor rods, yielding of the base-plate, and cracking of the concrete. It was also observed that the bond stresses between the anchor rods and the concrete foundation started degrading from the first cycles of loading. Finally, it was seen that the contact zone on the compression side of the connections increases with an increase of the axial load.

The base-plate connections with the anchor rods positioned inside the column flanges have also been tested as a part of full-scale experiments on metal building frames (Hong, 2007; Bajwa et al., 2010; Smith, 2013). A considerable rotational stiffness of the column base-plate connections was found and flange buckling near the knee joint regions was reported as main failure mode of the frames. It was also recommended that the rigidity and strength of "pinned" column base-plate connections on the overall lateral stiffness and strength of gabled frame systems is considered. Further, it was recommended that many more base-plate configurations are tested to determine the capacity and behavior of these connections.

2.1.2. Base-plate connections with anchor rods outside the column flanges

The column base-plate configurations in which the anchor rods are positioned outside the flanges have been tested extensively (El-Khoraibie, 1978; Picard and Beaulieu; 1985; Sato, 1987; Hon and Melchers, 1988; Astaneh et al., 1992; Melchers, 1992; Nakashima, 1992; Targowski et al., 1993; Jaspart and Vandegans, 1998; Fahmy, 1999; Camacho, 2007; Adany et al., 2010; Gomez et al., 2010; Stamatopoulos and Ermopoulos, 2011; Kanvinvde et al., 2012). Examples of typical base-plate configurations tested in these studies with the anchor rods positioned outside the flanges are shown in Figure 2.6. These tests were generally conducted under axial load and/or bending moment to investigate the plastic behavior of the column base-plate connections.

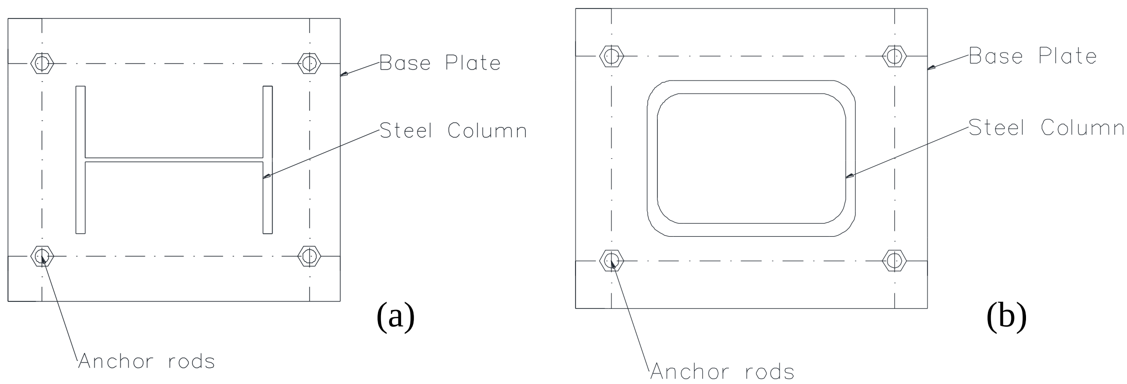

Figure 2.6. (a), (b) Typical four anchor rod base-plate connections tested in literature.

Researchers investigated the influence of different parameters such as column type and size, size of the base-plate, base-plate thickness, foundation properties, number of anchor rods, anchor rod diameter, and load eccentricity on the column base-plate connection behavior. The interaction between the anchor rod size, base-plate thickness, and load eccentricity was extensively studied by DeWolf and Sarisley (1980) and Thambiratnam and Paramasivam (1986). Figure 2.7 and Figure 2.8 show the test setups for the experimental programs in these two references. The experimental observations of these studies on column base-plate connections with a single anchor rod outside the column flanges were that the increase of the base-plate thickness leads to a decrease of the connection capacity since the base-plate behaves like a rigid plate. In addition, when the anchor rod diameter is larger relative to the base-plate thickness, the anchor rods do not reach their fully capacity prior to failure of the base-plate (DeWolf, 1978). This was especially true for connections with lower load eccentricities. Unlike DeWolf and Sarisley (1980), Thambiratnam and Paramasivam (1986) did not investigate the anchor rod size as a parameter. However, still it was concluded that connections with thicker base-plates exhibited lower capacities due to large bearing stresses under the base-plate, which resulted in premature crushing of the concrete (or grout). A similar trend was observed for eccentrically loaded columns.

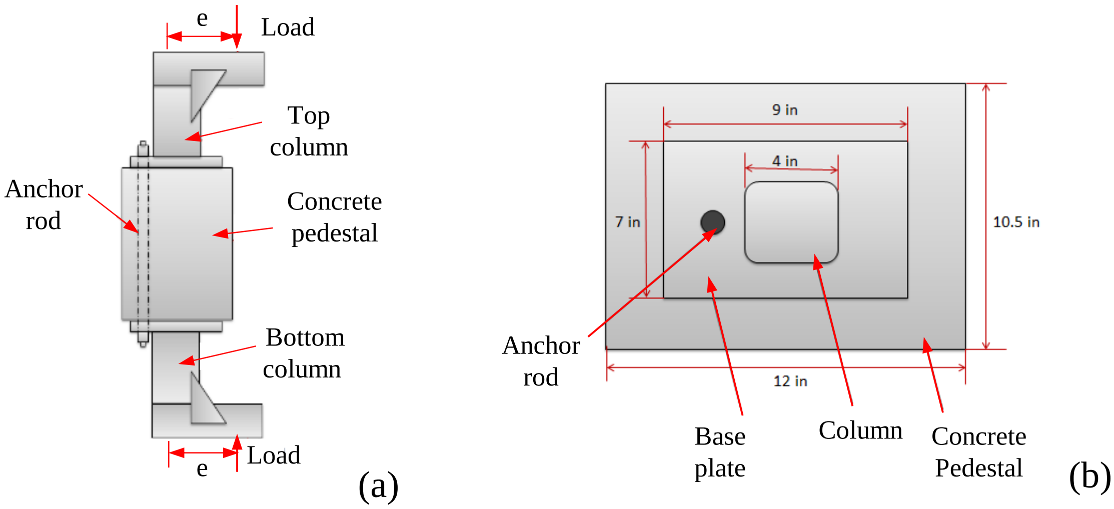

Figure 2.7. (a) Test set-up and (b) cross-sectional view (DeWolf and Sarisley 1980).

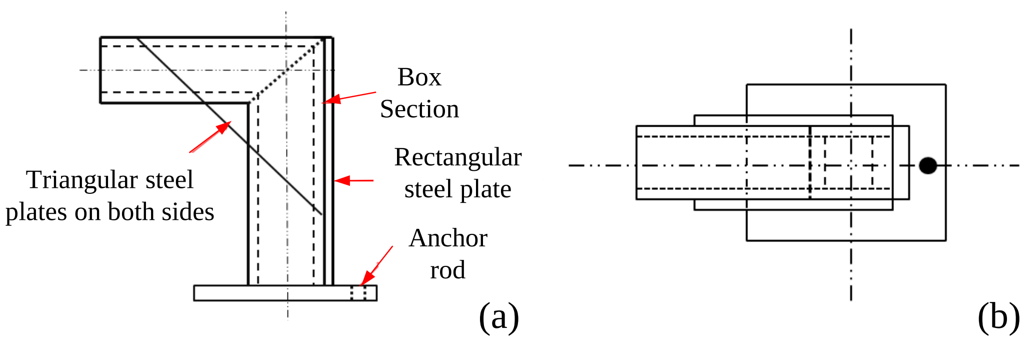

Figure 2.8. (a) Elevation view of the specimen and (b) plan view of the specimen (Thambiratnam and Paramasivam 1986).

Strength, ductility, and moment resistance of the base-plate connections are the features that were studied in different tests under various loading protocols. DeWolf (1982) recommended using the ultimate strength method for the column base design. In addition, it was suggested to use a concrete area to plate area ratio of unity. This is due to the fact that when the concrete pedestal has a larger surface than the base-plate, the bearing stresses are distributed to a larger area. Therefore, assuming the concrete surface to be equal to the base-plate surface leads to a higher concrete bearing stress. This suggestion is depicted in Table 22.8.3.2 of ACI 318 (2014) where the nominal bearing strength takes the minimum value when the concrete area to base-plate area ratio is equal to one. Picard and Beaulieu (1985) indicated that the axial loads applied to the column increase the rotational stiffness of the connection. Picard et al. (1987) investigated the effect of the rigidity ratio of the column base-plate connections on the calculation of the column effective length. The rigidity ratio is defined as the ratio of the summation of the column rigidity over the summation of the beam rigidity. The test results concluded that a rigidity ratio of 0.5 and 1.5 for weak axis and strong axis buckling respectively can be used to reduce the effective length of the column. Specifically, a design example provided in the study showed that when the proposed rigidity ratio mentioned above were employed, then the calculated column strength could be increased by up to 30%.

Sato (1987) performed an experimental study in order to investigate the influence of the diameter of the concrete foundation and anchor rods on the behavior of the base connection. A "yield ratio" was defined as the ratio of the yield strength over the tensile strength of the anchor rod. The base-plates used during the tests were thick enough in order to provide high stiffness to the connection. This high stiffness of the base-plate guaranteed the rotation of the column to occur through elongation of the anchor rods and the concrete compressive deformation. The specimens were subjected to cyclic loading and when a low yield ratio (approximately at 0.66) was used for the anchor rods, a ductile behavior with pinched hysteresis loops was observed for the connection. Base connections with low yield ratios did not experience any anchor rod rupture until rotations of about 0.1 rad while base connections with higher yield ratios, anchor rods ruptured in lower rotations (i.e., 0.03 rad)

It was observed from the studies that the base-plate thickness is a determining factor on column base-plate connections. Many researchers studied base-plate connections with various thicknesses to investigate the effect on the behavior of the connection. Astaneh et al. (1992) and Fahmy et al. (1999) proposed a classification according to the failure mechanisms based on the thickness being smaller, equal to, or greater than that required to form a plastic hinge in the plate. Four categories were reported: (1) plastic hinge in the column (weak column-strong connection), (2) plastic hinge in the base-plate (strong column-weak connection), (3) balanced mechanism, and (4) concrete failure. Figure 2.9 shows the three types of base-plates (thick, intermediate and thin) and a schematic representation of their deformed shapes. In parallel, researchers pointed out that tension fracture of anchor rods should be avoided. Here, the base-plate thickness plays an important role to avoid anchor rod rupture. Melenciuc et al. (2015) performed experiments using thick base-plates and large anchor rods in order to prove that it is desirable for the plastic hinge to form in the column and not in the base-plate for better seismic resistance.

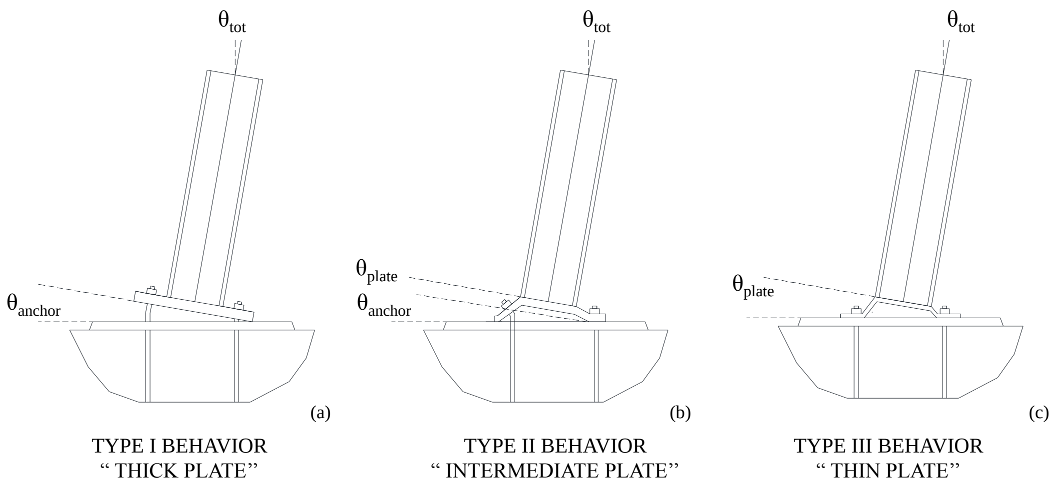

Figure 2.9. Behavior of base-plates commonly tested in the literature for (a) thick base-plates, (b) intermediate base-plates, and (c) for thin base-plates (Astaneh et al. 1992).

The first category of connections where the plastic hinge forms in the column (weak column-strong connection) is characterized by the formation of a plastic hinge at the base of the steel column. The rest of the connection components remain elastic or show moderate yielding. Experiments that have been conducted by Fahmy et al. (1999) and Adany et al. (2000) showed that even if the anchor rods and the base-plate reached their yield stress, the plastic hinge formed only in the column. Additionally, with this connection configuration, high strength and ductility with stable hysteresis loops was observed. The failure mechanism of the connections was mainly fracture of the welds connecting the column flanges to the base-plate. The second category of connections where the plastic hinge forms in the base-plate (strong column-weak connection) is characterized by the inelastic deformation or brittle failure of the base-plate or the anchor rods (DeWolf and Sarisley, 1980; Picard and Beaulieu, 1985; Thambiratnam and Paramisivam, 1986; Astaneh et al., 1992; Jaspart and Vandegans, 1998). An inelastic deformation of the base-plate is observed in the form of yield lines on the base-plate in addition to yielding of the anchor rods. Overall, this connections category showed high ductility, reduction of the stiffness, pinched hysteretic loops, but high energy dissipation. A combination of the two behaviors discussed above where the plastic hinge forms at the column (weak column-strong connection) and the plastic hinge forms at the base-plate (strong column-weak connection) is observed in the third category, which is the balanced mechanism. It was observed that in this case, the base-plate, anchor rods and column yielded approximately at the same time. The connection undergoes moderate inelasticity with no brittle failure of any of the components.

According to the studies in the database, different failure mechanisms govern the behavior of the base-plate connections with anchor rods positioned outside the column flanges. The percentage of the failure modes are shown in Figure 2.10.The most common failure mode was the base-plate yielding with 41%. Second is the anchor rod yielding or rupture with 38%. Other failure modes reported by researchers are column to base-plate weld rupture, concrete crushing, flange local buckling, cracking between the web and the flanges. The last group mentioned above is represented by ‘others’ in Figure 2.10.

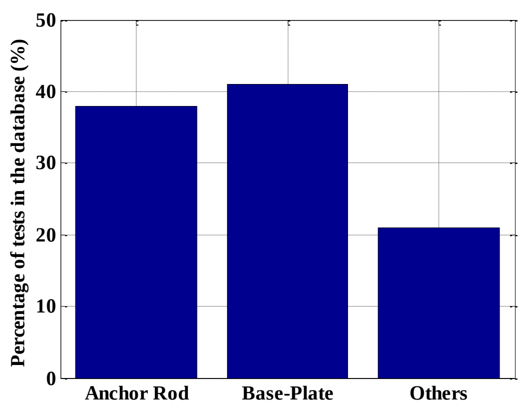

Figure 2.10. Percentage of tests in the database with different failure modes.

The seismic behavior of column base-plate connections was investigated by Astaneh et al. (1992). It was concluded that the yielding of the plate due to bending should govern the response and this would result in a ductile behavior of the base-plate connection. It was also recommended that the failure of the welds connecting the column to the base-plate should be avoided. It was proposed that the welds should resist 1.25 times the combined effects of the axial load, bending and shear developed in the column or the base-plate.

2.2. Previous Analytical Research on Column Base-Plate Connections

Researchers have estimated the rotational stiffness in exposed column base-plates experimentally, and using analytical models (Picard and Beaulieu, 1985; Sato, 1987; Penserini and Colson, 1989; Melchers, 1992; Targowski et al., 1993; Wald, 1995; Ermopoulos and Stamatopoulos, 1996; Wong and Chung, 2002; Bajwa et al., 2010; Verma, 2012). In this study the analytical modeling is used to indicate closed form expressions and/or finite element modeling. Melchers (1992) presented a mathematical model to calculate the rotational stiffness of column base-plate connections. The model was based on a total of 36 tests (including tests from Hon and Melchers, 1988). It was shown that the moment capacity of the base connections tested were governed by base-plate yielding. It was stated that the parameters that influences the rotational stiffness most are the anchor rod elongation, base-plate deformation and prying force. It was observed that the increase of the anchor rod diameter led to an increase of the rotational stiffness by keeping the base-plate thickness constant. It was also stated that the rotation of the footing could be significant in comparison to the rotation of the column base so it is suggested to be considered in the structural deflection estimation. Penserini and Colson (1989) created a mathematical model for determining the strength of the column base-plate connection. The mathematical model was created for pinned and fixed base connections and was used to calculate the ultimate strength of the column base-plate connection considering the ultimate strength of the concrete block, the anchor rods and the column with the base-plate. It was found that the calculated ultimate strength was in a good agreement with the experimental results.

Astaneh et al. (1992) recommended that the design of the column base-plate connections should follow the ultimate strength design procedures, and they suggested that in order to achieve a realistic response for the seismic applications, the base-plate connections should be modeled as semi-rigid rather than “pinned” or “fixed”. Ermopoulos and Stamatopoulos (1996) proposed an analytical formula which included closed formed equations relating the bending moment and rotation of the column base-plate connections. Their model was compared with analytical analysis which included finite element models for different compressive axial load levels and the results were found to be in a good agreement.

Thambiratnam and Krishnamurthy (1989) performed a parametric study to study the effect of the base-plate thickness and load eccentricity on the response of the base-plate connections. Their models showed a good match of the uplift of the base-plate and the pressure distributions under the base-plate area on the compression side in comparison to the experimental data. Targowski et al. (1993) performed analytical methods for investigating the nonlinear behavior of column base-plate connections. The challenges of the contact problem in the region between the base-plate and the anchor rods was underlined by the authors, and the necessity to investigate the contact problem in depth was pointed out. Detailed analytical models were also developed to quantify the “partial rigidity” of pinned column base-plate connections by Bajwa et al. (2010) and Verma (2012). These were correlated with experimentally obtained rotational stiffness and the necessity of detailed analytical models in order to evaluate the rotational stiffness and the behavior of the base-plate connections was underlined.

The necessity to take into consideration the rotational stiffness of pinned column base-plate connections in a frame analysis was first pointed out by Galambos (1960). Since then, several studies have found that the consideration of the base restraint could lead to non-negligible benefits in terms of the service deflections and strength demand for the frame design (El-Khoraibie, 1978; Vernon and Watwood, 1985; Robertson 1991; Yamada and Akiyama 1997; Kawano and Matsui 1998; Eroz et al., 2009; Bajwa et al., 2010). Particularly, El-Khoraibie (1978) examined the influence of the partially-restrained base connections in a frame analysis under different soil conditions. It was found that considering the partial base fixity in comparison with the "pinned" assumption resulted in a decrease of the effective length factor of the columns and caused in lighter column sections. Eroz et al. (2009), by modeling the partial-restraint of the base connections with two rotational springs in series (representing the base and the foundation), found that the frame service deflections and the member strength demand were reduced by 3-9%. The study also stated that the base-plate connection being considered as pinned, had a positive effect on the stability of the frames.

Parametric analyses performed by Fahmy (1999) on frame design having connections with rigid base-plates confirmed that the calculated drifts and developed moments will be very close to the ones obtained from frames with theoretical fixed supports (Fahmy, 1999). It was proposed that the base fixity of frames subjected to gravity and low lateral loads may be represented as "fixed" or "pinned" respectively. For a calculated rotational stiffness $S_{j,ini}$ higher than $30E \cdot I_c/L_c$, the base connection was assumed rigid while for a calculated rotational stiffness $S_{j,ini}$ lower than $30E \cdot I_c/L_c$, the base connection was considered as semi-rigid or pinned. Astaneh et al. (1992) proposed that under seismic loads, the column base-plate connection will be subjected to inelastic cycles and will act as a "semi-rigid" connection. Yamada and Akiyama (1997) and Kawano and Matsui (1998) investigated the effect of the semi-rigid base connection modelling on the frame analysis. Specifically, it was shown that the story drift and plastic hinges are distributed more equally along the height of the frame when semi-rigid column base-plate connections are used rather than perfectly fixed ones.

2.3. Design Codes Provisions

The current design provisions for the column base-plate connections include the design for gravity, wind and seismic loads. Murray (1983) proposed a method for designing column base-plate connections subjected gravity and uplift loads. The column base-plate connections designed to withstand gravity and wind loads are typically expected to ensure that the critical design loads combinations can be sustained without failure of any of the connection components (e.g., anchor rods, base-plate, concrete foundation). The available strength of each connection component is compared with the strength demand of the corresponding component. For example the axial tension is expected to be sustained by the anchor rods, the bending moments by the base-plate and the bearing stresses by the concrete foundation. In the case of the column base-plate connections designed to sustain seismic loads, the inelastic cyclic behavior need to be checked and accounted for. Therefore, in parallel with the strength, the deformation capacity of the connection needs to be accounted for.

The connections in the codes are mainly categorized according to the level of restraint they are designed for. According to their rigidity, they are categorized as rigid (or fully-restrained moment connections), pinned or as partially restrained moment connections. The column base-plate connections have attracted less attention compared to other connections such as the beam-to-column connections and therefore in most of the cases they are designed using concepts similar to beam-to-column connections. As described above, the most studied column base-plate connection used in the codes is the one with the anchor rods outside the flanges. Therefore, in most of the cases some assumptions need to be made in order to design a column base-plate connection that have anchor rods inside the flanges according to the code provisions. The considerations of the codes for calculating the capacity and the rigidity of the base-plate connections are described in the following sections. It should be noted that the American codes and design guides only deal with the strength design of a column base-plate connection while the European and Japanese provisions provide procedures for calculating the rotational stiffness of the connections in addition to the strength design.

2.3.1. AISC Design Guide 1 (Fisher and Kloiber, 2006)

AISC Design Guide 1 (Fisher and Kloiber, 2006) include provisions for strength design according the Allowable Stress Design (ASD) and the Load and Resistance Factor Design (LRFD). For the design of the reinforced concrete foundation and the embedment requirements for the anchor rods ACI 318 Appendix D (2014) is referenced. AISC Design Guide 1 (Fisher and Kloiber, 2006) provides the design requirements for column base-plate connections subjected to compressive and tensile axial loads, small and large moments and shear. Specifically, the design approach of AISC Design Guide 1 (Fisher and Kloiber, 2006) is based on the research that has been conducted by Drake and Elkin (1999) and modified by Fisher and Doyle (2005) based on the LRFD approach. According to this method, the applied factored moments and axial forces are resisted by the bearing in the concrete and the tensile resistance in the anchor rods. If the base-plate size is known, the bearing length Y and the anchor rod ultimate tensile force (see Figure 2.11) can be calculated from the two equilibrium Equations (2-1) and (2-2) as

$$\sum \mathrm{F_{vertical}} = 0 \rightarrow \mathrm{T_u} + \mathrm{P_u} - \varphi_c \cdot \mathrm{P_p} = 0, \qquad \text{(2-1)}$$

$$\sum \mathrm{M} = 0 \rightarrow \varphi_c \cdot \mathrm{P_p}\left(\frac{\mathrm{N}}{2} - \frac{\mathrm{Y}}{2} + \mathrm{f}\right) - \mathrm{P_u} \cdot (\mathrm{e} + \mathrm{f}) = 0\text{, and} \qquad \text{(2-2)}$$

$$\mathrm{P_p} = 0.85 \cdot \mathrm{f'_c} \cdot \mathrm{A_1} \cdot \sqrt{\frac{\mathrm{A_2}}{\mathrm{A_1}}} \quad \text{but} \quad \sqrt{\frac{\mathrm{A_2}}{\mathrm{A_1}}} \leq 2, \qquad \text{(2-3)}$$

where, T_u is the ultimate force in the anchor rod (kips) (see Figure 2.11), φ_c is the compression resistance factor equal to 0.60 per Section 9.3 of ACI 318 (2014), e is the eccentricity equal to the ratio of the applied moment over the applied axial load (inch), P_p is the ultimate force produced by the concrete block as defined in Equation (2-3) (kips), and Y is bearing length (see Figure 2.11) (inch).

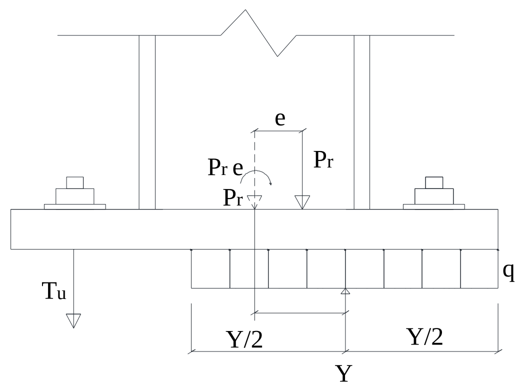

Figure 2.11. Base-plate with applied moments [(Fisher and Kloiber (2006)].

The anchor rod distance f from the column and base-plate centerline parallel to moment direction is shown in Figure 2.12.

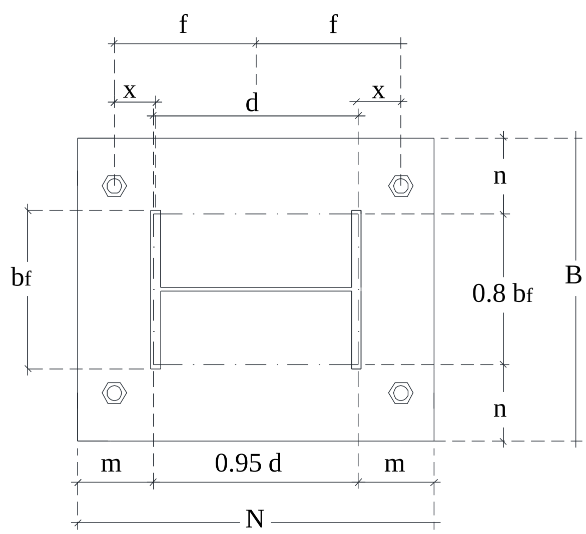

Figure 2.12. Base-plate geometric design variables [Drake and Elkin (1999)].

By solving Equations (2-1) and (2-2), the bearing concrete length Y and tensile resistance force in the anchor rod T_u (see Figure 2.11) are calculated according to Equations (2-4) and (2-5) as

$$Y = \left(f + \frac{N}{2}\right) \pm \sqrt{\left[-q \cdot \left(f + \frac{N}{2}\right)\right]^2 - \frac{2 \cdot P_u \cdot (f + e)}{q}} \text{ and} \tag{2-4}$$

$$T_u = q \cdot Y - P_u. \tag{2-5}$$

The anchor rods are designed according to the AISC Steel Constructional Manual Section J3.2 (2011) where the anchor rod shear strength V_{ub} and tensile force T_{ub} need to meet the requirements given in Equations (2-6) and (2-7) as

$$V_{ub} \le \varphi \cdot F_v \cdot A_b \text{ and} \tag{2-6}$$

$$T_{ub} \le \varphi \cdot F_t \cdot A_b, \tag{2-7}$$

where, F_v is the nominal shear strength of the anchor rod (kips), F_t is the nominal tensile strength (ksi), and A_b is the anchor rod area (inch^2).

The base-plate is then designed according to the flexural yielding limit states in AISC Steel Construction Manual (2001) Section F1 as

$$M_{pl} \le \varphi_b \cdot M_p, \tag{2-8}$$

where, M_p is the nominal plastic moment of the base-plate (kip-ft).

The base-plate thickness is then taken as larger than the value in Equations (2-9), (2-10) and (2-11) as

$$t_{p(req)} \ge 2.11 \cdot \sqrt{\frac{T_u \cdot x}{B \cdot F_y}}, \tag{2-9}$$

$$\text{If} \quad Y > m \quad \text{then} \qquad t_{p(req)} \ge 1.5m \cdot \sqrt{\frac{P_u}{B \cdot Y \cdot F_y}}, \text{ and} \tag{2-10}$$

$$\text{If} \quad Y < m \quad \text{then} \qquad t_{p(req)} \geq 2.11\sqrt{\frac{P_u \cdot \left(m - \frac{Y}{2}\right)}{B \cdot F_y}}, \tag{2-11}$$

where, F_y is the yield stress of the base-plate (ksi), x is the base tension interface cantilever parallel to moment direction (inch), B is the base-plate width perpendicular to the moment direction (inch), and m is the base-plate bearing interface cantilever direction parallel to moment direction (inch). These geometric quantities are shown Figure 2.12.

2.3.2. AISC Steel Construction Manual (2011)

According to Chapters J and K of the AISC Steel Construction Manual (2011), the connections are categorized based to their performance as "simple connections" whose moment capacity is negligible and allow unrestrained rotation between the connected elements, the "partially-restrained (PR) moment connections" whose moments and the rotation transmitted between the connected elements is not negligible, and the "fully-restrained (FR) moment connections" that transfer the moment with a negligible rotation between the connected elements. According to the AISC Steel Construction Manual (2011), the strength of the connection is calculated as a "proportion" of the required strength of the individual elements of a connection. The rotational stiffness of the connection is defined as the secant stiffness, K_s which is the ratio M_s/θ_s where M_s is the moment at the service loads and θ_s is the rotation at the service loads (see Figure 2.13). The AISC Steel Construction Manual (2011) uses a limiting value $K_s > 20 \cdot E \cdot I/L$ to define a fully-restrained connection and $K_s < 2 \cdot E \cdot I/L$ for a simple connection. Any connection with rotational stiffness between these two limits is defined as partially-restrained and it is suggested that its stiffness, strength and ductility should be considered in the design of the structure. For the partially restrained connections, it is suggested that an initial assumption can be done for their force-deformation characteristics, followed by iterative analysis of the structure until connection's performance is adequate for the structural design. Additionally, it is advised that the characteristics of partially restrained connections can be obtained from analytical studies, tests and simple component modeling.

The strength of the connection M_n (see Figure 2.13) is defined as the maximum moment that a connection is capable to sustain. It is suggested that the moment at a rotation of 0.02 radian is considered in case that the moment-rotation response does not exhibit a peak up to that rotation level. It should be noted that all the provisions of the AISC Steel Construction Manual (2011) for connections are for beam-column connections and $E{\cdot}I$ and L are referred to the bending rigidity and length of the beam, while there are no provisions for the column base-plate connections.

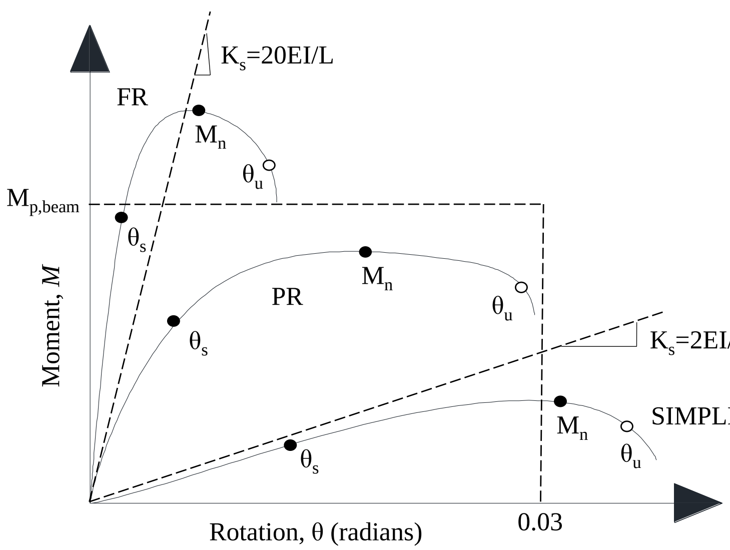

Figure 2.13. Classification of moment-rotation response of fully restrained (FR), partially restrained (PR) and simple connections [AISC Steel Construction Manual (2011)-Figure C-B3.3].

2.3.3. AISC Seismic Design Manual (2010)

The lack of research on column base-plate connections is underlined in AISC Seismic Design Manual (2010) especially for designing for high seismic loads. The Manual also acknowledges the influence of the column base-plate connection on the overall performance of the frame and underlines the high importance of the consideration of the column base-plate connection behavior in the frame design. It is suggested that the designer follows similar principles for the design and detailing of the column base-plate connection to the concepts for the beam-to-column connections. At the same time, the Commentary of the AISC Seismic Design Manual (2010) outlines the main differences between the beam-to-column connections and the column base-plate connections that need to be considered in the design. These differences are summarized below:

- The difference of the elongation of the anchor rods embedded inside the concrete in comparison with the steel bolts or weld strain capacity.
- The compressive capacity of the grout or the concrete foundation which is higher than the steel column flanges of the beam-to-column connections.
- The column base-plate connections need to sustain more axial load, while the beam-to-column connections need to sustain more shear load.
- The difference between the two shear mechanisms. In the case of the column base-plate connection, the shear forces are transmitted as a combination of surface friction between the grout/concrete and the steel base-plate, as well as bearing of the anchor rods on the steel base-plate. In contrast, the shear is transmitted from the steel beam end plate to the column flange through the bolts.
- The difference between the hole diameters for the anchor rods and the standard holes for high strength bolts.
- The foundation rocking behavior and the foundation rotation especially on isolated footings.

2.3.4. AISC Design Guide 25 (Kaehler et al., 2011)

The provisions for the design of frames with web-tapered sections are included in AISC Design Guide 25 (Kaehler et al., 2011). It is recommended that “partial-restrained” column base-plate connections could be included in the analysis of frames with the use of linear or nonlinear springs, if the moment-rotation response could be quantified. The AISC Design Guide 25 (Kaehler et al., 2011) refers to the research of Eroz et al. (2009) for more information about the modeling partially-restrained connections by using elastic-perfectly plastic rotational spring elements and their influence on the frame analysis.

2.3.5. Eurocode 3 (Design of Steel Structures – Part 1-8: Design of Joints)

Section 5.2.2.5 of Eurocode 3 (prEN1993-1-8) provides conditions to determine when a column base can be classified as rigid. The column base-plate connections can be classified as rigid under the following conditions.

- In frames where the bracing system reduces the horizontal displacement by at least 80 % and where the effects of deformation may be neglected

- If the slenderness ratio of the column is $\lambda_0 \leq 0.5$;
- If the slenderness ratio of the column is $0.5 < \lambda_0 < 3.93$; and $S_{j,ini} \geq 7(2\,\lambda_0 - 1)\,E \cdot I_c / L_c$
- If the slenderness ratio of the column is $\lambda_0 \geq 3.93$; and $S_{j,ini} \geq 48\,E \cdot I_c / L_c$

- Or if $S_{j,ini} \geq 30\,E \cdot I_c / L_c$

where, λ_0 is the slenderness ratio of a column in which both ends are assumed to be pinned, $S_{j,ini}$ is the rotational stiffness of the base connection (kip-ft/rad), I_c is the second moment of area of a column (inch^4), L_c is the story height of a column (inch).

Eurocode 3 (prEN1993-1-8) Section 6.3 provides a step-by-step procedure for calculating the rotational stiffness of column base-plate connections. This procedure follows the component-based method, in which the connection is considered to be a combination of individual components. The stiffness is determined through the analytical simulation of the mechanical model of the components of the connection. According to this model, the base-plate is modeled as a rigid bar connected with three springs. One of the springs represents the stiffness of the concrete, the second spring represents the anchor rods, and the third one represents the base-plate in tension. The springs representing the anchor rods and the base-plate in tension are in series and in parallel with the spring representing the concrete. Their stiffness are given by the Equations (2-12), (2-13) and (2-14) below:

Stiffness of the concrete in compression (including grout) is given by

$$k_{13} = \frac{E_c \cdot \sqrt{b_{eff} \cdot l_{eff}}}{1.275 \cdot E}, \tag{2-12}$$

where, E_c is the Young's of modulus of the concrete (ksi), E is the Young's of modulus of the steel (ksi), b_{eff} is the effective width of the T-stub flange (see Figure 2.14) (inch), and l_{eff} is the effective length of the T-stub flange (see Figure 2.14) (inch),

Stiffness of base-plate in bending under tension is given by Equation (2-13) as

$$k_{15} = \frac{0.425 \cdot l_{eff} \cdot t_p^3}{m^3}, \tag{2-13}$$

where, E_c is the Young's of modulus of the concrete (ksi), l_{eff} is the effective length of the T-stub flange (see Figure 2.14) (inch), t_p is the thickness of the base-plate (inch), and m is the rod to weld distance (inch).

Stiffness of the anchor rods in tension is given by Equation (2-14) as

$$k_{16} = \frac{2 \cdot A_s}{L_b}, \tag{2-14}$$

where, A_s is the area of the anchor rod (inch^2), and L_b is the elongation length of the anchor rod (inch).

Then the rotational stiffness is calculated according to Equation (2-15) as

$$S_j = \frac{E \cdot z^2}{\mu \cdot \sum_i \frac{1}{k_i}}, \tag{2-15}$$

where, E is the Young's of modulus of the steel (ksi), z is the distance of the resultant compressive force of the concrete to the tensile force of the rod (inch), k_i is the stiffness coefficient representing the stiffness of the components of the connection (kips-ft/rad), and μ is the stiffness ratio determined from the following condition in Section 6.3.1(6) of Eurocode 3 (prEN1993-1-8).

- if $M_{j,Ed} \leq 2/3\ M_{j,Rd}$, $\mu=1$
- if $2/3\ M_{j,Rd} < M_{j,Ed}, \leq M_{j,Rd}$, $\mu=(1.5\ Mj_{,Ed}/\ M_{j,Rd})^{\psi}$

where, $M_{j,Ed}$ *is* the applied moment (kips-ft), $M_{j,Rd}$ is the design moment resistance of the connection (kips-ft), and Ψ *is* a constant which depends from the type of the connection.

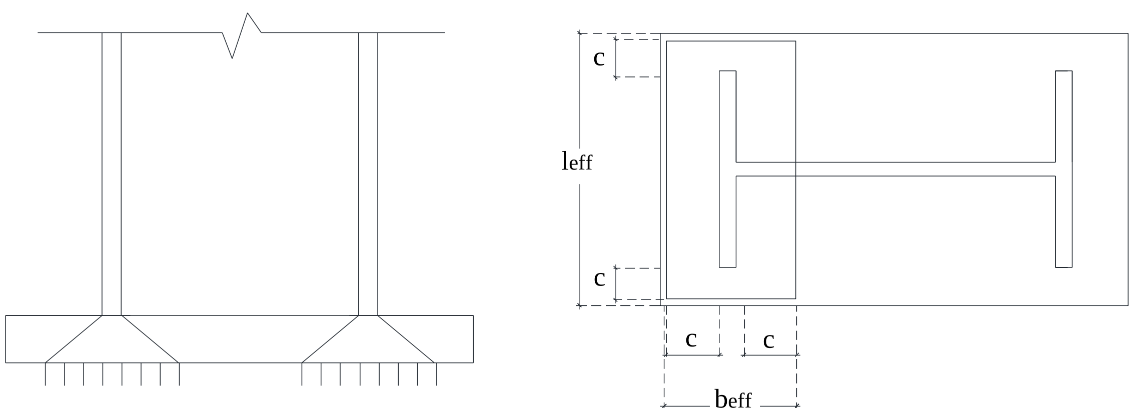

Figure 2.14. Area of equivalent T-stub in compression for large projection (prEN1993-1-8).

2.3.6. Japanese Code (AIJ, 2001)

The calculation of the rotational stiffness of the column base-plate connection provided by the provisions of the Japanese Code (AIJ, 2001) is given by Equation (2-16) as

$$K_{BS} = \frac{E \cdot n_t \cdot A_b \cdot (d_t + d_c)^2}{2 \cdot l_b}, \qquad (2\text{-}16)$$

where, E is the Young's of modulus (ksi), A_b is the cross section area of the anchor rods (inch^2), l_b is the embedment length of the anchor rods (inch), n_t is the number of the anchor rods, and d_t and d_c are given in Figure 2.15.

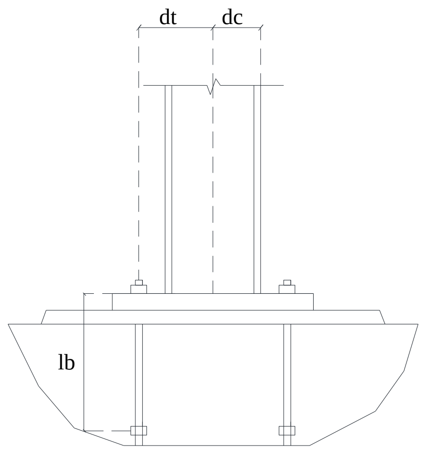

Figure 2.15. Dimensions included in the rotational stiffness formula according to Japanese Code (AIJ, 2001).

The provisions of the Japanese Code (AIJ, 2001) require that the rotational stiffness of the column base-plate connection need to be used for the calculation of the moment capacity of the connection. According to the Japanese Code (AIJ, 2001), the base connections are designed for different anchor rod behavior. Specifically, in the case that “ductile” anchor rods are used in the connection, the moment capacity M_u of the connection is calculated according to Equation (2-17) as

$$\mathrm{M_u} = \begin{cases} (\mathrm{N_u} - \mathrm{N}) \cdot \mathrm{d_t} & (\mathrm{N_u} \geq \mathrm{N} > \mathrm{N_u} - \mathrm{T_u}), \\ \mathrm{T_u} \cdot \mathrm{d_t} + \dfrac{(\mathrm{N} + \mathrm{T_u}) \cdot \mathrm{D}}{2}\left(1 - \dfrac{\mathrm{N} + \mathrm{T_u}}{\mathrm{N_u}}\right) & (\mathrm{N_u} - \mathrm{T_u} \geq \mathrm{N} > -\mathrm{T_u}), \\ (\mathrm{N} + 2 \cdot \mathrm{T_u}) \cdot \mathrm{d_t} & (-\mathrm{T_u} \geq \mathrm{N} \geq -2\mathrm{T_u}), \end{cases} \qquad (2\text{-}17)$$

where, N is axial force (kips), N_u is maximum compression strength of the concrete (ksi), T_u is maximum tensile strength of anchor rods on the tension side (ksi), F_c is concrete strength (ksi), and d_t is given in Figure 2.15.

In the research conducted by Hitaka et al, (2003), the requirements of the Japanese Code (AIJ, 2001) for the strength design of the connections are presented. The anchor rod yielding is permitted if their yield ratio is more than 0.75. It was estimated that a column base-plate connection consisting of anchor rods with this yield ratio, have plastic rotational capacity at a rotation more than 0.03 rad.

2.4. Conclusions

This study aims to characterize the rotational stiffness and moment capacity of pinned base-plate connections that are commonly used in low-rise metal building systems and its influence on the structural design. An extensive experimental program was being undertaken. All the connections which were part of the experimental program had asymmetric anchor rod arrangements with respect to the center of the base-plate and the length of the base-plate was equal to the column section depth (i.e., overhang equals to zero), see Figure 2.16. Thus, the configurations under investigation are distinctly different from those in literature and represent the actual details that are used in real metal buildings systems in the United States and around the world. The experimental data, which was generated on the rotational stiffness of “pinned” column base-plate connections was used to develop spring models which are implemented in analytical frame models. These analytical models were then used to determine the influence of column base-plate stiffness on the design of low-rise metal buildings. Additionally, the experimental results were used to validate detailed continuum analytical models of the connections including the foundation and the column stub. A parametric study was performed using validated models to evaluate the most influential parameters of the connections on the rotational stiffness and moment capacity. It is expected that the results from this study will inform future revisions of metal building design codes and standards by providing quantitative data based on large-scale experiments and validated numerical models of base-plate connections, potentially leading to cost savings in lateral resisting systems of this structural typology.

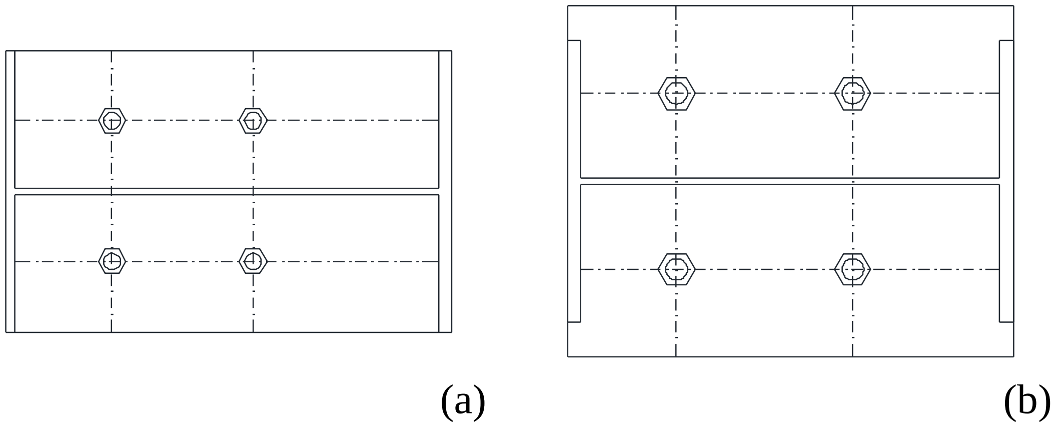

Figure 2.16. (a), (b) Typical base-plate configurations tested in the research.

3. EXPERIMENTAL PROGRAM AND RESULTS-PHASE 1

3.1. Test Configurations and Corresponding Frame Designs

Eight full-scale column base-plate connections were tested under combined axial and lateral loads in the first phase of the experimental program. These column base-plate connections were taken from eight different metal building designs that are representative of low-rise metal building construction in the United States. The dimensions of the column base-plate connections are symbolically shown in Figure 3.1(a) and the configuration of a column stub along with the loading directions are shown in Figure 3.1(b). The details of the column base-plate connections and those of the corresponding frames are presented in Table 3.1 and Table 3.2, respectively. Figure 3.1. The base-plate thicknesses varied from 3/8 inch to 3/4 inch. The flange thicknesses varied from 1/4 inch to 5/8 inch. Three different anchor rod diameters were used: 3/4 inch, 1 inch and 1 1/4 inch, with varying gage, setback, and pitch distances. All the base-plate connections, except for $S02_{phase1}$ had four anchor rods while $S02_{phase1}$ had six anchor rods. The smallest and largest base-plates had plan dimensions of 6 x 10 11/16 inches ($S01_{phase1}$) and 10 x 14 inches ($S08_{phase1}$), respectively.

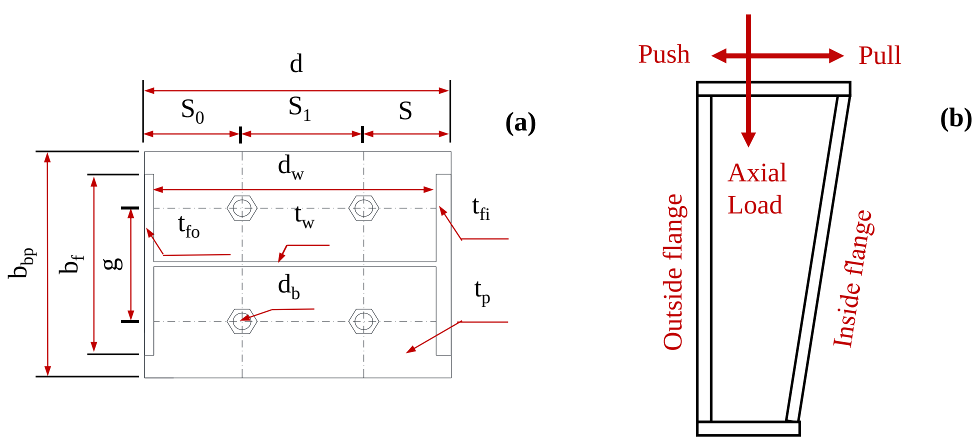

Figure 3.1. A generic base-plate connection configuration: (a) dimensional details, (b) elevation view.

Table 3.1. Details of the Tested Base-Plate Connections (refer to Figure 3.1).

Specimen ID	Web Depth	Flange Width	Web Thickness	Outside Flange Thickness	Inside Flange Thickness	Base-Plate Width	Base-Plate Thickness	Anchor Rod Diameter	No. of Anchor Rods	Pitch	Gage	Setback	Setback	Base Plate Depth	Axial load
	d_w	d_w	t_w	t_{fo}	t_{fi}	b_f	t_p	d_b	-	S_1	g	S_0	S	d	
	(inch)	(inch)	(inch)	(inch)	(inch)	(inch)	(inch)	(inch)		(inch)	(inch)	(inch)	(inch)	(inch)	(kips)
S01 $_{phase1}$	10	6	1/6	5/16	3/8	6	1/2	3/4	4	4	4	3	3 11/16	10 11/16	20.90
S02 $_{phase1}$	12	8	1/4	3/8	5/16	8	5/8	3/4	6	4	4	3	1 11/16	12 11/16	26.00
S03 $_{phase1}$	12	8	1/6	1/4	3/8	8	5/8	3/4	4	4	4	3	5 5/8	12 5/8	51.40
S04 $_{phase1}$	10	8	1/4	1/2	5/8	8	5/8	1	4	4	4	4	3 1/8	11 1/8	64.00
S05 $_{phase1}$	11 1/2	5	1/9	1/4	1/4	6	3/8	3/4	4	4	4	3	5	12	10.80
S06 $_{phase1}$	12	8	3/16	1/4	3/8	8	5/8	3/4	4	4	4	3	5 5/8	12 5/8	67.40
S07 $_{phase1}$	10	10	3/16	3/8	3/8	10	1/2	3/4	4	4	4	3	3 3/4	10 3/4	39.20
S08 $_{phase1}$	13	8	3/16	3/8	5/8	10	3/4	1 1/4	4	5	5	4	5	14	43.60

Table 3.2. Locations and Dimensions of the Corresponding Frames and Loading Details.

Specimen ID	Bldg Width	Bldg Length	Eave Height	Bay Width	Column Spacing	Slope (x in 12)	Weight	Load	Snow Pg	Wind	EQ	State	County
	(ft)	**(ft)**	**(ft)**	**(ft)**			**(psf)**	**(psf)**	**(psf)**	**(mph)**	**%**	**-**	**-**
S01 $_{phase1}$	100	100	25	25	0	1	~5	20	0	105	1	Texas	Harris
S02 $_{phase1}$	100	100	60	25	0	1	~5	20	0	123	1	Texas	Galveston
S03 $_{phase1}$	100	100	60	25	0	1	~5	20	0	85	17	California	Kern
S04 $_{phase1}$	120	100	35	25	0	1	~5	20	30	90	1	N Dakota	Williams
S05 $_{phase1}$	40	60	16	20	0	1	~5	20	10	90	27	Tennessee	Shelby
S06 $_{phase1}$	60	100	50	25	0	1	~5	20	40	90	5	Pennsylvania	Berks
S07 $_{phase1}$	300	300	35	30	50	1	75	20	40	90	8	Pennsylvania	Berks
S08 $_{phase1}$	80	100	50	25	0	1	~5	20	0	140	0	Florida	Broward

Figure 3.2 shows the dimensions of the tested connection configurations. Each connection had a unique geometry as explained above except for the fourth and the seventh. The only differences between $S03_{phase1}$ and $S06_{phase1}$ were the web thickness and the level of axial compressive load, the latter of which was a result of different frame dimensions. The drawings of the frames are given in Appendix B. As shown in Table 3.2, the span and width of the frames varied from 50 ft to 300 ft and from 40 ft to 300 ft, respectively. The frame of $S05_{phase1}$ had the smallest dimensions while the frame of $S07_{phase1}$ had the largest. The live load for all of the frames was 20 psf and the snow load varied from 0 psf to 40 psf depending on the state for which the frame was designed. Additionally, the wind load varied from 85 mph to 140 mph and the earthquake load varied from 0% (for the frame designed for Florida) up to 27% (for the frame designed for Tennessee). It should be noted that the snow pg is the equivalent roof load calculated according to American Society of Civil Engineers 7 (2010). Wind and earthquake (EQ) loads are the equivalent lateral forces calculated according to ASCE 7 (2010). Based on the structural analysis of the frames, the axial compressive load on the column base-plate connections varied from 10.8 kips for the frame of $S05_{phase1}$ to 67.4 kips for the frame of $S06_{phase1}$.

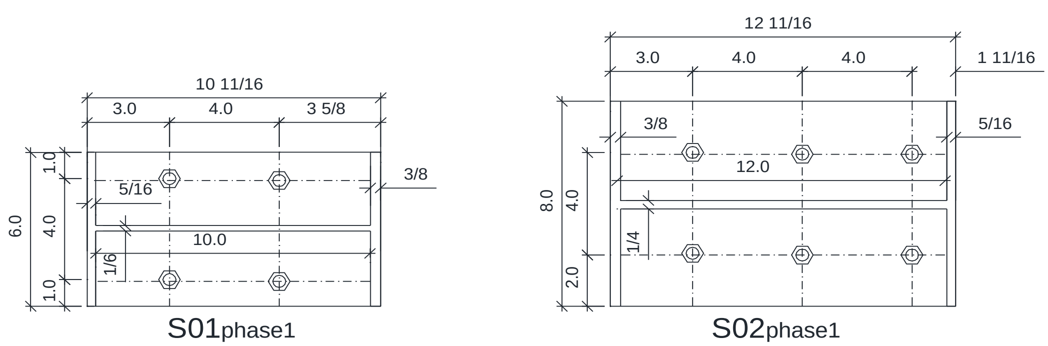

Figure 3.2. Tested web-tapered base-plate configurations (column base-plate connection 6 is the only non-web-tapered specimen). The drawings are created to follow the conventions of Figure 3.1.

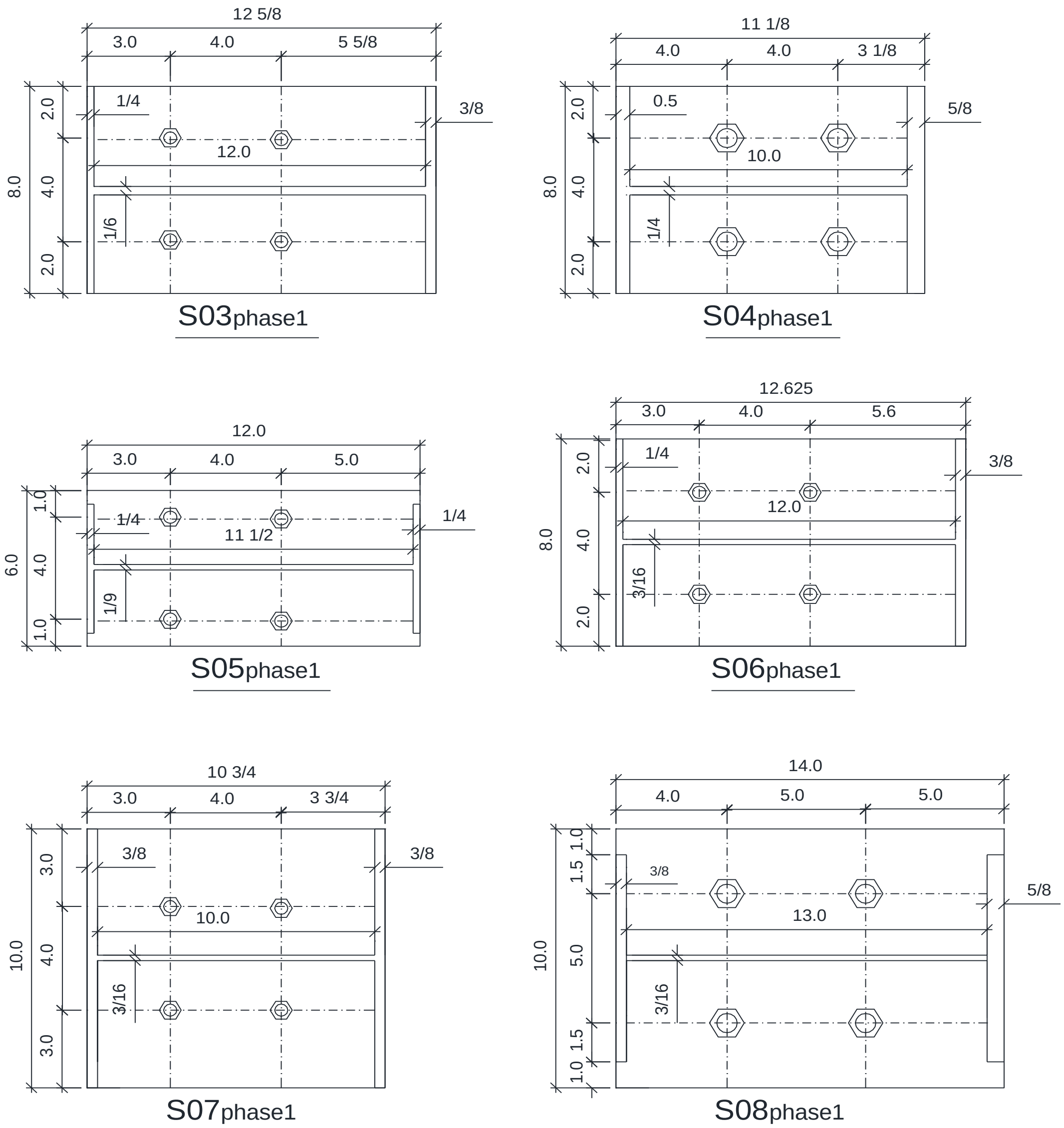

Figure 3.2. (Continued) Tested web-tapered base-plate configurations (column base-plate connection 6 is the only non-web-tapered specimen). The drawings are created to follow the conventions of Figure 3.1.

3.2. Test Setup

The test setup of the first phase of the experimental program, shown in Figure 3.3, was designed to remain elastic for the highest loads expected during the tests. The test setup components were fabricated at NCI Building Systems and assembled in the Thomas T. C. Hsu Structural Research Laboratory at the University of Houston. Three separate foundation built-up beams (24 inch depth × 12 inch flange width) were connected to each other through four channel sections (C15×50).

Only the two side beams were connected to the strong floor while the central one was connected to the side beams due to the pattern of the strong floor anchoring points. The column stubs were connected to the central foundation beam at the base, and connected to a 16 inch deep “transfer beam” at the top. The horizontal loads were applied to the specimens through an actuator with a capacity of 110 kips, which was connected to the transfer beam at one end and to a reaction frame at the other end. Additionally, a hydraulic jack with a capacity of 200 kips was placed atop the transfer beam to apply a constant axial compressive load in the columns ranging from 10 kips to 70 kips. The axial loads from the hydraulic jack were transferred to the foundation through a crossbeam sitting atop the jack and through two post-tensioning bars. Pin connections were used to provide a free rotation at the locations where the post-tensioning bars were connected to the side foundation beams. Two portal frames were built on each side of the column stub to prevent out-of-plane displacements. The columns of the portal frames were bolted to two base-beams that were fixed to the strong floor. The tested column stubs were 70 inch tall.

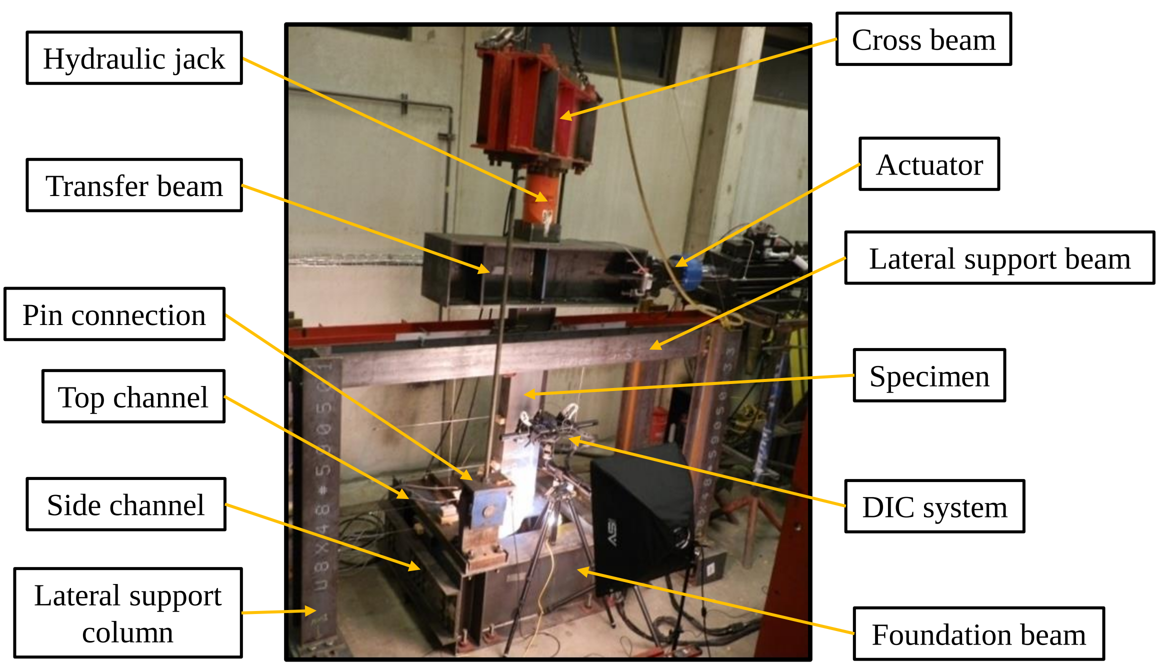

Figure 3.3. Illustration of the test setup.

3.3. Instrumentation and Data Acquisition

The deformations were measured using linear potentiometers, rotary (string) potentiometers and strain gauges. The global deformation and load measurements from the specimens included the displacement of the column stub at the location of the actuator connection, and the applied horizontal and axial loads. In addition, the deflections of the column stubs were measured using rotary (string) potentiometers at four points located along the height of the specimens. On one side of the columns, the deformations of the base-plate (uplift, in- and out-of-plane sliding, and torsion) were measured using linear potentiometers. The layout of the conventional instrumentation is shown in Figure 3.4. A Micro-Measurements System 7000 data acquisition system was used for all the tests. Strain gage data and high-level outputs such as those from linear potentiometers and rotary (string) potentiometers could be combined into groups of eight channels by choosing the suitable sensor cards in the data acquisition system. Each sensor was calibrated before testing and the Micro-Measurements data acquisition system was synchronized with the controller of the hydraulic actuator. The accuracy of the linear potentiometers was reported by the manufacturer as 0.15% of the full stroke which varied from 1/2 inch to 2 inch (for the linear potentiometers) and from 4 inch to 14 inch [for rotary (string) potentiometers]. A sampling frequency of 10 Hz was used in all of the tests.

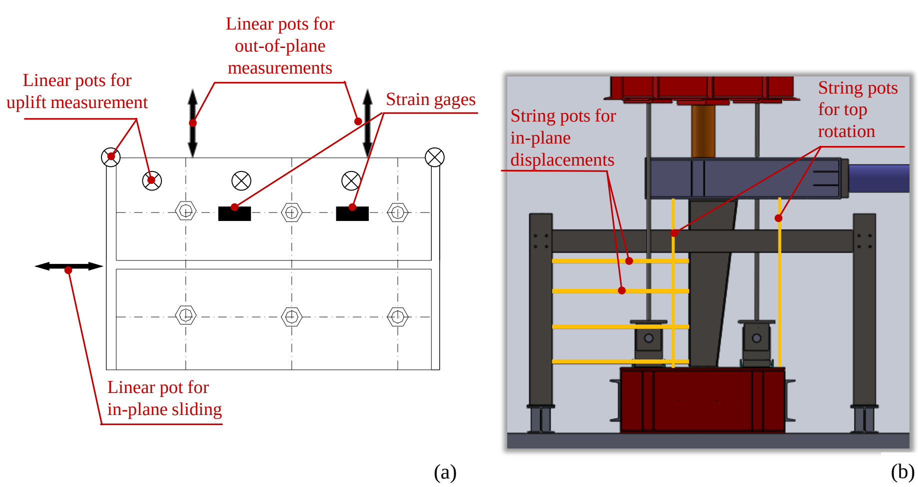

Figure 3.4. Layout of the conventional instrumentation: (a) plan, and (b) elevation view.

3.4. Loading Protocols

Three tests were conducted for each specimen. The drift was defined as the ratio of the displacement measured from the monitoring point over the height of the point from the base of the column given in Equation (3-1) as

$$\text{Drift (\%)} = \Delta/\text{H} \cdot 100, \tag{3-1}$$

where Δ and H are given in Figure 3.5.

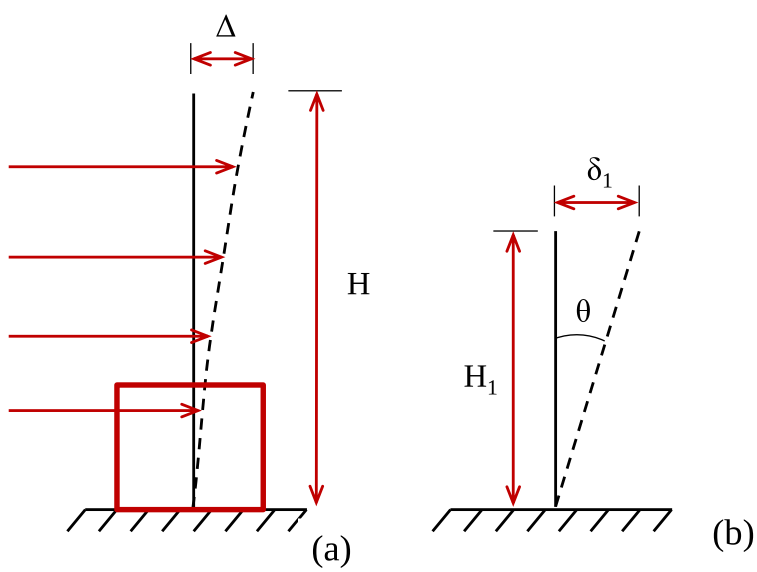

Figure 3.5 Definition of the drift.

In this Section the monitoring point is the point of the applied force from the actuator. First, a flexural cyclic test was performed up to a drift level of 1% under zero axial loading. The loading protocol along with the drift levels for this test is shown in Figure 3.6(a). In the second test, the same loading protocol was followed with the addition of a constant compressive load, which is given in Table 3.1 In the first two tests, two cycles were applied for each drift level up to 1% drift starting from 0.05% and increasing by 0.1% after the 0.1% drift level. These two tests were performed to obtain the elastic properties of the specimens with and without axial load. In the third test, cyclic displacements were increased up to 10% drift or until the specimens showed substantial degradation in capacity. These third tests were conducted under compressive axial loads. The loading protocol for the 10% drift test is shown in Figure 3.6(b), which began with 0.15% drift and increased by 0.1% after the first cycle and by 0.25% in the following cycles up to 1%. After 1% drift, two cycles of 1.5% drift were applied which was followed by 2% drift cycles, and cycles increasing in 1% drift increments thereafter.

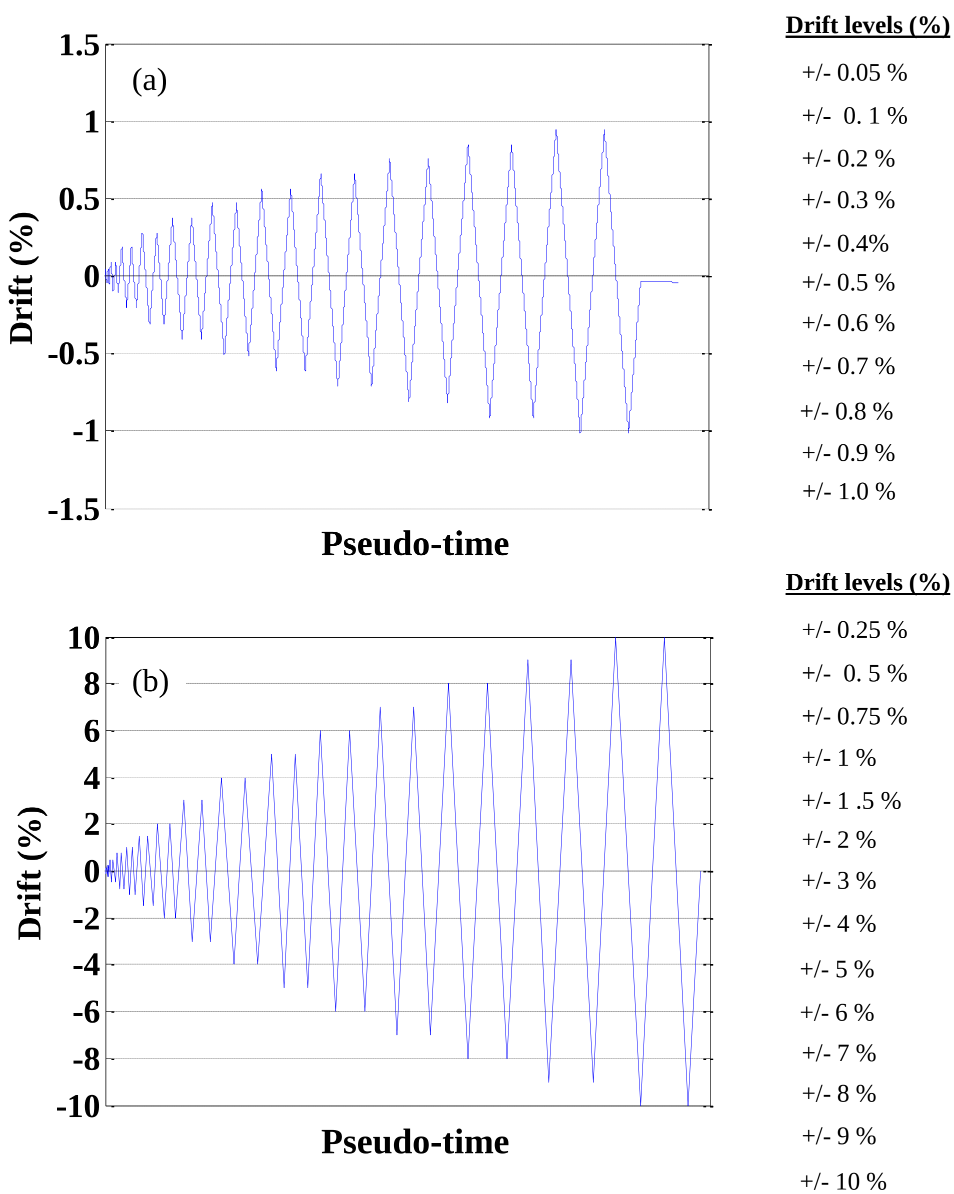

Figure 3.6 Loading protocols and drift levels for (a) 1%, and (b) 10% drift experiments.

3.5. Material Properties

As mentioned earlier and shown in Table 3.1, three different anchor rods diameters were used: 0.75 inch, 1.0 inch and 1 1/4 inch. The anchor rods were Grade 55 steel and had 10, 8 and had 7 threads per 1 inch for the 3/4 inch, 1 inch and 1 1/4 inch diameter anchor rods, respectively. To determine the stress-strain relationship, specimens selected from the same batch of anchor rods were tested under monotonically increasing displacements until rupture according to ASTM A370 (2015). An extensometer was used at the mid-gage of the samples to read the displacements [Figure 3.7(a)]. The results from the tensile tests are shown in Figure 3.7(b). The results from the tensile tests are shown in Table 3.3.

The columns were made of Grade 50 and coupons were cut from the flanges after the completion of the tests. The steel coupons were tested according to ASTM A370 (2015) [see Figure 3.8(a)], and representative stress-strain curves are shown in Figure 3.8(b). The same procedure as the anchor rod tests was followed and an extensometer was used at the mid-gage of the samples to measure the elongation and derive the strain. The main parameters of the stress-strain curves are presented in Table 3.4.

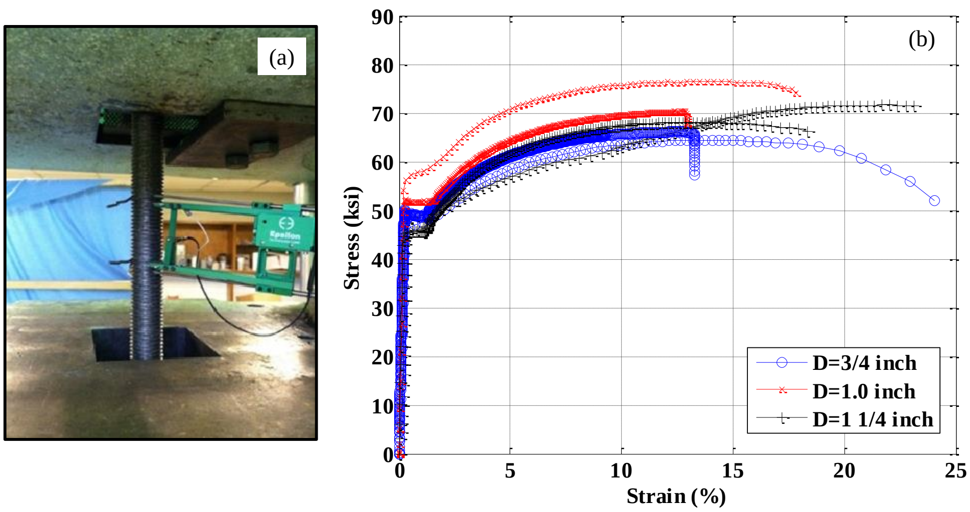

Figure 3.7. (a) Tensile testing of anchor rods, (b) stress-strain curves for anchor rods having different diameters.

Table 3.3. Steel Anchor Rods Test Results.

Diameter	Number of Anchor Rods	Young's Modulus	Yield Stress	Yield Strain	Peak Stress	Peak Strain	Ultimate Stress	Ultimate Strain
(inch)	-	(ksi)	(ksi)	(%)	(ksi)	(%)	(ksi)	(%)
3/4	3	28400	47.4	0.202	65.3	13.654	53.3	20.620
1	3	29200	56.7	0.210	73.6	12.362	70.6	17.430
1 1/4	3	29400	46.8	0.208	69.8	10.320	*	*

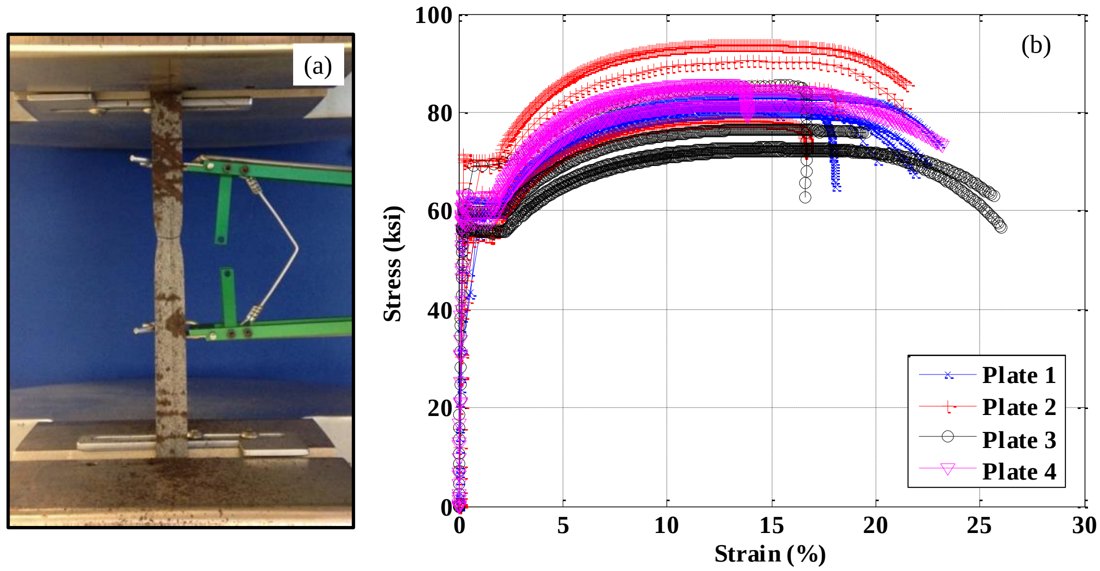

Figure 3.8. (a) Tensile testing of coupons, (b) stress-strain curves from coupon testing.

Table 3.4. Steel Coupon Test Results.

Coupon ID	Coupon ID*	Number of Coupons	Thickness	Young's Modulus	Yield Stress	Yield Strain	Peak Stress	Peak Strain	Ultimate Stress	Ultimate Strain
(inch)	-	-	(inch)	(ksi)	(ksi)	(%)	(ksi)	(%)	(ksi)	(%)
Plate 1	$S05_{phase1}$_IF,OF	7	1/4	28100	60.0	0.205	84.1	13.542	62.0	22.341
Plate 2	$S01_{phase1}$_IF	4	3/8	28900	63.7	0.210	87.0	13.968	81.0	23.074
Plate 3	$S04_{phase1}$_IF	4	1/2	29300	57.7	0.206	76.8	14.362	62.0	25.642
Plate 4	$S04_{phase1}$_OF	4	5/8	29700	59.7	0.214	84.1	15.354	72.0	22.630

*Coupon ID represents the specimen and location of the specimen that the coupon is coming from. IF: inside flange, OF: outside flange.

3.6. Definitions

3.6.1. Connection rotation

The rotation at the base-plate connections is evaluated using three different approaches each of which utilized information from different sets of sensors. In the first approach, the rotation was calculated using the rotary (string) potentiometers for measuring the in-plane displacement of the columns. The rotation was found according to Equation (3-2) and the variables are defined in Figure 3.9(a). The rotation is expressed as

$$\mathrm{Rotation}_1 = \tan^{-1} \delta_1/H_{1.} \tag{3-2}$$

However, since the column might deform due to the rotational stiffness of the connection, the rotation measurement based on different sensors at different heights along the column [see Figure 3.9(a)] might be different. The differences in the rotations obtained from different sensors for two representative specimens, $S03_{phase1}$ and $S06_{phase1}$, are shown in Figure 3.10. The rotations measured from rotary (string) potentiometers 1 (S.Pot. 1) and 2 (S.Pot. 2) (that are at 5 1/4 inch and 13 3/4 inch height from the base, respectively) differed only by 1-2%, the rotation measured from rotary (string) potentiometer 3 (at a height of 28 1/2 inch from the base) was on average 5% larger than the rotation measured from rotary (string) potentiometer 1, and the rotation measured from rotary (string) potentiometer 4 (S.Pot. 4) (located at 41 1/2 inch height from the base) was on average 10% larger than the rotation measured from rotary (string) potentiometer 1 (S.Pot. 1). However, it should be noted that these average differences are not uniform over all the drift range and for different specimens, and they are larger for larger drifts.

In the second approach for calculating the rotation, the uplift measurements of the base-plate from the linear potentiometers were used. The rotation was found according to Equation (3-3) and the variables are defined in Figure 3.9(b). The rotation is expressed as

$$\mathrm{Rotation}_2 = \tan^{-1} (\delta_{ul}/L_o). \tag{3-3}$$

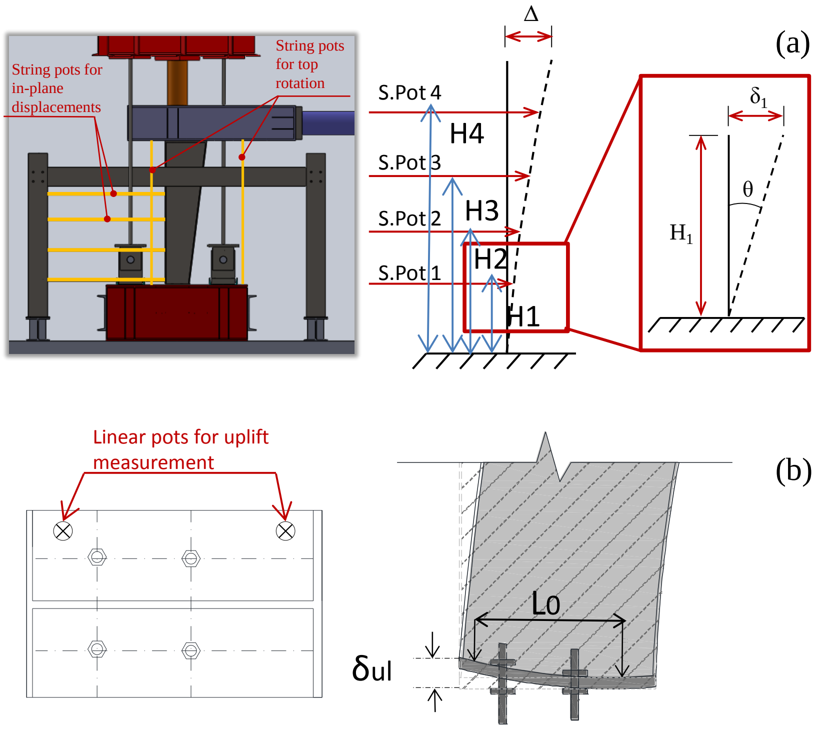

Figure 3.9. Calculation of the rotation: (a) based on the in-plane displacements of the columns, and (b) using the linear potentiometers measuring uplift.

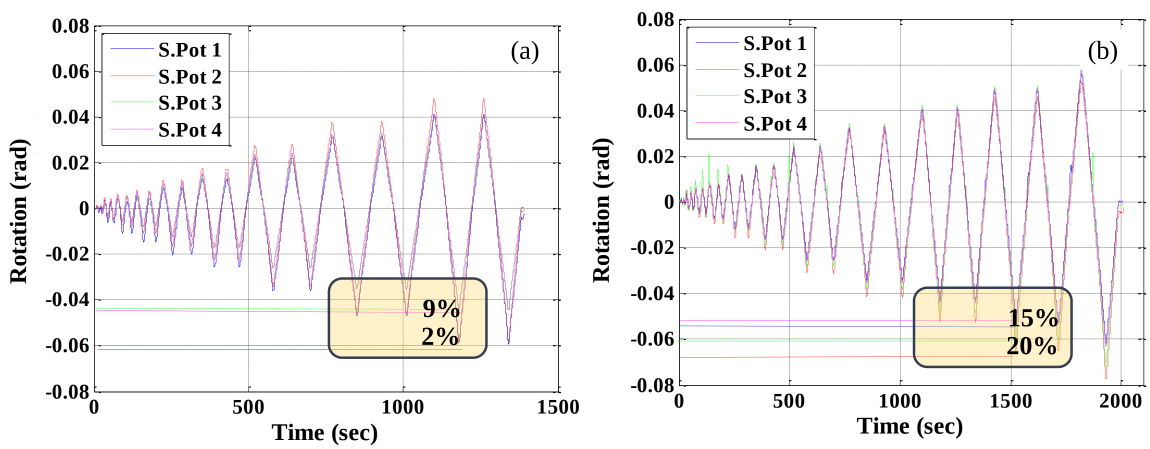

Figure 3.10. Average differences between the rotation measurements of the four rotary (string) potentiometers for $S03_{phase1}$ and $S06_{phase1}$ during the 10% drift tests.

As shown in Figure 3.11(b), for $S03_{phase1}$ as an example, the rotation measured form the linear potentiometers was 10-15% larger than that measured from the rotary (string) potentiometer located at 5 1/4 inch above the column base for the drift levels up to 4% drift level and approximately 20% larger at 5-6 % drift levels.

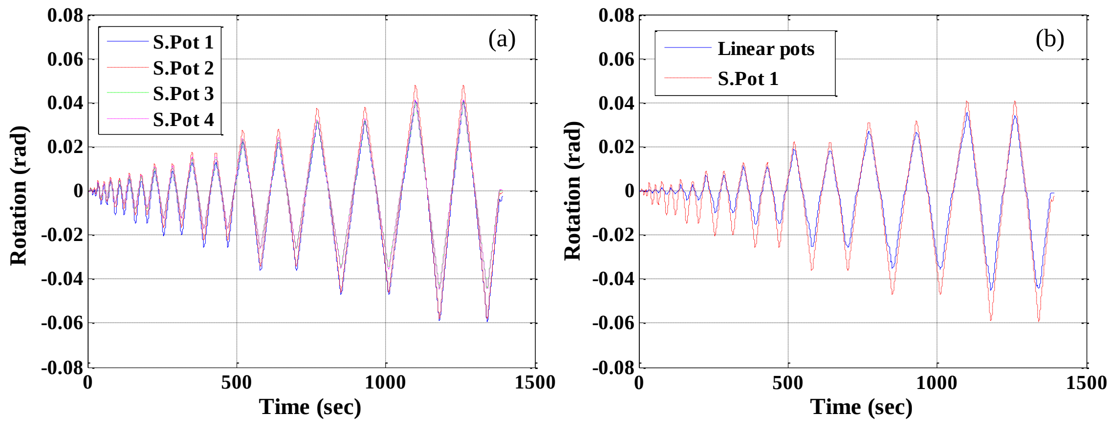

Figure 3.11. Calculation of the rotation for $S03_{phase1}$: (a) from the rotary (string) potentiometers measuring the in-plane displacement, and (b) from the linear potentiometers measuring the uplift compared to one of the rotary (string) potentiometer.

It was observed that the rotations obtained from different sensors using the first approach differed as much as 25%. Similarly, the rotations obtained according to the second approach differed from those measured based on the first approach by 8–17%. These two rotation definitions did not provide consistent results due to bending of the column stubs and base-plate, which depend on various parameters such as the plate thickness, and the number and diameter of the anchor rods. For this reason a third approach was adopted to develop a rotation definition which is less influenced by local deformations of the components and more representative of the global behavior, thereby, more applicable for use in the frame analysis.

In this approach, the force–displacement measurements at the top of the column stubs were used. A finite element model of each column stub was created using beam-column elements based on the Euler–Bernoulli formulation and a rotational spring was placed at the base [see Figure 3.12]. The frame analysis software ZEUS NL (Elnashai et al., 2010) was used for this purpose. Elastic properties were assigned to the tapered column sections to capture the deformations of the columns and an inelastic spring with a piecewise-linear moment–rotation envelope with four branches, shown in Figure 3.13, was used at the base to capture the connection behavior. As such, all the inelasticity at the column bases is captured by the rotational spring. The moment–rotation envelope of the rotational spring in push and pull directions was adjusted using an optimization procedure until a best fit was obtained to the measured force–displacement response. The force–displacement envelopes from the third cyclic tests conducted up to the failure of the specimens were used. The measured force–drift and the calculated moment–rotation envelopes are presented in Section 3.8.

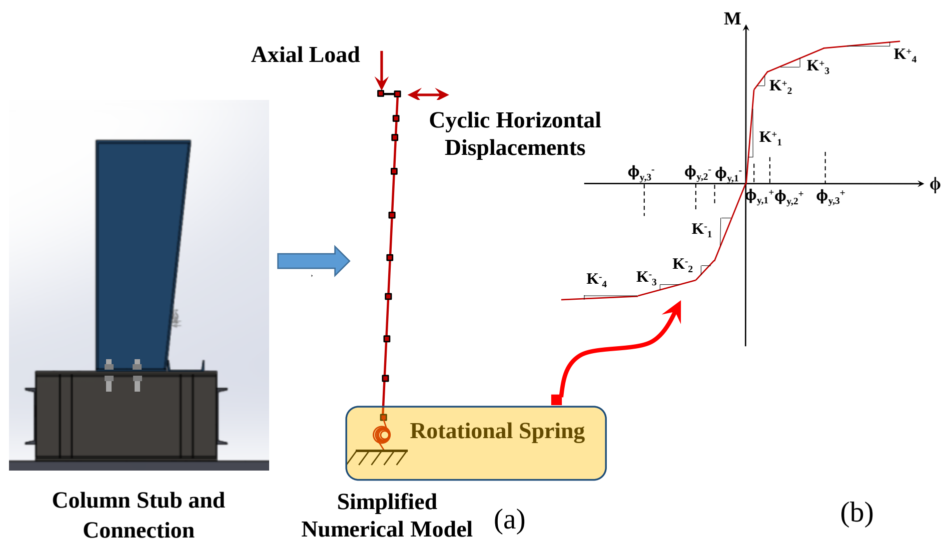

Figure 3.12. Numerical modeling for the rotation calculation: (a) analytical model, and (b) moment-rotation envelope with four branches.

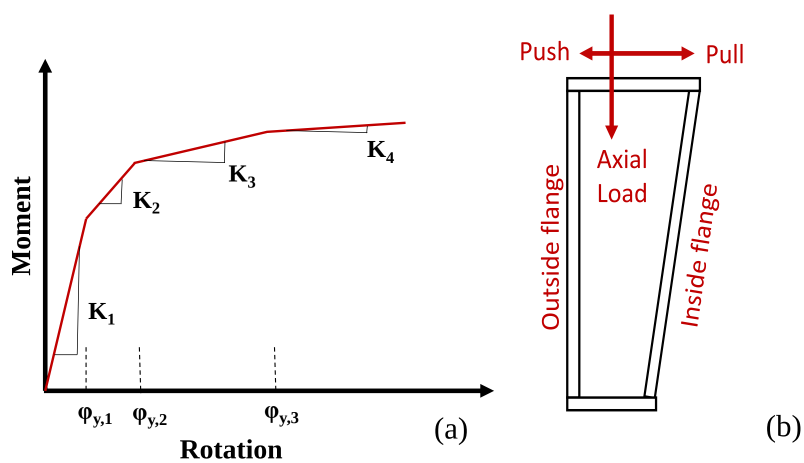

Figure 3.13. (a) Piece-wise linear approximation of the moment-rotation envelope curves, (b) illustration of the push and pull direction.

3.6.2. First- and second-order moments at the base

A schematic of the deformed configuration of the test specimens is shown in Figure 3.14. The first order moments were calculated by multiplying the force measured from the actuator load cell with the distance from the concrete foundation to the location of lateral load. The second-order moments created from the test setup were calculated and added to the first-order moments for the accuracy of the results. Second-order moments resulting from the weight of the actuator, the small eccentricity of the applied axial load, and that of the applied flexural load were separately calculated and summed. The calculations indicated that the second-order moments were approximately less than 10% of the total moment at 7% drift level and lower (higher) for lower (higher) drift levels. The second-order effects were not taken into consideration in the first phase of the experimental program.

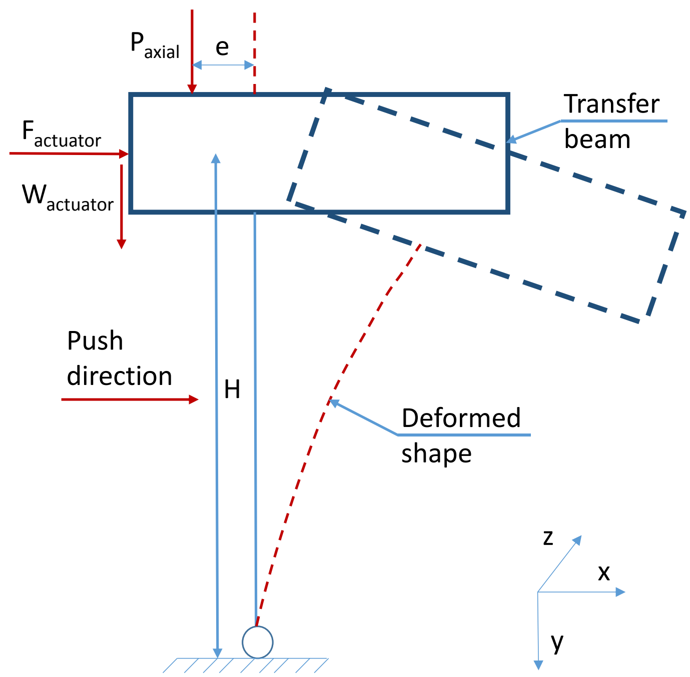

Figure 3.14. Deformed configuration of the test specimens for second-order moment calculations.

3.6.3. Lateral and rotational stiffness

The lateral stiffness in the push (K_{lat}^{+}) and pull (K_{lat}^{-}) directions was calculated at 0.2% drift level which was determined from the 1% drift tests with the axial compressive load applied. Specifically, the average slope of the chords connecting the origin with the two peaks in each of the push and pull directions was found [see Figure 3.15]. The lateral force measurement was obtained from the load cell mounted on the actuator and the drift (displacement) measurement was taken from the actuator linear variable differential transformer (LVDT), which is a displacement sensor. According to AISC Design Guide 3 (Fisher and West, 2004) and the AISC Steel Construction Manual (AISC, 2010), the serviceability design limit for frame lateral displacement is specified as H/500 (corresponding to 0.2% drift), where H is the frame height. The intent of this serviceability limit is to eliminate any damage to structural and nonstructural elements. The rotational stiffness of the base-plate connections was back calculated with the help of elastic analytical models discussed in Section 3.6.1.

It is important to note there that the lateral stiffness of the specimens depends on the height of the column stubs. The higher the columns stubs, the lower the lateral stiffness will be due to increased flexibility. In selecting the height of the columns, attention was given to the aspect ratio such that flexural (rather than shear) response would be observed similar to what would be expected for the gabled frames. Other than that, the column stubs were made as short as possible for the sake of logistics of specimen fabrication and testing. On the other hand, the rotational stiffness and moment capacity are expected to be invariant to the column height. Therefore, the lateral stiffness should be taken only as a comparative measure between the specimens tested here while the rotational stiffness may be used in absolute values for an identical base-plate connection configuration.

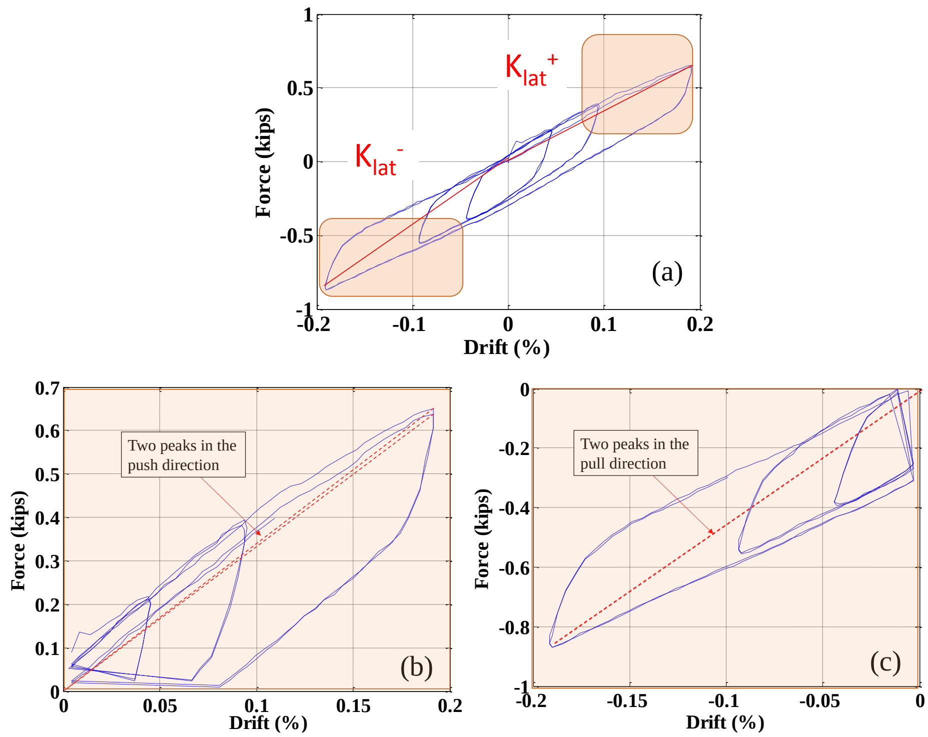

Figure 3.15. (a) Lateral stiffness calculation in push (K_{lat}^{+}) and pull (K_{lat}^{-}) directions for the 100% axial load level test for $S01_{phase1}$, (b) chords to the three peaks in push direction, (c) chords to the three peaks in the pull direction.

3.6.4. Strength and ductility

Strength degradation was not observed for the specimens of this experimental program up to drift levels of 6%, i.e., the column stubs showed a stable load carrying capacity with increasing rotation, unless anchor rod rupture took place (e.g., $S02_{phase1}$). The moment capacity was calculated as the peak moment and the ductility was not evaluated in this phase of the experimental program.

3.7. Elastic Behavior of the Connections

The lateral stiffness was calculated at a drift level of 0.2% from the elastic tests with compressive axial load as explained in Section 3.6.3. The force-drift relationships for all the specimens is shown in Figure 3.16. The lateral and rotational stiffness of the specimens calculated from the elastic tests under 100% axial load are provided in Table 3.5. As a result of the asymmetrical configuration of the base-plate connections, the push-to-pull lateral stiffness ratio varied from 0.7 to 1.4 while the push-to-pull rotational stiffness varied from 0.7 to 2.4.

$S07_{phase1}$ showed the highest rotational stiffness in the push direction. This could be caused by a combination of factors including the relatively thick base-plate with a shorter setback distance and relatively thick outside flange. On the other side, $S01_{phase1}$ showed the highest rotational stiffness in the pull direction. This behavior resulted from the fact that $S01_{phase1}$, similarly to $S07_{phase1}$, had relatively thick base-plate and inside flange thickness. It is noteworthy that both $S01_{phase1}$ and $S07_{phase1}$ had a higher taper angle compared to other specimens and they had a symmetrical anchor rod configurations with a lower base-plate depth resulting in smaller setback distances. On the other hand, $S05_{phase1}$ which had the thinnest base-plate (3/8 inch) was characterized by the lowest rotational stiffness (3301 kips-ft/rad in push and 5030 kips-ft/rad in pull direction) in both push and pull directions. $S05_{phase1}$ had the thinnest base-plate, web, and flanges, and it was the only non-web-tapered specimen. $S02_{phase1}$, $S05_{phase1}$ and $S06_{phase1}$ also showed a small difference between the positive and negative stiffness values (average 18% difference).

The presence of a compressive force increased elastic stiffness of the base-plate connections stiffness considerably. As shown in Figure 3.17, the stiffness increased in both loading directions considerably when the compressive axial load was applied. The lateral and rotational stiffness of the specimens calculated from the elastic tests at 0.2% drift level as explained in Section 3.6.3. Their calculated values from the 0% and 100% compressive axial load tests are provided in Table 3.6 and Table 3.7 respectively. It was calculated that the compressive axial load increased the lateral stiffness up to 46% and the rotational stiffness up to 51.5%. As a result of the asymmetrical configuration of the base-plate connections, the push-to-pull lateral stiffness ratio varied from 0.4 to 1.5 while the push-to-pull rotational stiffness varied from 0.5 to 2.6.

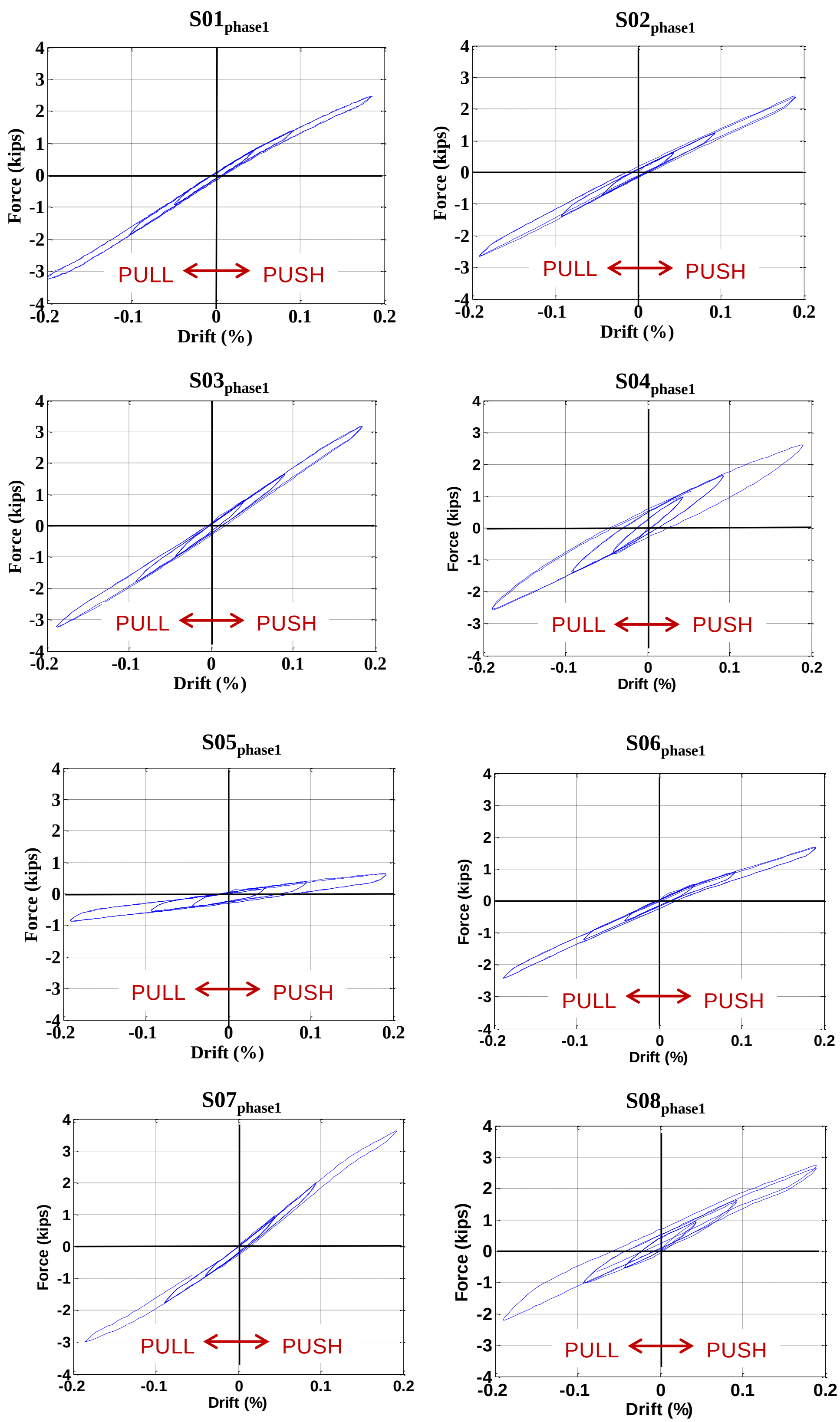

Figure 3.16. Force (kips)-drift (%) curves up to 0.2% drift level with compressive axial load.

Table 3.5. Elastic Lateral (K_{lat}) Calculated from the Elastic Tests under Axial Compressive Load and Rotational (K_{rot}) Stiffness Calculated as Explained in Section 3.6.3.

Specimen ID	K_{lat}^{+} (kips/in)	K_{lat}^{-} (kips/in)	K_{lat}^{+}/K_{lat}^{-}	K_{rot}^{+} (kips-ft/rad)	K_{rot}^{-} (kips-ft/rad)	K_{rot}^{+}/K_{rot}^{-}
$S01_{phase1}$	18.9	22.6	0.8	23206	24685	0.9
$S02_{phase1}$	18.1	19.8	0.9	13864	14921	0.9
$S03_{phase1}$	24.5	24.5	1.0	32505	17880	1.8
$S04_{phase1}$	19.3	13.5	1.4	13991	8834	1.6
$S05_{phase1}$	4.8	6.5	0.7	3301	5030	0.7
$S06_{phase1}$	12.6	18.2	0.7	9806	13568	0.7
$S07_{phase1}$	25.3	17.8	1.4	29715	11370	2.6
$S08_{phase1}$	20.4	16.2	1.3	13907	7735	1.8

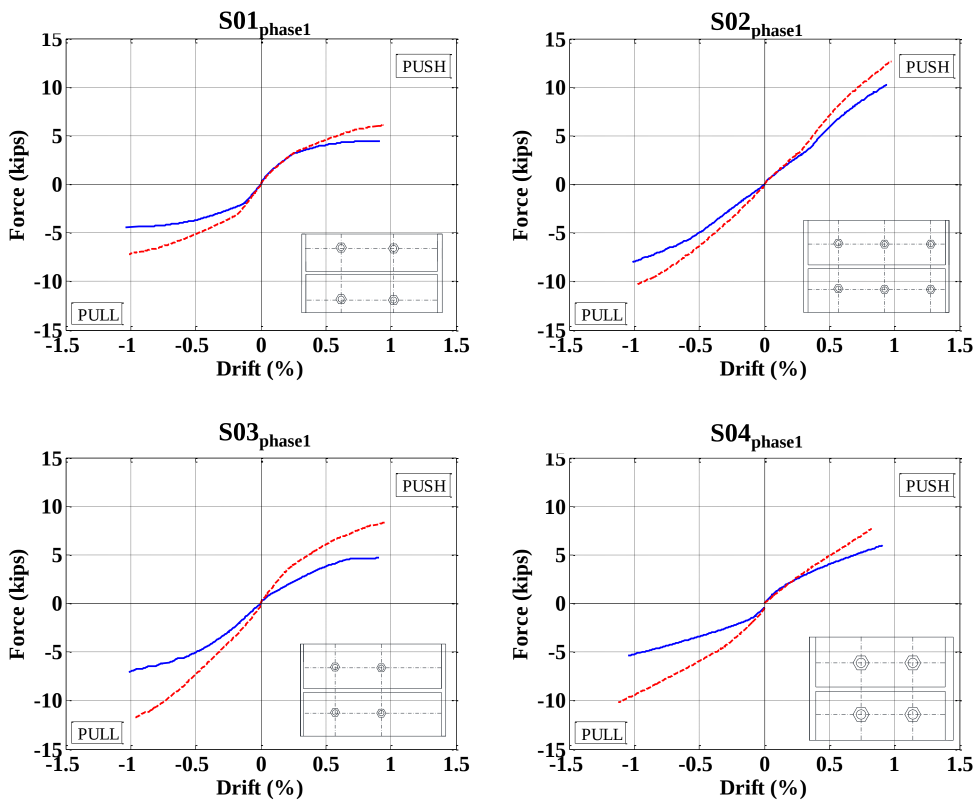

Figure 3.17. Force (kips)-drift (%) envelopes without (solid line) and with (dashed line) compressive load for all the specimens.

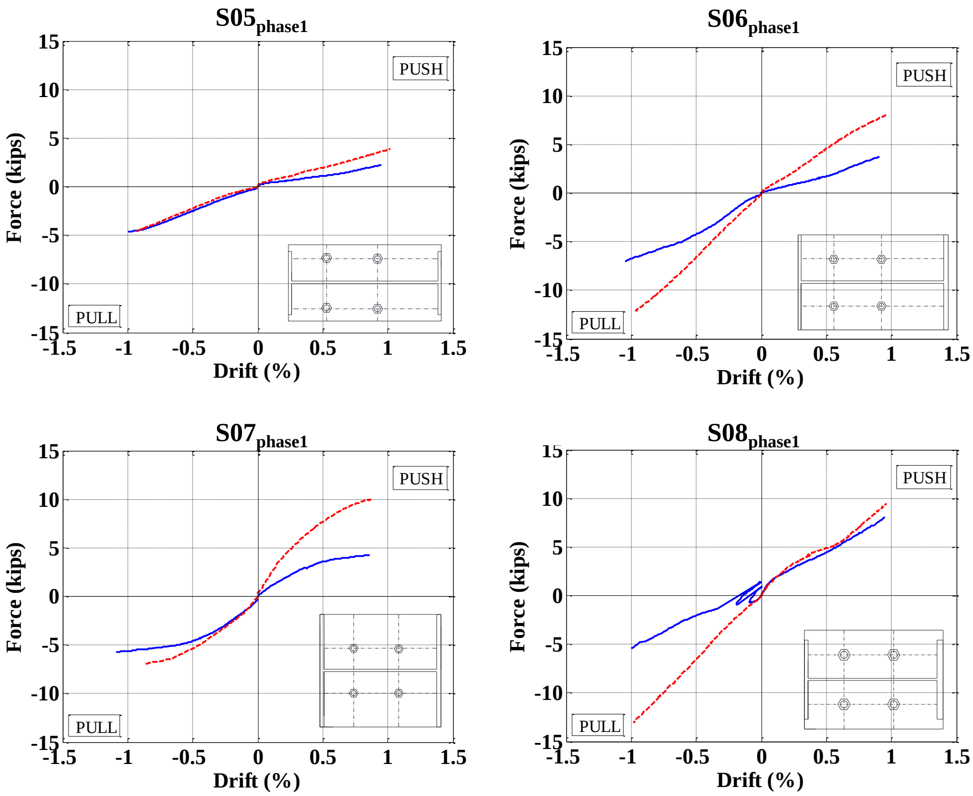

Figure 3.17. Force (kips)-drift (%) envelopes without (solid line) and with (dashed line) compressive load for all the specimens.

Table 3.6. Lateral Stiffness with and without Applied Compressive Load.

	Without axial load				With axial load				
Specimen ID	K_{lat}^{+} (kips/in)[a]	K_{lat}^{-} (kips/in)[b]	K_{aver}	K_{lat}^{+}/K_{lat}^{-}	K_{lat}^{+} (kips/in)[a]	K_{lat}^{-} (kips/in)[b]	K_{aver}	K_{lat}^{+}/K_{lat}^{-}	Influence of axial load on average stiffness (%)
$S01_{phase1}$	18.8	16.4	17.6	1.2	18.9	22.6	20.8	0.8	15.1
$S02_{phase1}$	15.1	13.6	14.4	1.1	18.1	19.8	19.0	0.9	24.3
$S03_{phase1}$	12.3	16.2	14.3	0.8	24.5	24.5	24.5	1.0	41.8
$S04_{phase1}$	13.7	11.9	12.8	1.2	19.3	13.5	16.4	1.4	21.8
$S05_{phase1}$	4.1	6.6	5.3	0.6	4.8	6.5	5.7	0.7	6.0
$S06_{phase1}$	4.8	12.4	8.6	0.4	12.6	18.2	15.4	0.7	44.0
$S07_{phase1}$	12.5	16.6	14.6	0.8	25.3	17.8	21.6	1.4	32.5
$S08_{phase1}$	11.9	7.8	9.9	1.5	20.4	16.2	18.3	1.3	46.0

[a]Secant lateral stiffness in push (positive) direction at 0.2% drift
[b]Secant lateral stiffness in pull (negative) direction at 0.2% drift

Table 3.7. Rotational Stiffness with and without Applied Compressive Load.

	Without axial load				With axial load				
Specimen ID	K_{rot}^{+} (kips-ft/rad)[a]	K_{rot}^{-} (kips-ft/rad)[b]	K_{aver}	K_{rot}^{+}/K_{rot}^{-}	K_{rot}^{+} (kips-ft/rad)[a]	K_{rot}^{-} (kips-ft/rad)[b]	K_{aver}	K_{rot}^{+}/K_{rot}^{-}	Influence of axial load on average stiffness (%)
$S01_{phase1}$	9707	7743	8725	1.3	23206	24685	23946	0.9	63.6
$S02_{phase1}$	7839	8449	8144	0.9	13864	14921	14393	0.9	43.4
$S03_{phase1}$	8341	7557	7949	1.1	32505	17880	25193	1.8	68.4
$S04_{phase1}$	7201	6029	6615	1.2	13991	8834	11413	1.6	42.0
$S05_{phase1}$	2533	4072	3302	0.6	3301	5030	4166	0.7	20.7
$S06_{phase1}$	3247	6945	5096	0.5	9806	13568	11687	0.7	56.4
$S07_{phase1}$	6976	7540	7258	0.9	29715	11370	20543	2.6	64.7
$S08_{phase1}$	7141	3304	5222	2.2	13907	7735	10821	1.8	51.7

[a]Secant rotational stiffness in push (positive) direction at 0.2% drift
[b]Secant rotational stiffness in pull (negative) direction at 0.2% drift

3.8. Non-Linear Behavior of the Connections

The moment capacity of the connections up to the drift level they were tested is shown in Table 3.8. Strength degradation was not observed and the columns (connections) showed a stable load (moment) carrying capacity with increasing drift (rotation), unless an anchor rod rupture took place ($S02_{phase1}$ and $S06_{phase1}$). The force-drift and moment-rotation curves of all the specimens are shown in Figure 3.18 and Figure 3.19 respectively. The results indicate that the base-plate connections showed significant drift capacity exceeding 6% in the inelastic range. A pinched behavior was observed in the moment-rotation and force-displacement responses, which is attributed to the rocking of the columns. Figure 3.20 shows the force-drift (from optimization) and moment-rotation envelopes (from optimization). The parameters of the multi-linear springs used to model the moment-rotation behavior of the base-plate connections are provided in Table 3.9. These spring models were used for pushover analyses of gabled frames as described in Section 5.1.

The damage to the base-plate connections occurred in the form of anchor rod elongation and rupture, yielding of the flanges and yielding of the base-plate. Based on visual observations, no yielding of the web was observed for any of the configurations. The influence of each of these parameters and an overall damage evaluation for each specimen is discussed in more detail in Section 3.10.

Table 3.8. Moment Capacity of the Column Base-Plate Connections.

Specimen ID	**Moment capacity M_m^+ (kips-ft)**	**Moment capacity M_m^- (kips-ft)**	**M_m^+/M_m^-**
$S01_{phase1}$	73.5	122.9	0.6
$S02_{phase1}$	112.7	150.7	0.7
$S03_{phase1}$	97.2	177.5	0.5
$S04_{phase1}$	147.3	183.9	0.8
$S05_{phase1}$	67.6	104.7	0.6
$S06_{phase1}$	117.4	160.1	0.7
$S07_{phase1}$	112.2	91.3	1.2
$S08_{phase1}$	235.5	297.8	0.8

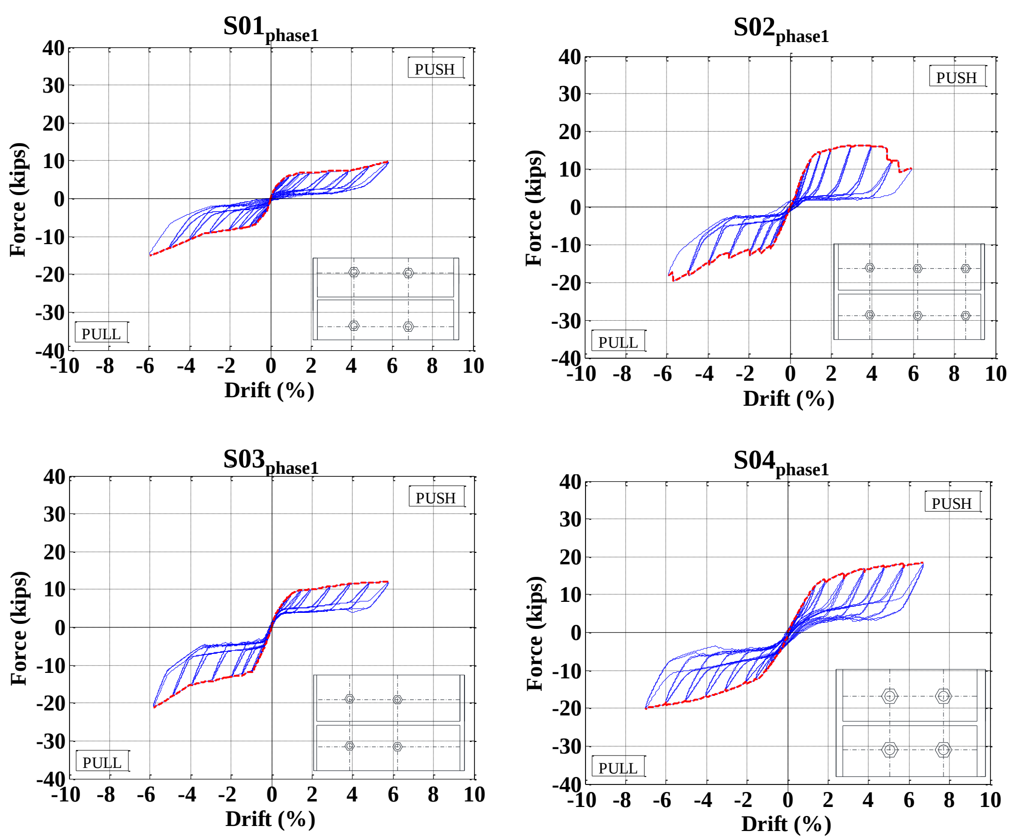

Figure 3.18. Force (kips)-drift (%) curves for the tested specimens.

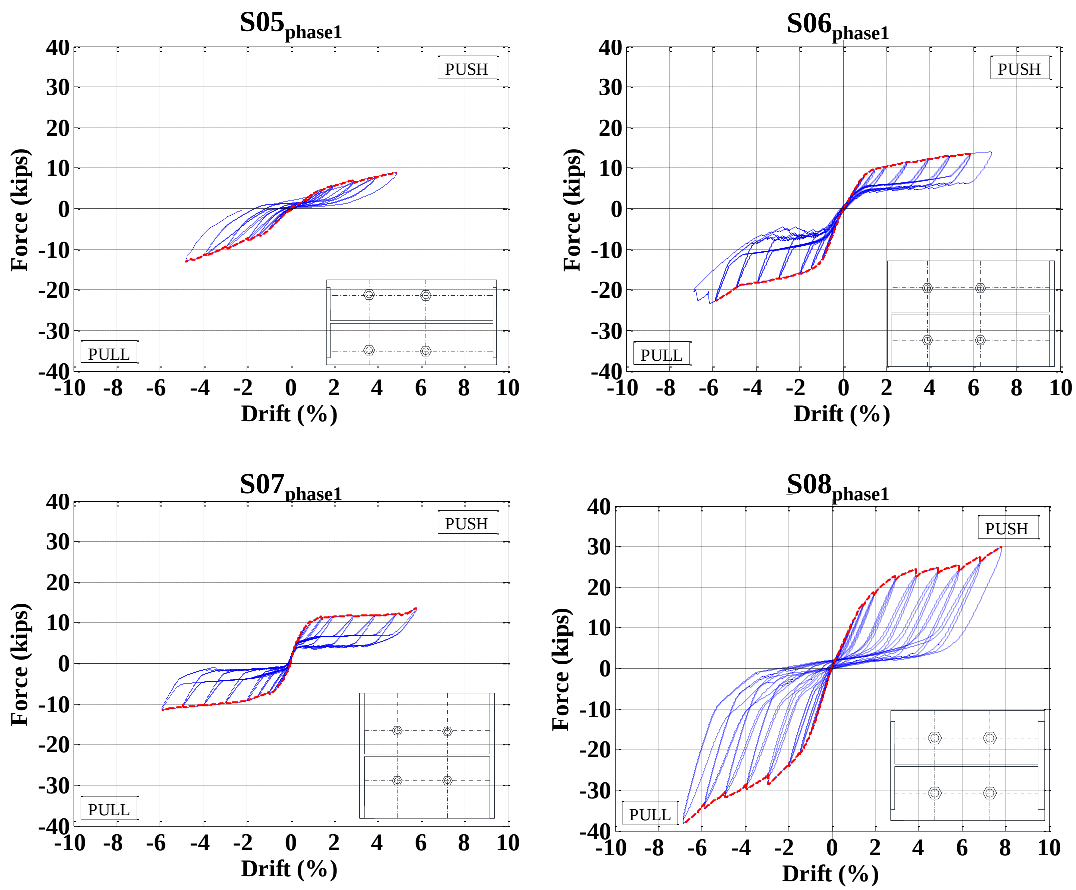

Figure 3.18. (Continued) Force (kips)-drift (%) curves for the tested specimens.

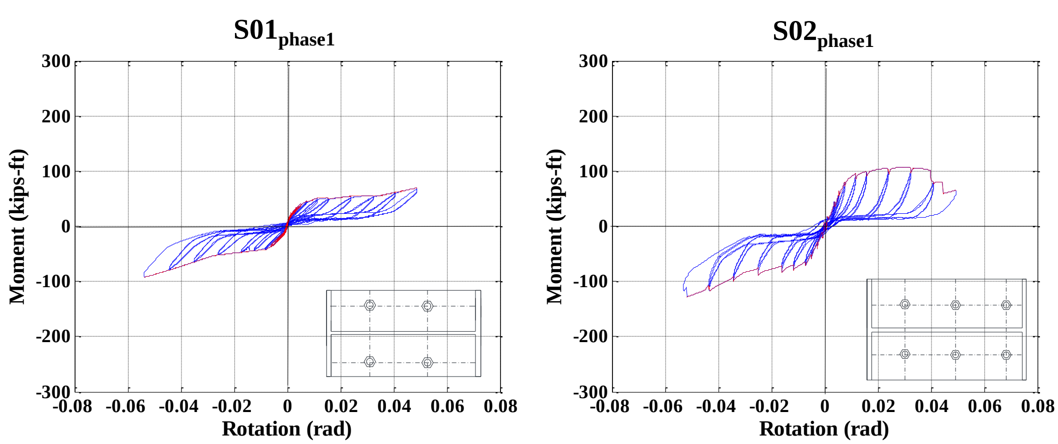

Figure 3.19. Moment (kips-ft)-rotation (degrees) curves for the tested specimens. The rotation was obtained from in-line rotary (string) potentiometer (see Figure 3.4).

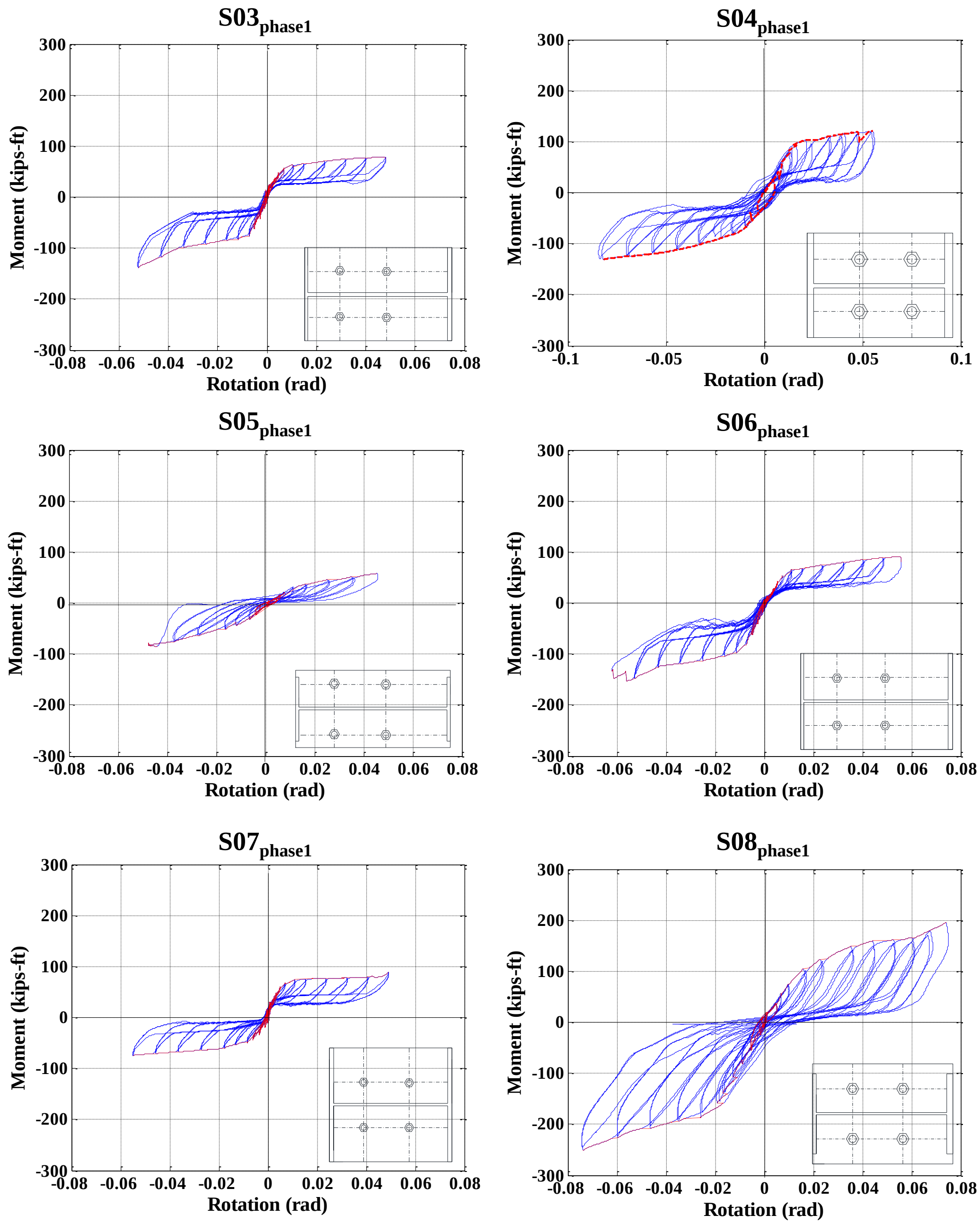

Figure 3.19. (Continued) Moment (kips-ft)-rotation (degrees) curves for the tested specimens. The rotation was obtained from in-line rotary (string) potentiometer (see Figure 3.4).

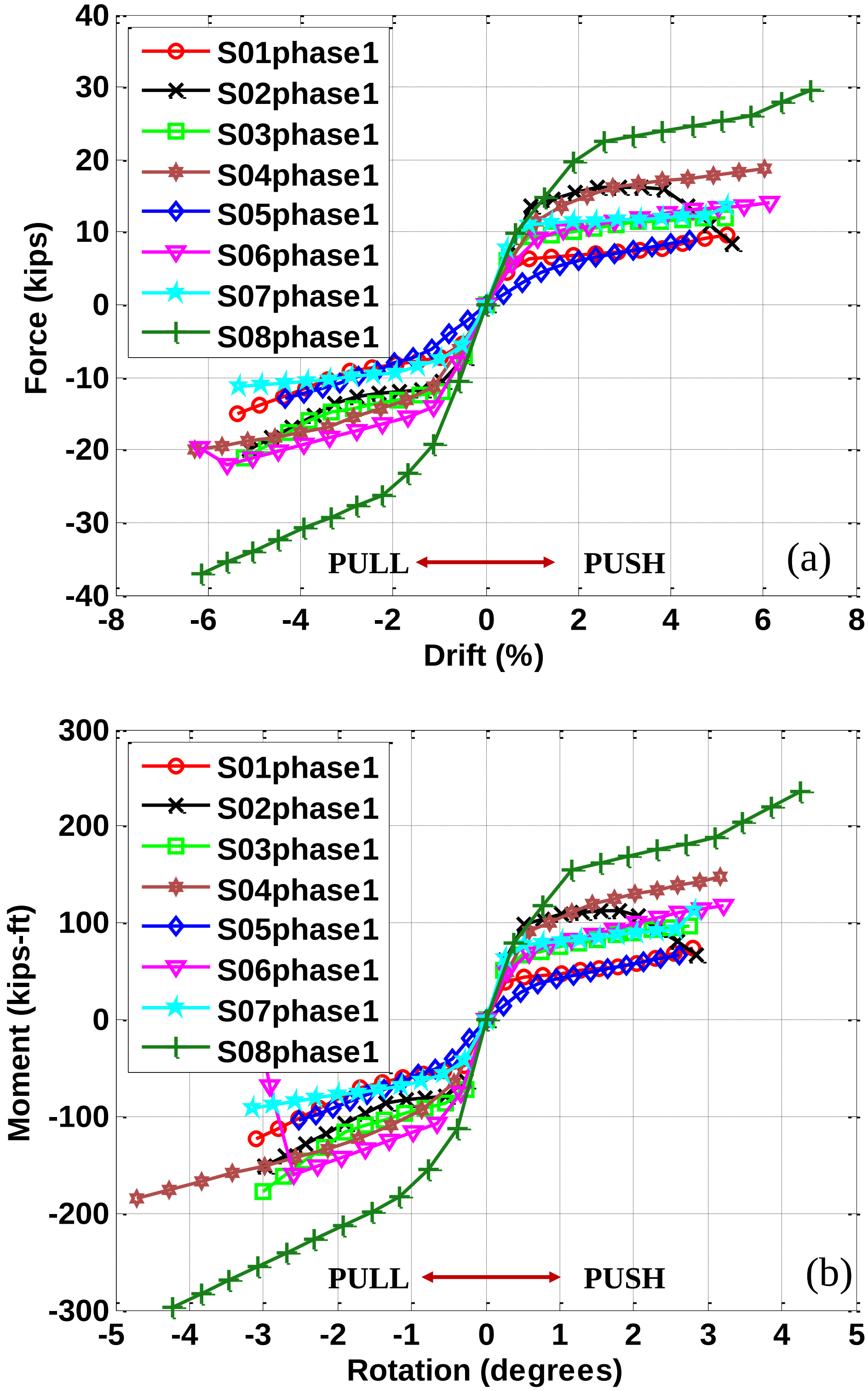

Figure 3.20. (a) Force-drift, and (b) moment-rotation envelope curves for the tested connections.

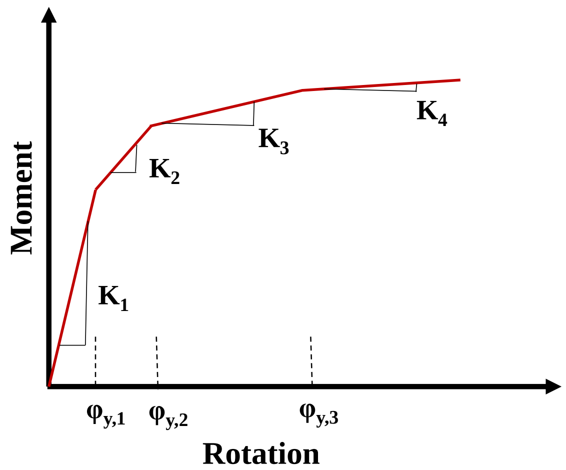

Figure 3.21. Piece-wise linear approximation of the moment-rotation envelope curves.

Table 3.9. Parameters of the Idealized Moment-Rotation Curves According to Figure 3.21.

Specimen ID	K_1^+ **(kips-ft/rad)**	$\varphi_{y,1}^+$ **(rad)**	K_2^+ **(kips-ft/rad)**	$\varphi_{y,2}^+$ **(rad)**	K_3^+ **(kips-ft/rad)**	$\varphi_{y,3}^+$ **(rad)**	K_4^+ **(kips-ft/rad)**	K_1^- **(kips-ft/rad)**	$\varphi_{y,1}^-$ **(rad)**	K_2^- **(kips-ft/rad)**	$\varphi_{y,2}^-$ **(rad)**	K_3^- **(kips-ft/rad)**	$\varphi_{y,3}^-$ **(rad)**	K_4^- **(kips-ft/rad)**
$S01_{phase1}$	23206	0.0010	4988	0.0051	452	0.0344	1217	24685	-0.0011	5410	-0.0050	795	-0.0280	2147
$S02_{phase1}$	13864	0.0069	1205	0.0201	115	0.0342	-3043	14921	-0.0004	3111	-0.0098	364	-0.0229	2278
$S03_{phase1}$	32505	0.0009	6171	0.0066	968	0.0309	537	17880	-0.0016	13780	-0.0054	1209	-0.0327	3242
$S04_{phase1}$	13991	0.0008	8961	0.0097	1864	0.0260	888	8834	-0.0082	4903	-0.0111	1915	-0.0335	1116
$S05_{phase1}$	3301	0.0100	1331	0.0141	1234	0.0201	858	5030	-0.0090	1716	-0.0173	2109	-0.0194	1661
$S06_{phase1}$	9806	0.0058	2781	0.0119	1082	0.0465	647	13568	-0.0070	3673	-0.0097	1568	-0.0466	-22783
$S07_{phase1}$	29715	0.0015	6340	0.0064	473	0.0465	6721	11370	-0.0029	4692	-0.0066	1543	-0.0168	659
$S08_{phase1}$	13907	0.0050	5833	0.0197	985	0.0542	2342	7735	-0.0001	16781	-0.0079	4151	-0.0210	2113

3.9. Repeatability of the Tests

The 10% drift test for $S03_{phase1}$ was repeated to check the repeatability of the test results. The failure of the specimen was mainly characterized by the anchor rod yielding. The same anchor rods were used in the repetition after tightening of the loosened anchor rods after the first test. It is seen in Figure 3.22 that the results were identical from both tests until anchor rod rupture was observed in the repetition due to cycling of the anchor rods to large strain reversals.

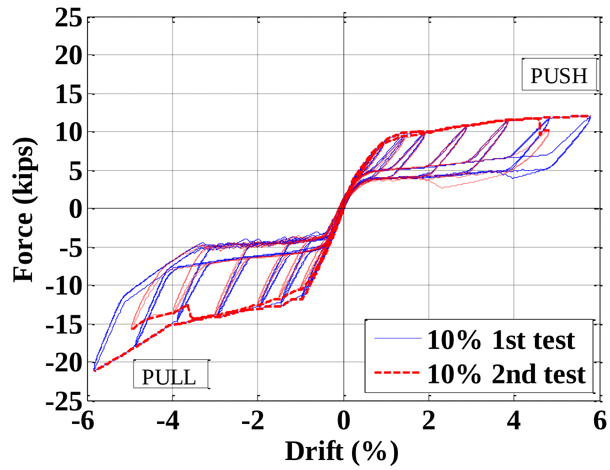

Figure 3.22. Force (kips)-drift (%) curves, initial (solid line) and repeated test (dashed line).

3.10. Semi-Qualitative Damage Evaluation of the Specimens

The failure modes observed during the tests were yielding of the inside flange, yielding of the outside flange, yielding of the base-plate, and yielding (and in some cases rupture) of the anchor rods. Accordingly, the specimens were grouped into three distinct categories based on the observed damage (as shown in Table 3.10).

- Specimens for which the energy dissipation was mainly achieved through the yielding of the flanges and the base-plate while only slight elongation of the anchor rods was observed ($S04_{phase1}$ and $S05_{phase1}$).

- Specimens for which the energy dissipation was achieved through combined yielding of the flanges, base-plate and the anchor rods ($S01_{phase1}$, $S03_{phase1}$ and $S08_{phase1}$).
- Specimens for which the flanges and base-plate remained linear elastic while anchor rods experienced excessive elongation and rupture in some cases ($S02_{phase1}$, $S06_{phase1}$ and $S07_{phase1}$).

Table 3.10 Grouping of the Specimens According to the Observed Damage.*

Damage Category	Specimen	Outside F.	Inside F.	Base Plate	Anchor Rods
1	**$S04_{phase1}$**	E	none	S	S
	$S05_{phase1}$	E	E	E	S
2	**$S01_{phase1}$**	S	M	M	M
	$S03_{phase1}$	none	S	none	M
	$S08_{phase1}$	S	M	S	S
3	**$S02_{phase1}$**	none	none	none	E/R
	$S06_{phase1}$	none	none	none	E/R
	$S07_{phase1}$	none	none	none	M

*S=slight, M=moderate, E=excessive, E/R=excessive/rupture

The average strains of the anchor rods are given in Table 3.11. Additional strain measurements for the additional components (flanges and base-plate) taken from the strain gage data are given in the presentation of the damage of each of the specimens.

Table 3.11. Summary of Average Strains in the Anchor Rods (%).

	Strain (%)					
Anchor Rod No	**$S02_{phase1}$**	**$S03_{phase1}$**	**$S04_{phase1}$**	**$S06_{phase1}$**	**$S07_{phase1}$**	**$S08_{phase1}$**
1	14	11.3	13.1	19.8*	12.7	13.6
2	10.5	14.7	13.3	9.8	17.4	10.8
3	19.9*	14.6	10.9	11.1	13	14
4	19.9*	8.2	14.1	27.4*	8.7	12.8
5	16.8					
6	21.1*					

* Anchor rod rupture

** Data for $S01_{phase1}$ and $S05_{phase1}$ were not collected

*** Numbering of anchor rods is shown in Figure 3.23

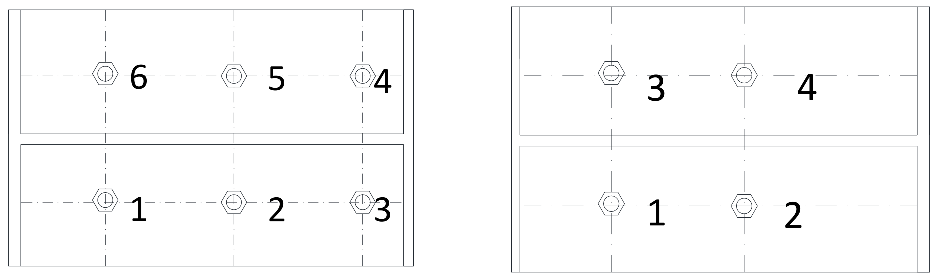

Figure 3.23. Anchor rod numbering refer in Table 3.11.

For the first group of specimens, the energy dissipation was mainly achieved by yielding of the flanges and the base-plate while slight elongation of the anchor rods was observed ($S04_{phase1}$ and $S05_{phase1}$). The base-plate configuration of $S04_{phase1}$ and the moment-rotation response of the specimen the inelastic area is shown in Figure 3.24(a) and Figure 3.24(b) respectively. $S04_{phase1}$ experienced excessive yielding of its outside flange reaching up to 15 inch height from the column base [see Figure 3.24(c)] while no yielding was measured from the strain gages or observed from the white wash in the inside flange [see Figure 3.24(d)]. Despite the relatively thick outside flange (1/2 inch) of $S04_{phase1}$ compared to other specimens, excessive yielding could be caused by the comparatively small deformations of the 1.0 inch diameter anchor rods. Particularly, the average strain experienced by the anchor roads was estimated as 14%, which was small in comparison to the anchor rods strains measured for the other specimens (see Table 3.11). The base-plate configuration of $S05_{phase1}$ and the moment-rotation response of the specimen the inelastic area is shown in Figure 3.25(a) and Figure 3.25(b), respectively. $S05_{phase1}$ experienced the most damage among all the specimens. No yielding was observed in the outside flange while significant yielding was observed in the inside flange [see Figure 3.25(c)]. Moreover, substantial uplift of the base-plate and permanent deformation was seen [see Figure 3.25(d)]. The relatively thin base-plate (3/8 inch) suffered substantial permanent deformation after the 7% drift loading cycle (corresponds to 0.037 rad rotation in push direction and 0.031 rad rotation in the pull direction). $S05_{phase1}$ was the only specimen with a constant cross-section (no taper). The combination of the low flange thicknesses (1/4 inch), web thickness (1/8 inch) and base-plate thickness (3/8 inch) with the asymmetric location of the anchor rods played a significant role in the behavior of the specimen and its moment capacity which was the lowest of all specimens.

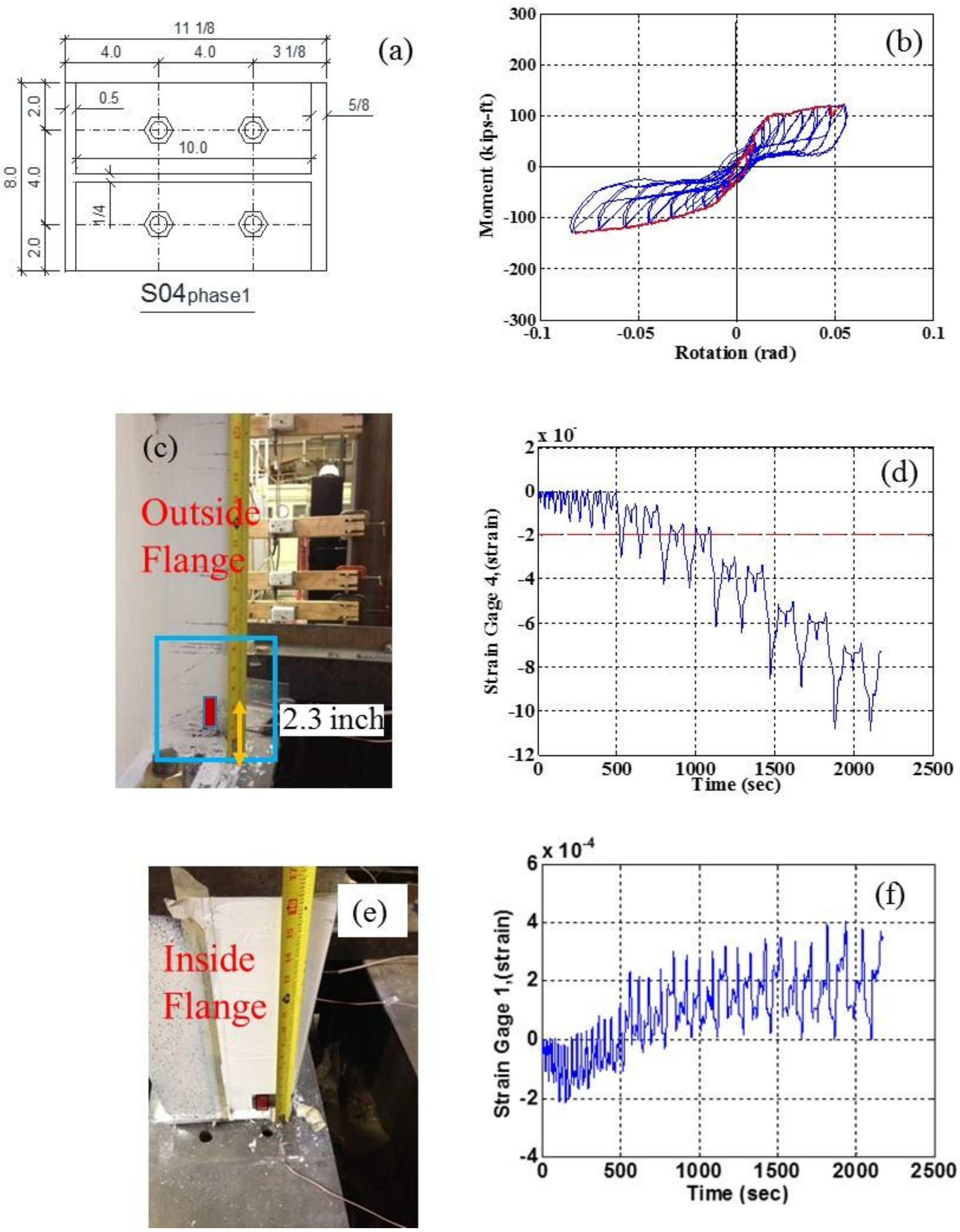

Figure 3.24. (a) $S04_{phase1}$ base-plate configuration, (b) moment-rotation response, (c) outside flange yielding up to 15 inch, (d) strain gage results, (e) no inside flange yielding and (f) strain gage results indicating no yielding in the inside flange.

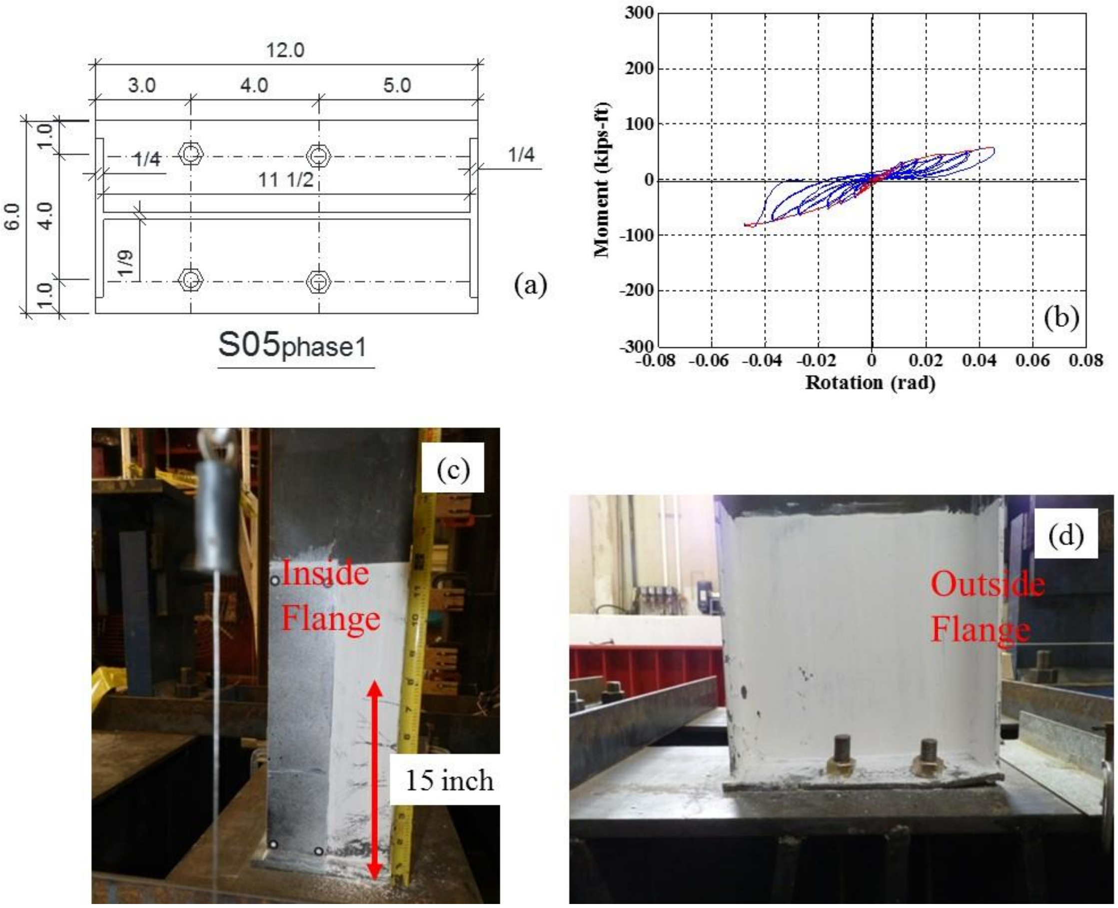

Figure 3.25. (a) $S05_{phase1}$ base-plate configuration, (b) moment-rotation response, (c) yielding of the inside flange, and (d) yielding and deformation of the base-plate.

The energy dissipation for the second group of specimens was achieved by combined damage to the flanges, base-plate and the anchor rods ($S01_{phase1}$, $S03_{phase1}$ and $S08_{phase1}$). The base-plate configuration of $S01_{phase1}$ and the moment-rotation response is shown in Figure 3.26(a) and Figure 3.26(b), respectively. In the case of $S01_{phase1}$, the outside flange experienced yielding reaching up to 7 inch height from the column base [see Figure 3.26(c)] and the strain gage measurement indicated that the yielding initiated at around 3% drift level (corresponds to 0.023 rad rotation in the push direction and 0.029 rad rotation in the pull direction) [see Figure 3.26(d)]. The base-plate configuration of $S03_{phase1}$ and the moment-rotation response is shown in Figure 3.27(a) and Figure 3.27(b), respectively. In the case of $S03_{phase1}$, the outside flange yielding initiated around 3% drift (corresponds to 0.012 rad rotation) [see Figure 3.27(c)]. Combined with the anchor rod yielding (with an average strain of 14.7%) this constituted the failure mechanism of the base-plate connection. No yielding was observed in the inside flange or the base-plate. The base-plate configuration of $S08_{phase1}$ and the moment-rotation response is shown in Figure 3.28(a) and Figure 3.28(b), respectively. In the case of $S08_{phase1}$, the outside flange at 2 1/2 inch height from the base-plate [see Figure 3.28(c)] initiated to yield at around 3% drift level (corresponds to 0.013 rad rotation) [see Figure 3.28(d)] and around 7% drift level (corresponds to 0.065 rad rotation) at 4 3/4 inch height. The yielding of the inside flange was observed around 2% drift (corresponding to 0.009 rad rotation) at 2 1/2 inch height from the base-plate. An anchor rod strain gage placed in the anchor rod indicated in Figure 3.28(e) indicated initiation of yielding around 3% drift (corresponds to 0.013 rad rotation) [see Figure 3.28(f)]. The yielding of the base-plate was also observed even though $S08_{phase1}$ had the thickest (3/4 inch) base-plate among all the specimens. Yielding and the permanent deformation of the base-plate could be caused by the larger anchor rod diameter (1 1/4 inch) resulting in the highest resistance.

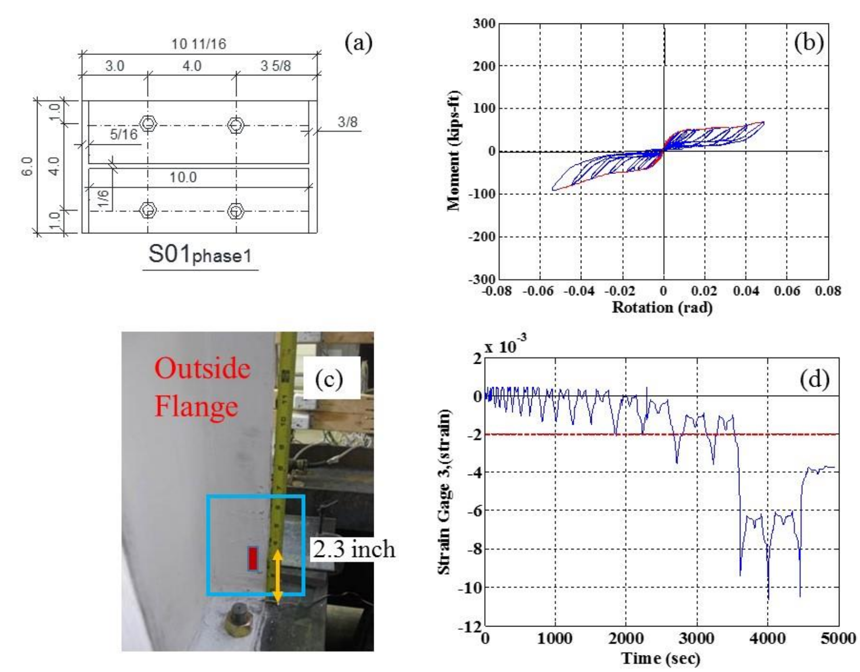

Figure 3.26. (a) $S01_{phase1}$ base-plate configuration, (b) moment-rotation response, (c) indication of yielding up to 7 inch height on the outside flange, and (d) strain gage data indicating yielding in the flange around 3% drift level (0.023 rad).

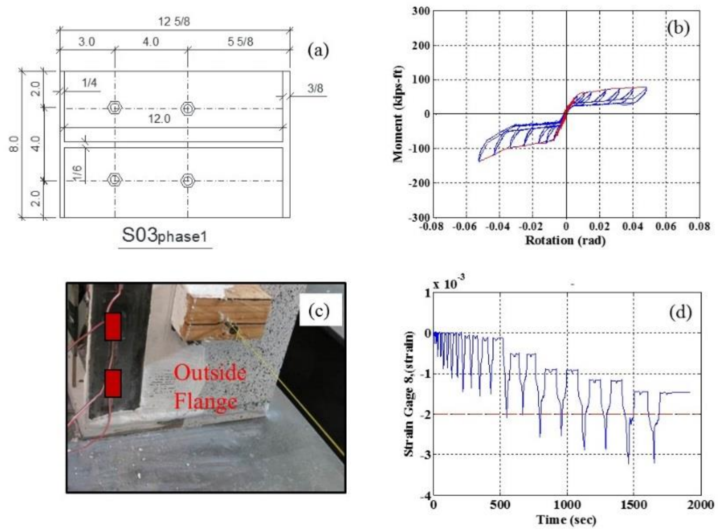

Figure 3.27. (a) $S03_{phase1}$ base-plate configuration, (b) moment-rotation response, and (c) yielding of the outside flange, and (d) strain gage measurement around 3% drift (0.012 rad).

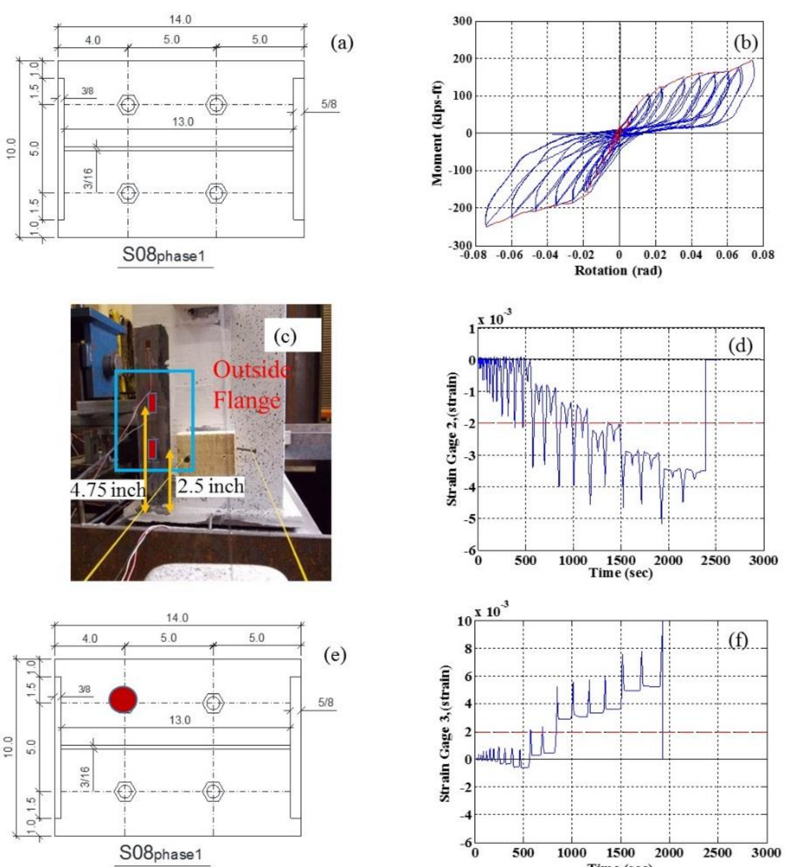

Figure 3.28. (a) $S08_{phase1}$ base-plate configuration, (b) moment-rotation response, (c) strain gages on the outside flange, (d) results from the strain gage, (e) anchor rod with installed strain gage is shown in red, and (f) anchor rod strain gage results.

The failure mechanism for the third group of specimens was characterized by excessive anchor rod elongation and rupture, while, the flanges and the base-plate remained in the elastic range ($S02_{phase1}$, $S06_{phase1}$ and $S07_{phase1}$). The average strains in the anchor rods after the 10% drift target tests are provided in Table 3.11. The anchor rods that ruptured during tests are indicated with red labels for $S02_{phase1}$ and $S06_{phase1}$ in Figure 3.29(e and f) and Figure 3.30(e and f), respectively. The thickness of base-plates for both specimens was 5/8 inch. The base-plate configuration of $S02_{phase1}$ and the moment-rotation response is shown in Figure 3.29(a) and Figure 3.29(b), respectively. $S02_{phase1}$ was the only specimen with 6 anchor rods and the distance from the last set of anchor rods to the inside flange was half of the setback distance (3 inch). Consequently, the forces created in the last set of anchor rods due to uplift was higher than the forces on the other side of the base-plate, and resulted in the rupture of this set of anchor rods [see Figure 3.29(c) and Figure 3.29(d)]. In Figure 3.29(e) the ruptured anchor rods are shown in red along with the anchor rod lengths before and after the test and the average strain in table in Figure 3.29(f).

The base-plate configuration of $S06_{phase1}$ and the moment-rotation response is shown in Figure 3.30(a) and Figure 3.30(b), respectively. The combination of the relatively thick base-plate and the small anchor diameter resulted in higher tensile forces in the first set of anchor rods (setback of 3 inch) and have led to their rupture [see Figure 3.30(c) and Figure 3.30(d)]. This observation was also made in the second phase of the experimental program (S01, S02). Additionally, the applied compressive force (67.4 kips) was significantly higher in comparison with the other specimens, which also contributed to the rupture of the anchor rods due to higher second order effects. In Figure 3.30(e), the ruptured anchor rods are shown in red along with the anchor rod lengths before and after the test and the average strain in table in Figure 3.30(f). No yielding of the flanges was measured from the strain gages placed at 2 1/2 inch height form the base-plate.

The base-plate configuration of $S07_{phase1}$ and the moment-rotation response is shown in Figure 3.31 (a) and Figure 3.31(b), respectively. $S07_{phase1}$, experienced the least damage in the column compared to other specimens [see Figure 3.31(c) and Figure 3.31(d)]. This phenomenon could be explained by the fact that S07$_{phase1}$ had relatively thick flanges and base-plate, and small diameter anchor rods (3/4 inch), which resulted in the concentration of damage in the anchor rods. In this specimen, the measured maximum average strain of the anchor rods was 17.4%.

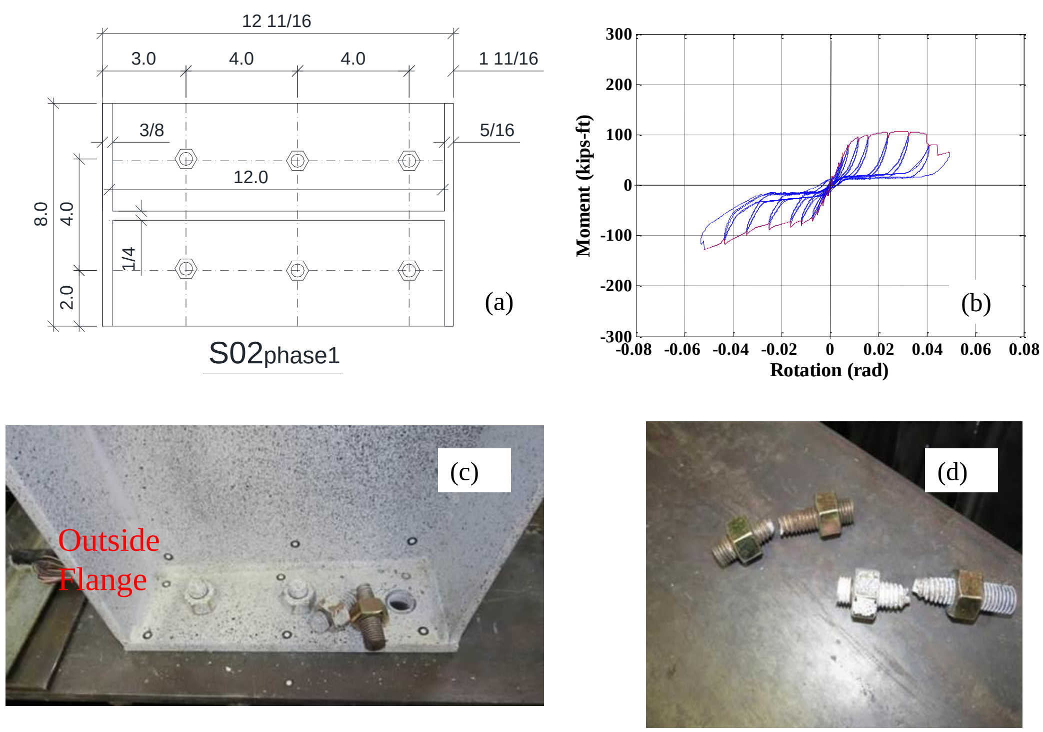

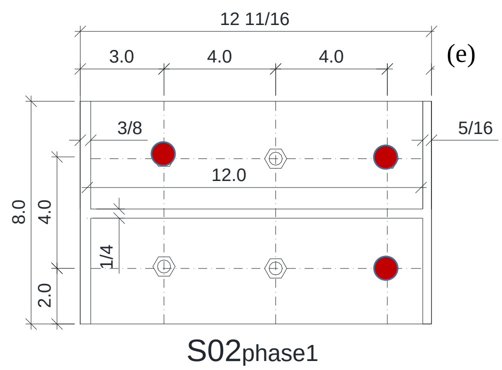

Anchor Rod	Before	After	Elongation (inch)	Average Strain (%)
1	3.99	4.35	0.36	14
2	4.05	4.32	0.27	10.5
3	4.12	4.63	0.51	19.9
4	3.87	4.38	0.51	19.9
5	3.9	4.33	0.43	16.8
6	4.05	4.69	0.64	21.1

(f)

Figure 3.29. (a) S02$_{phase1}$ base-plate configuration, (b) moment-rotation response, (c) ruptured anchor rods after the test, (d) ruptured anchor rods, (e) anchor rods ruptured indicated in red, and (f) anchor rod lengths before and after the test and the average strain.

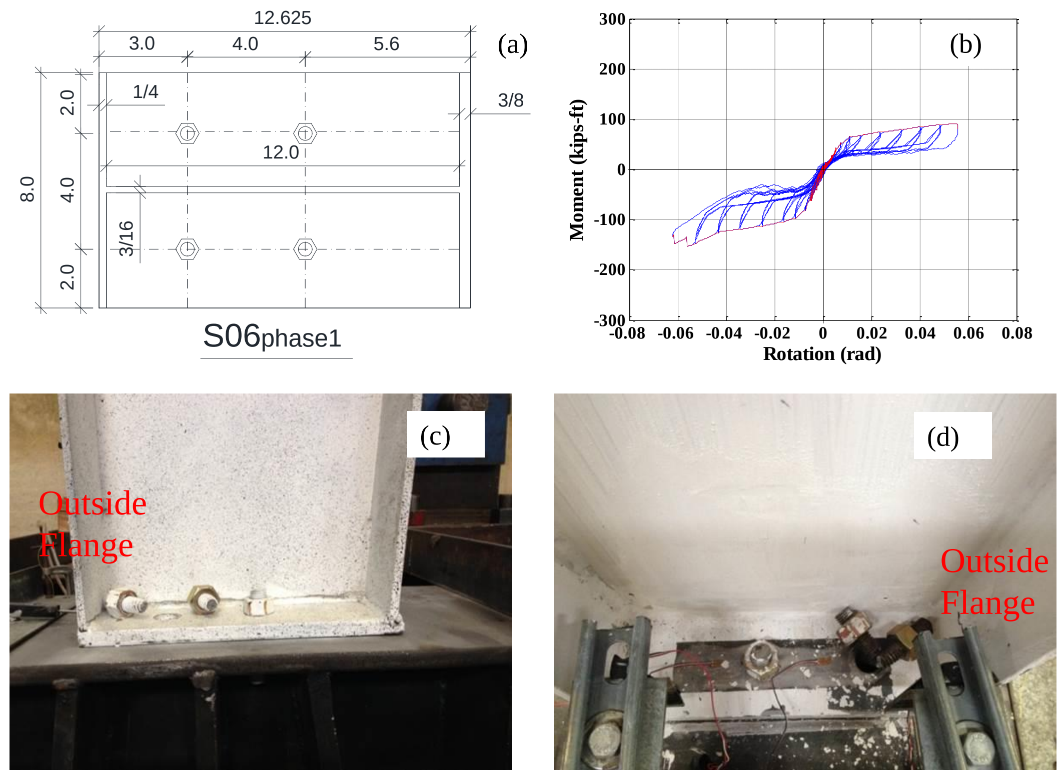

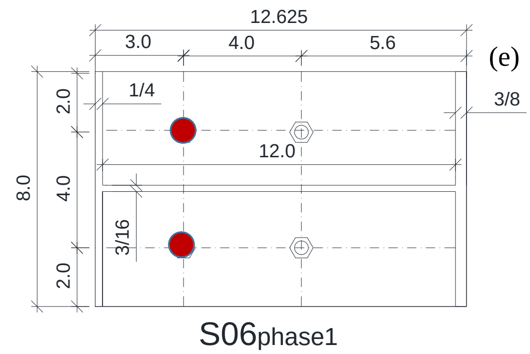

(f)

Anchor Rod	Before	After	Elongation (inch)	Average Strain (%)
1	3.99	4.498	0.51	19.8
2	4.001	4.251	0.25	9.8
3	4.002	4.286	0.28	11.1
4	3.936	4.638	0.7	27.4

Figure 3.30. (a) $S06_{phase1}$ base-plate configuration, (b) moment-rotation response, (c), (d) base-plate with ruptured anchor rods after the test, (e) the ruptured anchor rods are shown in red, and (f) anchor rod lengths before and after the test and the average strain.

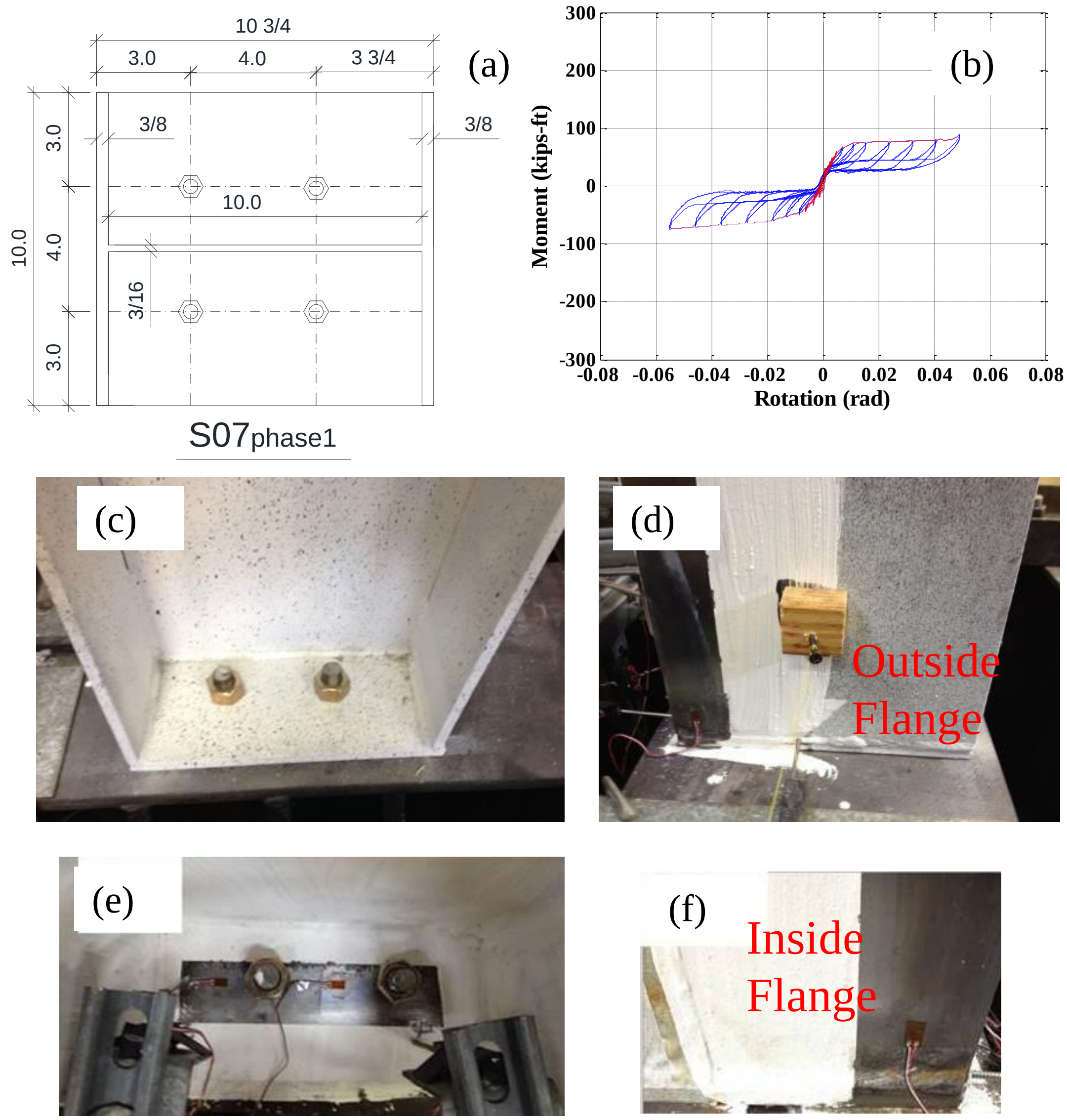

Figure 3.31. (a) $S07_{phase1}$ base-plate configuration, (b) moment-rotation response, (c), (d), (e) and (f) no yielding was observed in the flanges and the base-plate.

This first phase of the experiments warranted a second phase of experiments of column base-plate connections supported on concrete foundations which would give insights of the behavior of the connections under more realistic conditions. Further, in this second phase of testing, a systematic approach was taken to isolate the effect of key parameters such as anchor rod diameter, base-plate thickness, and number or anchor rods, among others, as presented in the next Chapter.

4. EXPERIMENTAL PROGRAM -PHASE 2

4.1. Test Configurations and Test Variables

Eleven full-scale column base-plate connections were tested under combined axial and lateral loads in the second phase of the experimental program. In this second phase, a systematic investigation of the influence of each parameter of the base-plate connection was conducted. Table 4.1 shows the investigated parameters; namely, the foundation material (steel versus reinforced concrete through S01 and $S06_{phase1}$ from the first phase of the experimental program), the pitch (through S01 and S02), the anchor rod diameter (through S01 and S03), the base-plate thickness (through S04 and S05, and S09 and S10), the number of anchor rods (through S07 and S08), and the repeatability (through S08 and S09). The four different tested base-plate connection configurations are compared in Figure 4.1. S11 was initially put in the test matrix and intended to be compared with $S06_{phase1}$ from the first phase of the experimental program. However, it was found that the anchor rods in the concrete foundation moved during casting and the base-plate had to be modified to match the pattern in the foundation. The base-plate was modified to match the new 4 1/2 inch pitch and 5.0 inch gage as opposed to originally intended 4.0 inch pitch and 4.0 inch gage distance just like in $S06_{phase1}$. For this reason S11, became a standalone test and it could not be compared to any other specimen in this parametric investigation.

Table 4.1 Parameters under Investigation.

Specimens*	Parameter under investigation	First specimen	Second specimen
S01-$S06_{phase1}$	Concrete-Steel Foundation	Concrete	Steel
S01-S02	Pitch	4 inch	6 inch
S01-S03	Anchor Rod Diameter	3/4 inch	1.0 inch
S04-S05	Base Plate Thickness	5/8 inch	3/8 inch
S04-S06	Flange Thicknesses	1/4-3/8 inch	1/2-5/8 inch
S07-S08	Number of Anchor Rods	6	8
S08-S09	Repeatability	-	-
S09-S10	Base Plate Thickness	5/8 inch	3/4 inch

*phase1 refers to the corresponding specimen from first phase of the experimental program.

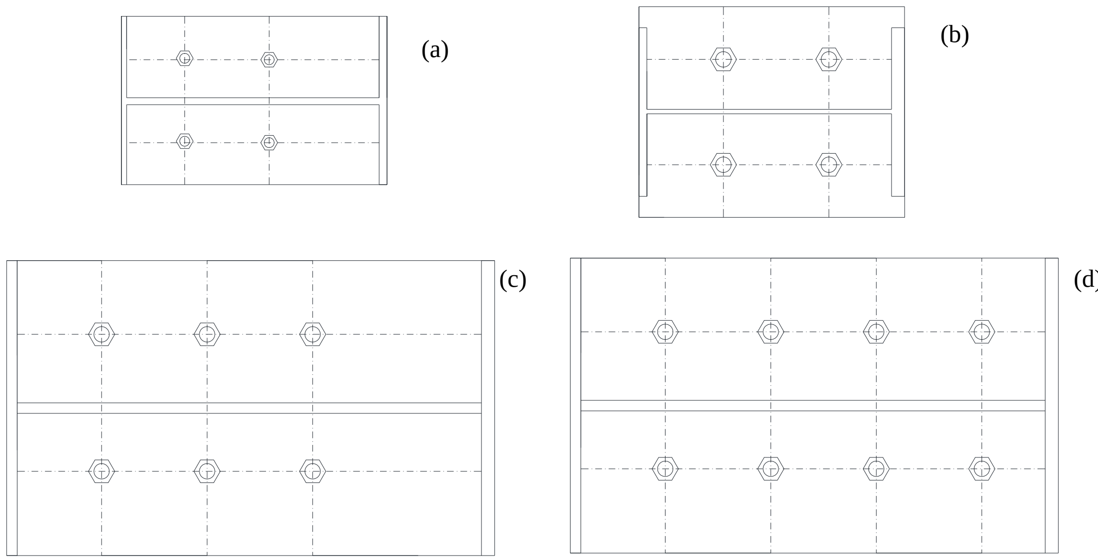

Figure 4.1. Tested base-plate connection configurations (a) S01-S03, S11 (b) S04-S06, (c) S07, (d) S08-S10 (to scale).

The details of the column base-plate connections are presented in Table 4.2 and in Figure 4.2. The specimens were divided in two categories according to their web depth. The first category included specimens with 10 inch and 12 inch web depths (S01-S06 and S11) and the second category included the specimens with 22 inch web depth (S07-S10). The base-plate thickness varied from 3/8 inch to 3/4 inch, while the outside flange and inside flange thicknesses varied from 1/4 inch to 1/2 inch and from 3/8 inch to 5/8 inch, respectively. Three different anchor rod diameters were tested: 3/4 inch, 1 inch and 1 1/4 inch, with varying gages, setbacks, and pitches. S01-S06 and S11 used four anchor rods while S07 used six anchor rods, and S08-S10 used eight anchor rods. The dimensional details of all the connection configurations are provided in Figure 4.3. The dimensional and reinforcement details of the 48 inch × 48 inch × 18 inch concrete foundations are shown in Figure 4.4. Both in transverse and longitudinal direction #6 reinforcement bars at 7 inches were used. The stirrups around the PVC pipes were fabricated using #4 reinforcement bars. The reinforcement ratios for the longitudinal and the transverse directions were 0.0071 while the same for the thickness direction was 0.0027.

Table 4.2 Details of the Tested Base-Plate Connections (refer to Figure 4.2).

Specimen ID	Web Depth	Flange Width	Web Thickness	Outside Flange Thickness	Inside Flange Thickness	Base-Plate Width	Base-Plate Thickness	Anchor Rod Diameter	No. of Anchor Rods	Pitch	Gage	Setback	Setback	Base Plate Depth	Axial load
	d_w	b_f	t_w	t_{fo}	t_{fi}	b_{bp}	t_p	d_b	-	S_1	g	S_0	S	d	
	(inch)	(inch)	(inch)	(inch)	(inch)	(inch)	(inch)	(inch)		(inch)	(inch)	(inch)	(inch)	(inch)	(kips)
S01	12	8	3/16	1/4	3/8	8	5/8	3/4	4	4	4	3	5 5/8	12 5/8	0, 25, 50, 67
S02						8	5/8	3/4	4	6	4	3	3 5/8	12 5/8	0, 25, 50
S03						8	5/8	1	4	4	4	4	4 5/8	12 5/8	0, 25, 50
S04						10	5/8	1 1/4	4	5	5	4	3 5/8	12 5/8	0, 25, 50
S05						10	3/8	1 1/4	4	5	5	4	3 5/8	12 5/8	0, 25, 50
S06				1/2	5/8	10	5/8	1 1/4	4	5	5	4	3 1/8	13 1/8	0, 25, 50
S07	22	14	1/4	1/2	5/8	14	5/8	1 1/4	6	5	5	4	9 1/8	23 1/8	0, 50, 100
S08								1 1/4	8	5	5	4	4 1/8	23 1/8	0, 50, 100
S09								1 1/4	8	5	5	4	4 1/8	23 1/8	0, 50, 100
S10							3/4	1 1/4	8	5	5	4	4 1/8	23 1/8	0, 50, 100
S11	10	10	3/16	3/8	3/8	10	1/2	3/4	4	4 1/2	5	3	3 1/4	10 3/4	0, 25, 50

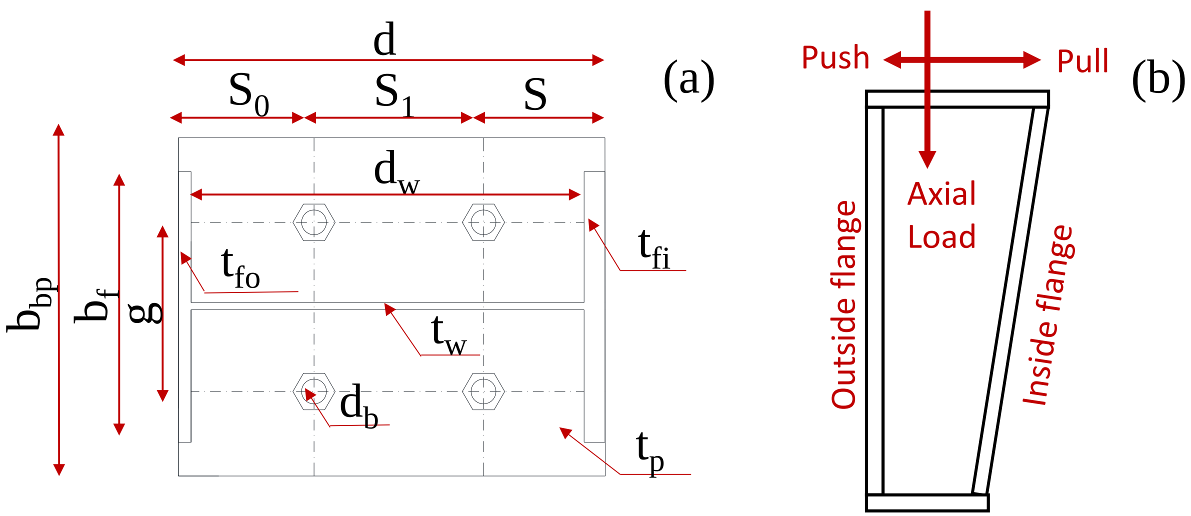

Figure 4.2. A generic base-plate connection configuration: (a) dimensional details, (b) elevation view.

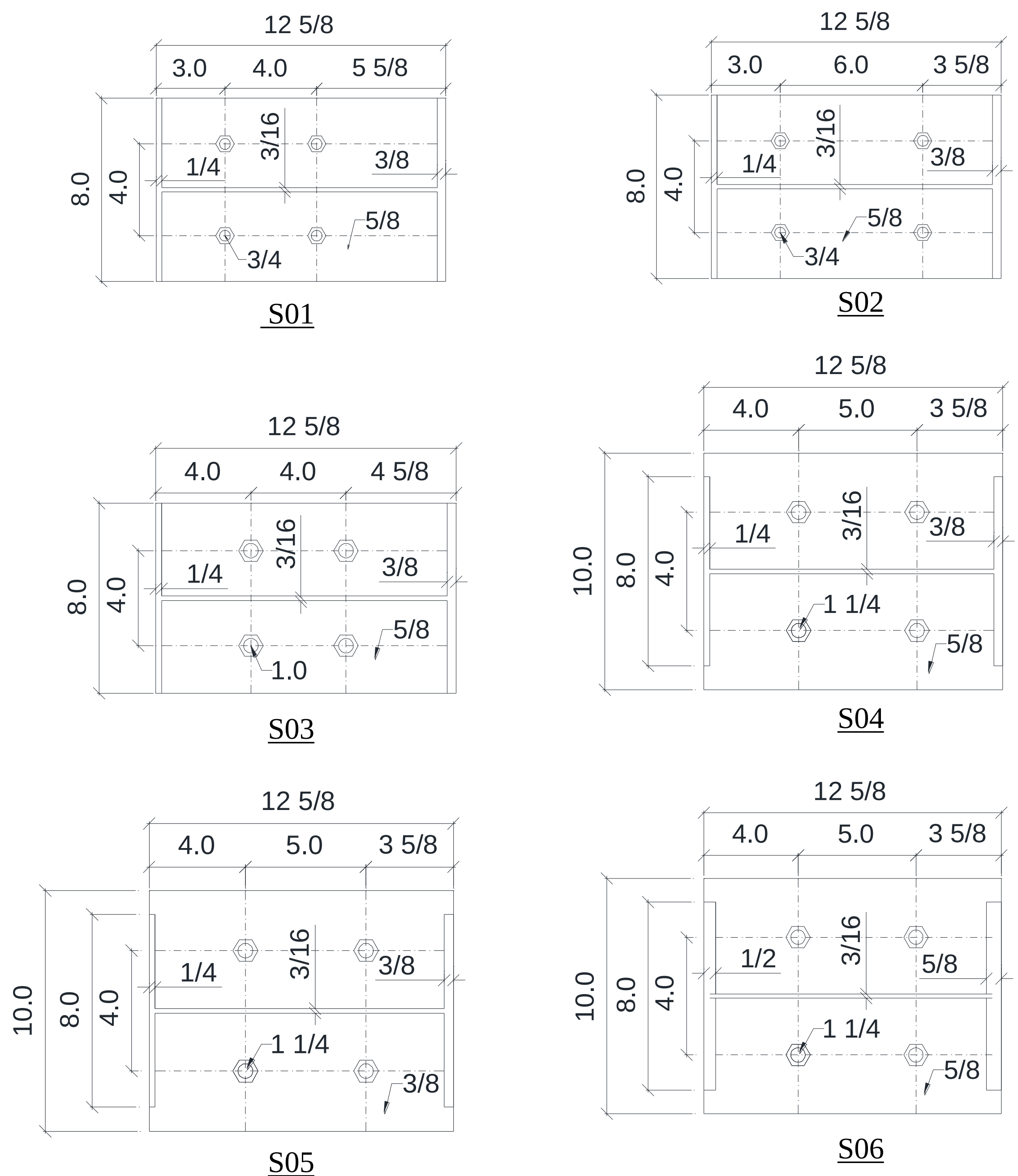

Figure 4.3. Tested web-tapered base-plate connection configurations.

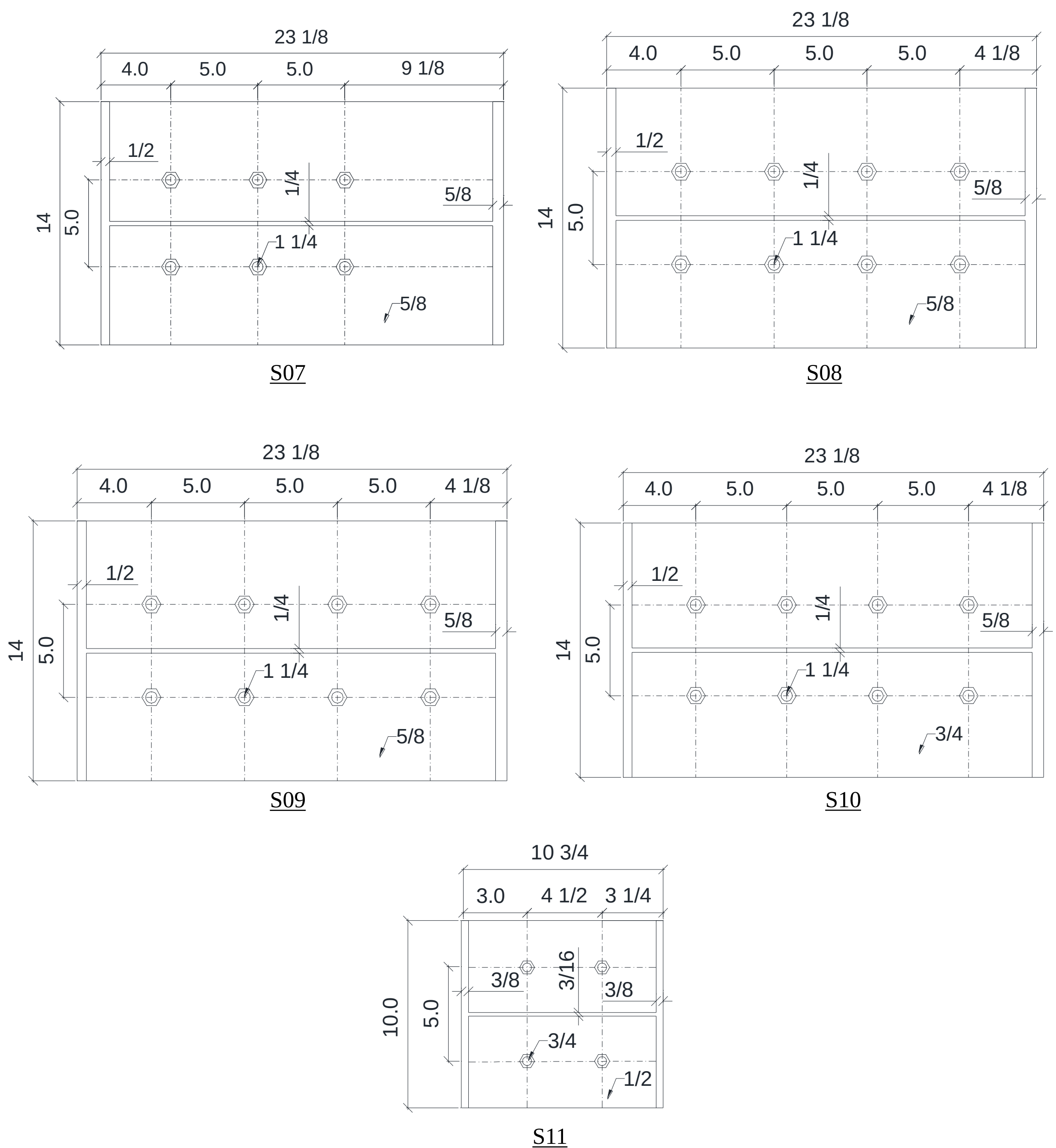

Figure 4.3. (Continued) Tested web-tapered base-plate connection configurations.

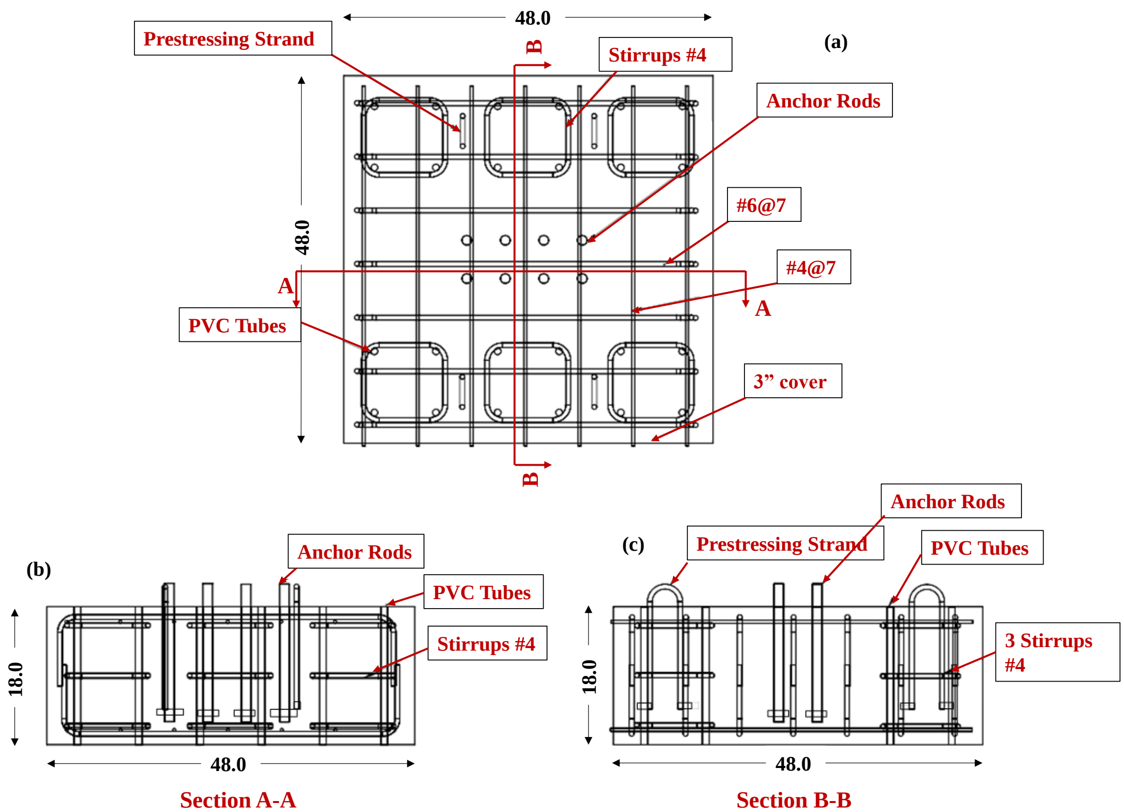

Figure 4.4. (a) Plan view of the foundations, (b) and (c) sections A-A and B-B respectively (note that the anchor rod layout corresponds to one of the specimens while all the other properties are generic to all the specimens).

4.2. Test Setup

The test setup of the second phase of the experimental program is shown in Figure 4.5. The test setup components were provided by the Metal Building Manufacturers Association (MBMA) and assembled in the Structural Research Laboratory at the University of Houston. Eleven reinforced concrete foundations were cast at Locke Solutions in Houston, Texas on February 27, 2015 using one batch of concrete for all the specimens. The concrete foundations were connected to a self-reacting frame using twenty-four 30 inch long steel threaded rods. The column stubs (with the base-plates) were connected to the center of the reinforced concrete foundation at the base, and connected to a “transfer beam” at the top. The horizontal loads were applied to the specimens through an actuator with a capacity of 110 kips, which was connected to the transfer beam at one end and to the horizontal wall of the reaction frame at the other end. Additionally, two hydraulic jacks with a capacity of 60 kips were placed atop the transfer beam to produce a constant compressive load in the columns ranging from 25 kips to 100 kips. The axial loads from the hydraulic jacks were transferred to the foundation through a transverse beam beneath the jacks and two post-tensioning bars. Pin connections were used to provide a free rotation at the locations where the post-tensioning bars were connected to the reaction floor using threaded rods that pass through the through holes in the concrete foundations. A portal frame was placed on either side of the column stubs to prevent out-of-plane displacements. The columns of the portal frames were bolted on the strong floor. The tested columns stub were 66 inch tall and had a constant taper of 0.08 inch/inch.

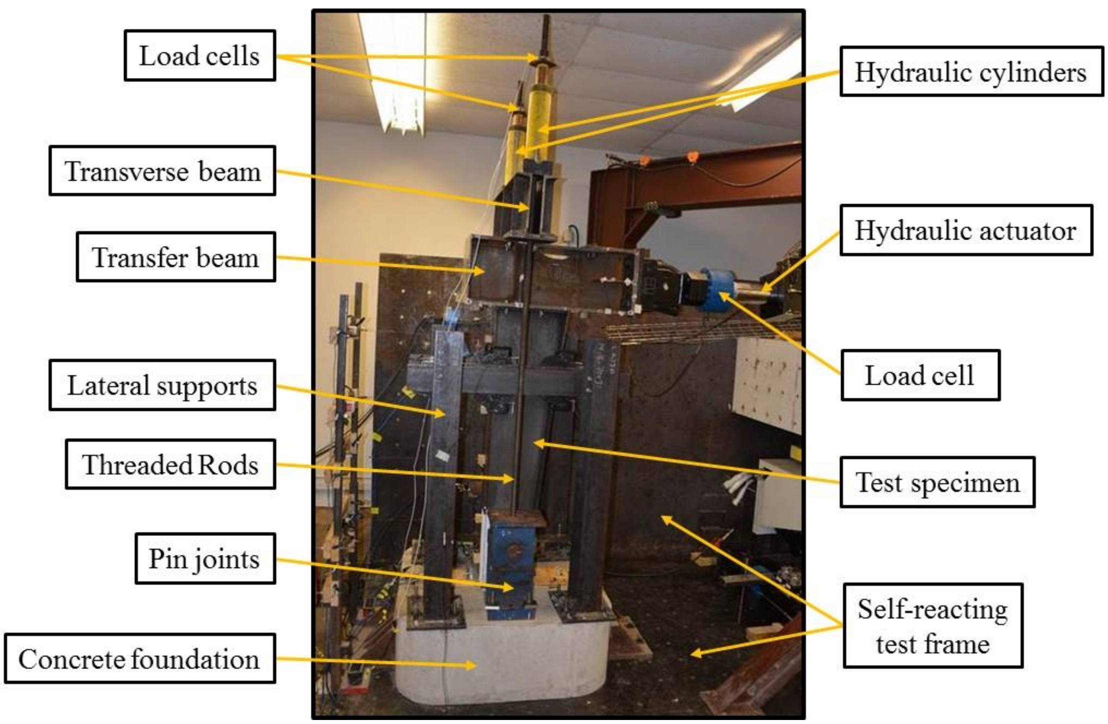

Figure 4.5. Illustration of the test setup.

4.3. Instrumentation and Data Acquisition

The instrumentation layout for the second phase of the experimental program is shown in Figure 4.6. The deformations were measured using linear potentiometers, rotary (string) potentiometers, and strain gauges. The global deformation and load measurements from the specimens included the displacement of the column stub at the location of the actuator connection, and the applied horizontal and axial loads. Load cells were connected to the two hydraulic jacks to measure the axial load during the experiments while the load cell attached to the actuator was used for the lateral load measurements. Six rotary (string) potentiometers [those for out-of-plane movement and in-plane rotation are shown in Figure 4.6(b)] were used to monitor the rigid body motion of the transfer beam in all six degrees-of-freedom. This information was later on used to calculate the second-order moments at the base of the specimen. In addition, the in-plane deflections of the column stubs along their height were measured using rotary (string) potentiometers at 5 1/2 inches, 16 inches, 30 1/2 inches, 42 inches and 57 1/2 inches measured from the base of the column. On one of side of the columns, the deformations of the base-plate and elongation of the anchor rods were measured using linear potentiometers. Moreover, two rotary (string) potentiometers were connected with the specimens' flanges to measure the uplift at those locations. Strain gages were placed on the inside and outside flanges at 3 inch, 6 inch and 9 inch from the base-plate in order to measure the extent of yielding of the two flanges. Additionally, two strain gages were placed on the base-plate one at approximately 2 inch from the outside and the other at approximately 2.5 inches the from inside flange. A Micro-Measurements System 7000 data acquisition system was used in all of the tests. The sampling frequency was set at 1 Hz.

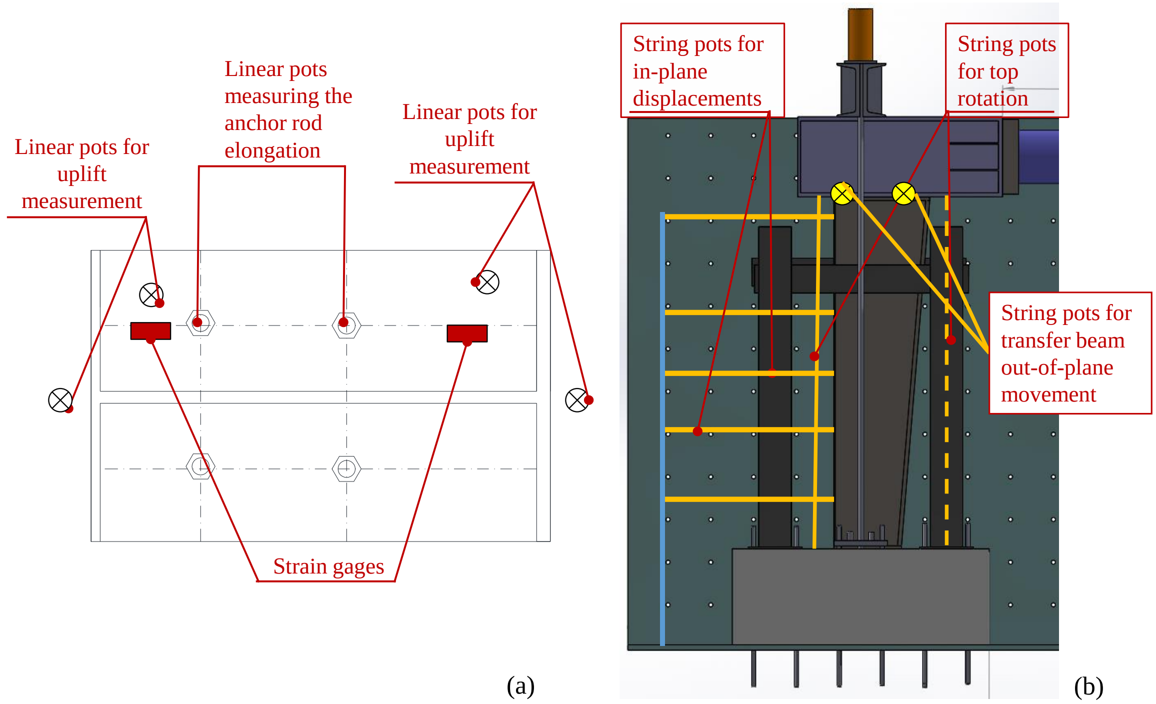

Figure 4.6. Instrumentation layout: (a) plan, and (b) elevation view.

4.4. Loading Protocols

In the second experimental program four tests were conducted for each specimen. First, a flexural cyclic test was performed consisting of three full cycles at 0.75% drift level under zero axial load. The loading protocol along with the drift levels for this test are shown in Figure 4.7(a). In the second and third tests, the same loading protocol was followed with the addition of a constant compressive load corresponding to the 50% and 100%, respectively, of the expected service load. The expected service load was determined as 50 kips for S01-S06 and S11, and 100 kips for S07-S10. These three tests were performed to characterize the elastic properties of the specimens with and without axial load. In the fourth test, cyclic displacements were increased until the specimens showed substantial degradation in capacity or up to a maximum drift of 10%, whichever is reached first. These fourth tests were conducted under 100% of the expected service axial load. The loading protocol for the 10% drift test is shown in Figure 4.7(b).

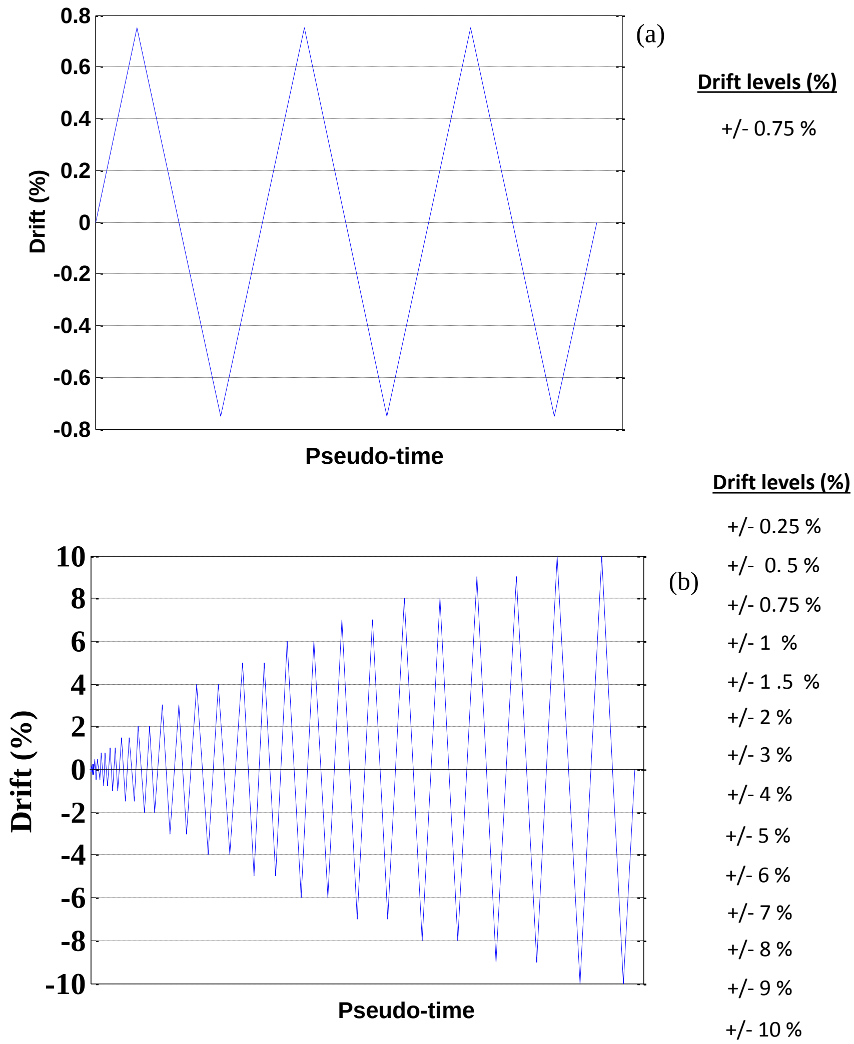

Figure 4.7. Loading protocol for (a) elastic range, and (b) inelastic range experiment.

4.5. Material Properties

The reinforced concrete foundations were designed according to ACI 318 (2014). The steps followed in construction of the foundations are shown in Figure 4.8. A total of 100 cylinders (4×8 inch) for compression and split tension testing and 27 prisms (6×6×21 inch) for modulus of rupture testing were prepared according to ASTM C31 (2015) from the same batch of concrete used in casting the foundations. The concrete cylinders and prisms were kept in the same environmental conditions as the concrete foundations. The material specimens were tested 7 days and 28 days after curing, and on the same day of connection tests. Compressive and splitting tensile tests [see

Figure 4.9(a) and Figure 4.9(b)] were conducted on concrete cylinders according to ASTM C39 (2016) and C496 (2011), respectively, while the modulus of rupture tests [see Figure 4.9(c)] were conducted according to ASTM C78 (2015). To determine the axial and diametrical deformations (see Figure 4.9) of the cylinders, and therefore, the modulus of elasticity and Poisson's ratio, from the compressive tests, a compressometer [see Figure 4.8(a)] was used in 28 days testing. The modulus of elasticity and the Poisson's ratio were calculated according to ASTM C469 (2014). The results from the compression, split tension and modulus of rupture tests are shown in Table 4.3, Table 4.4 and Table 4.5, respectively.

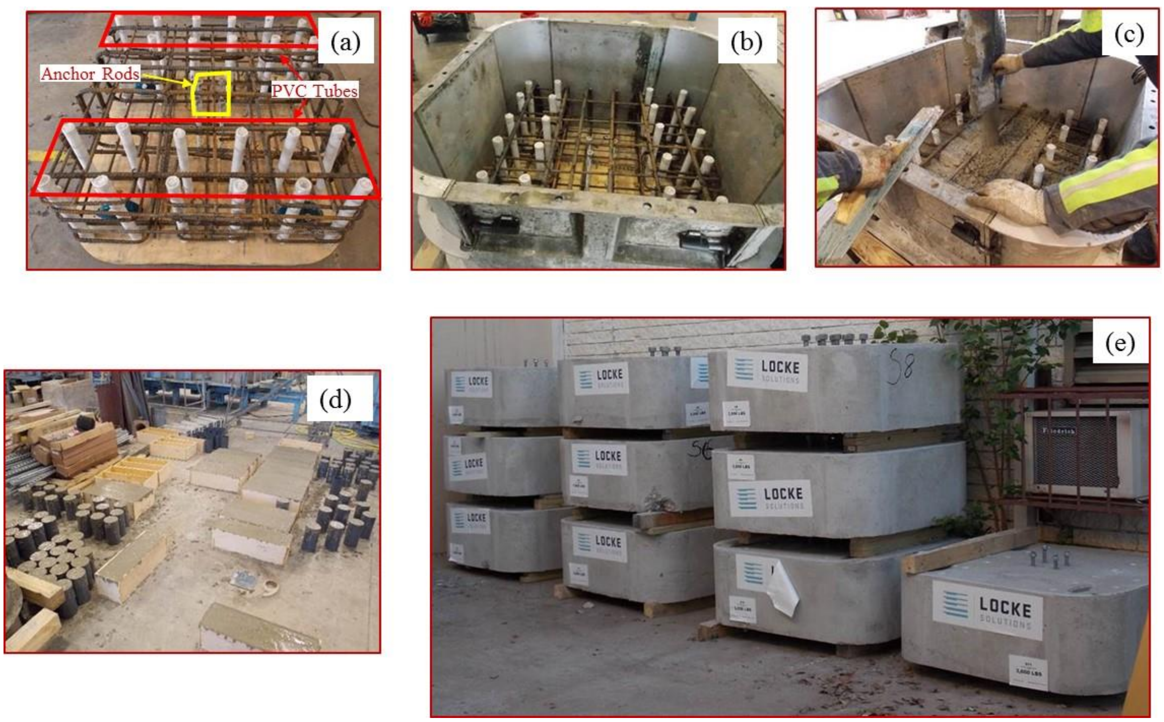

Figure 4.8. (a) Rebar cage, (b) formwork, (c) casting of the reinforced concrete foundations (d) preparation of material specimens, and (e) delivered concrete foundation at the University of Houston Structural Research Laboratory.

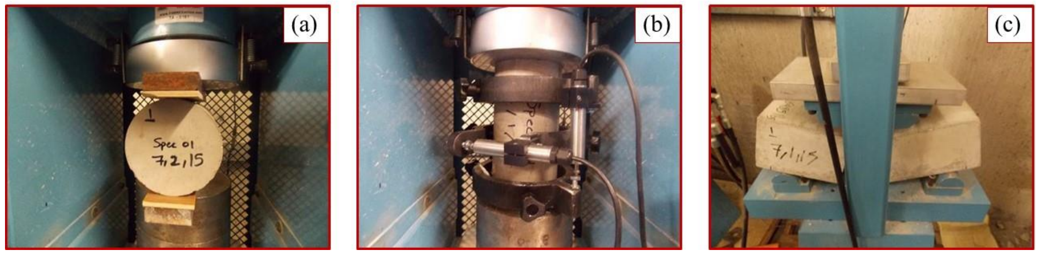

Figure 4.9. (a) Cylinders compression tests, (b) cylinders split tension tests, and (c) prism modulus of rupture tests.

Table 4.3 Compression Test Results.

Days/Specimen	Average Compressive Strength (ksi)	Standard Deviation (ksi)	Coefficient of Variation	Age of Concrete	Number of Specimens	Date
7 days	3.06	0.14	0.05	7 days	6	3/3/2015
28 days	4.34	0.39	0.09	28 days	4	3/27/2015
S01	4.08	0.14	0.04	127 days	4	7/2/2015
S02	5.70	0.23	0.04	139 days	4	7/15/2015
S03	5.32	0.17	0.03	161 days	4	8/7/2015
S04	4.75	0.13	0.03	161 days	3	8/7/2015
S05, S06	4.85	0.18	0.04	173 days	6	8/19/2015
S07, S08	5.06	0.17	0.03	189 days	5	9/5/2015
S09, S10, S11	4.86	0.23	0.05	249 days	6	11/4/2015
Additional*	4.92	0.15	0.03	279 days	7	12/4/2015

*Additional cylinders tested after the completion of the experiments.

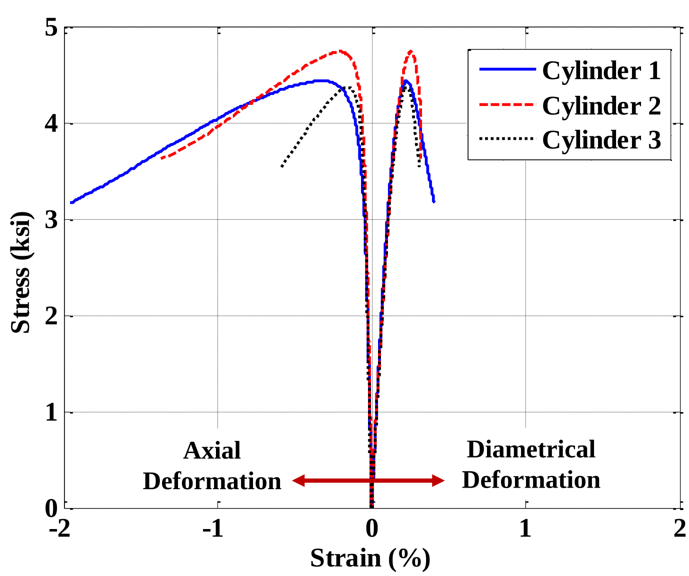

Figure 4.10. Stress strain curves for cylinders at 28 days curing.

Table 4.4 Split Tension Tests Results.

Days/Specimen	Average Split Tensile Strength (ksi)	Standard Deviation (ksi)	Coefficient of Variation	Age of Concrete	Number of Specimens	Date
7 days	0.27	0.03	0.12	7 days	4	3/3/2015
28 days	0.54	0.02	0.04	28 days	3	3/27/2015
S01	0.56	0.07	0.12	127 days	3	7/2/2015
S02	0.64	0.04	0.06	139 days	3	7/15/2015
S03	0.54	0.04	0.08	161 days	3	8/7/2015
S04	0.61	0.06	0.10	161 days	3	8/7/2015
S05, S06	0.55	0.02	0.05	173 days	5	8/19/2015
S07, S08	0.54	0.04	0.08	189 days	4	9/5/2015
S09, S10, S11	0.54	0.04	0.07	249 days	5	11/4/2015
Additional*	0.56	0.17	0.31	279 days	4	12/4/2015

*Additional cylinders tested after the completion of the experiments.

Table 4.5 Modulus of Rupture Tests Results.

Days/Specimen	Average Modulus of Rupture (ksi)	Standard Deviation (ksi)	Coefficient of Variation	Age of Concrete	Number of Specimens	Date
7 days	0.60	0.06	0.09	7 days	4	3/3/2015
28 days	0.67	0.06	0.08	28 days	4	3/27/2015
S01	0.66	0.08	0.12	127 days	3	7/2/2015
S05, S06	0.75	0.14	0.18	173 days	4	8/19/2015
S09, S10, S11	0.68	0.03	0.05	249 days	5	11/4/2015
Additional*	0.70	0.04	0.06	279 days	7	12/4/2015

*Additional cylinders tested after the completion of the experiments.

The columns were made of Grade 55 plates from seven different batches of steel. Coupons from each batch of steel were tested according to ASTM A370 (2015) [see Figure 4.11(a)], and representative stress-strain curves are shown in Figure 4.11(b). An extensometer was used at the mid-gage of the samples to measure the elongation and derive the strain. The main parameters of the stress-strain curves are presented in Table 4.6.

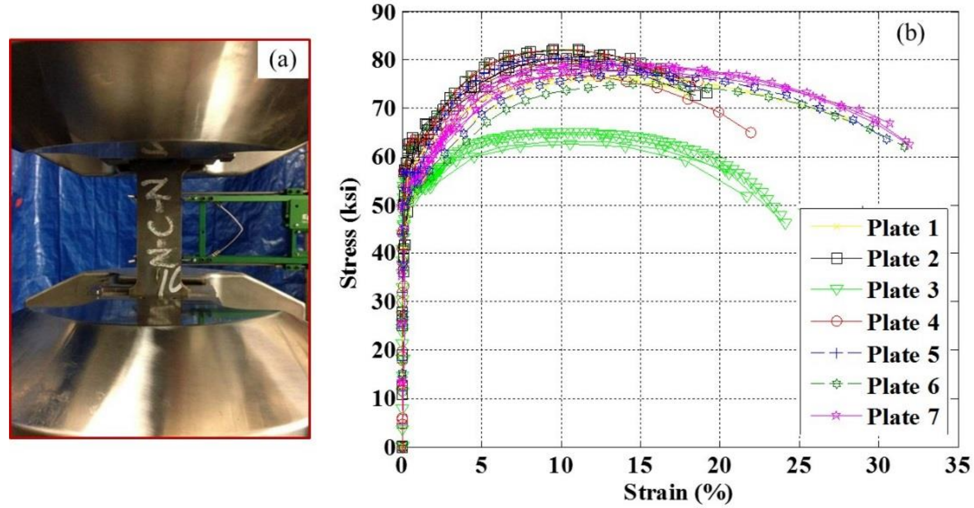

Figure 4.11. (a) Tensile testing of coupons, (b) representative stress-strain curves from coupon testing.

Table 4.6 Steel Coupon Test Results.

Plate ID	Cooupon ID*	Number of coupons	Thickness	Young's modulus	Yield stress	Yield strain	Peak stress	Peak strain	Ultimate stress	Ultimate strain
			(inch)	(ksi)	(ksi)	(%)	(ksi)	(%)	(ksi)	(%)
1	S02_OF, S03_OF	5	1/4	29100	64.7	0.223	82.5	13.157	56.0	18.767
2	S01_IF, S02_IF, S03_IF, S04_IF, S05_IF, S05_BP, S06_IF, S11_OF	5	3/8	29500	61.4	0.208	81.8	12.086	68.3	19.891
3	S06_OF, S07_OF, S08_OF, S09_OF, S10_OF, S11_BP	4	1/2	27000	54.9	0.203	63.9	12.622	43.9	23.866
4	S01_BP, S02_BP, S06_BP, S06_IF	4	5/8	28100	57.4	0.204	78.2	12.657	58.9	23.985
5	S03_BP, S04_BP	4	5/8	29800	60.5	0.203	81.5	12.298	71.0	18.881
6	S07_BP, S07_IF, S08_BP, S08_IF, S09_BP, S09_IF	4	5/8	27700	55.8	0.201	77.0	12.578	64.7	24.972
7	S10_BP	4	3/4	27300	55.3	0.202	79.3	13.011	67.1	24.436

*Coupon ID represents the specimen and location of the specimen that the coupon is coming from. IF: inside flange, OF: outside flange, BP: base-plate.

Three different diameter (3/4 inch, 1 inch and 1 1/4 inch) Grade 50 anchor rods were used for the specimens as presented earlier. The anchor rods had 10, 8 and 7 threads per 1 inch for the 3/4 inch, 1 inch and 1 1/4 inch diameter anchor rods, respectively. To determine the stress strain relationship, anchor rods selected from the same batch of anchor rods placed inside the foundations were tested according to ASTM A370 (2015) under monotonically increasing displacements until rupture. An extensometer was used at the mid-gage of the samples to read the displacements [see Figure 4.12(a)] and representative stress-strain curves are shown in Figure 4.12(b). The results from the tensile tests are shown in Table 4.6.

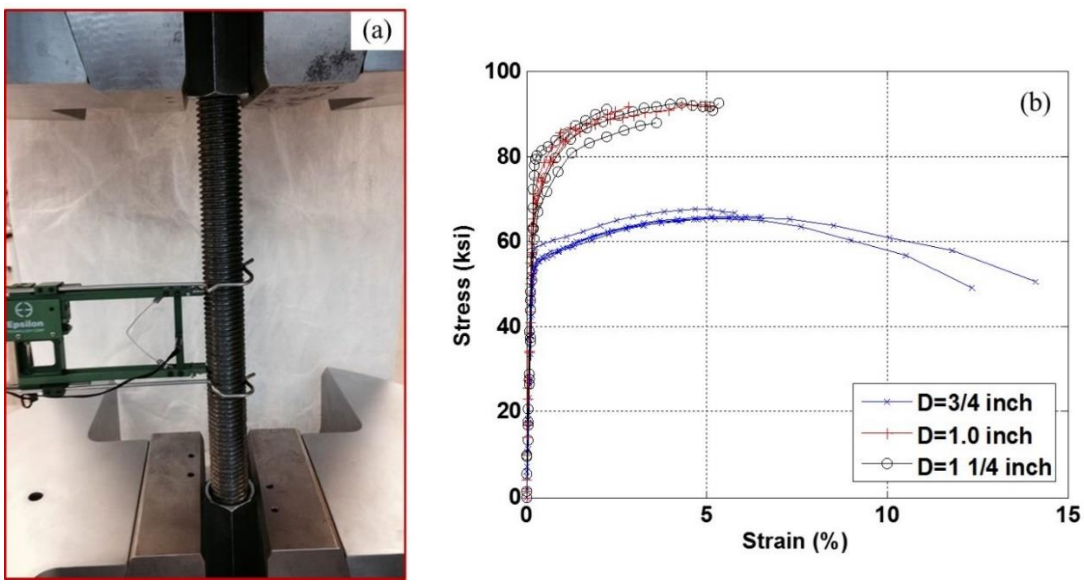

Figure 4.12. (a) Tensile testing of anchor rods, (b) representative stress-strain curves for anchor rods.

Table 4.7 Anchor Rod Tests Results.

Diameter	Number of Anchor Rods	Young's Modulus	Yield Stress	Yield Strain	Peak Stress	Peak Strain	Ultimate Stress	Ultimate Strain
(inch)	-	(ksi)	(ksi)	(%)	(ksi)	(%)	(ksi)	(%)
3/4	5	27600	57.7	0.204	66.0	6.314	52.6	9.418
1	3	29800	74.3	0.213	92.8	4.926	*	*
1 1/4	3	29300	76.3	0.207	92.5	4.937	*	*

*The extensometer was removed before rupture of the specimen to prevent damage to the sensor. Therefore, these values were not recorded.

4.6. Definitions

4.6.1. Connection rotation

The rotation of the base-plate connections has been calculated using two different approaches, each of which utilized information from different sets of sensors. In the first approach for calculating the rotation, the uplift measurements of the two rotary (string) potentiometers placed at the center of the flanges at a height of approximately 5 inch from the base-plate [see Figure 4.13(a)] were used. The rotation measurements presented here have been used for the calculation of the rotational stiffness presented later on. The rotation was found using Equation (4-1) as

$$\mathrm{Rotation} = (\delta_1 - \delta_2)/\mathrm{L}_{\mathrm{SP1SP2}}, \tag{4-1}$$

where, δ_1 is the uplift measurement from rotary (string) potentiometer 1 (SP1) (inch), δ_2 is the uplift measurement from rotary (string) potentiometer 2 (SP2) (inch), and L_{SP1SP2} is the distance between SP1 and SP2 [see Figure 4.13(a)] (inch).

In the second approach, the rotation was calculated using the rotary (string) potentiometers for measuring the horizontal displacement of the columns at various heights from the base-plate level [see Figure 4.13 (b)] according to Equation (4-2) as

$$\mathrm{Rotation}_{\mathrm{i}} = \tan^{-1}(\delta_{\mathrm{i}}\,/\mathrm{H}_{\mathrm{i}}), \tag{4-2}$$

where, δ_i is the in-plane measurement from rotary (string) potentiometer i (S.Pot i) (inch), and H_i is the height (measured from the base-plate) of that rotary (string) potentiometer (inch).

These measurements are presented in Appendix A and may be used to quantify the bending of the column stub because in an ideally pinned condition, the rotations measured from these sensors would be identical. In the research these rotation measurements have not be used for any of the rotation calculations.

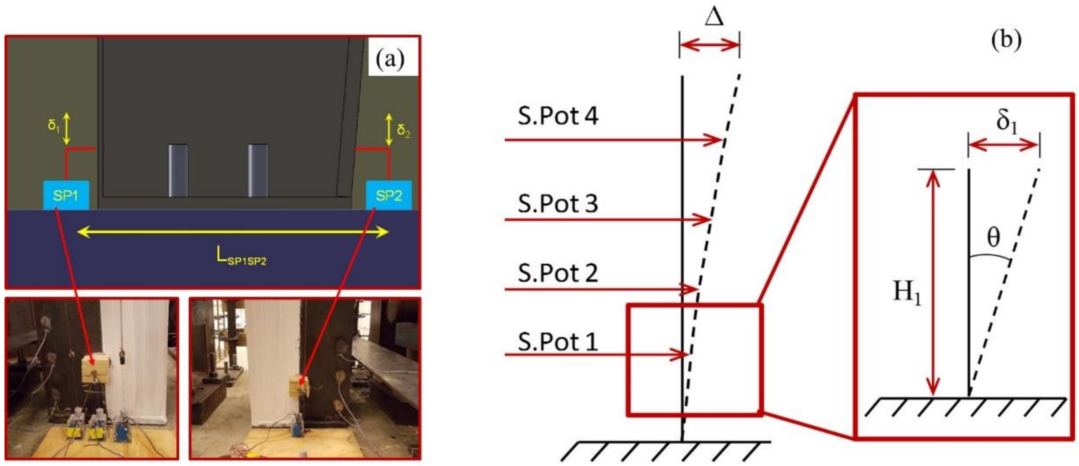

Figure 4.13. Calculation of the rotation: (a) using the uplift of the base-plate at the flanges, and (b) based on in-plane deflection of the column.

It was observed that the rotations obtained from SP1 and SP2 [see Figure 4.13(a)] using the first approach differed from those measured based on the second approach [see Figure 4.13(b)] from 0% up to 12% [see Figure 4.14(a)]. This rotation definition provided consistent results. In addition, they were reliable and representative of the connection behavior. For this reason in the second phase of the experimental program the third numerical approach adopted in the first phase and presented in Section 3.6.1 was not used.

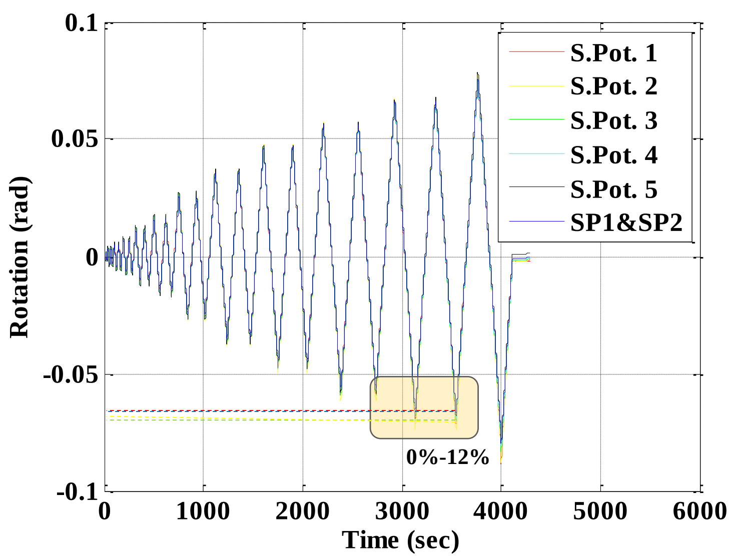

Figure 4.14. Average differences between the rotation measurements of the SP1 and SP2 with the five rotary (string) potentiometers for S02.

4.6.2. First- and second-order moments at the base

The definition of the first and second order moments at the base are defined as explained in Section 3.6.2. The graphs comparing the first- and second-order moments for all the specimens of the second experimental program can be found in Appendix A. Note that since the second-order moments are proportional to the deformation (no second-order effects in undeformed configuration), only the results from the inelastic tests are presented. The second-order moments in the elastic tests, were negligible. The calculations indicated that the second-order moments were approximately 10% to 15% of the total moment at 7% drift level and lower (higher) for lower (higher) drift levels. The second-order effects were taken into consideration and the total (first- plus second-order) moment versus rotation curves are presented.

4.6.3. Lateral and rotational stiffness

The lateral stiffness in the push (K_{lat}^{+}) and pull (K_{lat}^{-}) directions was calculated from the 0.75% drift level elastic tests. Specifically, the average slope of the chords connecting the origin with the three peaks in each of the push and pull directions was found [see Figure 4.15]. The lateral force measurement was obtained from the load cell mounted on the actuator and the drift (displacement) measurement was taken from the actuator linear variable differential transformer (LVDT), which is a displacement sensor.

As explained earlier in Section 3.6.3, the lateral stiffness should be taken only as a comparative measure between the specimens tested here while the rotational stiffness may be used in absolute values for an identical base-plate connection configuration. The rotational stiffness in the push (K_{rot}^{+}) and pull (K_{rot}^{-}) directions was calculated using the same approach as for the lateral stiffness explained above. The total (first- plus second-order) moments described in Section 3.6.2 and the first rotation measurement approach described in Section 4.6.1 were used. The rotations derived from the elastic tests (three cycles of 0.75% drift) for the specimens with 22 inch deep webs (S07-S10) were very small, considering the scale of these specimens and their behavior under small deformations. Consequently, the first rotation definition did not give reasonable results for these large base-plate connections up to 0.75% drift. As a result, the two 1.5% drift cycles that were executed at the beginning of the inelastic tests to calculate the rotation of the base-plate connections using the same approach explained in Section 4.6.3. However, since the inelastic tests were conducted only under the 100% axial load level, the influence of the effect of axial load on the rotational stiffness could not be derived for these larger base-plate connections (S07-S10).

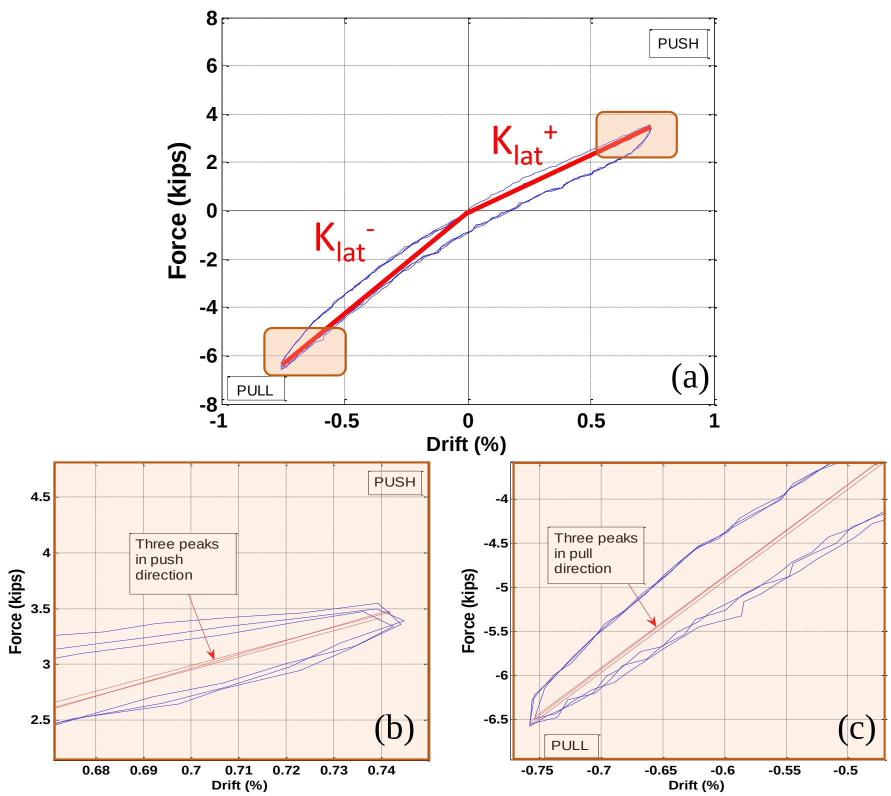

Figure 4.15. (a) Lateral stiffness calculation in push (K_{lat}^{+}) and pull (K_{lat}^{-}) directions for the 100% axial load level test for S04, (b) chords to the three peaks in push direction, (c) chords to the three peaks in the pull direction.

4.6.4. Idealized piecewise linear response

For representing the moment-rotation behavior of the specimens beyond the elastic range, a piecewise linear best-fit to the moment-rotation envelopes was used. As shown in Figure 4.16, the piecewise linear response fits consisted from four branches and was characterized by seven parameters in each direction. The piecewise linear response fitting of S04 is shown in Figure 4.17. In the first branch, the stiffness is dictated by the rotational stiffness, which was calculated as described in Section 4.6.3 above, and only the rotation corresponding to the first change in the stiffness (i.e., end of the first branch) was obtained from the fit. For the remainder of the branches, a best-fit that minimizes the error between the idealized curve and the enveloped obtained from the experiments was used to determine the parameters.

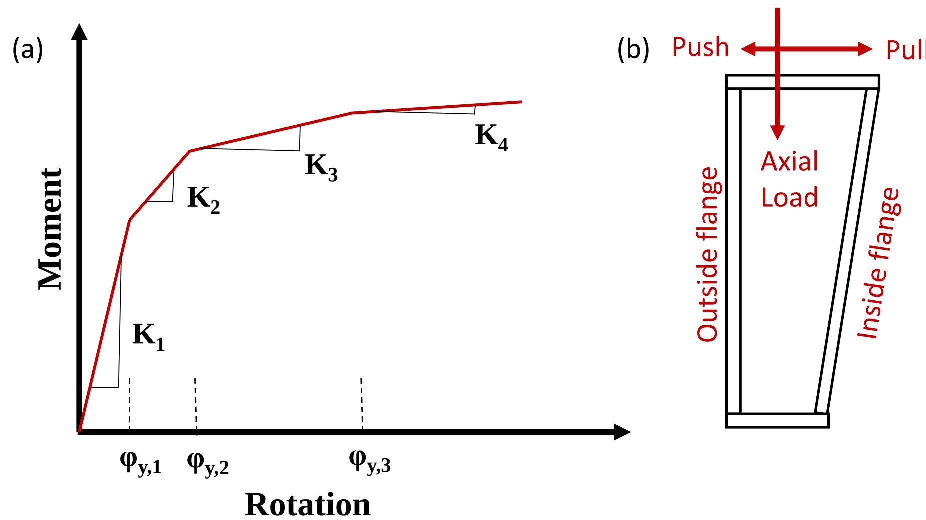

Figure 4.16. (a) Piece-wise linear approximation of the moment-rotation envelope curves, (b) indication of the push and pull direction.

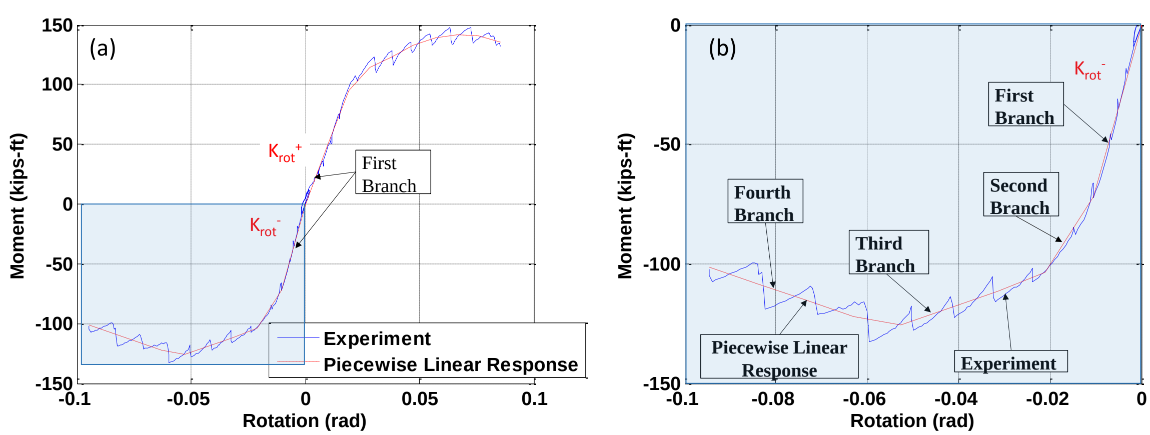

Figure 4.17. (a) Piecewise linear response fitting composed of four branches in push (K_{rot}^{+}) and pull (K_{rot}^{-}) directions for the 100% axial load level test (S04), (b) four branches of the piecewise linear response.

4.6.5. Hysteretic behavior

To enable a quantitative comparison of the performance of the tested eleven column base-plate connections, the moment capacity, M_m, and rotational ductility, μ_ϕ, values of the specimens were used as metrics. As shown in Figure 4.18, the energy absorption, E_a, was taken equal to the area inside of the hysteresis loops up to 0.05 radian for the specimens with smaller web depths (10 inch and 12 inch) and up to 0.02 radian for the specimens with a larger web depth (22 inch). The yield rotation, ϕ_y, was taken as the rotation corresponding to 75% of the maximum moment, M_m. The rotational ductility values in push, μ_ϕ^+, and pull directions, μ_ϕ^-, were defined as the ratio of the rotation at peak moment, ϕ_m, to the rotation at yielding, ϕ_y. It is noted here that this definition of the rotational ductility is somewhat tests is that corresponding to the largest rotation up to which the specimen was tested.

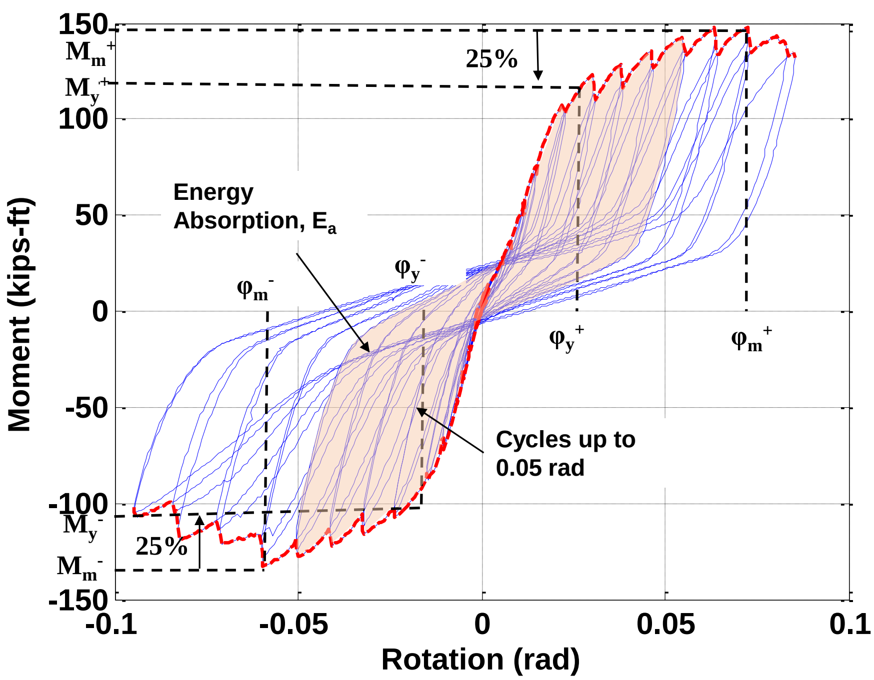

Figure 4.18. Definition of energy absorption, E_a, yield rotations in push (ϕ_y^+) and pull (ϕ_y^-) directions corresponding to 0.75% of the maximum moments (M_y^+, M_y^-), and maximum rotations in push (ϕ_m^+) and pull (ϕ_m^-) directions corresponding to the maximum moments (M_m^+, M_m^-).

4.7. Elastic Behavior of the Connections

In Figure 4.19, the force-drift relationships for the three elastic tests with varying axial load levels are presented. The average lateral stiffness values were normalized by the no axial load case to investigate the influence of the axial load, and the results are plotted in Figure 4.20. These results are also summarized in Table 4.8. It is reemphasized here that the absolute values of the lateral stiffness reported here should be used with caution as they depend on the height of the column stubs tested. The absolute values of the lateral stiffness are reported here for completeness and to facilitate a comparison of different connection configurations. The average (of positive and negative) lateral stiffness of the specimens increased from 6.0% to 46% when the axial load increased from 0% to 50%, and it increased from 8.3% to 29.8% when the axial load increased from 50% to 100%. An increase in the average lateral stiffness from 19.8% to 89.5% was calculated when the axial load increased from 0% to 100%.

In addition, as a result of the asymmetrical configuration of the base-plate connections, the lateral stiffness in push and pull directions differed significantly. For example, as shown in Table 4.8, the push-to-pull ratios differed from 0.4 to 1.7 for the tests with 0% axial load, from 0.3 to 1.4 for the tests with 50% axial load, and from 0.4 to 1.1 for the tests with 100% axial load. Additionally, it was observed that specimens that had a more symmetrical anchor rod configuration with respect to the axes of symmetry of the base-plate (e.g., S02, S05, and S08) had push-to-pull ratios closer to unity in the elastic tests with 100% axial load. This is a combined effect of the symmetric base-plate connection configuration and the axial load.

S06 experienced the highest average lateral stiffness in the push and pull directions under 100% axial load among all the 10-12 inch web depth specimens (i.e., S01–S06 and S11), with the reason being the geometric characteristics. Specifically, S06 consisted of the thickest base-plate: 5/8 inch, column flanges: 5/8 inch (outside flange) and 1/2 inch (inside flange), and largest anchor rod diameter: 1 1/4 inch among all the 10-12 inch web depth specimens. The 22 inch web depth specimens (i.e., S07–S10) showed a higher average lateral stiffness in comparison with the 10-12 inch web depth specimens. Among these specimens, S07 exhibited the lowest lateral stiffness in push direction. The reason for this was that S07 had six anchor rods as opposed to eight in the case of S08–S10. Therefore, in the push direction, there was only one pair of anchor rods in tension for S07 as opposed to two pairs for S08–S10.

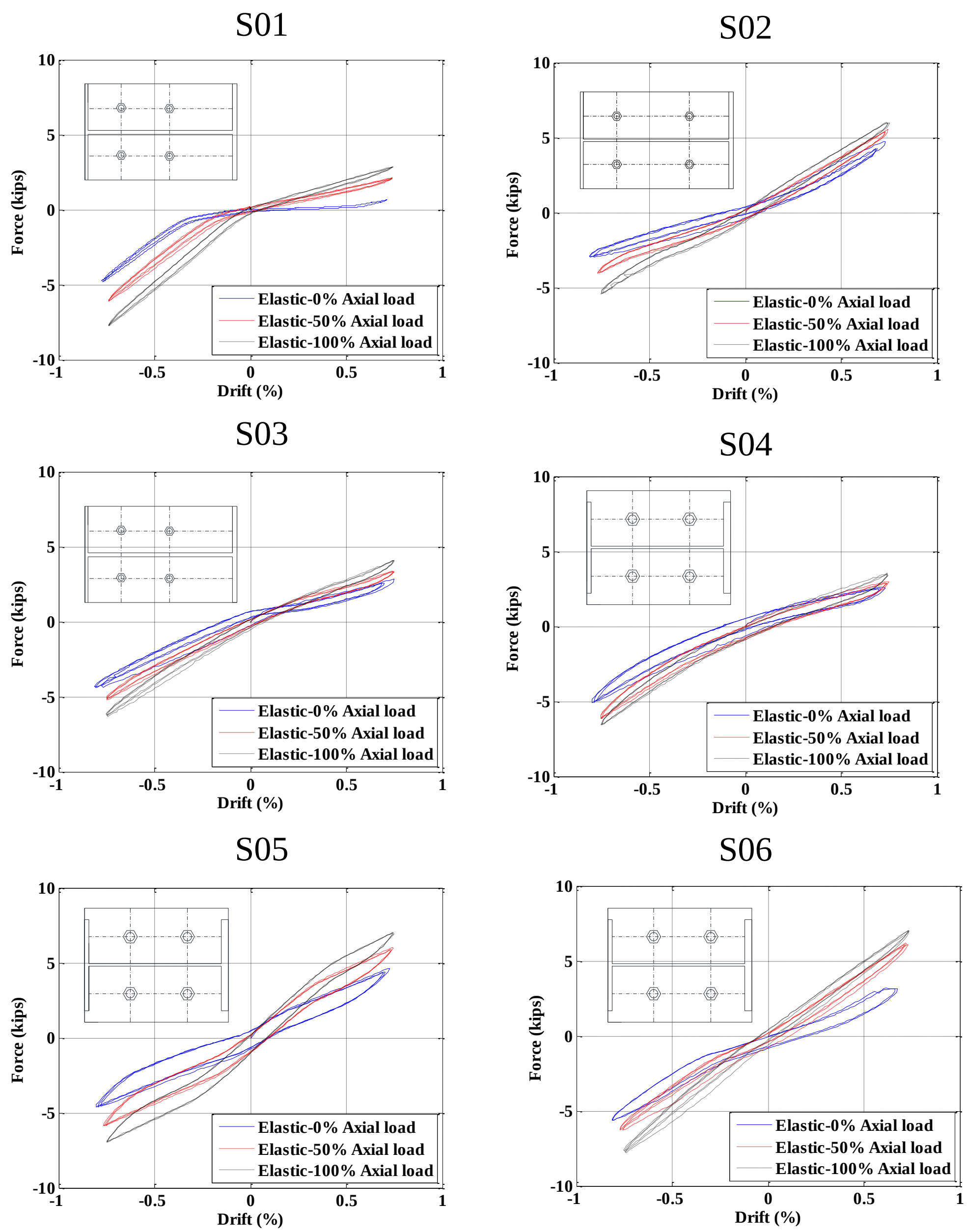

Figure 4.19. Load versus drift curves for the elastic tests under 0%, 50% and 100% axial load level.

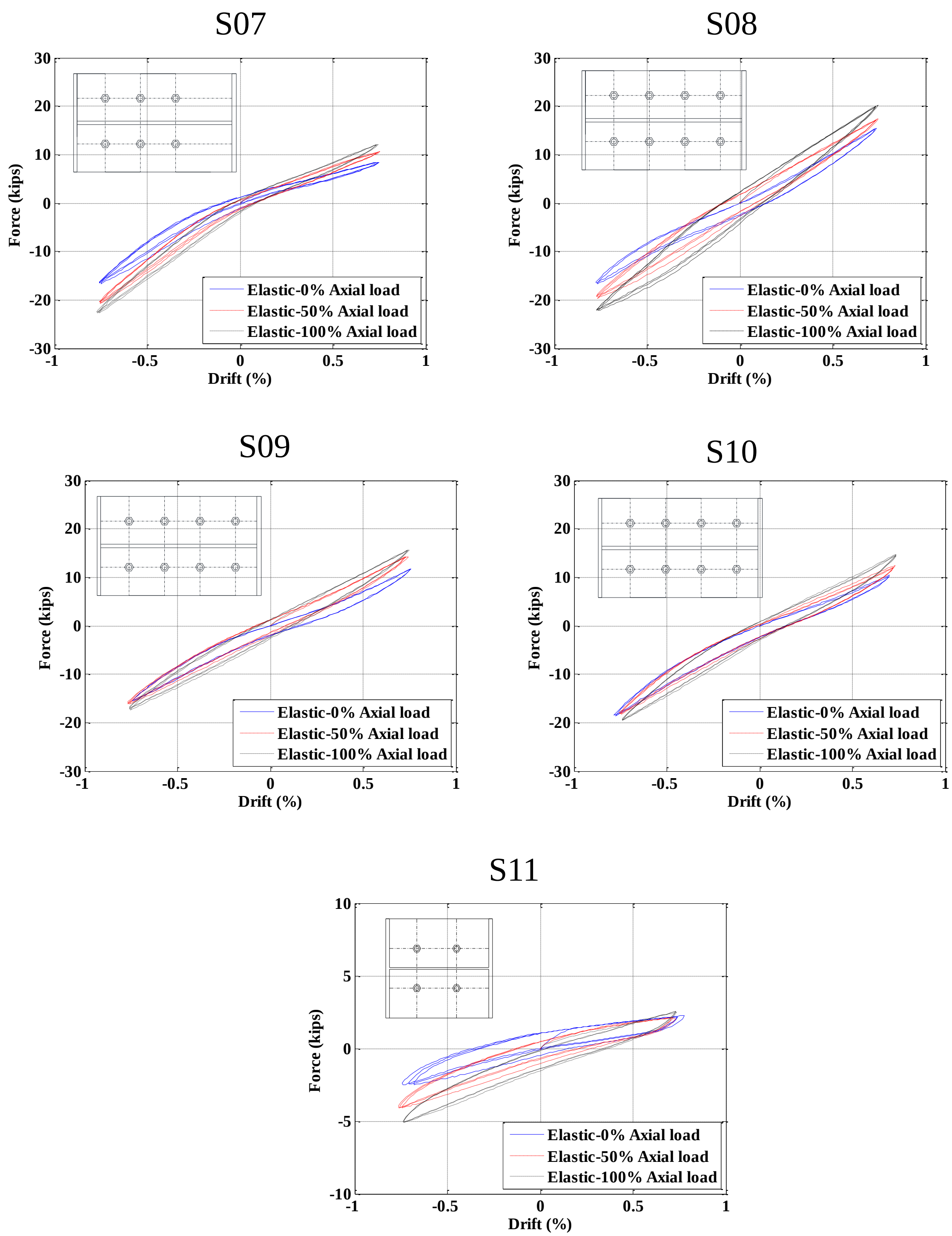

Figure 4.19 (Continued) Load versus drift curves for the elastic tests under 0%, 50% and 100% axial load level.

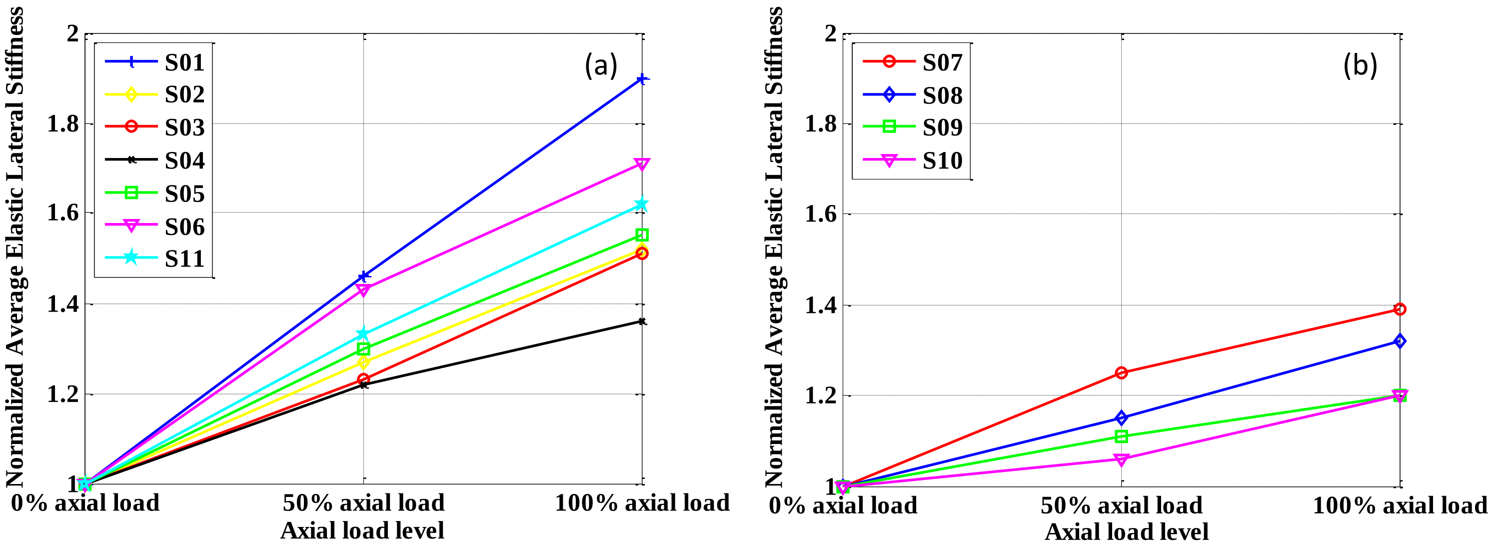

Figure 4.20. (a) Normalized lateral stiffness for (a) S01-S06 an0% axial d S11, and (b) S07-S10.

Table 4.8 Lateral Stiffness under 0%, 50% and 100% Applied Axial Load.

	0% Axial load				50% Axial load				100% Axial load				Influence of axial load on average stiffness (%)		
Specimen ID	K^+ (kips/in)	K^- (kips/in)	K^+/K^-	K_{ave} (kips/in)	K^+ (kips/in)	K^- (kips/in)	K^+/K^-	K_{ave} (kips/in)	K^+ (kips/in)	K^- (kips/in)	K^+/K^-	K_{ave} (kips/in)	0-50%	50-100%	0-100%
S01	2.8	7.5	0.4	5.1	3.9	11.1	0.3	7.5	5.3	14.2	0.4	9.7	46.0	29.8	89.5
S02	8.6	5.0	1.7	6.8	10.1	7.0	1.4	8.6	10.9	9.8	1.1	10.3	26.6	20.5	52.5
S03	5.1	7.4	0.7	6.2	6.0	9.4	0.6	7.7	7.4	11.4	0.7	9.4	23.4	22.2	50.7
S04	4.8	8.7	0.5	6.7	5.3	11.1	0.5	8.2	6.4	11.9	0.5	9.2	21.6	11.6	35.6
S05	8.5	7.9	1.1	8.2	10.9	10.5	1.0	10.7	12.7	12.6	1.0	12.7	30.1	18.8	54.6
S06	6.4	9.4	0.7	7.9	11.5	11.1	1.0	11.3	13.0	14.0	0.9	13.5	42.8	19.8	71.1
S07	15.4	29.6	0.5	22.5	19.2	37.2	0.5	28.2	22.2	40.2	0.6	31.2	25.3	10.6	38.6
S08	28.5	29.2	1.0	28.9	31.7	34.6	0.9	33.1	37.1	39.1	0.9	38.1	14.7	15.0	31.9
S09	21.2	28.4	0.7	24.8	26.3	28.5	0.9	27.4	28.4	30.9	0.9	29.7	10.7	8.3	19.8
S10	20.1	32.2	0.6	26.2	22.7	32.7	0.7	27.7	27.0	35.9	0.8	31.4	6.0	13.4	20.2
S11	4.0	4.8	0.8	4.4	4.2	7.4	0.6	5.8	4.7	9.4	0.5	7.0	33.0	21.5	61.6

In Figure 4.21, the moment-rotation relationships for the three elastic tests with varying axial load levels are presented. The rotational stiffness values were normalized by the no axial load case to investigate the influence of the axial load, and plotted in Figure 4.22. As described in Section 4.6.3, the influence of the effect of axial load on the rotational stiffness could not be derived for the 22 inch deep webs connections (S07-S10). Consequently, the average rotational stiffness shown in Figure 4.22(b) were evaluated from the 1.5% drift cycles of the inelastic tests as explained previously. All the results are summarized in Table 4.9. The average (positive and negative) rotational stiffness of the subset of specimens (S01-S06 and S11) increased from 10.2% to 80.7% when the axial load increased from 0% to 50%, and it increased from 13.9% to 35.9% when the axial load increased from 50% to 100%. An increase in the average rotational stiffness from 33.2% to 145.6% was observed when the axial load increased from 0% to 100%.

In addition, as a result of the asymmetrical configuration of the base-plate connections, the rotational stiffness in push and pull directions differed significantly. As shown in Table 4.9, the push-to-pull ratios varied from 0.2 to 1.4 for the tests with 0% axial load, from 0.2 to 1.2 for the tests with 50% axial load, and from 0.3 to 1.3 for the tests with 100% axial load. Additionally, it was observed that specimens that had a more symmetrical anchor rod configuration with respect to the axes of symmetry of the base-plate (e.g., S02 and S08) had push-to-pull ratios closer to unity when tested under 100% axial load.

S06 showed the highest average rotational stiffness under 100% axial load among all the 10-12 inch web depth specimens (i.e., S01–S06 and S11), with the reason being the geometric characteristics as explained above. Similarly, S10 showed the highest average rotational stiffness in the push and pull direction among the 22 inch web depth specimens (i.e., S07–S10) for the same reasons. Specifically, S10 consisted of the thickest base-plate (3/4 inch), among all the 22 inch web depth specimens, while the other geometrical characteristics were identical (column flanges, web, anchor rods) to S07-S09. S07 showed the lowest rotational stiffness in push direction. The reason for this was that S07 had six anchor rods as opposed to eight in the case of S08–S10 as explained above.

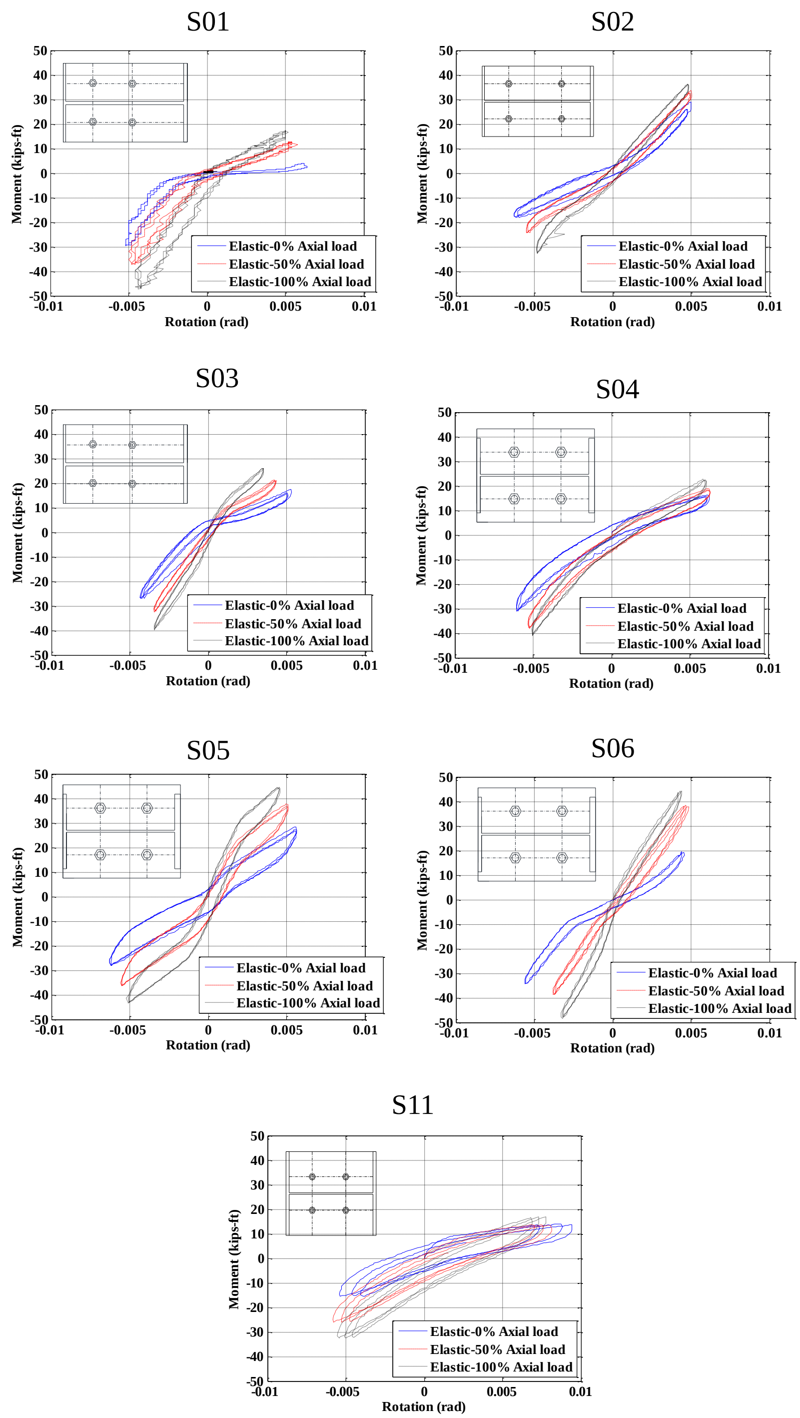

Figure 4.21. Moment versus rotation curves for the elastic tests under 0%, 50% and 100% axial load level. Note that the results for S07-S10 are not presented because the rotation was only calculated from the inelastic tests at 1.5% drift level.

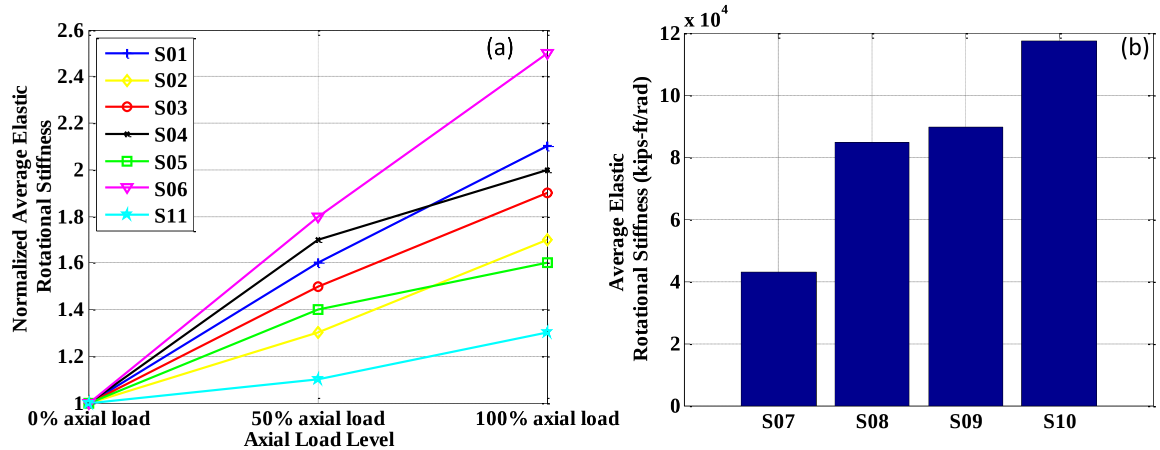

Figure 4.22. (a) Normalized rotational stiffness for S01-S06 and S11, (b) Average rotational stiffness for S07-S10 under 100% axial load.

Table 4.9 Rotational Stiffness under 0%, 50% and 100% Applied Axial Load.

	0% Axial load				50% Axial load				100% Axial load				Influence of axial load on average stiffness (%)		
Specimen ID	K^+ (kips-ft/rad)	K^- (kips-ft/rad)	K^+/K^-	K_{ave} (kips-ft/rad)	K^+ (kips-ft/rad)	K^- (kips-ft/rad)	K^+/K^-	K_{ave} (kips-ft/rad)	K^+ (kips-ft/rad)	K^- (kips-ft/rad)	K^+/K^-	K_{ave} (kips-ft/rad)	0-50%	50-100%	0-100%
S01	1273	5115	0.2	3194	1978	8227	0.2	5102	3456	9722	0.4	6589	59.7	29.1	106.3
S02	4800	3548	1.4	4174	5660	5275	1.1	5467	6091	8030	0.8	7060	31.0	29.1	69.2
S03	2696	6982	0.4	4839	4351	9794	0.4	7073	6862	11994	0.6	9428	46.2	33.3	94.8
S04	2601	3360	0.8	2981	3203	6698	0.5	4951	4300	7226	0.6	5763	66.1	21.1	101.2
S05	4734	4579	1.0	4657	7362	6130	1.2	6746	10462	7762	1.3	9112	44.9	13.9	65.0
S06	3355	6901	0.5	5128	7800	10733	0.7	9266	9882	15312	0.6	12597	80.7	35.9	145.6
S07	-*	-	-	-	-	-	-	-	28171	58142	0.5	43156	-	-	-
S08	-	-	-	-	-	-	-	-	83889	85372	1.0	84630	-	-	-
S09	-	-	-	-	-	-	-	-	44942	134574	0.3	89758	-	-	-
S10	-	-	-	-	-	-	-	-	120672	113821	1.1	117247	-	-	-
S11	1206	3240	0.4	2223	1450	3451	0.4	2450	1896	4027	0.5	2962	10.2	20.9	33.2

*The data was not available for these specimens

4.8. Non-Linear Behavior of the Connections

The force-drift and moment-rotation curves of all the specimens under large drift reversals are shown in Figure 4.23 and Figure 4.24, respectively. The force-drift envelopes using the piece-wise linear approximation discussed in Section 4.6.4 are shown in Figure 4.25(a) and Figure 4.25(b). The experiments indicated that the base-plate connections showed significant drift capacity, in the inelastic range, reaching up to 10%. The energy absorption characteristics due to different mechanisms are explained in detail for each specimen in Section 4.10. Strength degradation was observed mainly after a specimen experienced anchor rod rupture, weld rupture, or excessive cracking of the concrete foundation. Specifically, the strength degradation of S01, S02 and S11 occurred due to the failure of the anchor rods and for S03 and S04 through combined yielding of the flanges, the base-plate and the web. Additionally, the strength degradation of S05 and S06 occurred when the welds between the flanges, web and the base-plate ruptured. The strength degradation of S07–S10 occurred mainly due to excessive cracking and failure of the reinforced concrete foundation.

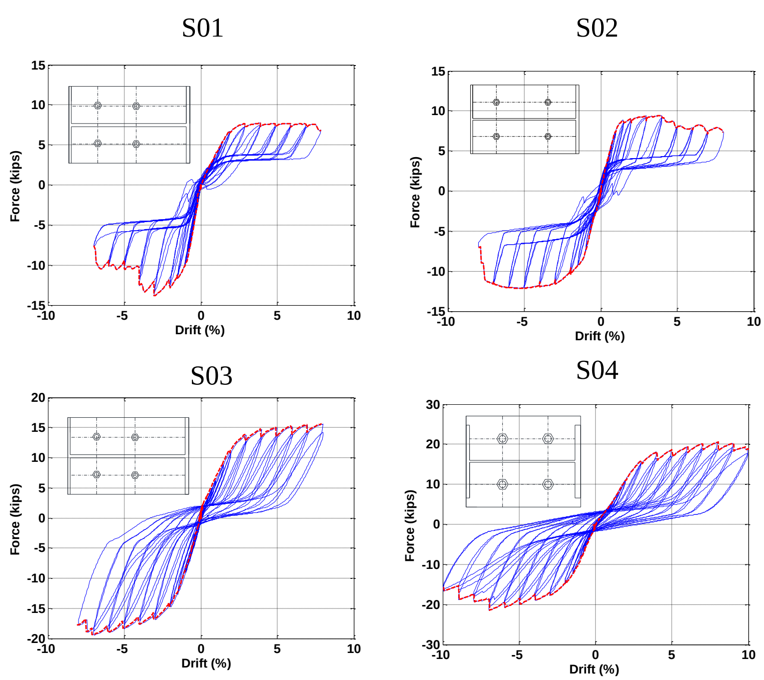

Figure 4.23. Cyclic force-drift curves.

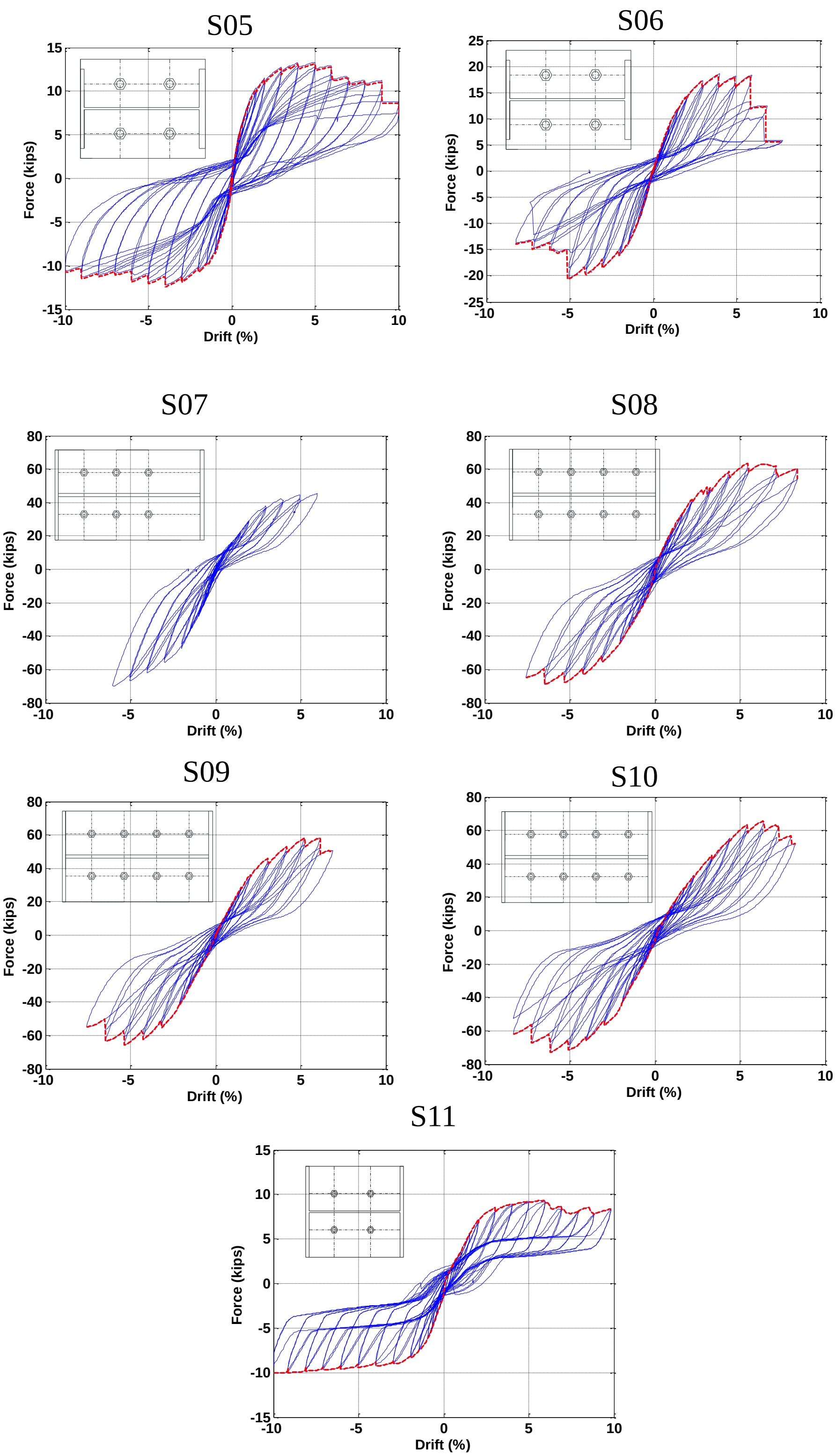

Figure 4.23. (Continued) Cyclic force-drift curves.

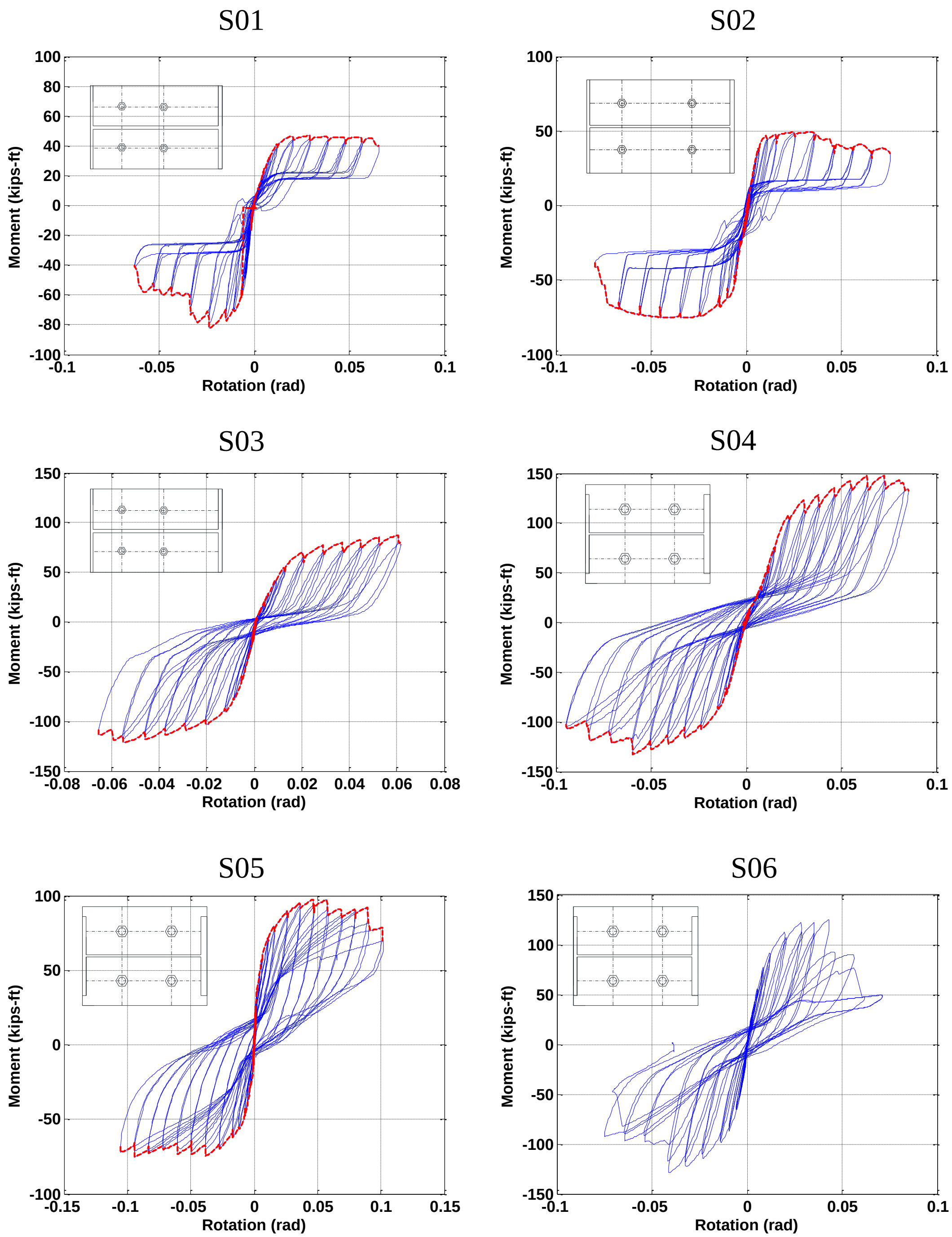

Figure 4.24. Cyclic moment-rotation curves.

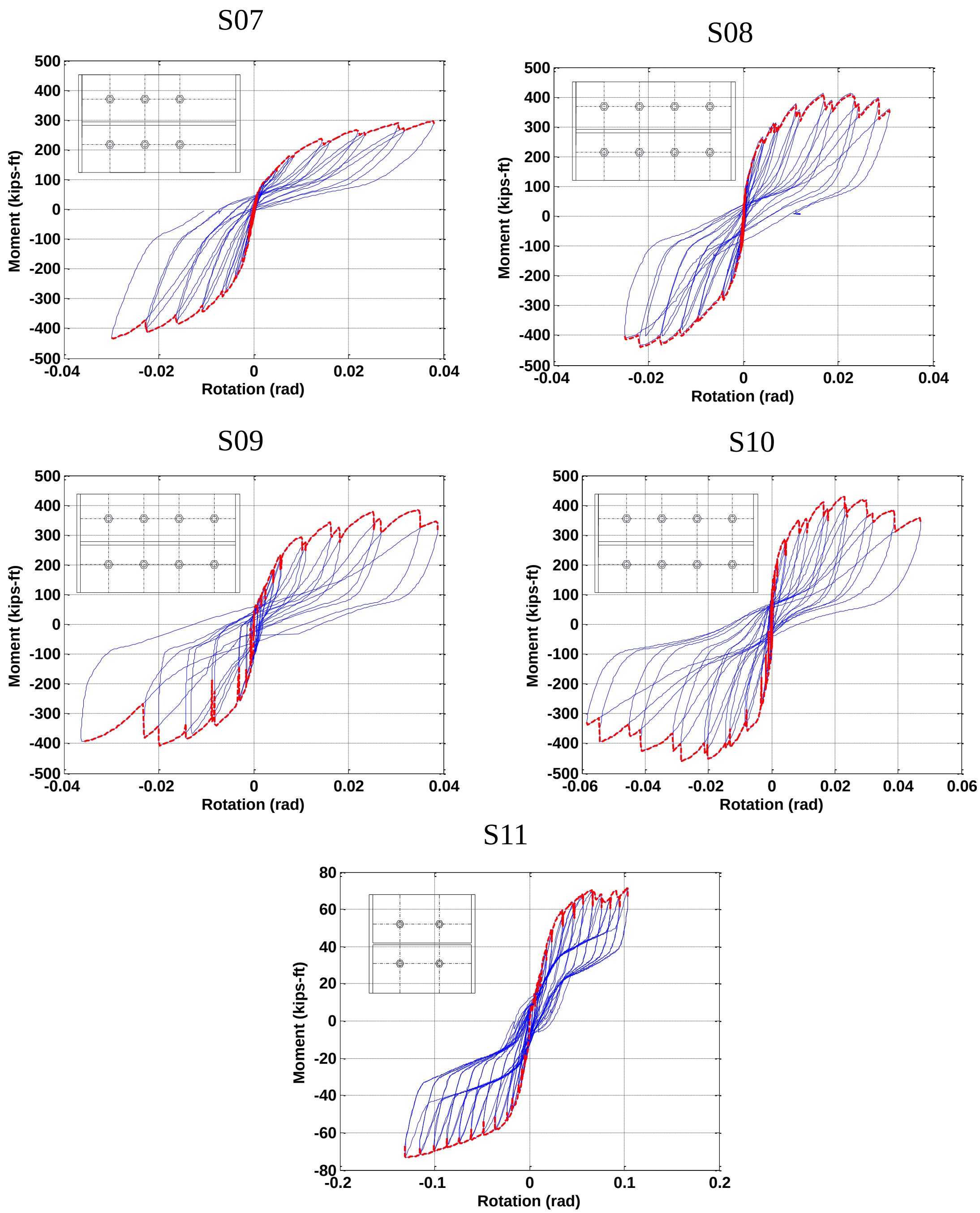

Figure 4.24. (Continued) Cyclic moment-rotation curves.

The moment-rotation envelopes from the inelastic 10% drift tests were idealized using a piecewise linear approximation with four branches in each of the push and pull directions as described in Section 4.6.4. The idealized curves are characterized by seven parameters in each direction. Due to asymmetric nature of the base-plate connections (unequal flange thicknesses, tapered column web and anchor rods not being centered on the base-plate), the behavior in the push and pull direction is presented separately in Table 4.10. The idealized moment-rotation envelopes are shown in Figure 4.26(a) and Figure 4.26(b).

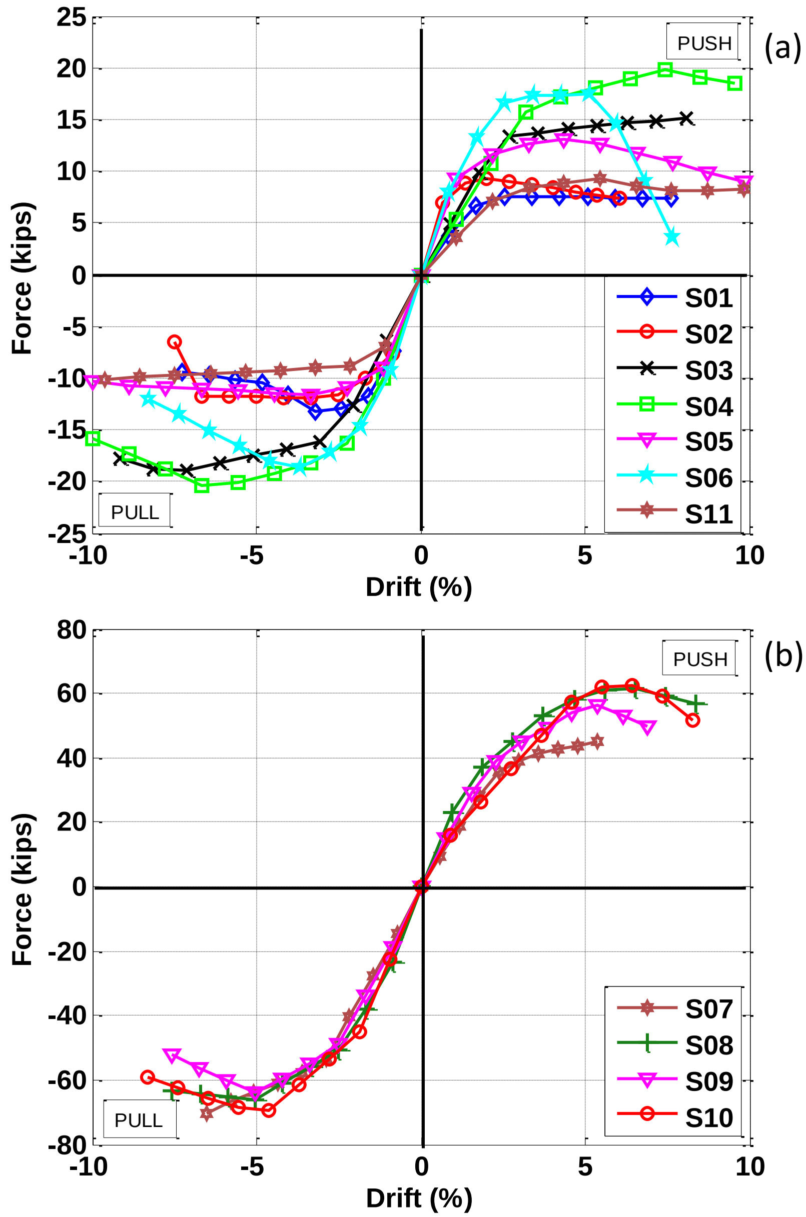

Figure 4.25. (a) Force-drift envelopes for S01-S06 and S11, and (b) force-drift envelopes for S07-S10.

Table 4.10. Parameters of the Idealized Moment-Rotation Curves. Refer to Section 4.6.4 for a Detailed Description of These Parameters.

Specimen ID	K_1^+	$\varphi_{y,1}^+$	K_2^+	$\varphi_{y,2}^+$	K_3^+	$\varphi_{y,3}^+$	K_4^+	K_1^-	$\varphi_{y,1}^-$	K_2^-	$\varphi_{y,2}^-$	K_3^-	$\varphi_{y,3}^-$	K_4^-
	(kips-ft/rad)	**(rad)**	**(kips-ft/rad)**	**(rad)**	**(kips-ft/rad)**	**(rad)**	**(kips-ft/rad)**	**(kips-ft/rad)**	**(rad)**	**(kips-ft/rad)**	**(rad)**	**(kips-ft/rad)**	**(rad)**	**(kips-ft/rad)**
S01	3456	0.0114	962	0.0173	-34	0.0618	-1289	9722	0.0004	4944	-0.0095	737	-0.0206	-743
S02	6091	0.0073	274	0.0332	-753	0.0463	-109	8030	-0.0074	1579	-0.0267	-156	-0.0711	-3641
S03	6862	0.0010	1196	0.0159	403	0.0630	807	11994	-0.0056	2172	-0.0153	560	-0.0530	-738
S04	4300	0.0263	1344	0.0535	284	0.0712	-528	7226	-0.0094	1734	-0.0203	678	-0.0550	-657
S05	10462	0.0061	1074	0.0311	-128	0.0869	-1014	7762	-0.0061	900	-0.0217	432	-0.0318	7
S06	9882	0.0068	256	0.0178	351	0.0393	-2499	15312	-0.0049	338	-0.0281	-554	-0.0348	-859
S07	28171	0.0053	20588	0.0100	5049	0.0213	1543	58142	-0.0043	4783	-0.0095	8518	-0.0142	3751
S08	83889	0.0030	9859	0.0146	160	0.0224	-4316	85372	-0.0029	11317	-0.0118	8232	-0.0168	-1798
S09	44942	0.0034	26912	0.0079	3799	0.0332	-8264	134574	-0.0013	7940	-0.0048	10277	-0.0148	-1229
S10	120672	0.0017	34437	0.0062	6367	0.0211	-3083	113821	-0.0013	33796	-0.0044	9352	-0.0184	-2491
S11	1896	0.0291	132	0.0578	-51	0.0949	557	4027	-0.0091	370	-0.0264	192	-0.0984	93

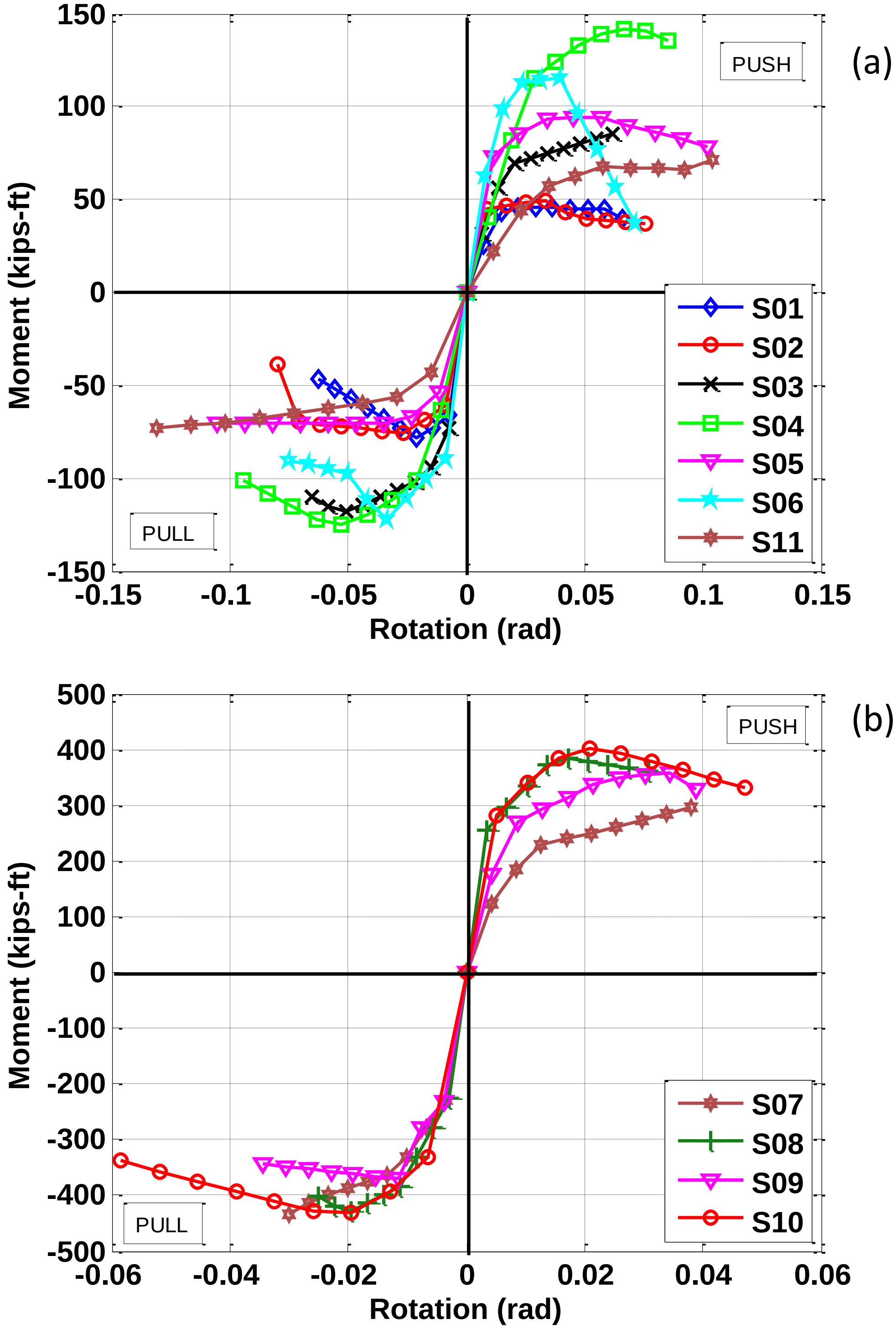

Figure 4.26. (a) Moment-rotation envelopes for S01-S06 and S11, and (b) moment-rotation envelopes for S07-S10.

4.9. Parameters Under Investigation

The base-plate connection configurations were selected such that a systematic investigation of the key parameters could be performed. Figure 4.17 shows these parameters investigated through the experimental program; namely, the foundation material (concrete versus steel), pitch, anchor rod diameter, base-plate thickness, number of anchor rods, and repeatability. In the following sections, the influence of each of the parameters listed in Table 4.1 on the lateral stiffness, rotational stiffness, and the moment capacity of the base-plate connections is discussed in detail.

4.9.1. Foundation material

S01 in the current study had identical connection configuration with $S06_{phase1}$ from the first phase of the experimental program. The only difference between the two tested specimens was the foundation on which they were supported. S01 was tested on a reinforced concrete foundation while $S06_{phase1}$ was tested on a steel foundation. Both specimens were tested in the elastic range under a 67 kips axial load. However, the axial load of S01 was decreased to 50 kips for the inelastic range to be consistent with the specimens in the test matrix of this paper. The results are shown in Figure 4.27and Figure 4.28. It was found that the average rotational stiffness of $S06_{phase1}$ was 26% and 37.5% higher compared to S01 under 0% and 100% axial load, respectively (note that no testing of $S06_{phase1}$ had been conducted under the 50% axial load level). These results are expected because the steel foundation serves almost like a rigid block with very little deformability while the concrete foundation has a significantly lower modulus of elasticity. The reinforced concrete foundation also results in seating of the specimen and sometimes loosening of the anchor rods under small drift cycles due to minor crushing of the rough concrete surface under the base-plate. It was also observed that $S06_{phase1}$ had 95.6% and 84.9% higher moment capacity in the push and pull directions, respectively, in comparison to S01, which was tested on a concrete foundation. S01 had anchor rods with a yield strength of 57.7 ksi and an ultimate strength of 52.6 ksi while $S06_{phase1}$ had anchor rods with a yield strength of 47.4 ksi and an ultimate strength of 53.6 ksi. The higher yield strength of the anchor rods in S01 might have reduced an otherwise higher difference in the moment capacity between the two specimens; however, the influence is estimated to be rather low. The response of both of these specimens were governed by anchor rod elongation. S01 had longer anchor rods embedded in the concrete foundation while $S06_{phase1}$ had shorter anchor rods. Anchor rod rupture was observed in both specimens; however, during cyclic loading, the bond between the anchor rods and the concrete degraded for S01 which resulted in a lower strength. In addition, the degradation of the top concrete layer underneath the base-plate in S01 reduced the moment capacity of the connection.

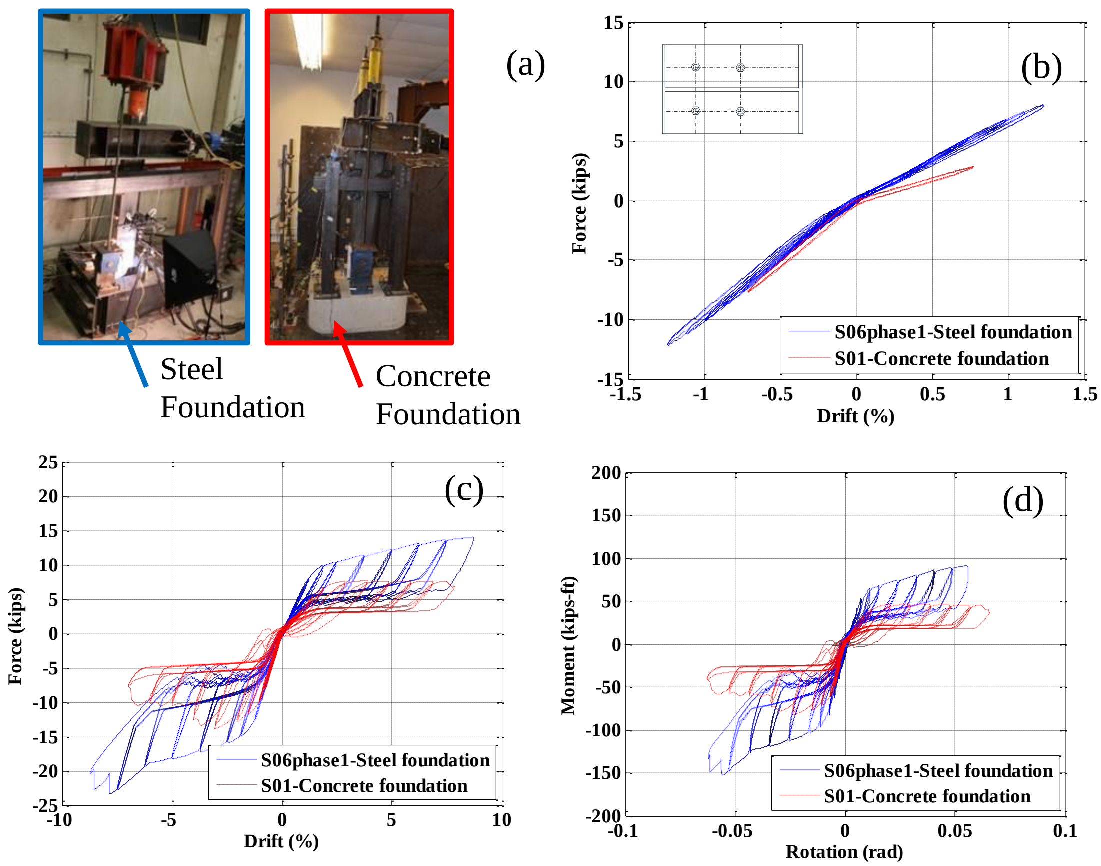

Figure 4.27. (a) Comparison of specimen configurations, (b) elastic force-drift response under 100% axial load, (c) inelastic force-drift response, and (d) inelastic moment-rotation response.

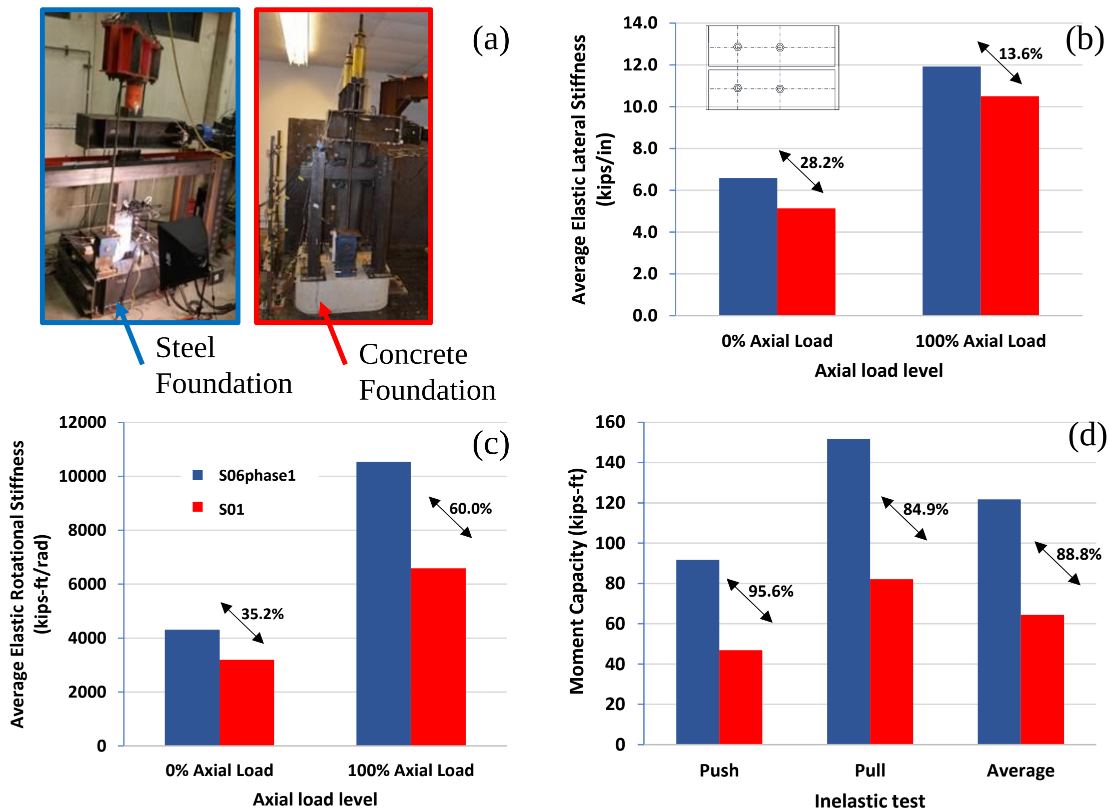

Figure 4.28. (a) Comparison of specimen configurations, (b) comparison of average lateral stiffness, (c) comparison of average rotational stiffness, and (d) comparison of moment capacity.

4.9.2. Pitch

S01 and S02 had identical connection configurations except for the pitch (distance between the anchor rods in the longitudinal direction). For S01, the pitch was 4 inch while the same for S02 was 6 inch. The test results are shown in Figure 4.29 and Figure 4.30. The results showed that the average lateral stiffness of S02 was 24.2%, 12.5% and 5.8% higher than S01 under 0%, 50% and 100% axial load. The results showed that the average rotational stiffness of S02 was 23.5%, 6.7% and 6.7% higher than S01 under 0%, 50% and 100% axial load. It was also observed that an increase of the pitch increased the moment capacity of S02 by 5.1% in the push direction and decreased the same by 9.2% in the pull direction. This is because the cantilevered section of the base-plate reduced in the push direction for S02 with 6 inch pitch, resulting in a higher strength. Additionally, with similar setback distances in both directions, the connection exhibited a more symmetric response with 6 inch pitch in comparison to 4 inch pitch. However, this led to a reduced moment capacity in the pull direction in comparison to 4 inch pitch.

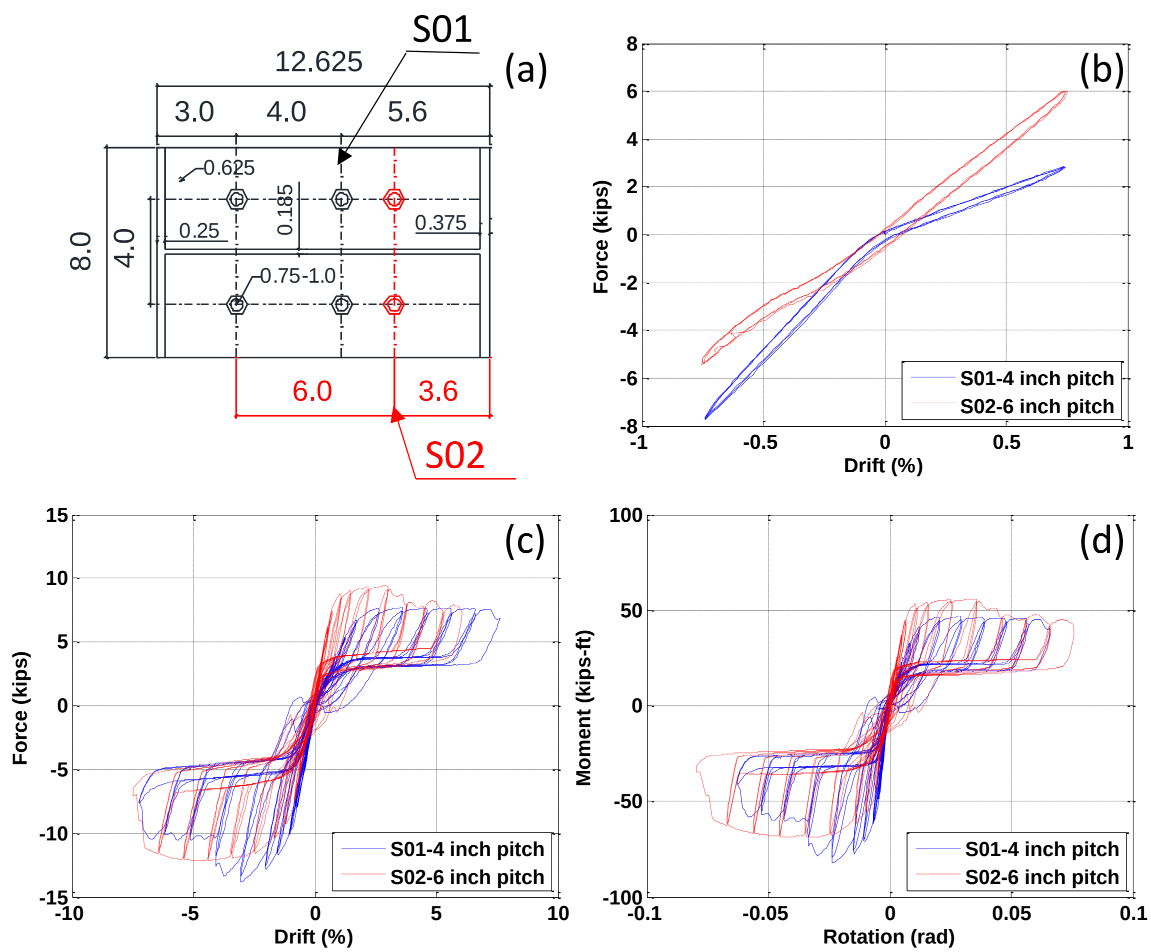

Figure 4.29. (a) Comparison of specimen configurations, (b) elastic force-drift response under 100% axial load, (c) inelastic force-drift response, and (d) inelastic moment-rotation response.

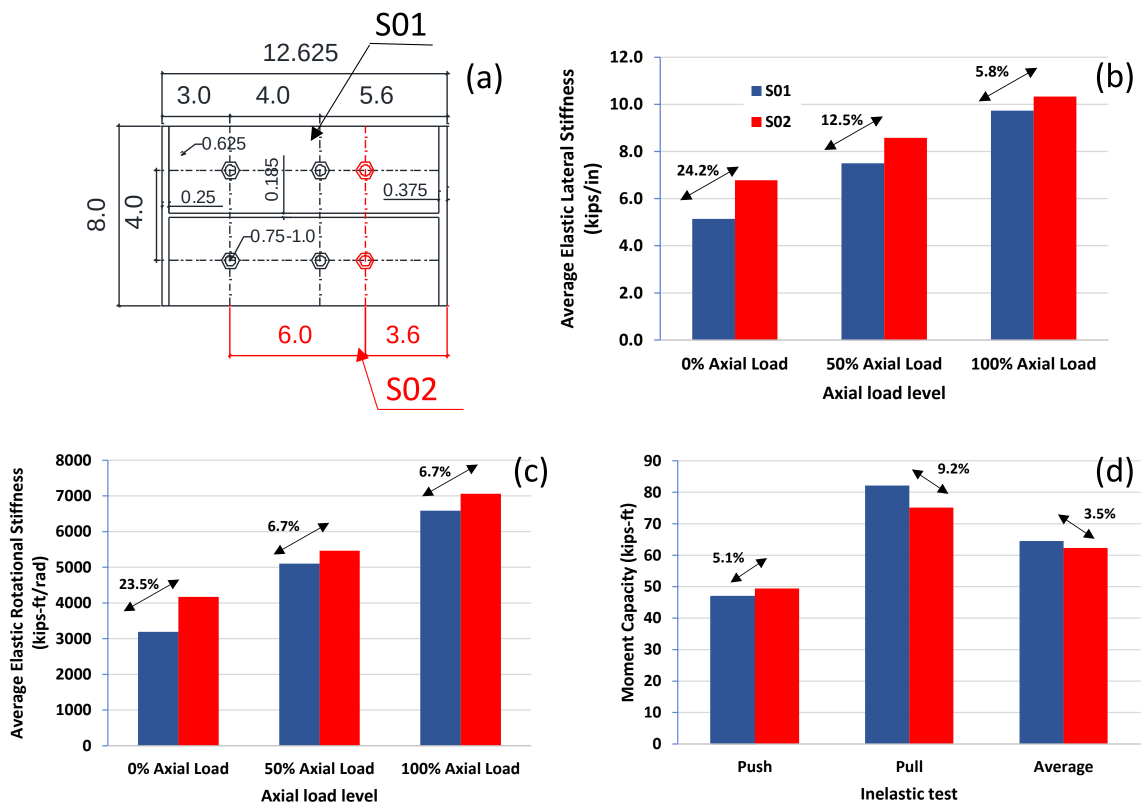

Figure 4.30. (a) Comparison of specimen configurations, (b) comparison of average lateral stiffness, (c) comparison of average rotational stiffness, and (d) comparison of moment capacity.

4.9.3. Anchor rod diameter

Between S01 and S03, the influence of the anchor rod diameter was studied. S01 had 3/4 inch diameter anchor rods while S03 had 1 inch diameter anchor rods. The results are shown in Figure 4.31 and Figure 4.32. It was found that an increase of the anchor rod diameter led to an increase in the average lateral stiffness of 17.8% and 2.7% when the specimens were tested under 0% and 50% axial load; while, there was a 3.4% decrease when the specimens were tested under 100% axial load. The differences of the lateral stiffness under 50% and 100% axial load were negligible and within the repeatability that could be achieved at this scale of testing. The average rotational stiffness of the connection with the greater anchor rod diameter increased by 34% in the 0% axial load, by 27.9% in the 50% axial load elastic test and by 30.1% at the 100% axial load test [see Figure 4.31(c) and Figure 4.32(b)]. The differences in the impact of the anchor rod diameter on the elastic lateral and rotational stiffness resulted from the fact that an increase in the anchor rod diameter resulted in lower rotations of the base-plate by 20.2%, 26.4% and 37% when the specimens were tested under 0% and 50% axial load, respectively, due to higher restraint at the base with the larger diameter anchor rods. It was also observed that the increase of the anchor rod diameter increased the moment capacity of the connection by 46.4% and 32.2% in the push and pull directions, respectively [see Figure 4.31(d) and Figure 4.32(d)].

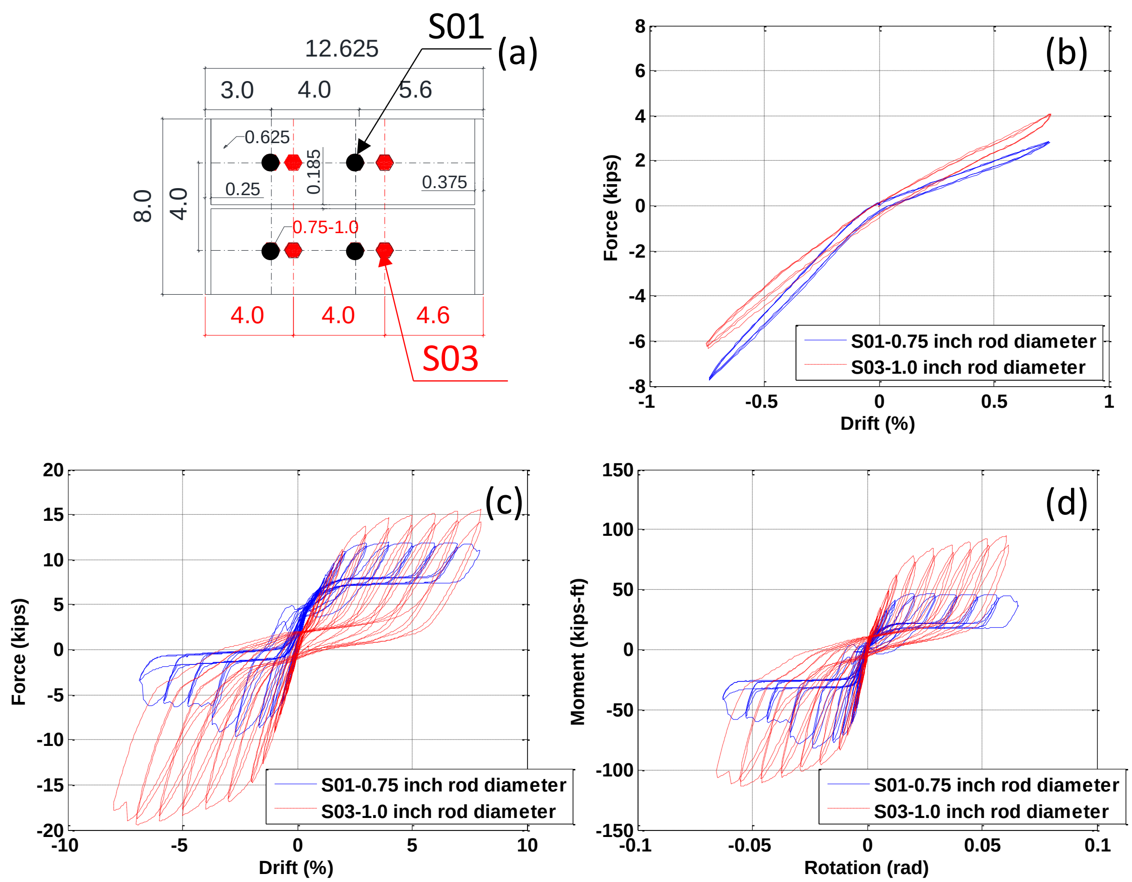

Figure 4.31. (a) Comparison of specimen configurations, (b) elastic force-drift response under 100% axial load, (c) inelastic force-drift response, and (d) inelastic moment-rotation response.

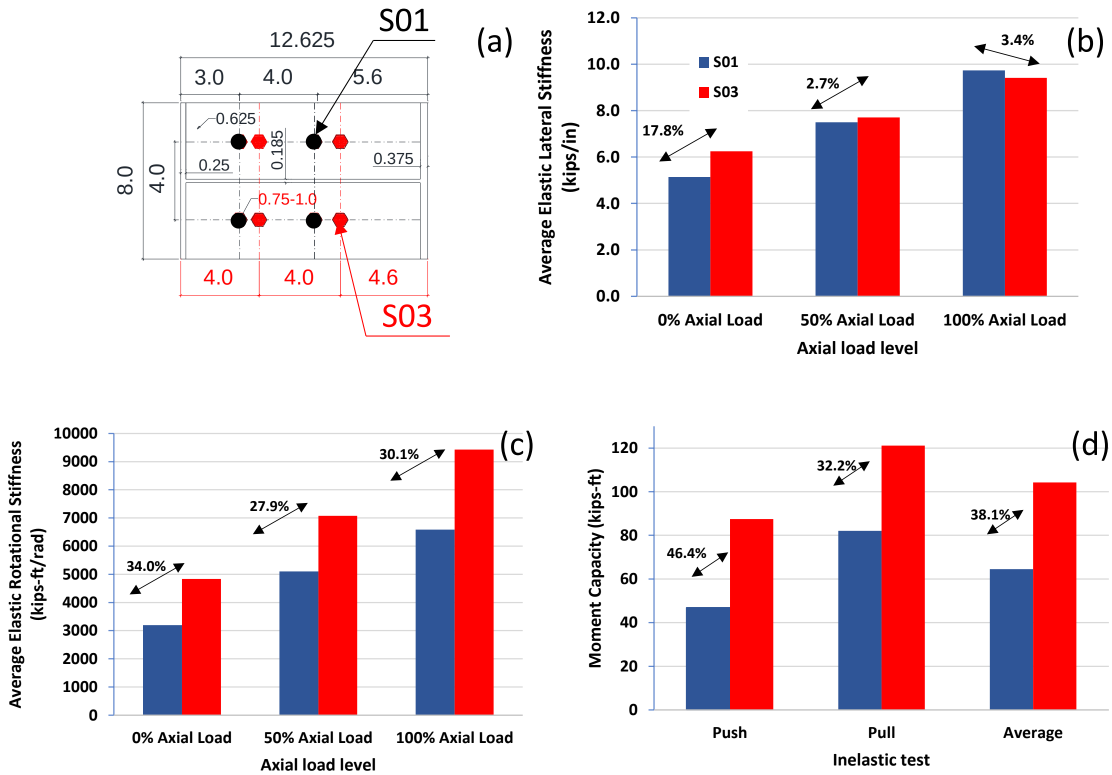

Figure 4.32. (a) Comparison of specimen configurations, (b) comparison of average lateral stiffness, (c) comparison of average rotational stiffness, and (d) comparison of moment capacity.

4.9.4. Base-plate thickness

Between S04 and S05, the influence of the base-plate thickness was studied. S04 had a 5/8 inch thick base-plate while the same for S05 was 3/8 inch. The test results are shown in Figure 4.33 and Figure 4.34. Counterintuitively, S05 with the thinner base-plate showed 17.6%, 23.0% and 27.7% higher average lateral stiffness compared to S04 with the thicker base-plate when the specimens were tested under 0%, 50% and 100% axial load, respectively. Similarly, S05 showed a higher average rotational stiffness of 36.0%, 26.6% and 36.8% when the specimens was tested under 0%, 50% and 100% axial load. With regards to the moment capacity, S04 had lower moment capacity by 51.8% and 67.2% in the push and pull directions, respectively, in comparison to S05.

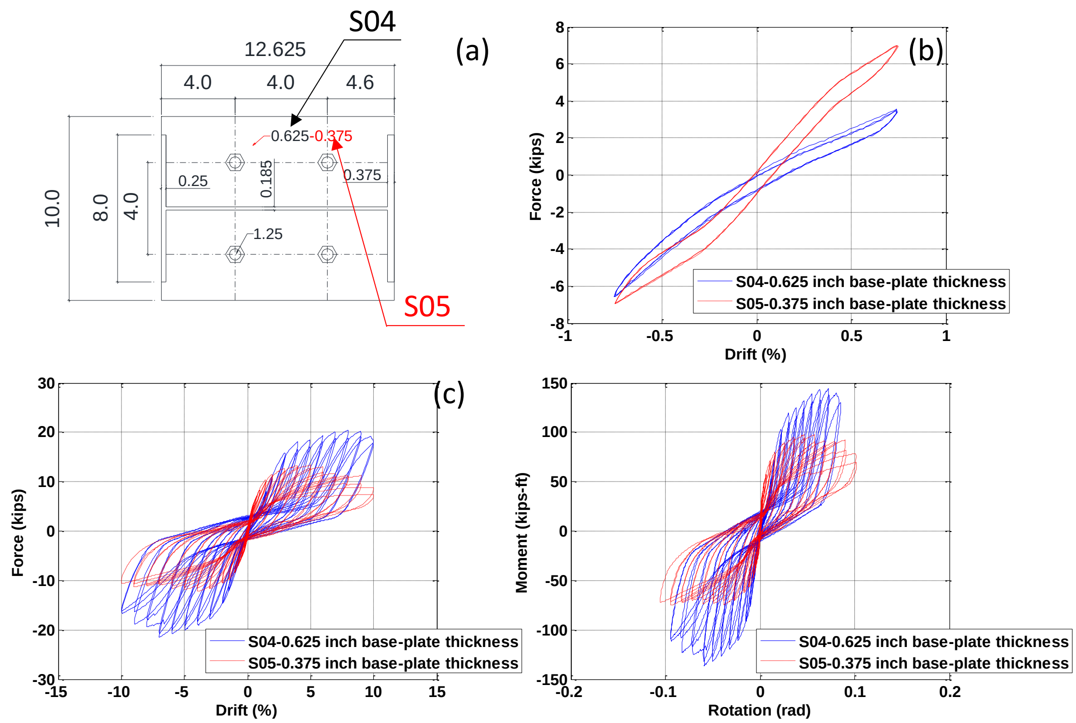

Figure 4.33. (a) Comparison of specimen configurations, (b) elastic force-drift response under 100% axial load, (c) inelastic force-drift response, and (d) inelastic moment-rotation response.

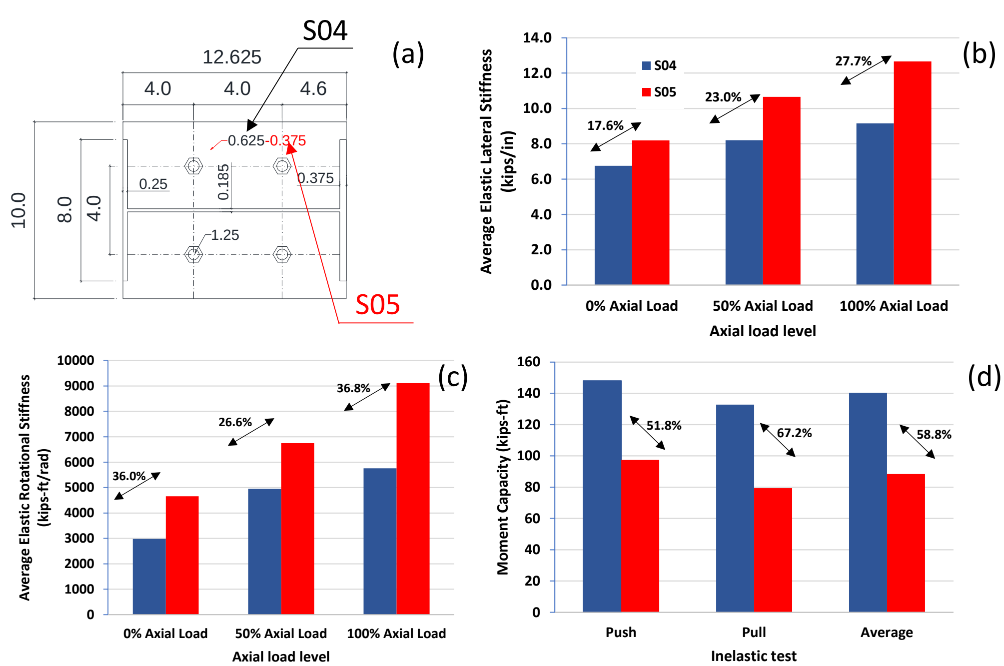

Figure 4.34. (a) Comparison of specimen configurations, (b) comparison of the average lateral stiffness, (c) comparison of the average rotational stiffness, and (d) comparison of moment capacity.

With regards to these counterintuitive stiffness values obtained from the tests, it is postulated here that the increase in the average rotational stiffness of the connection with thinner base-plate configuration is because the overall stiffness of these two connections were governed by the axial stiffness of the anchor rods. The axial stiffness, k_{axial}, of a tension member is given by

$$\mathrm{k_{axial}} = \mathrm{AE/L}, \tag{4-3}$$

where, A is the area of the tension member (inch^2), E is the elastic modulus (ksi), and L is the length of the tension member (inch).

The thinner base-plate results in a reduced length and hence a higher axial stiffness of the anchor rods. The axial stiffness of an individual anchor rod for thinner base-plate configuration (S05) was calculated as 74,936 lb/inch while the same number for the thicker base-plate was (S04) was 44,962 lb/inch. The former is 67% higher than the latter, which partially explains the higher stiffness of the configuration with the thinner base-plate (or anchor rods with shorter unrestraint portion).

In the inelastic range, the two specimens (S04 and S05) showed two different behavior. Specifically, S04 (5/8 inch thick base-plate) showed a rocking behavior while Specimen 05 (3/8 inch thick base-plate) showed a more flexural bending behavior. As a result, the specimen with thicker base-plate (S04) showed a significantly higher lateral strength compared to the specimen with the thinner base-plate (S05). The results from these two specimens cannot be generalized to all the connection configurations. A more systematic investigation looking into combined effect of anchor rod diameter and number of anchor rods along with the base-plate thickness needs to be conducted for a better understanding of the connection stiffness and strength. This point is further reflected upon through the comparison below of S09 and S10, which also had identical base-plate connection configurations except for the base-plate thickness.

The second comparison for the base-plate thickness was made between S09 and S10. The base-plate thickness of S09 was 5/8 inch while the same for S10 was 3/4 inch. The test results are shown in Figure 4.35 and Figure 4.36. It was found that the average lateral stiffness of the connection corresponding to thicker base-plate (S10) was 5.3%, 1.1% and 5.6% higher when the specimens were tested under 0%, 50% and 100% axial load, respectively. Similarly, the rotational stiffness of S10 was 3.5% higher than S09 when tested under 100% axial load. As explained previously, no data was available to quantify the rotational stiffness of S07-S10 under 0% and 50% of axial load. It was also observed that S10 had 10.5% and 11.3% higher moment capacity in the push and pull directions, respectively.

The higher average elastic lateral and rotational stiffness of S10 with the thicker base-plate in comparison to S09 could be explained as follows. Note that this finding was contrary to what was observed for S04 and S05. First, the difference in the base-plate thicknesses of S09 and S10 was marginal (1/8 inch) and accordingly the differences in the elastic average lateral stiffness were minimal ranging from 1.1% to 5.6%. S10 had 23.4% higher average rotational stiffness compared to S09 under 100% axial load. The differences in the impact of the base-plate thickness on the rotational stiffness resulted from the fact that an increase in the base-plate thickness resulted in lower rotations of the base-plate by 20.4% when the specimens were tested under 100% axial load, due to higher restraint at the base with the larger base-plate thickness. Second, S09 and S10 both had eight 1 1/4 inch diameter anchor rods in comparison to S04 and S05 which had four 1 ¼ inch diameter anchor rods. It may be partially concluded that when the number of anchor rods is higher (8 versus 4 in this case), the elastic lateral and rotational stiffness of the column base-plate connection is not highly dependent on the anchor rod axial stiffness, rather, it is dependent on the base-plate thickness because the connection shows a more flexural bending behavior than a rocking behavior as a result of higher fixity. Again, further research is needed to investigate the influence of number of anchor rods and anchor rod diameter in relation to the base-plate thickness.

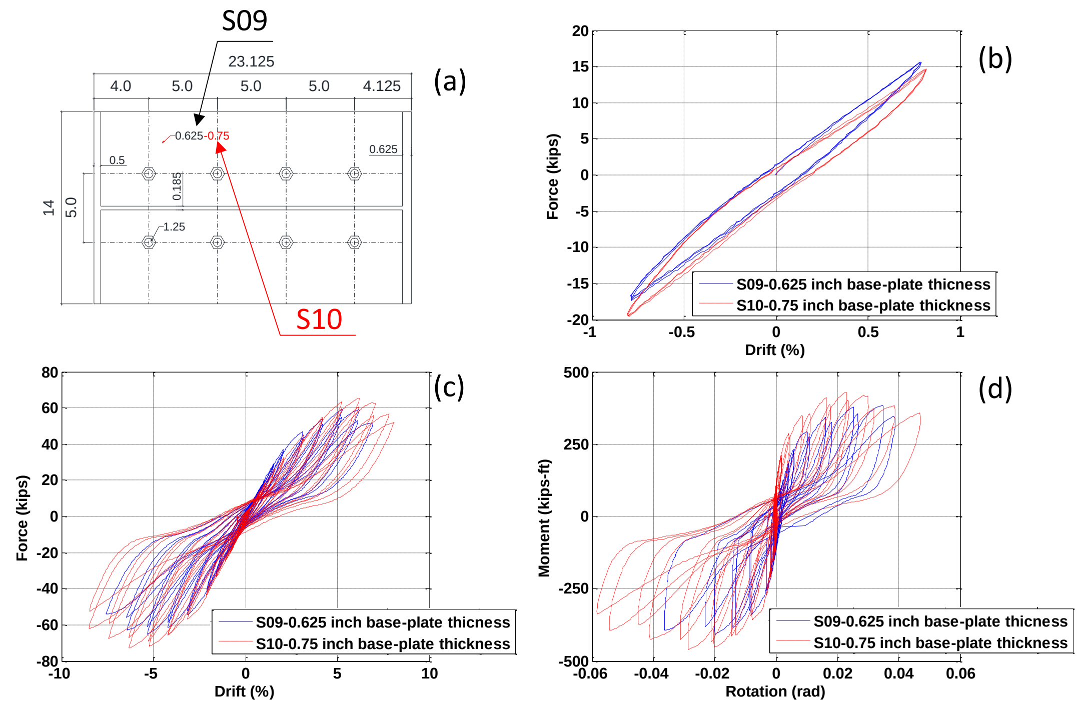

Figure 4.35. (a) Comparison of specimen configurations, (b) elastic force-drift response under100% axial load, (c) inelastic force drift response, and (d) inelastic moment-rotation response.

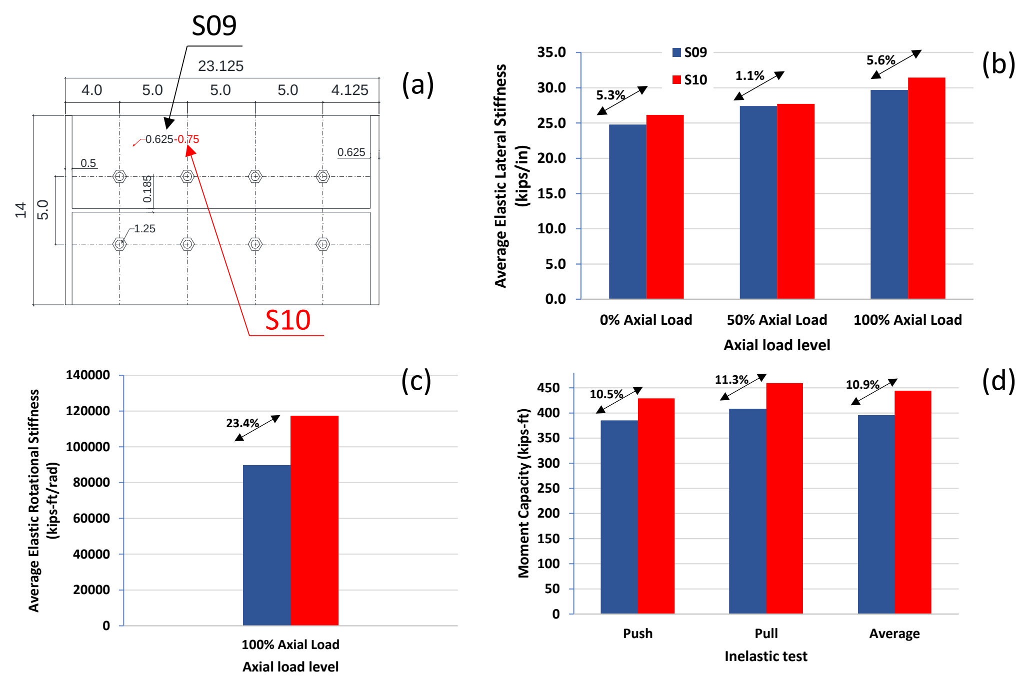

Figure 4.36. (a) Comparison of specimen configurations, (b) comparison of lateral stiffness, (c) comparison of rotational stiffness, and (d) comparison of moment capacity.

4.9.5. Flange thickness

Between S04 and S06, the influence of the flange thickness on the stiffness and strength of the connections was studied. The outside and inside flanges of S04 were 1/4 inch and 3/8 inch thick, respectively, while for S06 these were 1/2 inch and 5/8 inch. The test results are presented in Figure 4.37 and Figure 4.38. It was found that an increase in the flanges thicknesses (S06) led to 14.5%, 27.2% and 32.2% higher average lateral stiffness, respectively, compared to the specimen with thinner flanges (S04) when the specimens were tested under 0%, 50% and 100% axial load. Similarly, the connection with thicker flanges (S06) had 41.9%, 46.6% and 54.3% higher average rotational stiffness when the specimens were tested under 0%, 50% and 100% axial load, respectively. It was also observed that the specimen with thicker flanges (S06) had 19.5% and 2.0% less moment capacity in the push and pull directions, respectively, than the specimen with thinner flanges (S04). This was due to the failure mode of the connections. S06 ultimately failed due to rupture of the welds between the base-plate and the web and flanges, which was characterized by a more brittle failure at a drift level of approximately 8%. On the other hand, a more ductile behavior was observed for S04, and the failure was achieved through combined yielding of the flanges, the base-plate and the web, and moderate cracking of the concrete foundation while the anchor rods were slightly damaged. In summary, for the two connection configurations compared here, an increase in the flanges thicknesses led to increased elastic average lateral and rotational stiffness; however, it led to reduced lateral strength and moment capacity of the connection due to weld failure.

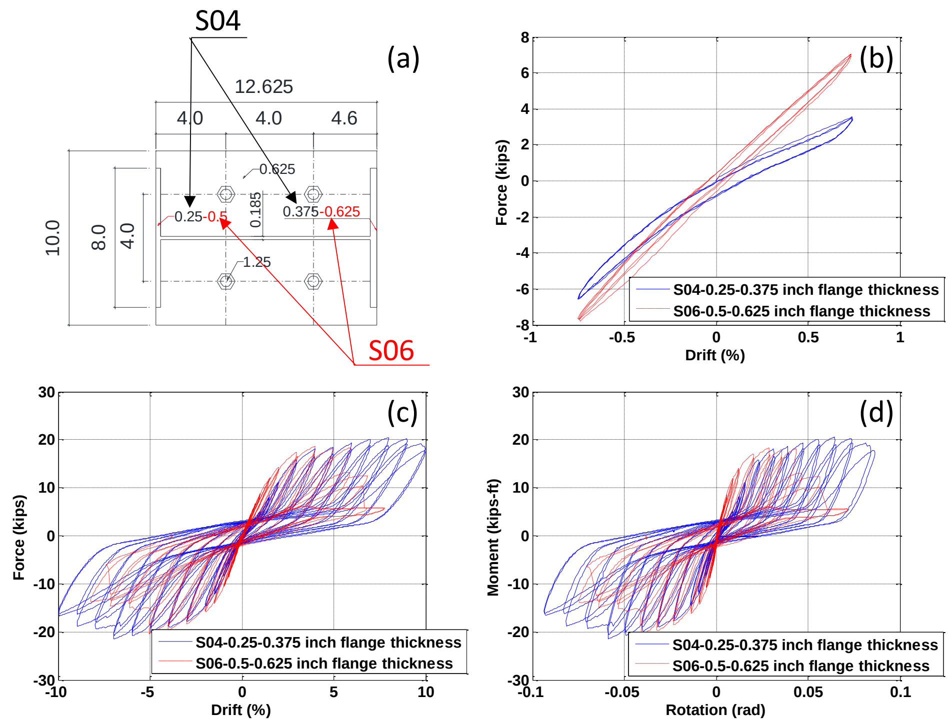

Figure 4.37. (a) Comparison of specimen configurations, (b) elastic force-drift response under 100% axial load, (c) inelastic force-drift response, and (d) inelastic moment-rotation response.

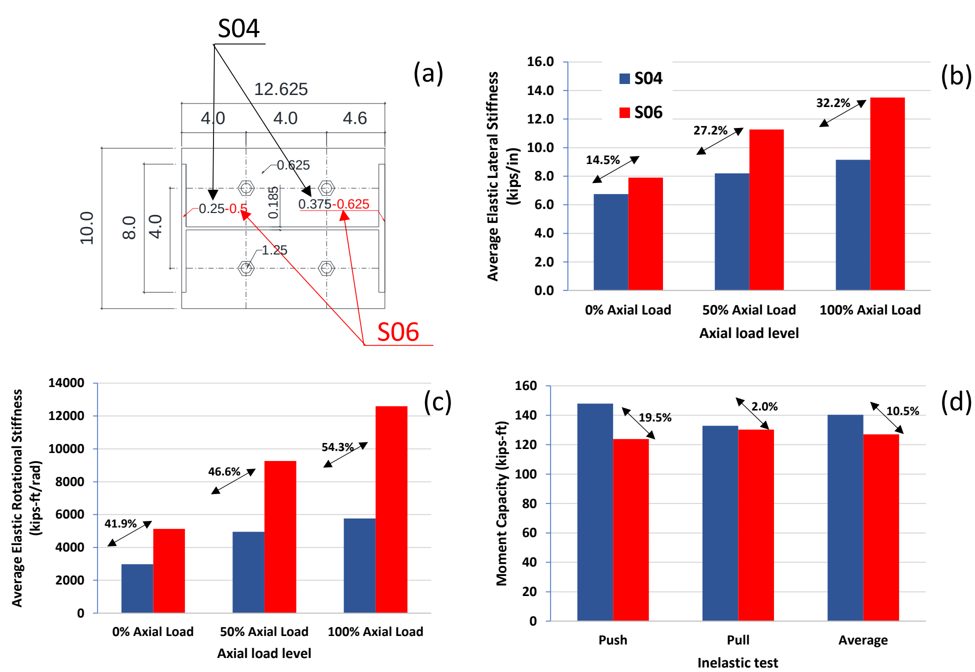

Figure 4.38. (a) Comparison of specimen configurations, (b) comparison of average lateral stiffness, (c) comparison of average rotational stiffness, and (d) comparison of moment capacity.

4.9.6. Number of anchor rods

Between S07 and S08, the influence of the number of anchor rods was studied. S07 had six anchor rods while S08 had eight anchor rods. The results are shows in Figure 4.39 and Figure 4.40. It was found that the base-plate connection with the eight anchor rods (S08) had 22.1%, 14.9% and 18.2% higher average lateral stiffness compared to the specimen with six anchor rods (S07) when the specimens were tested under 0%, 50% and 100% axial load. In addition, it was found that the base-plate connection with eight anchor rods (S08) had 49.0% higher average elastic rotational stiffness compared to S07 under 100% axial load. It was also observed that S08 had 27.1% and 1.4% higher moment capacity in the push and pull direction, respectively. The asymmetrical configuration of the anchor rods on the base-plate of S07 led to different elastic stiffness and moment capacity in the push and pull directions, while S08 had a more symmetric response as shown in Figure 4.39 (d).

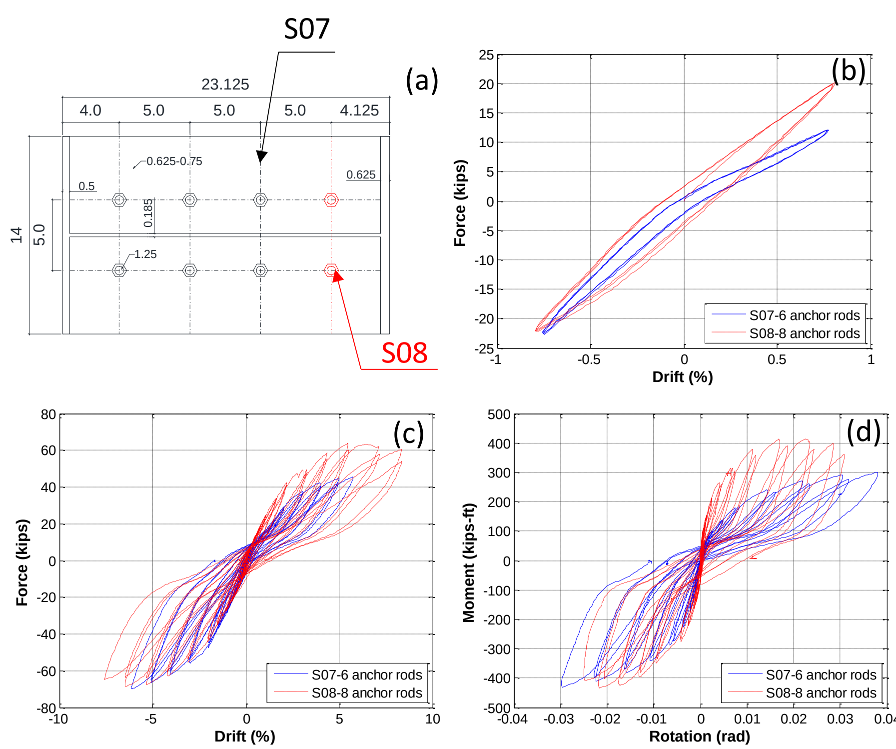

Figure 4.39. (a) Comparison of specimen configurations, (b) elastic force-drift response under 100% axial load, (c) inelastic force-drift response, and (d) inelastic moment-rotation response.

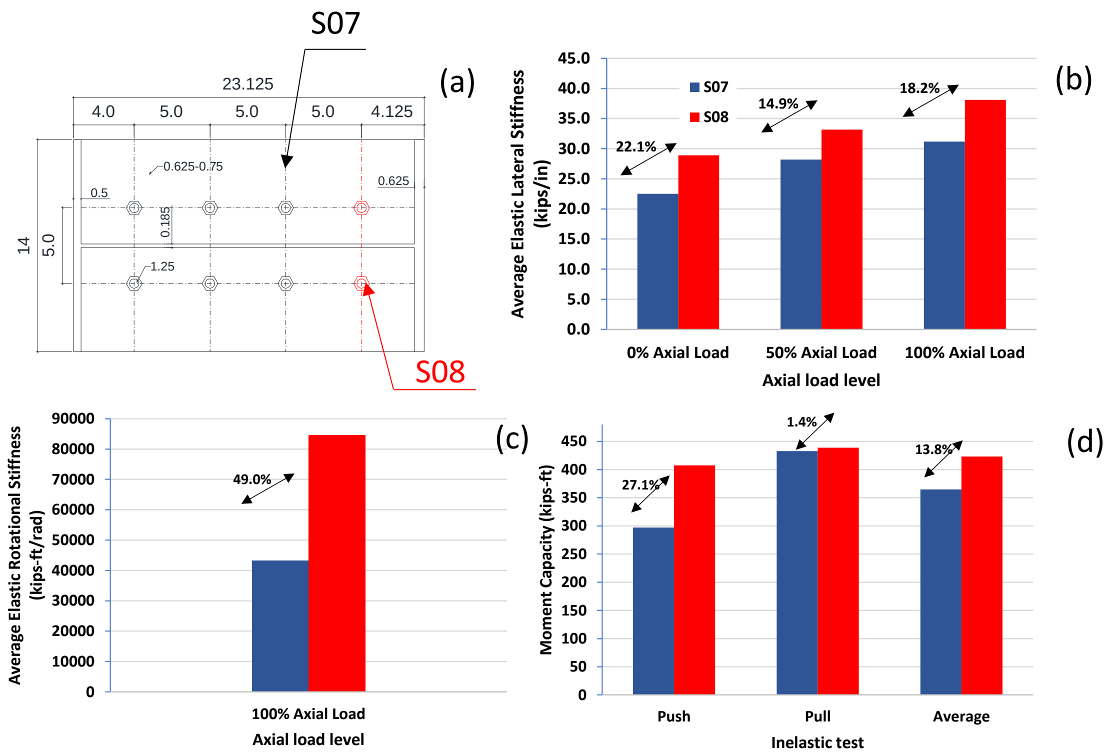

Figure 4.40. (a) Comparison of specimen configurations, (b) comparison of average lateral stiffness, (c) comparison of average rotational stiffness, and (d) comparison of moment capacity.

4.9.7. Repeatability

S08 and S09 had the identical connection configuration. Between these two specimens, the potential variability in the results due to fabrication and construction tolerances and the material properties of the reinforced concrete foundation was checked. The results are shown in Figure 4.41 and Figure 4.42. It was found that the average lateral stiffness differed by 13.4% when the specimens were tested under 100% axial load. Note that the average lateral stiffness calculated from the inelastic tests at 2% drift level are used for this comparison. The average rotational stiffness differed up to 5.7% under the 100% axial load. It was also observed that the moment capacity differed by 6.0% and 7.7% in the push and pull directions, respectively.

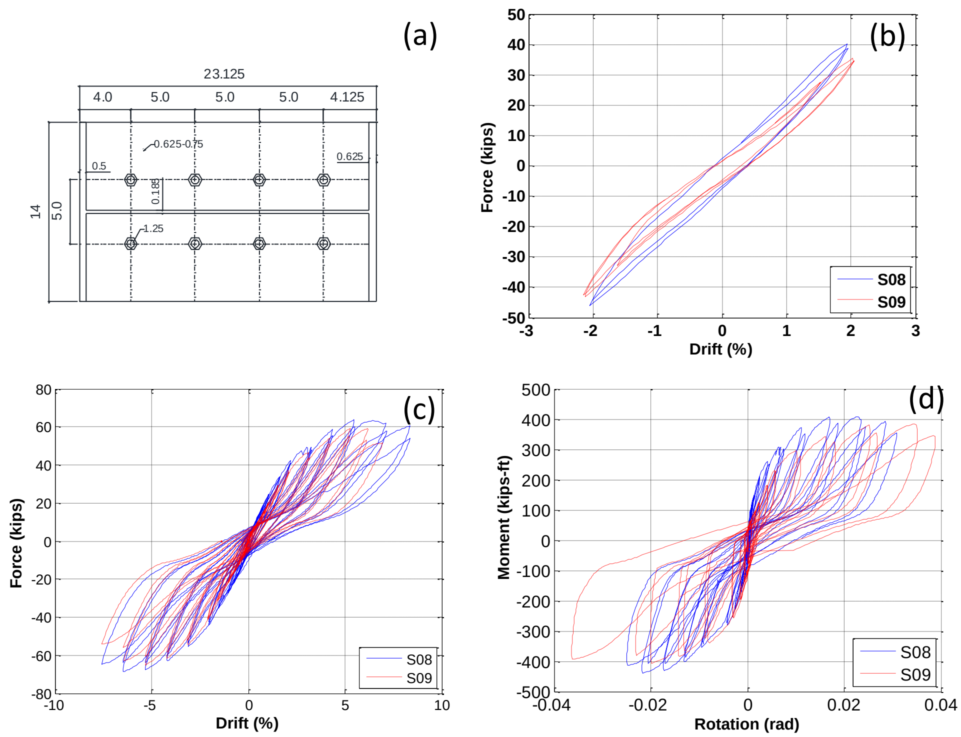

Figure 4.41. (a) Specimens configuration, (b) elastic force-drift response at 2% drift limit under 100% axial load, (c) inelastic force-drift response, and (d) inelastic moment-rotation response.

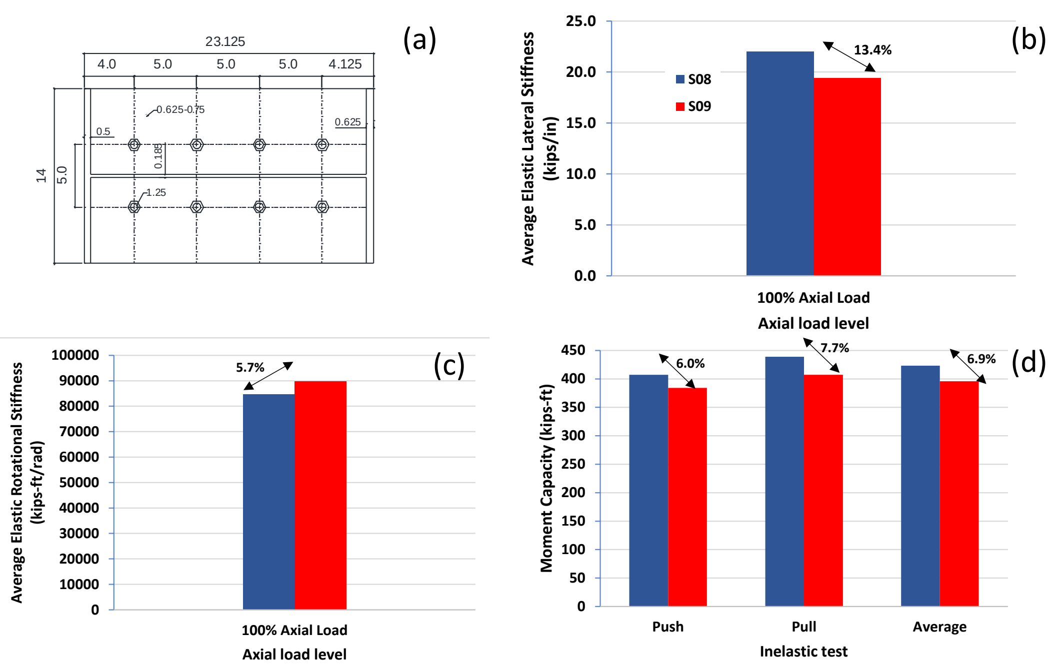

Figure 4.42. (a) Specimens configuration, (b) comparison of average lateral stiffness, (c) comparison of average rotational stiffness, and (d) comparison of moment capacity.

4.10. Damage Evaluation of the Specimens

The specimens were grouped into four categories according to their failure mechanisms as shown in Table 4.11. Each of the damage states were quantitatively determined according to the criteria shown in Table 4.12. The damage observed for each group and each specimen are presented in detail in Sections 4.10.1-4.10.4

Table 4.11. Grouping of the Specimens According to Observed Damage.

Group	Specimen	Outside F.	Inside F.	Base Plate	Web	Foundation	Anchor Rods
1	**01**	N	N	S	N	S	E/R (1)
	02	S	N	S	N	S	E/R (2)
	11	S	N	S	S	S	E
2	**03**	M	M	M	S	M	S
	04	M	M	E/WR	M	M	S
3	**05**	M	E/WR	E/WR	M	N	N
	06	E/WR	E/WR	E/WR	M	N	S
4	**07**	S	N	M	N	E	S
	08	S	N	M	N	E	S
	09	S	N	M	N	E	S
	10	S	N	M	S	E	S

*N=None, S=Slight, M=Moderate, E=Excessive, E/R=Excessive/Rupture (number of anchor rods ruptured), E/WR=Excessive/Weld Rupture

Table 4.12 Quantitative Evaluation of the Observed Damage.

Observed Damage	Flanges	Base Plate	Anchor rods	Web*	Foundation
None	0-800 μstrain	0-800 μstrain	0-800 μstrain	No white wash flaking	No cracking
Slight	800-1500 μstrain	800-1500 μstrain	800-1500 μstrain	White wash flaking up to 2 inches height	Cracking underneath the base-plate area
Moderate	1500-2500 μstrain	1500-2500 μstrain	1500-2500 μstrain	White wash flaking up to 4 inches height	Cracking underneath and around the base-plate area
Excessive	Rupture of the welds between the base-plate and the flanges	Rupture of the welds between the base-plate and the flanges and web	>2500 μstrain or rupture	Rupture of the welds between the base-plate and the web	Cracking of the entire concrete foundation

*Strain gages were not placed on the web.

The failure modes observed during the tests were yielding of the flanges, the base-plate, and the web, yielding and rupture (in some cases) of the anchor rods, rupture of the welds between the column and the base-plate, and cracking of the concrete foundations. These four categories are described below.

Specimens for which the energy absorption was mainly achieved through excessive yielding of the anchor rods while slight or no yielding of the flanges, the web and the base-plate, and slight cracking of the reinforced concrete foundation were observed (S01, S02 and S11). The ultimate failure was due to rupture of the anchor rods.

Specimens for which the energy absorption was mainly achieved through combined yielding of the flanges, the base-plate and the web, and moderate cracking of the concrete foundation while the anchor rods slightly yielded (S03 and S04).

Specimens for which the energy absorption was mainly achieved by yielding of the flanges and the web. The ultimate failure was due to rupture of the welds between the base-plate and the web, and the base-plate and the flanges. The concrete foundation did not experience any significant damage and the anchor rods had slight to no damage (S05 and S06).

Specimens for which the energy absorption was mainly achieved through excessive cracking of the concrete foundations while the base-plate had moderate damage and the flanges and anchor rods had slight to no damage (S07, S08, S09 and S10).

4.10.1. Damage group 1

The behavior of the first group of specimens (S01, S02 and S11) was dominated by a rocking behavior with energy absorption mainly occurring through yielding of the anchor rods and the ultimate failure occurring due to anchor rod rupture. The behavior of each specimen of this group is presented below.

The geometric characteristics of S01 and its moment versus rotation response are shown in Figure 4.43(a) and (b), respectively. The condition of the specimen and the foundation after the completion of the test are shown in Figure 4.43(c) to (f). The energy absorption of S01 mainly occurred through yielding of the anchor rods and slight yielding of the base-plate and the foundation cracking underneath the base-plate area. The ultimate failure was due to rupture of one of the anchor rods at the second cycle of the 7% drift level (corresponds to 0.058 rad rotation) in the pull direction. The combination of the relatively thick base-plate (5/8 inch) and the small anchor rods (3/4 inch diameter) induced this failure mode.

The geometric characteristics of S02 and its moment versus rotation response are shown in Figure 4.44(a) and (b), respectively. The condition of the specimen and the foundation after the completion of the test are shown in Figure 4.44(c) to (f). The energy absorption of S02 mainly occurred through yielding of the anchor rods and slight yielding of the base-plate, the web and the outside flange. The foundation was slightly cracked underneath the base-plate area. The ultimate failure was due to rupture of two of the anchor rods at the first cycle of the 8% drift level (corresponds to 0.08 rad rotation) in the pull direction. The combination of the relatively thick base-plate (5/8 inch) and the small anchor rod diameter (3/4 inch diameter) induced this failure mode.

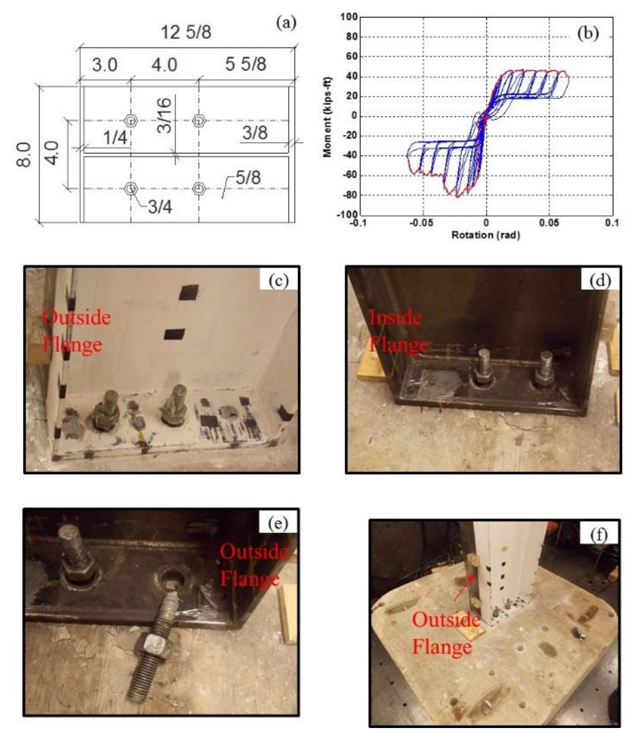

Figure 4.43. (a) S01 base-plate configuration, (b) moment-rotation response, (c) no yielding in the flanges and base-plate, (d) slight concrete cracking under the base-plate, (e) rupture of the anchor rod, and (f) concrete foundation and column after testing.

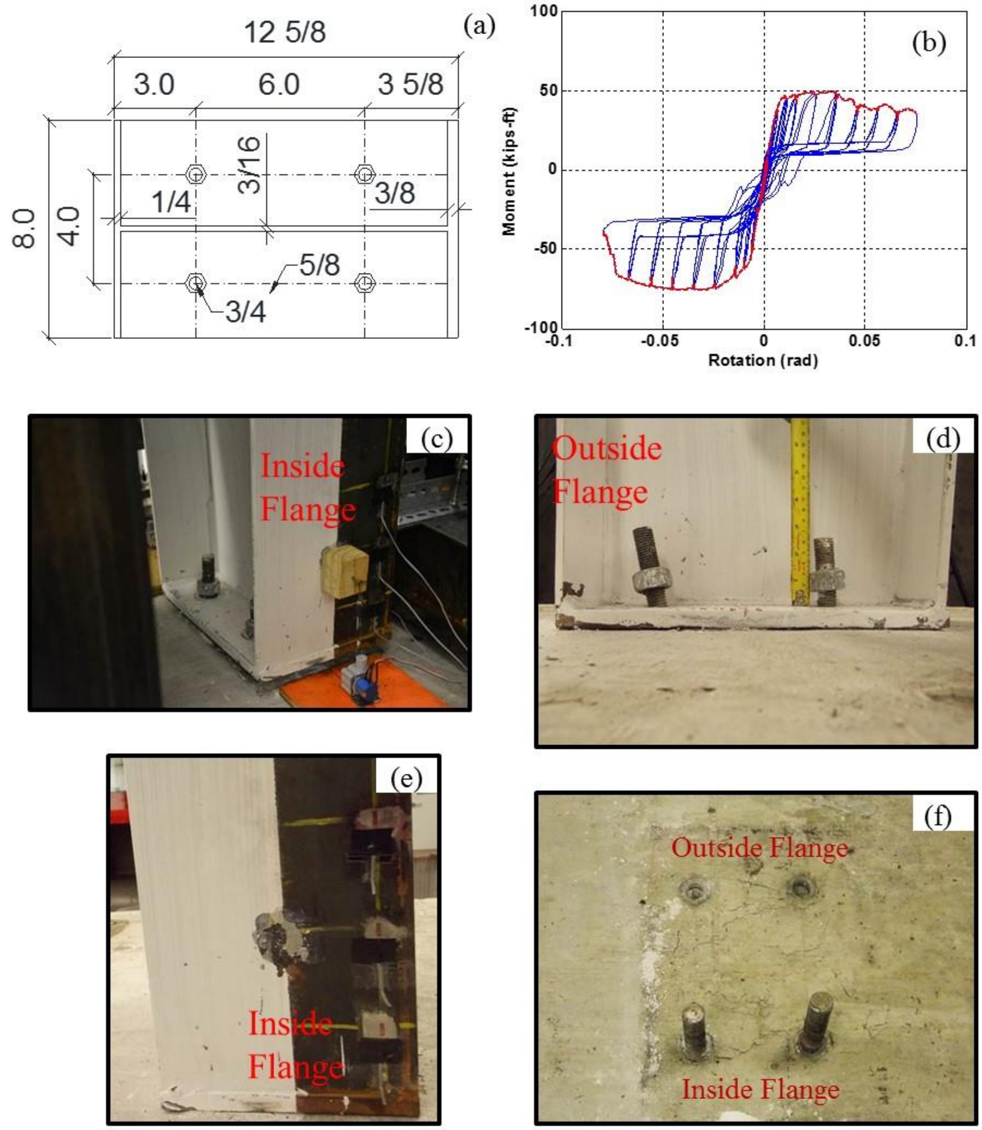

Figure 4.44. (a) S02 base-plate configuration, (b) moment-rotation response, (c), (d) and (e) no yielding in the flanges and the base-plate, and (f) rupture of the anchor rods closer to the outside flange and slight concrete cracking under the base-plate.

The geometric characteristics of S11 and its moment versus rotation response are shown in Figure 4.45(a) and (b), respectively. The condition of the specimen and the foundation after the completion of the test are shown in Figure 4.45(c) to (f). The energy absorption of S11 mainly occurred through yielding of the anchor rods and slight yielding of the base-plate, the web and the outside flange. The foundation underneath the base-plate area cracked slightly. The ultimate failure was due to the excessive yielding of the anchor rods. S11 was tested up to 10% drift level (corresponds to 0.1 rad rotation in the push direction and 0.13 rad rotation in the pull direction). The combination of the relatively thick base-plate (1/2 inch) and the small anchor rods (3/4 inch diameter) induced this failure mode.

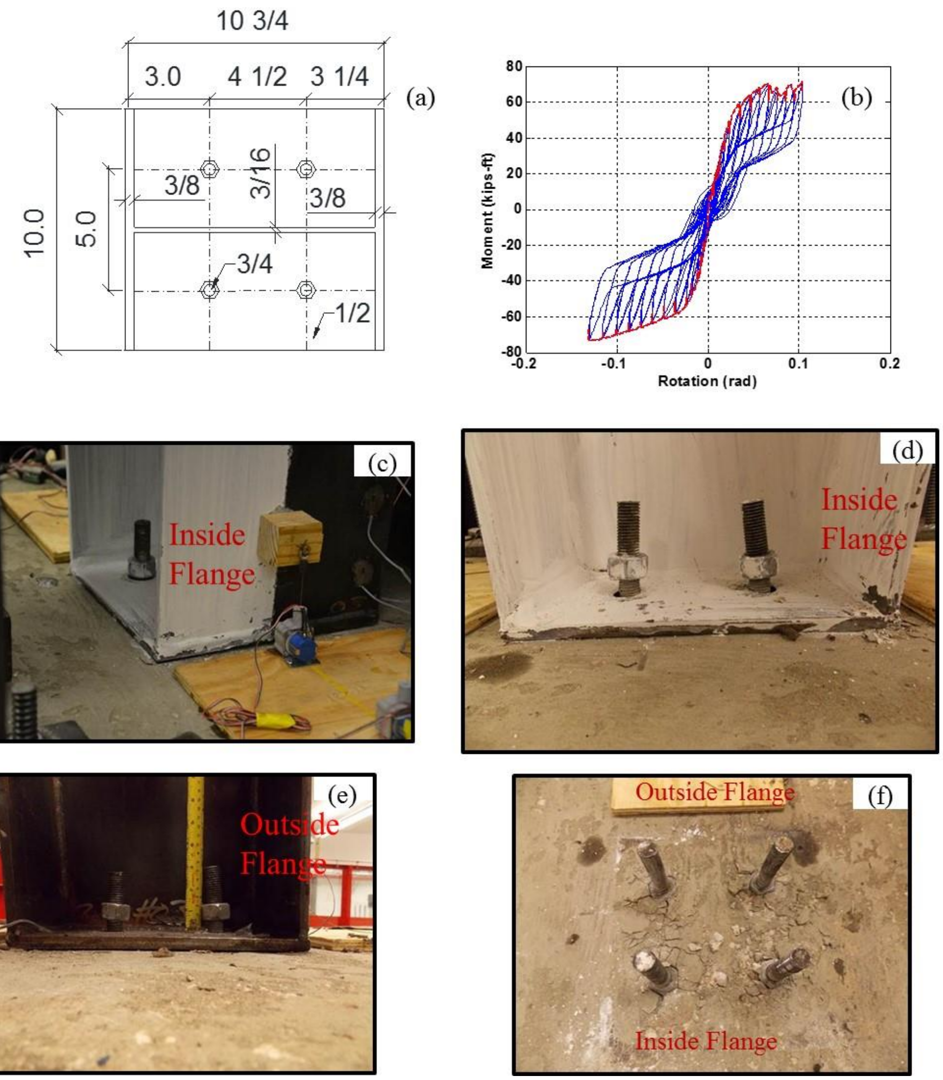

Figure 4.45. (a) S11 base-plate configuration, (b) moment-rotation response, (c) no yielding in the flanges and base-plate, (d), (e) yielding of the anchor rods, (f) concrete cracking under the base-plate after testing.

4.10.2. Damage group 2

The specimens (S03 and S04) in the second damage group were dominated by a more flexural response. Their energy absorption was mainly achieved through combined yielding of the flanges, the base-plate and the web, and moderate cracking of the concrete foundation while the anchor rods were slightly damaged. The damage evaluation of the specimens consisting this group are presented below.

The geometric characteristics of S03 and its moment versus rotation response are shown in Figure 4.46(a) and (b) respectively. The condition of the specimen and the foundation after the completion of the test are shown in Figure 4.46(c) to (f). The energy absorption of S03 mainly occurred through moderate yielding of the flanges and the base-plate, slight yielding of the web and the anchor rods, and moderate cracking of the foundation underneath the base-plate area. S03 was tested up to 8% drift level (corresponds to 0.061 rad rotation in push direction and 0.066 rad rotation in pull direction). The combination of the relatively thick base-plate (5/8 inch) and the large anchor rods (1 inch diameter) induced this failure mode.

The geometric characteristics of S04 and its moment versus rotation response are shown in Figure 4.47(a) and (b), respectively. The condition of the specimen and the foundation after the completion of the test are shown in Figure 4.47(c) to (f). The energy absorption of S04 mainly occurred through excessive yielding of the base-plate, moderate yielding of the flanges and the web, slight yielding of the anchor rods and moderate cracking of the foundation underneath and around the base-plate. S04 was tested up to 10% drift level (corresponds to 0.084 rad rotation in push direction and 0.095 rad rotation in the pull direction). S04 was the only specimen which showed buckling of the outside flange [see Figure 4.47(e)]. Additionally, S04 experienced base-plate rupture between the anchor rods and the weld that connects the web with the base-plate [see Figure 4.47(c)]. The combination of the relatively thick base-plate (5/8 inch) and the large anchor rods (1 1/4 inch diameter) induced this failure mode.

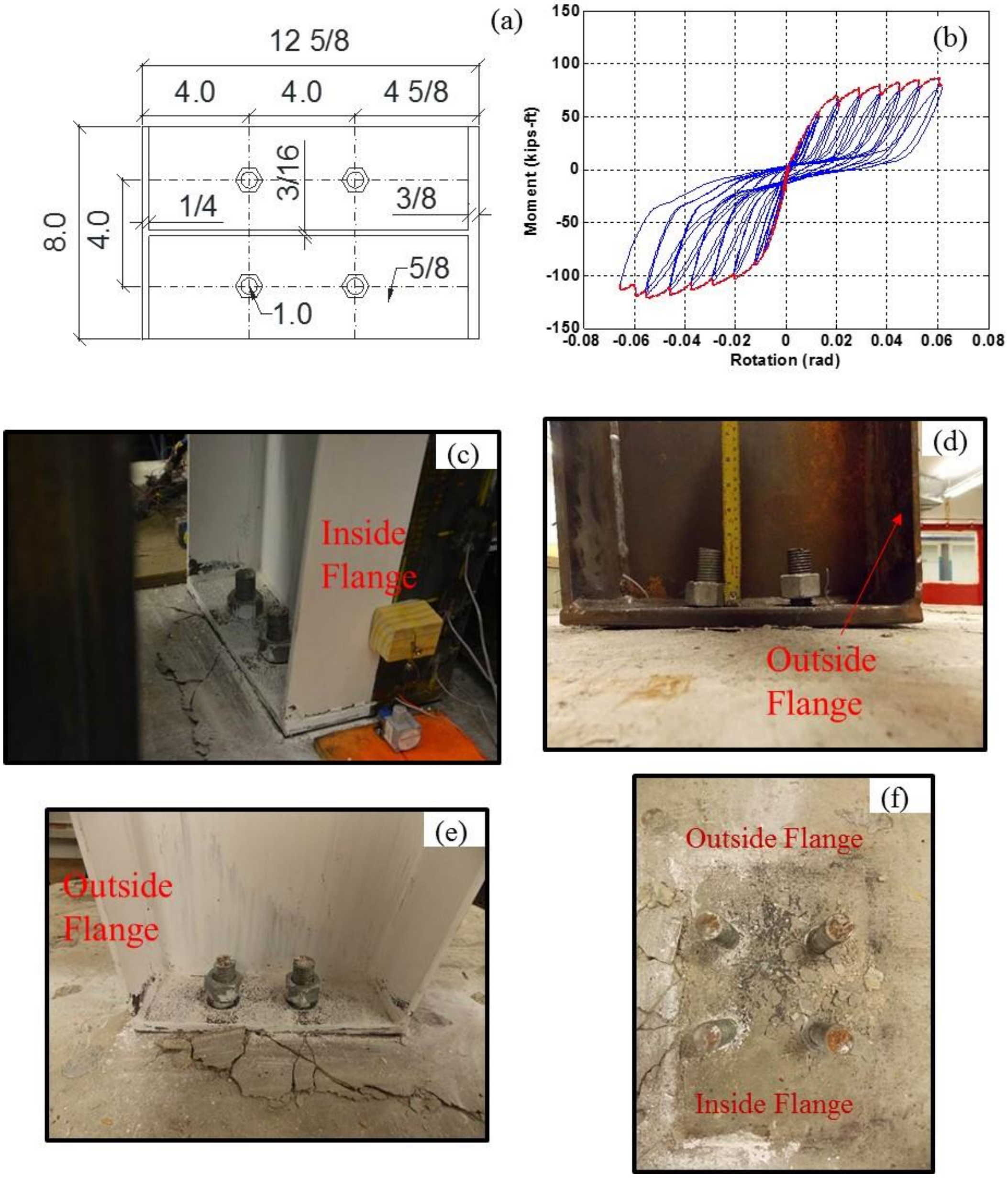

Figure 4.46. (a) S03 base-plate configuration, (b) moment-rotation response, (c) flaking of white wash in the flanges and base-plate, (d) permanent deformation of the base-plate, (e) and (f) moderate concrete cracking around the base-plate.

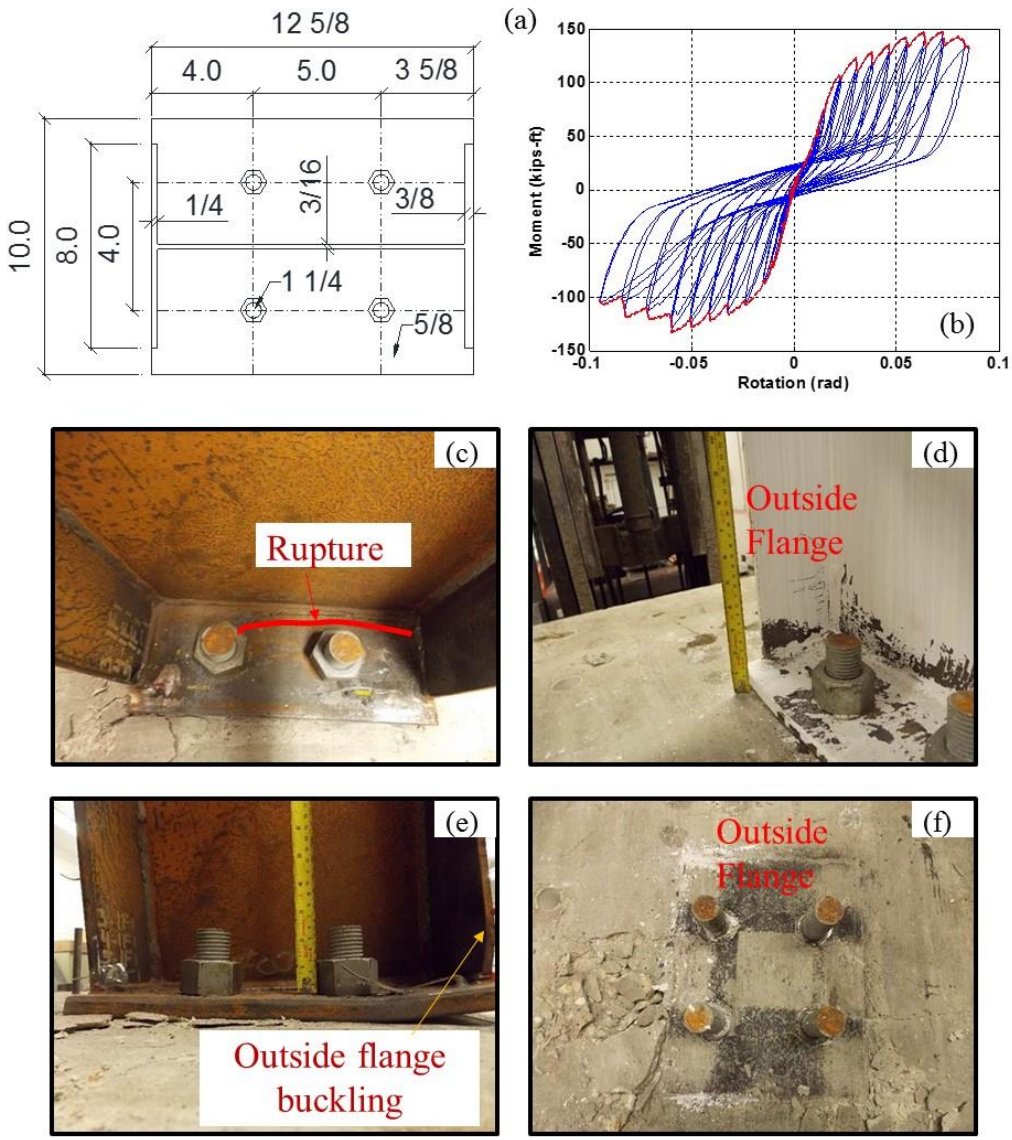

Figure 4.47. (a) S04 base-plate configuration, (b) moment-rotation response, (c) weld rupture between web and base-plate and base-plate rupture, (d) moderate yielding of the flange, web and the base-plate, (e) outside flange buckling, and (f) concrete cracking.

4.10.3. Damage group 3

The energy absorption for the third group of specimens (S05 and S06) was mainly achieved through yielding of various components of the base-plate connection. The ultimate failure was due to the rupture of the welds between the base-plate, the flanges and the web. The concrete foundation did not experience significant damage and the anchor rods had slight to no damage. The damage evaluation of S05 and S06 consisting this damage group are presented below.

The geometric characteristics of S05 and its moment versus rotation response are shown in Figure 4.48(a) and (b), respectively. The condition of the specimen and the foundation after the completion of the test are shown in Figure 4.48(c) to (f). The energy absorption of S05 mainly occurred through moderate yielding of the outside flange and the web while no cracking of the foundation underneath the base-plate area was observed. S05 was tested up to 10% drift level (corresponds to 0.1 rad rotation in the push and pull directions). At the ultimate stage, rupture of the welds connecting the base-plate to the flanges and the web was observed. The combination of the relatively thin base-plate (3/8 inch) and large anchor rods (1 1/4 inch diameter) and relatively thick flanges (1/4 inch outside and 3/8 inch the inside flange) led to a more flexurally dominated behavior of the specimen and induced this failure mode.

The geometric characteristics of S06 and its moment versus rotation response are shown in Figure 4.49(a) and (b), respectively. The condition of the specimen and the foundation after the completion of the test are shown in Figure 4.49(c) to (f). The energy absorption of S06 mainly occurred through moderate yielding of the web while no cracking of the foundation underneath the base-plate area was observed. S06 was tested up to 8% drift level in the pull direction (corresponds to 0.07 rad). At the ultimate stage, rupture of the welds connecting the base-plate to the flanges and the web was observed. The combination of the relatively thick base-plate (5/8 inch), the large anchor rods (1 1/4 inch diameter) and thick flanges (1/2 inch outside and 5/8 inch the inside flange) led to a more rocking dominated behavior of the specimen and induced its failure mode. The rocking mode for this specimen was different than what has been observed for the others and with the rupture of the welds, it happened through the interface between the column and the base-plate rather than at the interface between the base-plate and the concrete foundation.

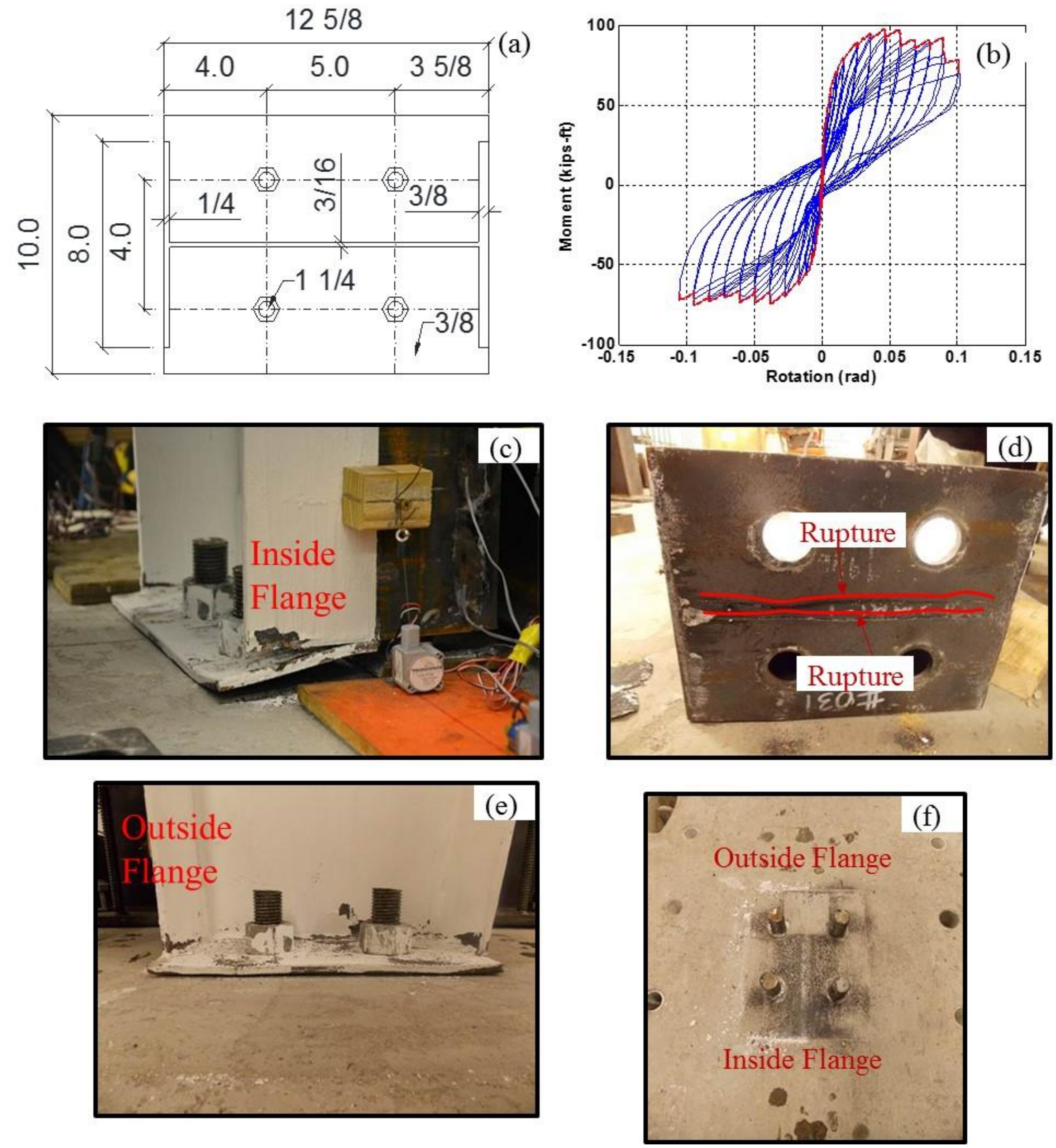

Figure 4.48. (a) S05 base-plate configuration, (b) moment-rotation response, (c) rupture of the weld connecting the inside flange with the base-plate, (d) rupture of the weld connecting the web and the base-plate, (e) and (f) no cracking of the concrete.

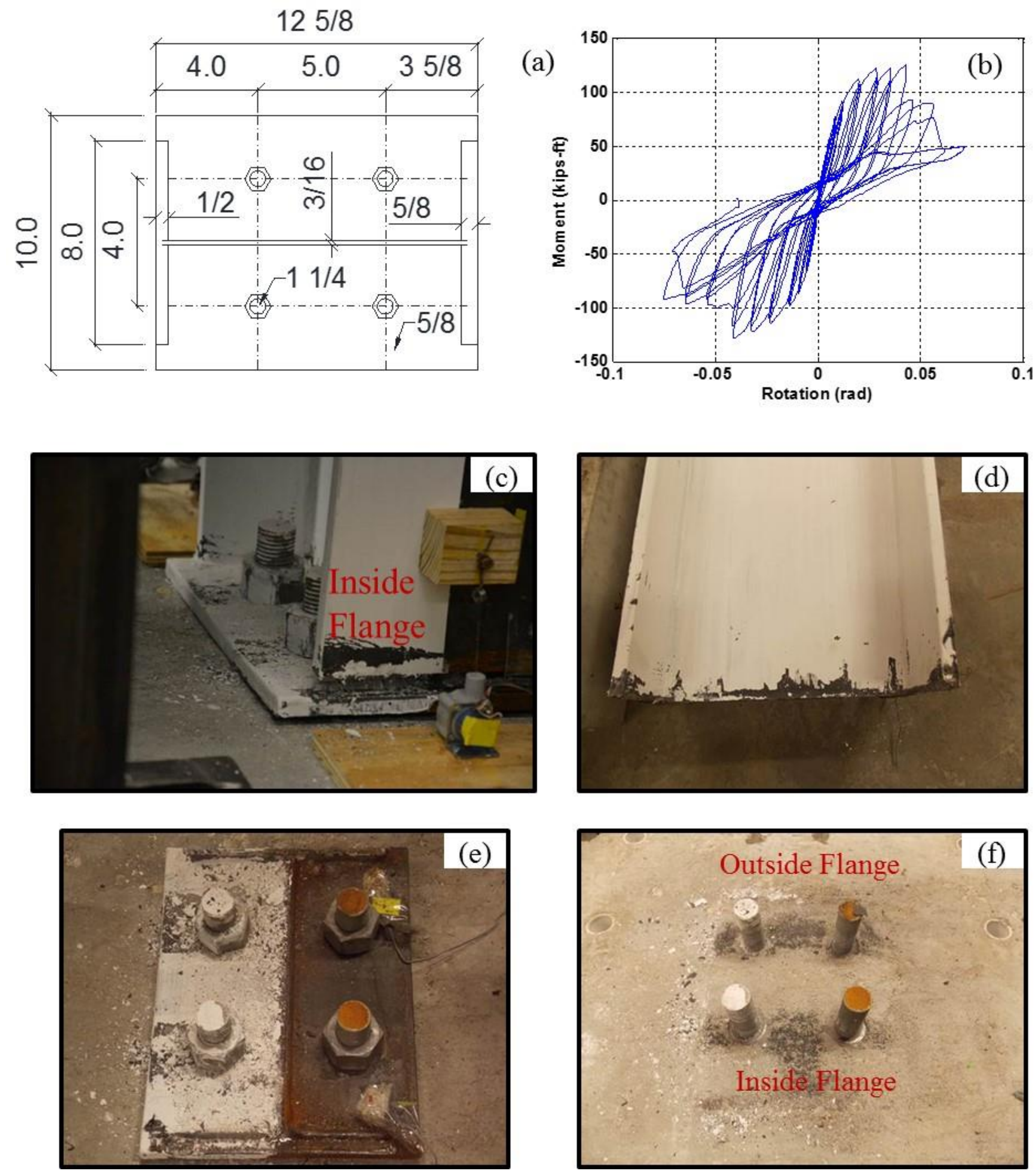

Figure 4.49. (a) S06 base-plate configuration, (b) moment-rotation response, (c) rupture of the inside flange-base-plate weld, (d) column stub after complete detachment from the base-plate, (e) base-plate on the foundation, and (f) no cracking of the concrete.

4.10.4. Damage group 4

The energy absorption for the fourth group of specimens (S07, S08, S09 and S10) was mainly achieved through extensive damage of the concrete foundation, moderate damage of the base-plate while the flanges and anchor rods remained mostly elastic. This behavior was observed for all the specimens in this group and all the tests were terminated when the reinforced concrete foundation experienced extensive cracking and crushing. The damage evaluation of S07, S08, S09 and S10 belonging to this damage group are presented below.

The geometric characteristics of S07 and its moment versus rotation response are shown in Figure 4.50(a) and (b) respectively. The condition of the specimen and the foundation after the completion of the test are shown in Figure 4.50(c) to f). The energy absorption of S07 mainly occurred through excessive cracking of the concrete foundation while the base-plate had moderate damage, the outside flange were slightly damaged and the web and inside flange did not experience any damage. S07 was tested up to 6% drift level (corresponds to 0.038 rad rotation in the push direction and 0.03 rad rotation in the pull direction). Cracks on the concrete foundation initiated from 2.0% drift level cycles (corresponds to 0.007 rad rotation in the push direction and 0.0065 rad rotation in the pull direction) and propagated in the subsequent loading cycles. Among the 22 inch web depth specimens, S07 was the one with the lower number of anchor rods (6 anchor rods in comparison to 8 anchor rods for S08, S09 and S10).

The geometric characteristics of S08 and its moment versus rotation response are shown in Figure 4.51(a) and (b), respectively. The condition of the specimen and the foundation after the completion of the test are shown in Figure 4.51(c) to (f). The energy absorption of S08 mainly occurred through excessive cracking of the concrete foundation while the base-plate had moderate damage, the outside flange were slightly damaged and the web and inside flange did not experience any damage. S08 was tested up to 7% drift level in the pull direction (corresponds to 0.025 rad rotation). Cracks on the concrete foundation initiated from 1.5% drift level cycles (corresponds to 0.004 rad rotation in the push direction and 0.0035 rad rotation in the pull direction) and propagated in the subsequent loading cycles.

The geometric characteristics of S09 and its moment versus rotation response are shown in Figure 4.52(a) and (b), respectively. The condition of the specimen and the foundation after the completion of the test are shown in Figure 4.52(c) to (f). The energy absorption of S09 mainly occurred through excessive cracking of the concrete foundation while the base-plate had moderate damage, the outside flange were slightly damaged and the web and inside flange did not experience any damage. S09 was tested up to 7% drift level (corresponds to 0.039 rad rotation). Cracks on the concrete foundation initiated from 1.5% drift level cycles (corresponds to 0.0035 rad rotation in the push and 0.003 rad rotation in the pull direction) and propagated in the subsequent loading cycles.

The geometric characteristics of S10 and its moment versus rotation response are shown in Figure 4.53(a) and (b), respectively. The condition of the specimen and the foundation after the completion of the test are shown in Figure 4.53(c) to (e). The energy absorption of S10 mainly occurred through excessive cracking of the concrete foundation while the web, base-plate had moderate damage, the outside flange were slightly damaged and the inside flange did not experience any damage. S10 was tested up to 9% drift level (corresponds to 0.047 rad rotation in the push direction and 0.058 rad rotation in the pull direction). Cracks on the concrete foundation initiated from 1.0% drift level cycles (corresponds to 0.002 rad rotation in the push direction and 0.003 rad rotation in the pull direction) and propagated in the subsequent loading cycles. This specimen had the thicker base-plate in comparison with the 22 inch web depth specimens.

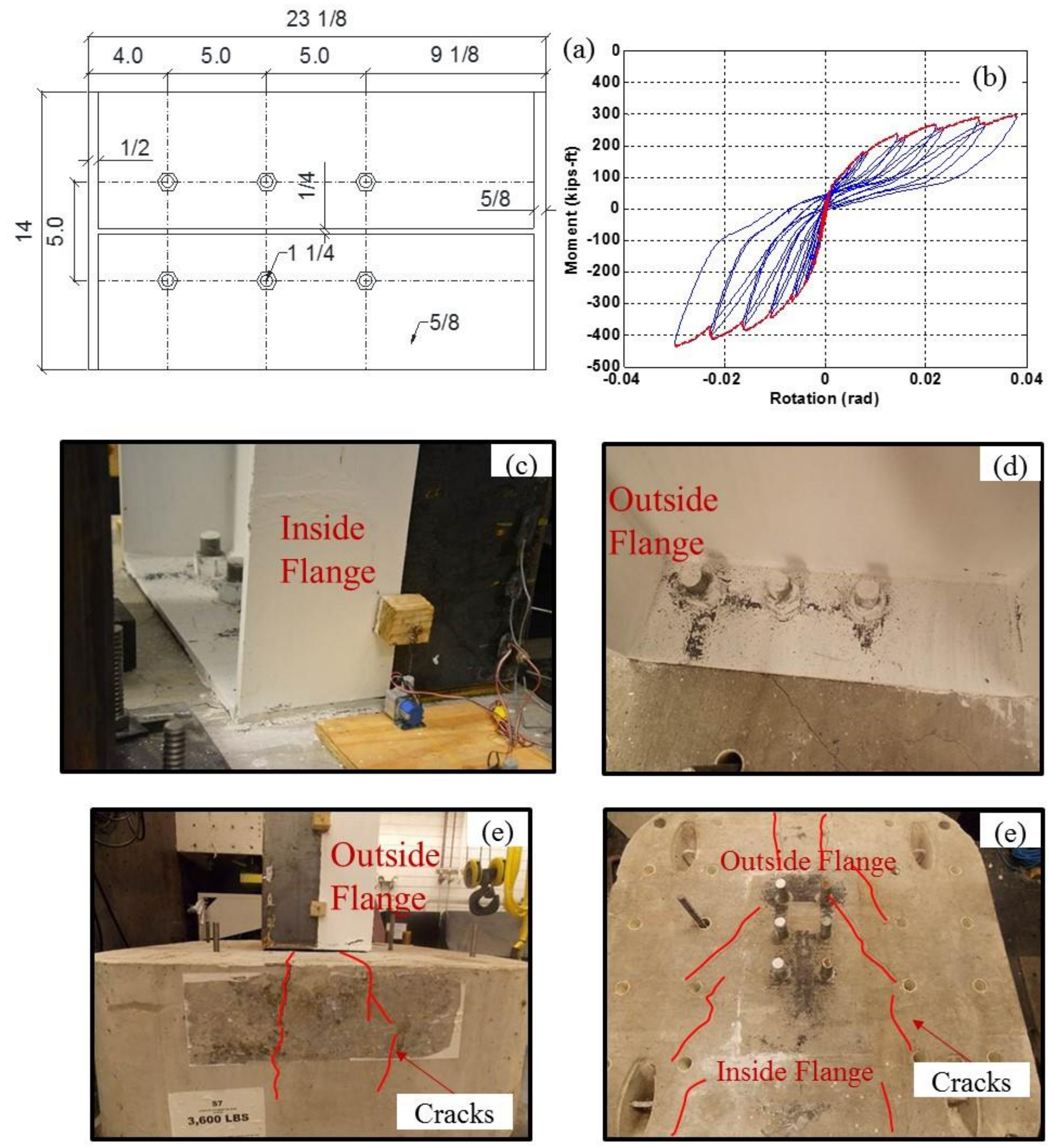

Figure 4.50. (a) S07 base-plate configuration, (b) moment-rotation response, (c) no yielding in the flanges and yielding at the base-plate, (d) slight yielding of the base-plate around the anchor rods, (e)and (f) concrete foundation cracking.

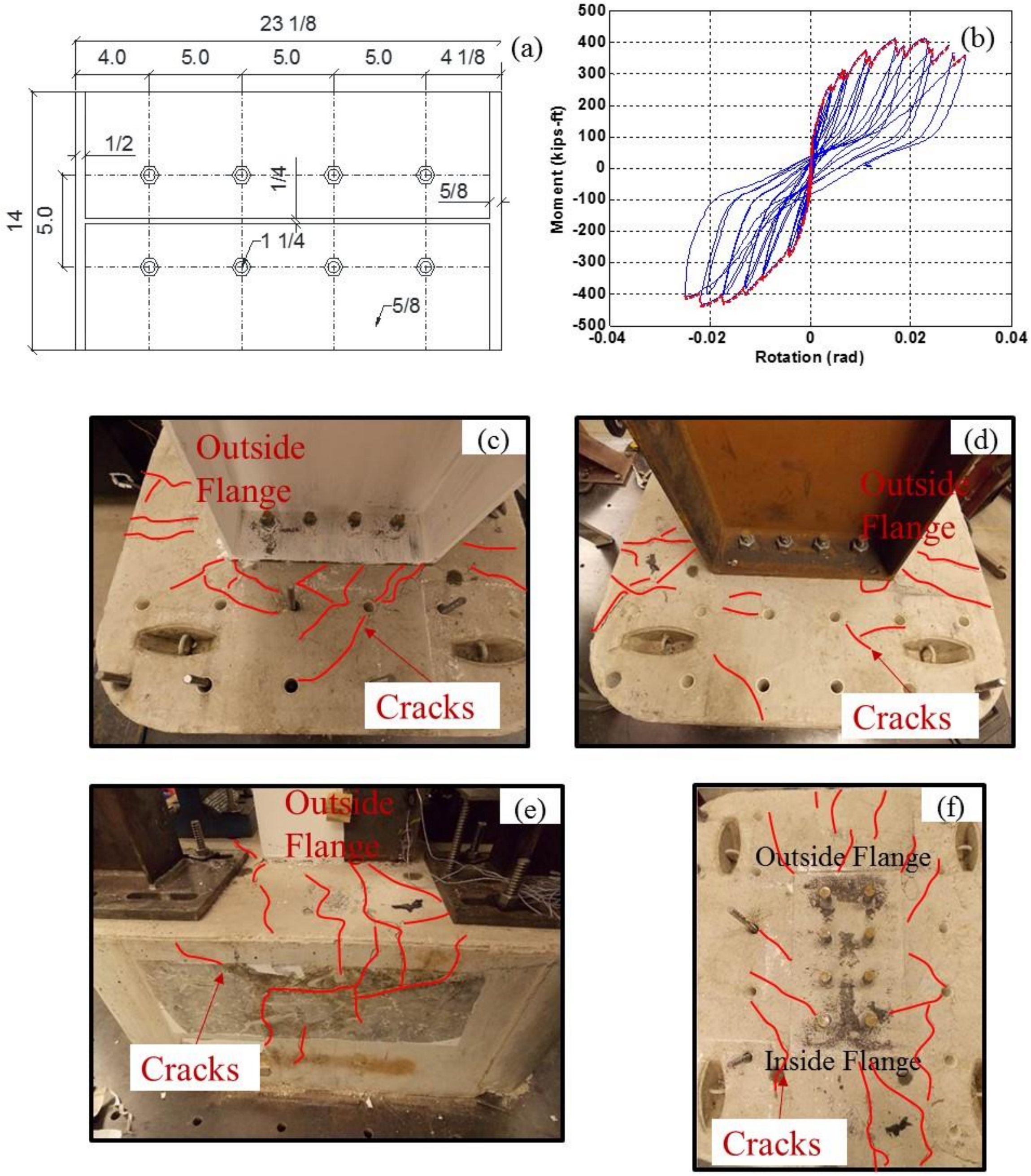

Figure 4.51. (a) S08 base-plate configuration, (b) moment-rotation response, the condition of S08 after the test: (c) white wash flaking in the base-plate around the anchor rods and no white wash flaking in the flanges, (d), (e) and (f) concrete foundation cracking.

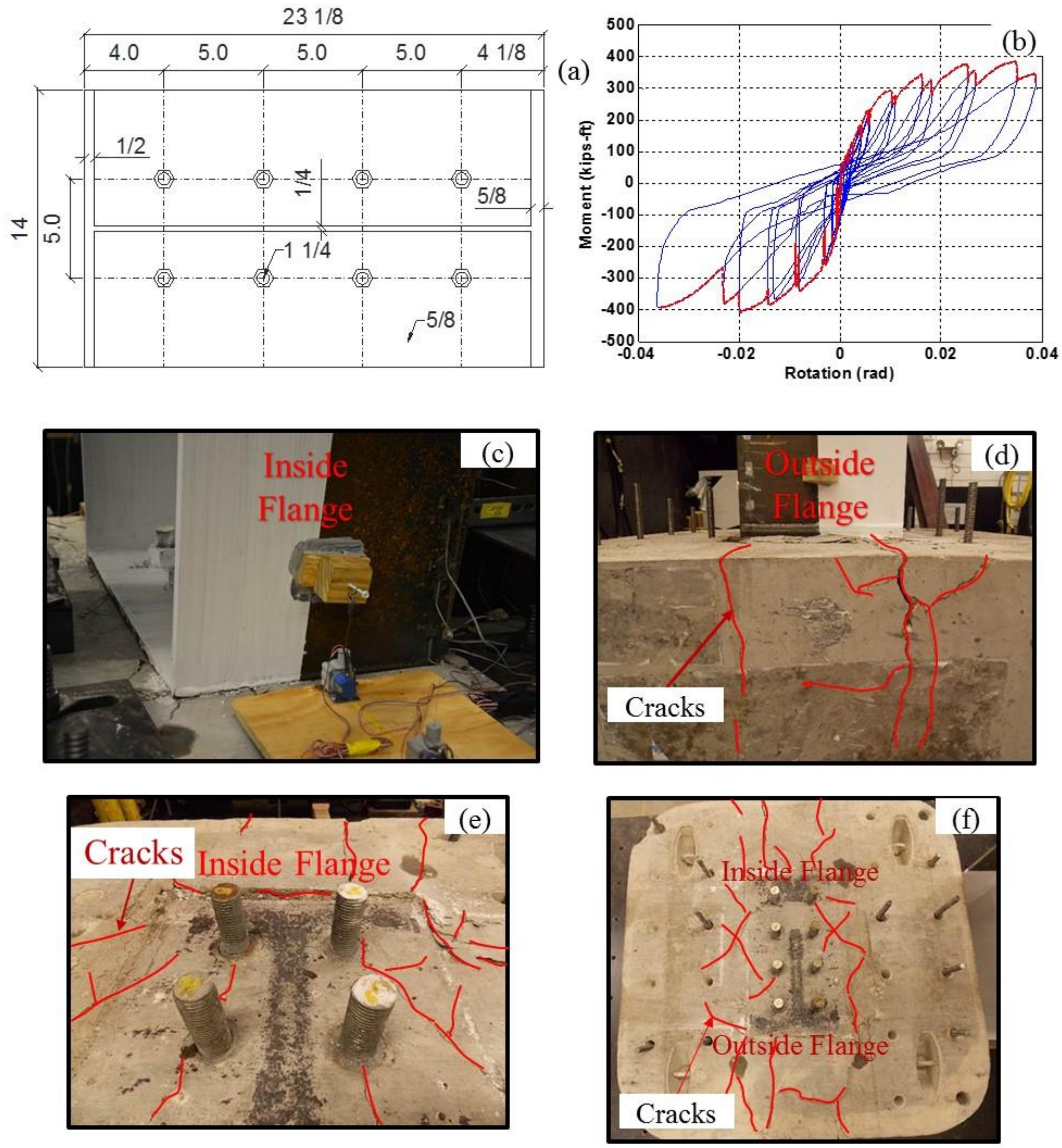

Figure 4.52. (a) S09 base-plate configuration, (b) moment-rotation response, the condition of S09 after the test: (c) no white wash flaking in the flanges, (d), (e) and (f) concrete foundation cracking.

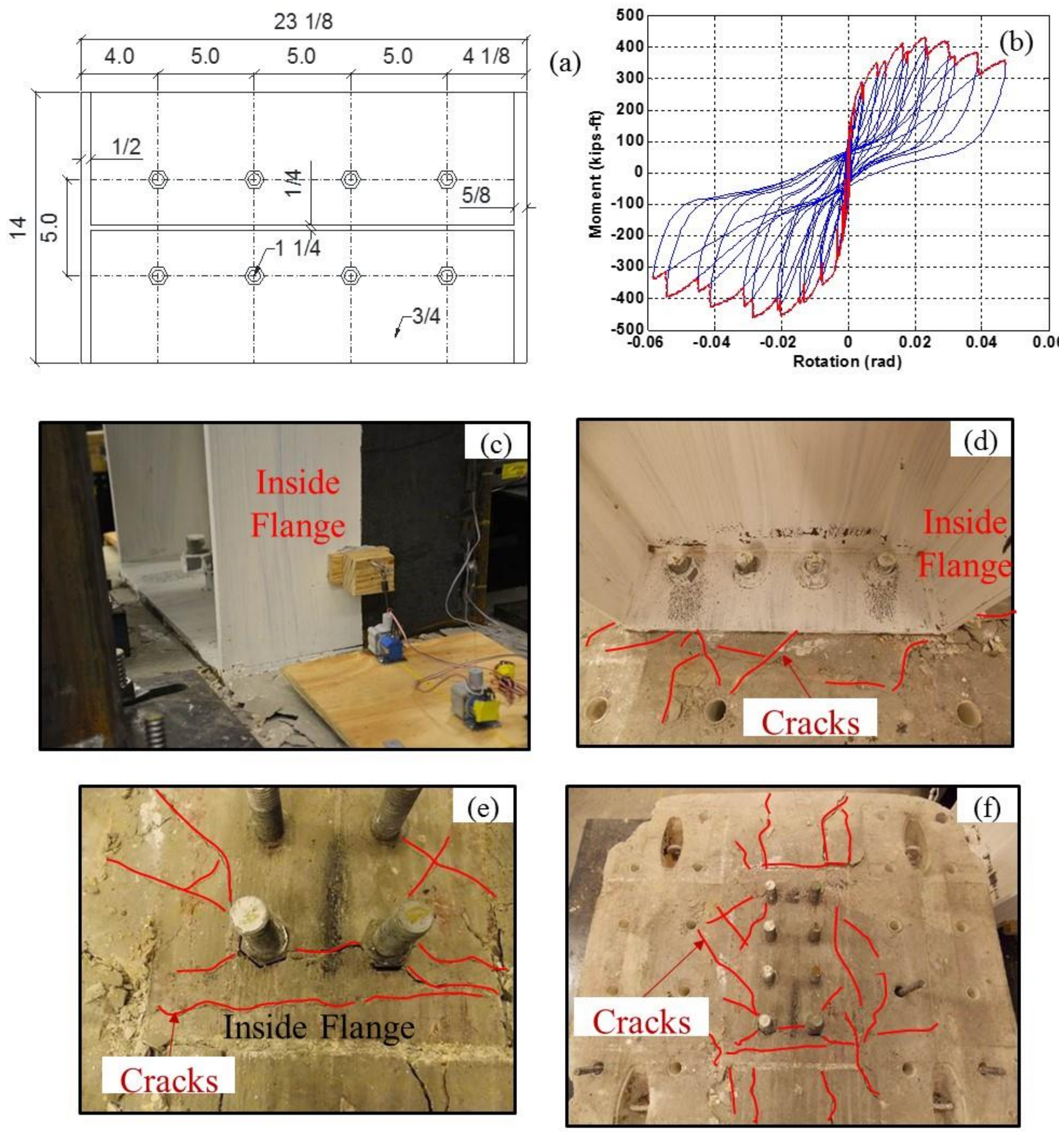

Figure 4.53. (a) S10 base-plate configuration, (b) moment-rotation response, the condition of S10 after the test: (c) no white wash flaking in the flanges and white wash flaking in the base-plate, (d) slight yielding of the base-plate and web, (e) and (f) concrete foundation cracking.

4.11. Hysteretic Behavior of the Specimens

Based on the definitions presented in Section 4.6.5, the energy absorption, lateral strength, moment capacity, and the displacement and rotational ductility of the specimens were calculated. The results are presented in Table 4.13 and Table 4.14. The first three damage groups reported in Table 4.11 include specimens with smaller web depths: 10 inch and 12 inch while the fourth damage category include specimens with larger web depth: 22 inch. For the first damage group, where the anchor rod behavior governed the behavior of the connection, lowest energy absorption compared to the other two damage categories with similar web depths was observed. For the fourth damage category with the larger web depth, excessive cracking of the concrete foundation governed the behavior of the connection, the energy absorption of the specimens was observed to be higher but not comparable with the other groups due to large differences in connection dimensions.

It was observed that S04 and S06 had greater lateral strength and moment capacity among the 10-12 inch web depth specimens (i.e., S01–S06 and S11). This behavior was a result of their geometric characteristics. Both S04 and S06 had thicker base-plates (5/8 inch) with larger anchor rods (1 1/4 inch diameter). The only varying parameter was the flange thicknesses: 1/4 inch and 3/8 inch for S04 versus 1/2 inch and 5/8 inch for S06. Comparing the overall behavior of S04 and S06, it was observed that the increased flange thicknesses led to a more brittle behavior (S06) in comparison with the ductile behavior that the specimen with the thinner flanges (S04) exhibited. Among all the 22 inch web depth specimens (S07–S10), S10 showed the highest lateral strength and moment capacity. S10 had the thickest base-plate amongst S07–S10.

It was also observed that S03 and S04 experienced the highest displacement ductility in comparison with the 10-12 inch web depth specimens. This behavior was a result of the geometric characteristics of these connections and therefore their failure mode. S03 and S04 were very similar with the only varied parameter being the anchor rod diameter (and setback which is a function of the anchor rod diameter). Specifically, S03 had 1.0 inch diameter anchor rods while S04 had 1 1/4 inch diameter anchor rods. The failure of the connections was due to the yielding of different components of the connections while no concentrated damage was observed to one of the components of the connections. The damage mode of all the connections is explained in Section 4.10. The 22 inch web depth specimens experienced the lowest displacement ductility amongst all the specimens. Specifically, it was observed that the failure of 22 inch web depth specimens was due to the excessive cracking of the concrete foundation; therefore, these specimens experienced a less ductile behavior.

Finally, S05 experienced the highest rotational ductility amongst all the specimens. S05 had the thinnest base-plate (3/8 inch) among all the specimens. In the elastic range, the behavior of S05 was dominated by the stiffness of the anchor rods which resulted the specimen to experience small rotations. On the other hand, in the inelastic range S05 showed a more flexural bending behavior with large rotations of the base-plate. S04 and S06 showed the lowest rotational ductility amongst all the specimens. Both S04 and S06 had thicker base-plates (5/8 inch) with larger anchor rods (1 1/4 inch diameter) which resulted in the lowest rotational ductility of the specimens.

Table 4.13. Lateral Strength (V_m^+, V_m^-) and Displacement Ductility (μ_Δ^+, μ_Δ^-). See Figure 4.18 for definition of the variables.

Damage Group	Specimen ID	Lateral Strength (V_m^+)	Lateral Strength (V_m^-)	V_m^+ / V_m^-	Displacement Ductility (μ_Δ^+)	Displacement Ductility (μ_Δ^-)	$\mu_\Delta^+ / \mu_\Delta^-$
		(kips)	(kips)	-	-	-	-
1	S01	7.6	13.8	0.55	2.6	2.8	0.93
	S02	9.4	12.1	0.78	3.3	3.6	0.92
	S11	9.3	10	0.93	2.8	-	-
2	S03	15.6	19.4	0.80	-	3.7	-
	S04	20.6	21.50	0.96	3.6	3.5	1.03
3	S05	13.3	12.22	1.09	3.3	3.1	1.06
	S06	18.4	20.5	0.90	2.4	2.8	0.86
4	S07	45.4	70.05	0.65	-	-	-
	S08	63.7	68.72	0.93	2.1	2.5	0.84
	S09	59.1	65.13	0.91	2.3	2.1	1.10
	S10	65.4	72.94	0.90	1.7	2.3	0.74

Table 4.14. Energy Absorption (E_a), Moment Capacity (M_m^+, M_m^-) , and Rotational Ductility (μ_ϕ^+, μ_ϕ^-). See Figure 4.18 for definition of the variables.

Damage Group	Specimen ID	Energy Absorption (E_a)	Moment Capacity (M_m^+)	Moment Capacity (M_m^-)	M_m^+ / M_m^-	Rotational Ductility (μ_ϕ^+)	Rotational Ductility (μ_ϕ^-)	μ_ϕ^+/μ_ϕ^-
		(kips-ft/rad)	(kips-ft)	(kips-ft)	-	-	-	-
1	S01	1.9	46.9	82.1	0.57	3.4	3.5	0.97
	S02	1.6	49.4	75.2	0.66	4.3	4.5	0.96
	S11	1.6	71.5	73.4	0.97	3.8	-	-
2	S03	2.5	87.4	121.1	0.72	-	4.2	-
	S04	2.8	147.9	132.8	1.11	3.1	3.2	0.97
3	S05	2.2	97.4	79.4	1.23	3.9	4.9	0.80
	S06	2.8	123.8	130.2	0.95	3.3	3.2	1.03
4	S07	3.0	297.0	432.7	0.69	-	-	-
	S08	3.4	407.3	438.8	0.93	3.6	2.7	1.33
	S09	3.0	384.1	407.3	0.94	3.7	3.7	1.00
	S10	2.8	429.1	459.5	0.93	3.4	3.2	1.06

The energy absorption, moment capacity and rotational ductility also differed amongst the damage groups presented in Section 4.10. Specifically, a representative moment versus rotation response, a full loading cycle and the energy absorption versus rotation graphs of all the specimens consisting each damage category are presented in Figure 4.54, Figure 4.55, Figure 4.56 and Figure 4.57.

The moment versus rotation response of S02 is shown in Figure 4.54(a), which is representative of the behavior of all the specimens in the first damage category (i.e., S01, S02 and S11). As mentioned in Section 4.10, the anchor rod behavior (3/4 inch diameter) governed the failure of this group of specimens. In this case, mostly a rigid-body type rocking motion was seen, which resulted in the severe "necking" at the zero force level in the moment-rotation response [see Figure 4.54(b)]. The energy absorption increased with increasing rotation levels [see Figure 4.54(c)] but it was relatively low in comparison to specimens from damage groups 2 and 3 (see Section 4.10). The common geometric characteristic of the specimens of this first damage category was that they had the lowest anchor rod diameter (3/4 inch) among specimens from damage groups 1-3. The rotational ductility of S01 and S02, respectively, was 3.4 and 3.5 in the push direction and 4.3 and

4.5 in the pull direction, while the ductility for S11 was calculated only in the push direction as 3.8 (see Table 4.14). S02 had the highest rotational ductility among the specimens of the first damage category. As mentioned above, the failure of these connections occurred due to anchor rod rupture. The pitch of the anchor rods affected the rotational ductility of the connection. When the anchor rods had a pitch of 4 inch (i.e., S01) and 4 1/2 inch (i.e., S11), the pair of anchor rods farther from the tension flange elongated more compared to the case when the anchor rods had a pitch of 6 inch (i.e., S02). Therefore, these pair of anchor rods in the 4 inch (i.e., S01) and 4 1/2 inch (i.e., S11) pitch configurations started to degrade in stiffness and strength at lower rotations than the same pair of anchor rods for the 6 inch pitch (i.e., S02) configuration, leading to a lower rotational ductility.

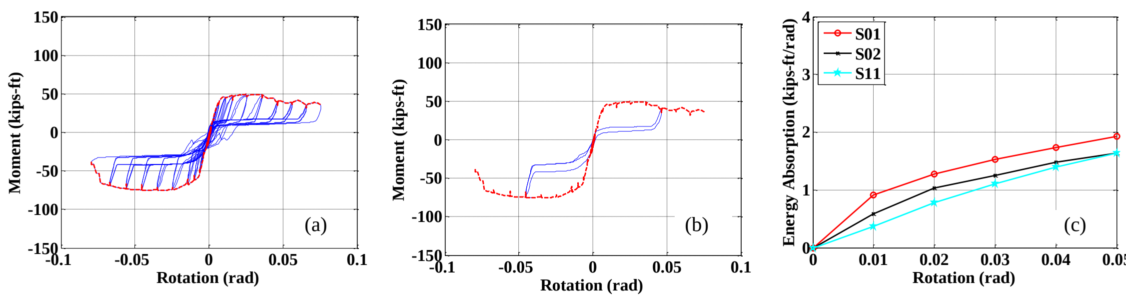

Figure 4.54. Representative moment-rotation response (S02) of the first damage group of specimens: (a) overall moment-rotation response, (b) a complete loading cycle at 0.045 radian, (c) energy absorption versus rotation.

The moment versus rotation response of S03 is shown in Figure 4.55(a) and a complete 0.05 radian rotation cycle is shown in Figure 4.55(b). This response is representative of the two specimens consisted the second damage group (i.e., S03 and S04). The failure of the connections of the second damage group, as mentioned in Section 4.10, was due to combined yielding of the flanges, the base-plate and the web, and moderate cracking of the concrete foundation while the anchor rods were slightly damaged. The energy absorption was relatively higher in comparison to the specimens of the first damage category where the failure was concentrated in the anchor rods. The overall behavior of S03 and S04 was a result of their geometric characteristics. Specifically, the varied parameters between the specimens were the anchor rod diameter, setback and the base-plate width which is a function of the anchor rod diameter. Specifically, S03 had 1.0 inch diameter anchor rods while S04 had 1 1/4 inch diameter anchor rods, S03 had a 8 inch wide base-plate while S04 had a 10 inch wide base-plate. These geometric characteristics led to the difference in the energy absorption of S03 and S04 [see Figure 4.55(c)]. The energy absorption of S04 was 10% higher than that of S03 after the completion of the 5 radians rotation cycles. Base-plate rupture and outside flange buckling were occurred for S04 which led to a lower rotational ductility in comparison with S03. The difference in the anchor rod diameter was the main reason for this behavior.

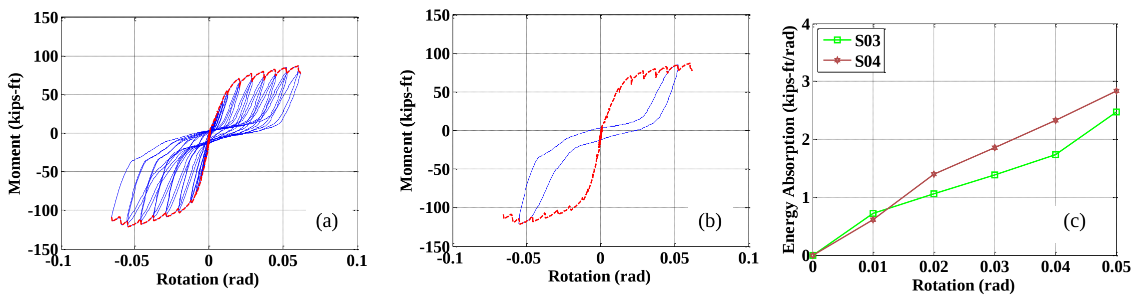

Figure 4.55. Representative moment-rotation response (S03) of the second damage group of specimens: (a) overall moment-rotation response, (b) a complete loading cycle 0.05 radian, (c) energy absorption versus drift.

The moment versus rotation response of S05 is shown in Figure 4.56(a) and a complete loading cycle at 0.05 radian rotation cycle is shown in Figure 4.56(b). This response is representative of the two specimens consisting the third damage category (i.e., S05 and S06). As mentioned in Section 4.10, the ultimate failure of S05 and S06 was due to weld rupture between the flanges and the base-plate, while prior to that yielding of the flanges and the web was observed. The concrete foundation did not experience any significant damage and the anchor rods had slight to no damage. The overall behavior of S05 and S06 was a result of their geometric characteristics. Specifically, among all the specimens with smaller web depths (10 inch and 12 inch), S05 had the thinnest base-plate (3/8 inch) and thinner flanges (1/4 inch and 3/8 inch) while S06 had the thicker base-plate (5/8 inch) and thickest flanges (1/2 inch and 5/8 inch). These geometric characteristics led to low and high energy absorption of S05 and S06, respectively [see Figure 4.56(c)]. The energy absorption of S06 was 21% higher than that of S05 after the 0.05 radians rotation cycles. However, for both specimens, the anchor rods were large enough to limit the damage to the flanges, web and the base-plate. It was also observed that due to thinner members, S05 had a more flexurally dominated behavior which led to a more ductile response while S06 showed a more rocking rigid-body-motion behavior. The rotational ductility of S05 was 3.9 and 4.9 in push and pull directions, respectively, while the same for S06 was 3.3 and 3.2 in push and pull directions, respectively (see Table 4.14).

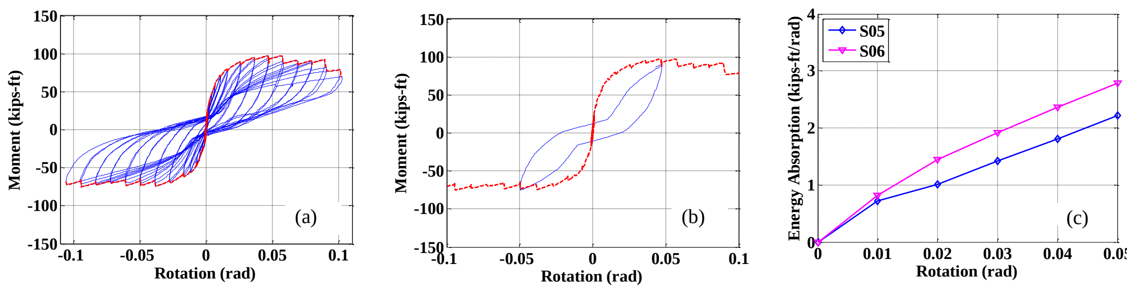

Figure 4.56. Representative moment-rotation response (S05) of the third damage group of specimens: (a) overall moment-rotation response, (b) a complete loading cycle 0.05 radian, (c) energy absorption versus drift.

The moment versus rotation response of S08 is shown in Figure 4.57(a) and a complete loading cycle at 0.018 radian is shown in Figure 4.57(b). This response is representative of the four specimens consisting the fourth damage category. The damage of the specimens, as mentioned in Section 4.10, was governed by the excessive cracking of the concrete foundations and potentially yielding of the reinforcing steel (although this was not measured), while the flanges, anchor rods and base-plate had slight to no damage. The specimens in this group had very similar geometric characteristics with a 22 inch web depth. The only differences were S07 had 6 anchor rods while S08 to S10 had 8 anchor rods, and S10 had 1/8 inch thicker base-plate compared to S07 to S09. The energy absorption of this group of specimens was observed to be higher but not comparable with the other groups due to large differences in connection dimensions [see Figure 4.57 (c)]. The rotational ductility of S08 was 3.6 and 2.7 in push and pull directions, respectively, while the same for S09 was 3.7 in push and pull directions, and for S10 it was 3.4 and 3.2 in push and pull directions, respectively (see Table 4.14). The specimens showed the same overall behavior which led to the small differences in the rotational ductility among the specimens.

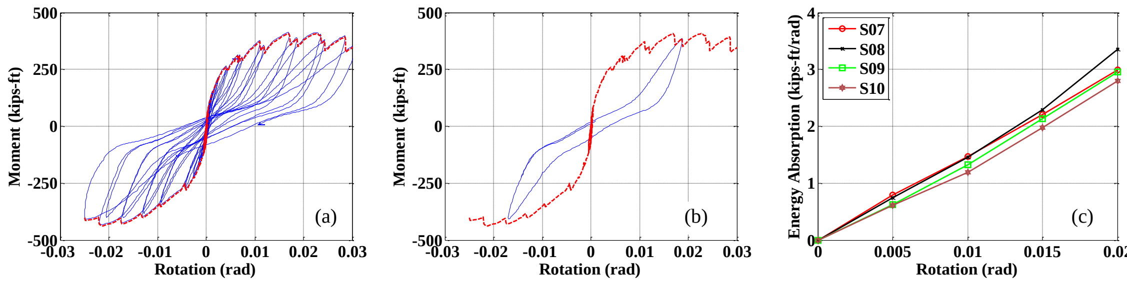

Figure 4.57. Representative moment-rotation response (S08) of the fourth damage group of specimens: (a) overall moment-rotation response, (b) a complete loading cycle 0.018 radian, (c) energy absorption versus drift.

5. ANALYTICAL RESULTS

5.1. Frame Optimization-Phase 1

As mentioned earlier, the tested column stubs of the first phase of the experimental program were extracted from actual frame designs that are representative of low-rise metal building construction in the United States. The frame dimensions are presented in Table 3.2 and their drawings are given in Appendix B. These frames are modeled and analyzed in R-Frame, an in-house design software for performing linear elastic analysis, used by one of the largest metal building manufacturers in the United States. The purpose of the analysis conducted here was to investigate the potential weight savings that can be achieved in the frame designs when semi-rigid (rather than pinned) connection response is considered in the column bases.

The drift limit state is established as H/60 and H/40 (where H is the building height) for wind and the earthquake limit states, respectively, according to AISC Design Guide 3 (Fisher et al., 2004). For this reason, a secant rotational stiffness corresponding to a drift limit of H/60 in the tested column stubs was calculated from the moment-rotation envelope curves shown in Figure 3.19 and the values as well as the moments corresponding to this drift level are presented in Table 5.1. As an input to the design software used here, the average secant rotational stiffness in the push (positive) and pull direction (negative) was given. From the analysis results, which are presented below, rotational stiffness estimate at a drift limit of H/60 provides a conservative upper bound. An optimization algorithm was then run to minimize the total weight of each frame. Note that the initial frame designs were also optimized. The design variables for optimization included the number of sections to be used along the length of the columns and rafters, and the flange and web thicknesses. The web-taper and flange widths were not considered as design variables in the optimization. The constraints of the optimization were the segmentation of the frame as it relates to the fabrication, shipping and construction limitations in addition to the design constraints specified in AISC Design Guides 1 and 25 (Fisher et al., 2006; Kaehler et al., 2011).

Table 5.1. Rotational Stiffness Corresponding to H/60 Drift Limit.

Frame ID	Push Direction Moment at H/60 Drift	Pull Direction Moment at H/60 Drift	Push Direction Secant Rotational Stiffness	Pull Direction Secant Rotational Stiffness	Average Secant Rotational Stiffness
F1	(kips-ft)	(kips-ft)	(kips-ft/rad)	(kips-ft/rad)	(kips-ft/rad)
F2	46.0	56.0	3381	3964	3672
F3	101.0	81.0	7062	5595	6328
F4	71.0	91.5	5426	6318	5872
F5	102.4	97.0	6749	5735	6242
F6	42.0	53.0	2865	3617	3241
F7	75.0	111.0	5375	7759	6567
F8	78.5	60.0	5625	3862	4744

Table 5.2 presents the results of the optimization and structural analysis of all of the frames considered in this study based on two column base conditions, pinned and semi-rigid. For each frame, the maximum drift, the corresponding load combination and the moment at the base connections are reported for comparison between the two designs. The last column of Table 5.2 presents the weight decrease of the frames that can be achieved by accounting for the base rotational stiffness in the frame design.

Table 5.2. Frame Analysis Results.

Frame ID	Max. Drift Load Combination	Pinned Base	Semi-rigid Base			
		Max. Column Drift	Max. Column Drift	Rotational Stiffness (kips-ft/rad)	Moment at Base at Max. Drift (kips-ft)	Decrease in Frame Weight (%)
F1	1.0 Wind Load	H/361	H/436	3799	23	0.5%
F2	1.0 Wind Load	H/69	H/78	3609	130	7.1%
F3	0.74 Dead Load +1.0 Earthquake Load	H/48	H/70	6018	29	9.8%

Table 5.2. (Continued) Frame Analysis Results.

Frame ID	Max. Drift Load Combination	Pinned Base	Semi-rigid Base			
		Max. Column Drift	Max. Column Drift	Rotational Stiffness (kips-ft/rad)	Moment at Base at Max. Drift (kips-ft)	Decrease in Frame Weight (%)
F4	1.0 Roof Snow Load	H/253	H/328	6838	45	0.0%
F5	0.71 Dead Load +1.0 Earthquake Load	H/67	H/206	35075	5	2.0%
F6	1.0 Wind Load	H/81	H/125	6567	87	11.4%
F7	0.84 Dead Load +1.0 Earthquake Load	H/56	H/64	4746	26	0%
F8	0.6 Wind Load	H/99	H/117	8490	104	7.5%

The frames were designed for dead, wind, snow, and earthquake load combinations, which varied according to the location of the frames. Frames 1 and 4 were governed by the strength limits (maximum column drift design varied from H/253 to H/426) and they did not show any significant reduction in the total weight (about 0% to 0.5%) after the addition of the rotational stiffness of the base-plate connections. However, the deflections of the frames decreased by 9% (for F1) and 17% (for F4). For F5 and F7 the member dimensions were governed by the slenderness limits in AISC Design Guide 25 (Kaehler et al., 2011). Most of the components of these frames had flange thicknesses of 1/4 inch, which is the minimum permitted flange thickness to prevent flange local buckling as the dominant failure mode. Consequently, Table 5.2 indicates that no further reduction of the frame weight could be achieved by considering the rotational stiffness of the base connection in the design. However, the deflections of the frames decreased by 19.4% (for F5) and 34% (for F7). For F2, F3, F6, and F8, the design was governed by drift limits under the wind and earthquake dominated load combination. With nominally pinned bases, the frames exhibited maximum drifts ranging from H/99 to H/48. By considering the rotational stiffness of the bases, the weights of the frames were reduced by between 7.1% and 11.4%. Lateral deflection for these frames also decreased by between 21 and 34%.

Further modeling of the frames was performed to compare the effects of different modeling assumptions on the lateral stiffness and strength of the frames. The same modeling approach (fiber-based beam-column elements) that was adopted to obtain the moment-rotation envelopes (see Section 3.6.1) from the force-drift envelopes was used. In this approach, the column base-plate connection rotational behaviors were modeled using zero-length spring elements, whose properties are presented in Table 3.9.

For each of the original frames, three models were created with pinned, semi-rigid, and fixed base connection assumptions. For each frame, a fourth model was created using the optimized frame dimensions from elastic analysis and semi-rigid base connections. Then pushover analysis was performed for each of the models. The results for all the frames are shown in Figure 5.1. The differences of the lateral stiffness of the pinned and semi-rigid frames ranged from 20% to 34% while the differences of the peak base shears ranged from 13% to 30%. The differences of the lateral stiffness of the pinned and semi-rigid-optimized frames ranged from 0% to 15% while the differences of the peak base shears ranged from 7% to 25%.

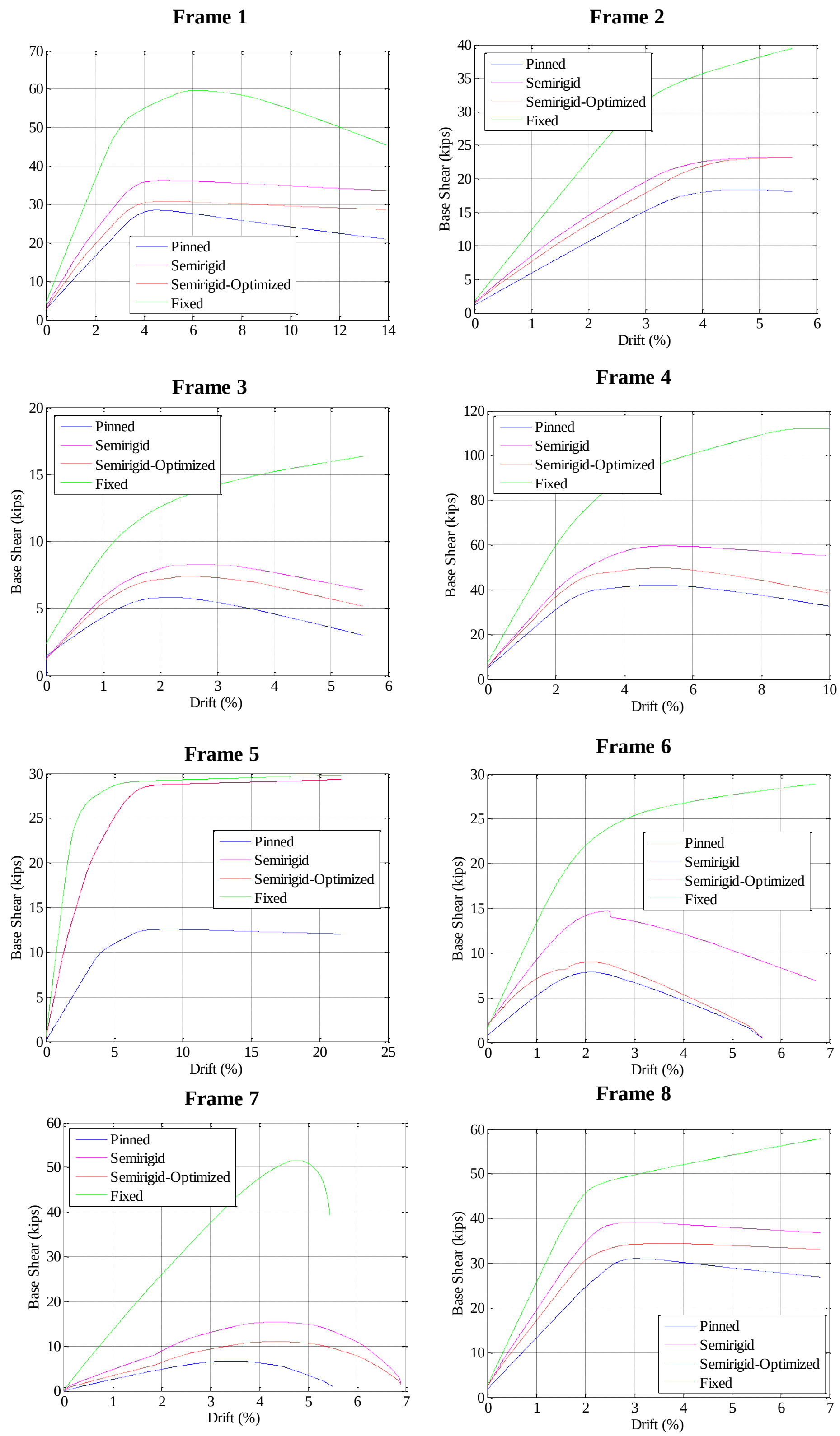

Figure 5.1. Pushover curves for the frames examined in the first phase of the experimental program with different restraints at the column base-plate connections.

5.2. Numerical Analysis and Results – Phase 2

Detailed three-dimensional analytical models were generated in ATENA 3D (2016) based on the column base-plate connection tests conducted in the second phase of the experimental program. A representative analytical model of S04 is shown in Figure 5.2(a). Separate macro-elements were used for each of the components forming the column base-plate connection and the test setup. The macro-elements had material properties as shown in Figure 5.3. Specifically, the following macro-elements were used:

- The strong floor [see Figure 5.2(a)] was modelled as an elastic plate with very high stiffness and fixed supports at the bottom.
- The reinforced concrete pad [see Figure 5.2(b)] was modelled using a fracture-plastic material model [see Figure 5.3(a)]. The fracture-plastic material model combines constitutive models for tensile (fracturing) and compressive (plastic) behavior. The material properties for each of the specimens are given in Table 5.3. The reinforced concrete foundation was connected to the strong floor which was represented by the elastic plate described above with the help of 24 anchors rods. These anchors were modelled as one dimensional cable elements [see Figure 5.2(b)] passing through but not attached to the concrete foundation in order to capture the most realistic conditions of the test setup. Elastic material properties were given to the cables shown in Figure 5.3(d) with assigned Young's modulus equal to 25200 ksi. For the embedment of the one dimensional cable elements, small nut plates [see Figure 5.2(b)] were modelled on the top of the reinforced concrete foundation. These plates had elastic properties shown in Figure 5.3(d) with assigned Young's modulus equal to 29000 ksi, and served the purpose of holding the one dimensional cables only. The other ends of the cables were embedded into the elastic plate representing the strong floor but the cables were not

connected to the surrounding concrete. The nuts and the concrete foundation was also connected.

- The base-plate was modelled as shell/plate element [see Figure 5.2(a)]. Von Mises plasticity model was used to represent the behavior of the base-plate. This model allowed cyclic analysis with the Bauschinger effect included [see Figure 5.3(b)]. The material properties for the base-plate of each specimen are given in Table 5.3.In order to connect the base-plate with the reinforced concrete foundation, holes were create in the base-plate for passing the anchor rods.
- The anchor rods were modelled as three-dimensional solid square elements with area equal to the effective area of the actual anchor rods used in the experiments. Von Mises plasticity model was used for describing the material behavior of the anchor rods. This model allowed cyclic analysis with the Bauschinger effect included [see Figure 5.3(b)]. The material properties of the anchor rods for each of the specimens are given in Table 5.3.The anchor rods were embedded into the concrete pad with a perfect connection [see Figure 5.2(b)]. On top of the base-plate, nut plates with the same size as the ones used during the experiments, were placed. The anchor rods were embedded in the nut plates. However, a contact surface interaction was introduced between the anchor rods and the base-plate and the anchor rods and the side surfaces of the holes. The contact surface interaction had zero tensile strength.
- The web was modelled as shell/plate element [see Figure 5.2(a)]. Von Mises plasticity model for its material modeling was used. The material stress-strain behavior is shown in Figure 5.3(c). The material properties of the web for each of the specimens are given in Table 5.4.The web was perfectly connected to the base-plate and the flanges.
- The flanges were modelled as shell/plate elements [see Figure 5.2(a)]. The material properties of the flanges (inside and outside) for each of the specimens are given in

Table 5.4. Von Mises plasticity model was used for both of the flanges and they were connected to the web and base-plate with a perfect connection. The material stress-strain behavior is shown in Figure 5.3(c).

- The top plate [see Figure 5.2(a)] of the column connecting the column stub with the transfer beam was modelled as shell/plate element. The top plate had elastic properties shown in Figure 5.3(d) with assigned Young's modulus equal to 29000 ksi. The top plate was connected to the web and flanges with a perfect connection.

- The beam used for transferring the axial and flexural loads to the specimen was modeled as a plate with linear elastic properties [see Figure 5.2(a)]. The material stress-strain behavior is shown in Figure 5.3(c). The height of the plate was half the height of the transfer beam used in the experiments in order to apply the axial compressive load and the lateral displacements of the specimen at the points of the actual application during the tests. The stiffness of this plate was selected to be very high to avoid any local deformation and this plate was perfectly connected to the top plate of the column.

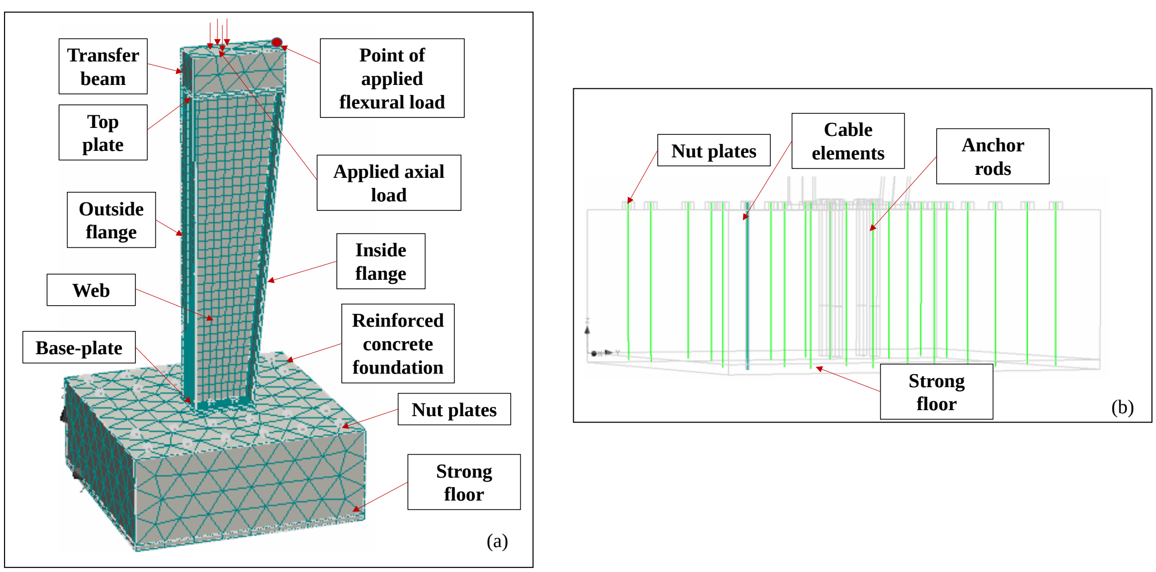

Figure 5.2. (a) Detailed three-dimensional analytical model, and (b) concrete pad modelling.

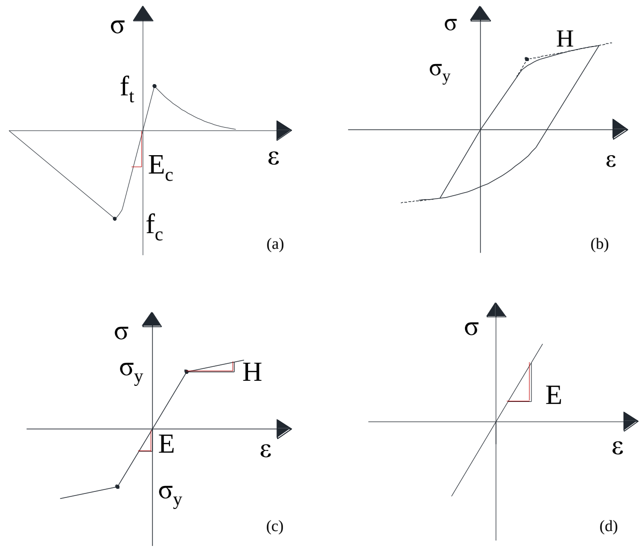

Figure 5.3. Material properties (a) fracture-plastic material model, (b) for steel account Bauschinger effect, (c) bilinear behavior stress-strain behavior, and (d) linear elastic behavior.

Table 5.3. Material Propeties Assigned to the Concrete Foundation, Anchor Rod and Base-Plate.

Specimen ID	Young's modulus, E_c	Poisson's ratio	Tensile strength, f_t	Compressive strength, f_c	Young's modulus, E	Poisson's ratio	Yield strength, σ_y	Hardening modulus, H	Young's modulus, E	Poisson's ratio	Yield strength, σ_y	Hardening modulus, H
	(ksi)	-	(ksi)	(ksi)	(ksi)	-	(ksi)	(ksi)	(ksi)	-	(ksi)	(ksi)
S01	4900	0.2	0.55	-4.10	28100	0.3	55.8	290	28100	0.3	57.4	290
S02	4900	0.2	0.64	-5.70	28100	0.3	55.8	290	28100	0.3	57.4	290
S03	4800	0.2	0.56	-5.30	29800	0.3	74.3	551	29800	0.3	60.6	551
S04	4900	0.2	0.61	-4.80	29300	0.3	76.3	290	29800	0.3	60.6	551
S05	4900	0.2	0.55	-6.38	29300	0.3	76.3	290	29000	0.3	61.0	290
S06	4900	0.2	0.55	-6.38	29300	0.3	76.3	290	28100	0.3	57.4	290
S07	4300	0.12	0.55	-4.93	29300	0.3	76.3	290	27700	0.26	55.8	290
S08*	4300	0.12	0.55	-4.93	29300	0.3	76.3	290	27700	0.26	55.8	290
S10	4300	0.12	0.55	-4.93	29300	0.3	76.3	290	27000	0.26	55.8	290
S11	4900	0.2	0.55	-4.93	28100	0.3	55.8	290	27000	0.2	54.8	145

Table 5.4. Material Propeties Assigned to the Inide and Outside Flanges.

	Inside Flange				Outside Flange				Web			
Specimen ID	Young's modulus, E	Poisson's ratio	Yield strength, σ_y	Hardening modulus, H	Young's modulus, E	Poisson's ratio	Yield strength, σ_y	Hardening modulus, H	Young's modulus, E	Poisson's ratio	Yield strength, σ_y	Hardening modulus, H
	(ksi)	-	(ksi)	(ksi)	(ksi)	-	(ksi)	(ksi)	(ksi)	-	(ksi)	(ksi)
S01	29000	0.3	61.0	290	28200	0.3	54.8	290	29000	0.3	54.8	290
S02	29000	0.3	61.0	290	29100	0.2	64.7	522	29000	0.3	54.8	290
S03	29000	0.3	61.0	290	29100	0.2	64.7	522	29000	0.3	54.8	290
S04	29000	0.3	61.0	290	29100	0.2	64.7	522	29000	0.3	54.8	290
S05	29000	0.3	61.0	290	29100	0.2	64.7	522	29000	0.3	54.8	290
S06	28100	0.3	57.4	290	27000	0.2	54.8	145	29000	0.3	54.8	290
S07	27700	0.26	55.8	290	27000	0.2	54.8	145	29000	0.3	54.8	290
S08*	27700	0.26	55.8	290	27000	0.2	54.8	145	29000	0.3	54.8	290
S10	27700	0.26	55.8	290	27700	0.2	55.8	290	29000	0.3	54.8	290
S11	27000	0.26	55.8	290	29000	0.3	61.0	290	29000	0.3	54.8	290

The numerical models were able to match the mechanism of the connections that was observed during the experiments. The mechanisms were presented in Section 4.10 through the four damage groups. The mechanism of S02 which is representative of the first damage group presented in Section 4.10.1, is shown in Figure 5.4. As it is referred in Section 4.10.1, the behavior of the first damage group (S01, S02 and S11) was dominated by a rocking behavior with energy absorption mainly occurring through yielding of the anchor rods and the ultimate failure occurring due to anchor rod rupture [see Figure 5.4(a)]. From the deformed shape of the connection in the pull direction during the experiment [see Figure 5.4(b)] it was observed a rigid behavior of the base-plate. This behavior was matched in the numerical models as it is shown in Figure 5.4(c). Additionally, the Von Misses contour is shown in Figure 5.4(d) where stress concentration was observed in the first pair of anchor rods in tension. In parallel, no stress concentration was reported in the base-plate, web and flanges which matched the experimental results.

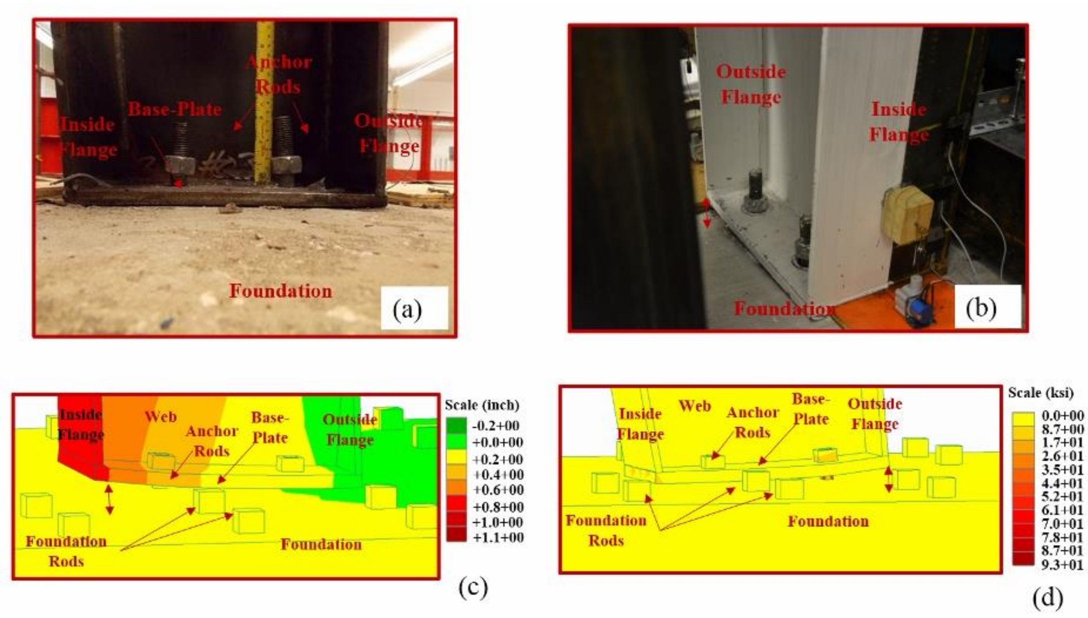

Figure 5.4. (a), (b) Behavior of damage group 1 (S02) and (c) deformation pattern extracted from the numerical models, and (d) stress pattern extracted from the numerical models.

The mechanism of S03 which is representative of the second damage group presented in Section 4.10.1, is shown in Figure 5.5. As it is referred in Section 4.10.2, the behavior of the second damage group (S03 and S04) was dominated by combined yielding of the flanges, the base-plate and the web, and moderate cracking of the concrete foundation while the anchor rods were slightly damaged. The condition of S03 after the experiments, which is representative of the second damage group, is shown in Figure 5.5(a) and Figure 5.5(b). Bending behavior of the base-plate was observed which matched in the numerical models as it is shown in Figure 5.5(c). Additionally, the Von Misses contour is shown in Figure 5.5(d) where stress concentration was observed in the base-plate and flanges.

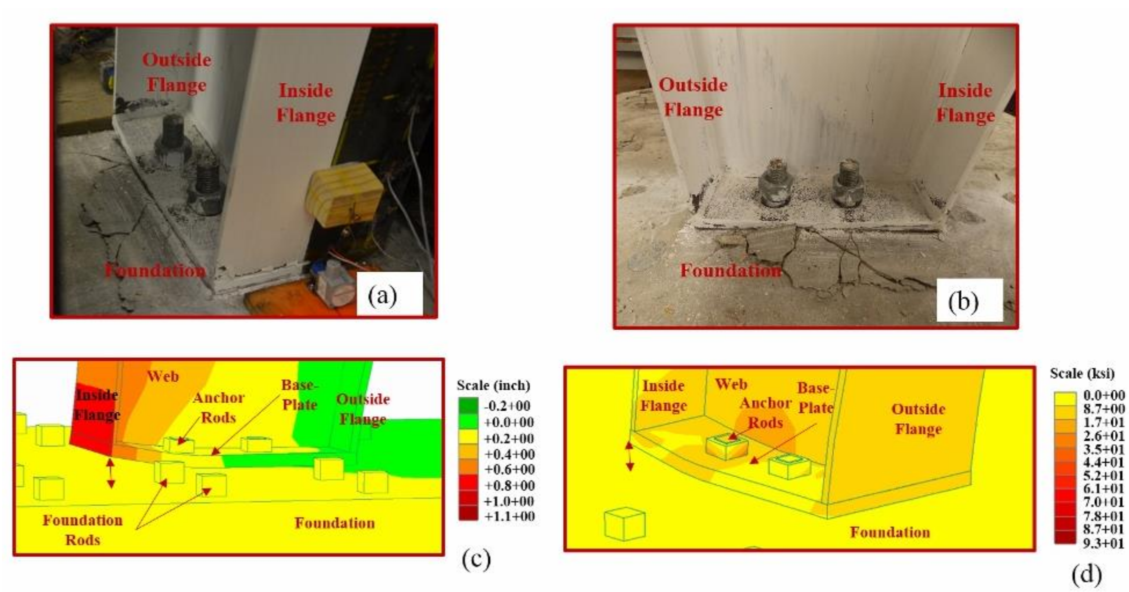

Figure 5.5. (a), (b) Behavior of damage group 2 (S03) and (c) deformation pattern extracted from the numerical models, and (d) stress pattern extracted from the numerical models.

The mechanism of S05 which is representative of the third damage group presented in Section 4.10.1, is shown in Figure 5.6. As it is referred in Section 4.10.3, the behavior of the third damage group (S05 and S06) was determined by yielding of various components of the base-plate connection. The ultimate failure was due to the rupture of the welds between the base-plate, the flanges and the web. The condition of S05 after the experiments, which is representative of the third damage group, is shown in Figure 5.6(a) and Figure 5.6(b). A more flexurally dominated behavior of the base-plate was observed which matched in the numerical models as it is shown in

Figure 5.6(c). Additionally, the Von Misses contour is shown in Figure 5.6(d) where stress concentration and yielding was observed in the base-plate, web and flanges.

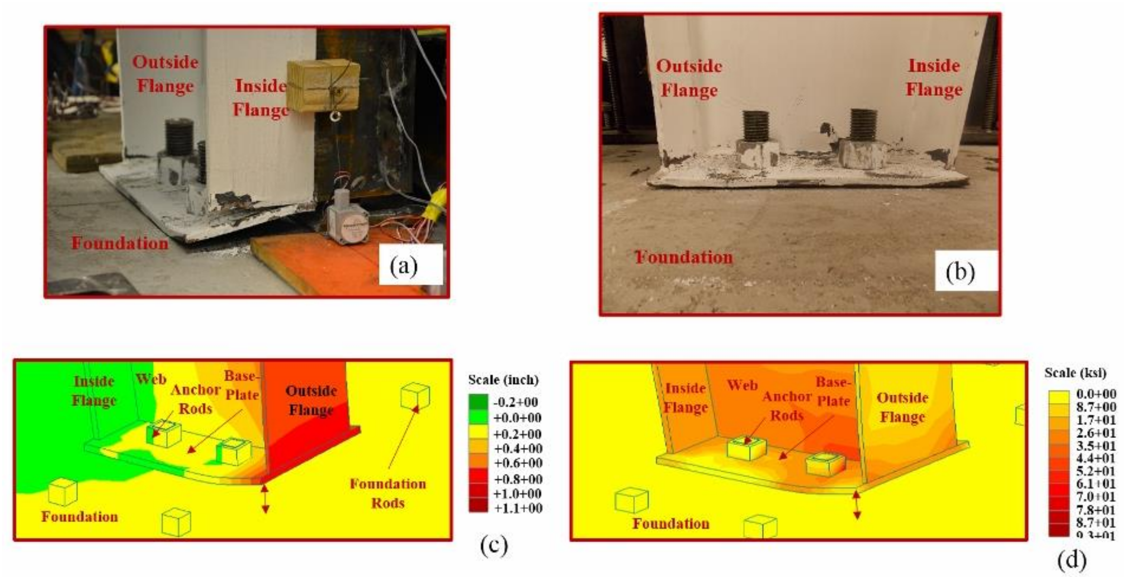

Figure 5.6. (a), (b) Behavior of damage group 3 (S05) and (c) deformation pattern extracted from the numerical models, and (d) stress pattern extracted from the numerical models.

The mechanism of S08 which is representative of the fourth damage group presented in Section 4.10.1, is shown in Figure 5.7. As it is referred in Section 4.10.4, the behavior of the fourth damage group (S07, S08, S09 and S10) was mainly achieved through extensive damage of the concrete foundation, moderate damage of the base-plate while the flanges and anchor rods remained mostly elastic. The condition of S08 after the experiments, which is representative of the fourth damage group, is shown in Figure 5.7(a) and Figure 5.7(b). Excessive cracking and bending behavior of the base-plate was observed which matched in the numerical models as it is shown in Figure 5.7(c). Additionally, the Von Misses contour is shown in Figure 5.7(d) where stress concentration and yielding was observed in the base-plate, web and flanges.

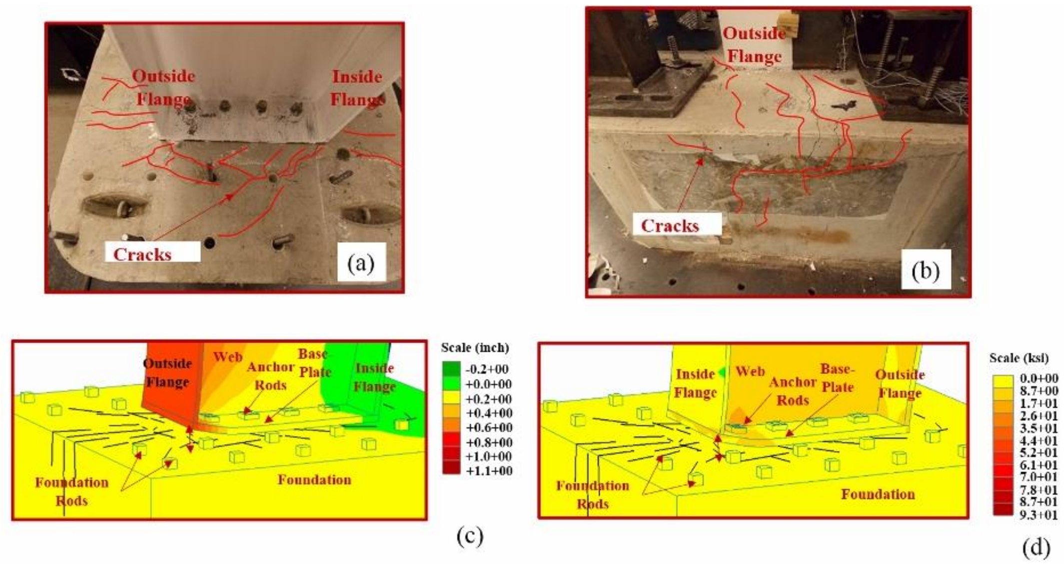

Figure 5.7. (a), (b) Behavior of damage group 4 (S08) and (c) deformation pattern extracted from the numerical models, and (d) stress pattern extracted from the numerical models.

The flexural load was measured at each applied displacement increment (0.1 inch) to the transfer beam [see Figure 5.2(a)]. Note that this was a displacement controlled simulation. The compressive axial load was applied as pressure acting atop of the transfer beam in the location that it was applied during testing [see Figure 5.2(a)]. Additional boundary conditions were not applied in the column, the foundation or the transfer beam. Figure 5.8 shows the moment-rotation response of the analytical models compared with the response of the specimens obtained from testing. The secant rotational stiffness of the analytical models is calculated at a rotation of an average of 0.003 radians with a chord passing from the origin. The moment-rotation response of the connections (as well as the response of the numerical models presented in Section 5.3 and this rotation range was characterized as a good estimation for the rotation in the elastic region. A comparison of the rotational stiffness and moment capacity of the connections obtained from the analytical analysis and the experiments are summarized in Table 5.5. There is a discrepancy between the rotational stiffness obtained from the analytical models and the experiments. It should be noted that even if the discrepancy of rotational stiffness was significant for certain cases, given the sensitivity of the rotation measurements at very small values, these results were found reasonable. On the other hand, it was observed that the moment capacity of the base-plate connections estimated with the analytical models is in a good agreement with the ones calculated from the experimental results. Specifically, the rotational stiffness obtained from the three-dimensional analytical models varies from 0% up to 73.3% in push direction, from 1.9% up to 62.1% in pull direction and their average from 2.5% up to 41.0% in comparison with the rotational stiffness reported from the experiments. The moment capacity obtained from the three-dimensional analytical models varies from 2.1% up to 33.5% in push direction and from 0.7% up to 23.5% in pull direction in comparison with the moment capacity reported from the experiments.

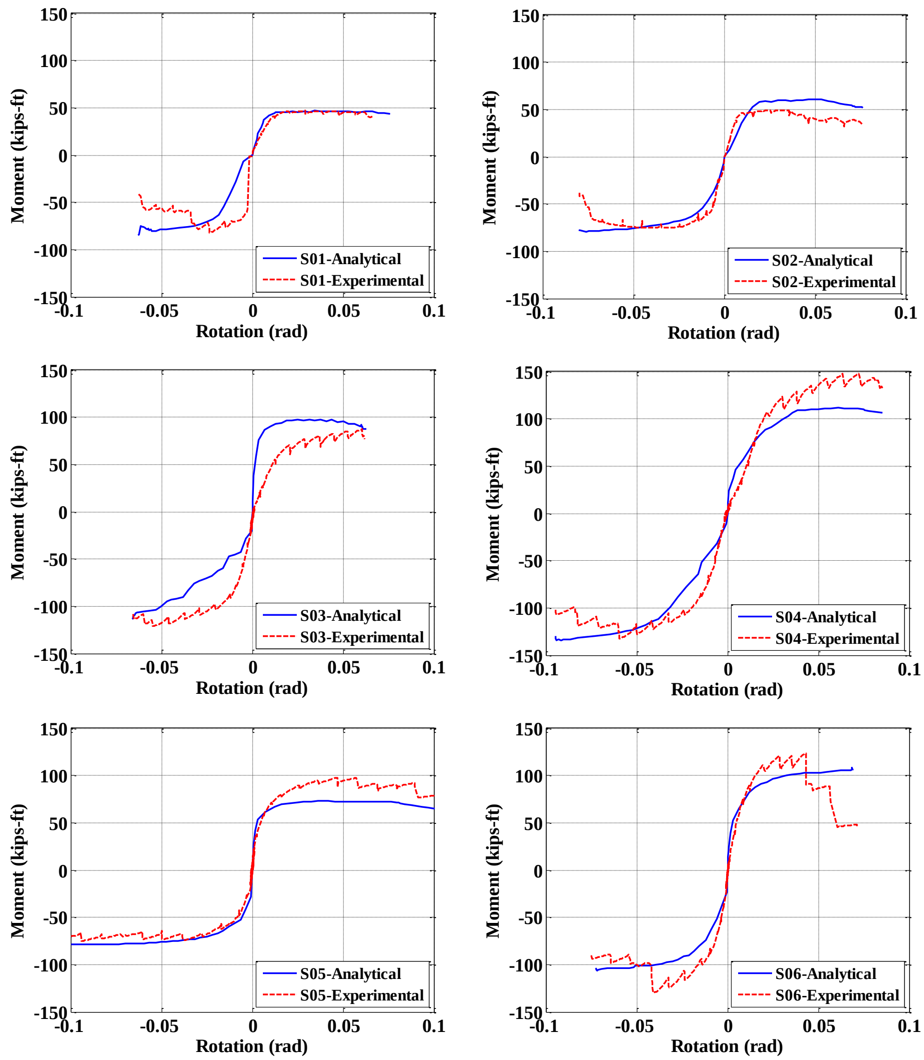

Figure 5.8. Comparison of the analytical (blue) and experimental (red) moment-rotation responses.

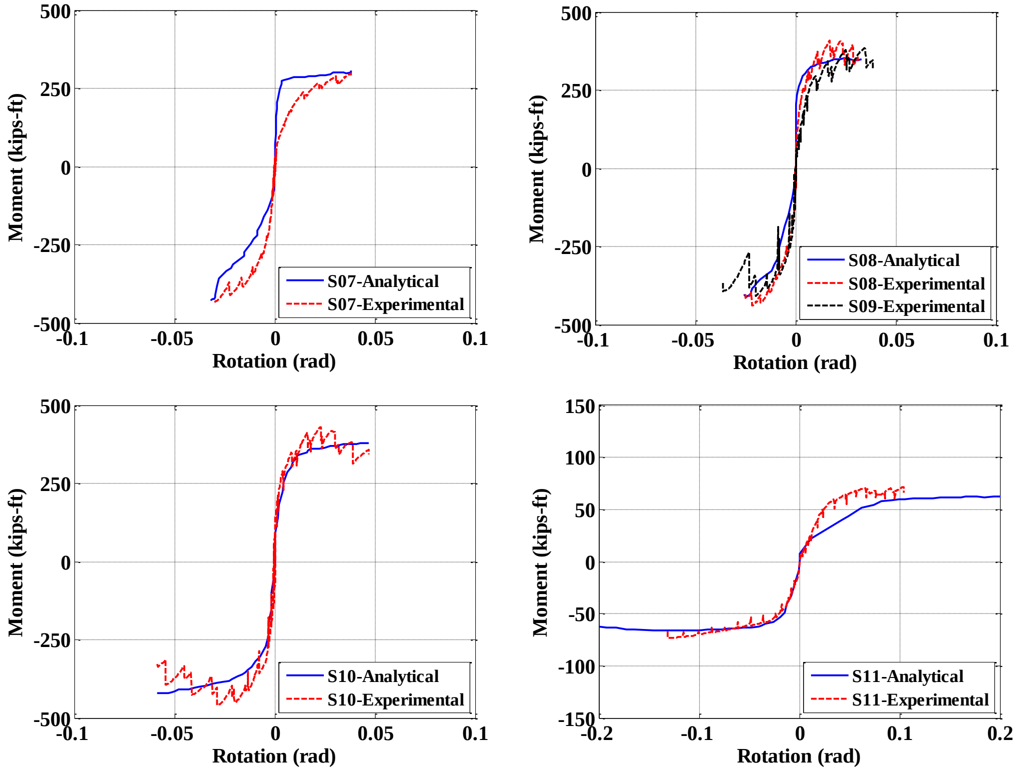

Figure 5.8. (Continued) Comparison of the analytical (blue) and experimental (red) moment-rotation responses.

Table 5.5. Comparison of the Rotational Stiffness and Moment Capacity between the Analytical Models and the Experimental Results for the Specimens Tested in the Second Phase of the Experimental Program.

	Rotational Stiffness-Analytical Model			Rotational Stiffness-Experiments			Moment Capacity Analytical Model		Moment Capacity Experiments		Difference Analytical-Experimental				
Specimen ID	K^+	K^-	K_{aver}	K^+	K^-	K_{aver}	M_m^+	M_m^-	M_m^+	M_m^-	K^+	K^-	K_{aver}	M^+	M^-
-	(kips-ft/rad)			(kips-ft/rad)			(kips-ft)		(kips-ft)		(%)			(%)	
S01	6208	13624	9916	3456	9722	6589	45.9	80.5	46.9	82.1	44.3	28.6	33.6	2.1	2.0
S02	3649	8182	5915	6091	8030	7061	61.0	79.0	49.4	75.2	66.9	1.9	19.4	19.0	4.9
S03	13118	8247	10683	6862	11994	9428	97.0	113.5	87.4	121.1	47.7	45.4	11.7	9.9	6.7
S04	12526	6694	9610	4300	7226	5763	111.5	133.8	147.9	132.8	65.7	7.9	40.0	32.7	0.7
S05	16372	8031	12201	10462	7762	9112	73.0	78.5	97.4	79.4	36.1	3.3	25.3	33.5	1.2
S06	7920	12019	9970	9882	15312	12597	105.4	105.4	123.8	130.2	24.8	27.4	26.4	17.5	23.5
S07	105611	40636	73123	28171	58142	43157	289.0	426.0	297.0	432.7	73.3	43.1	41.0	2.8	1.6
S08	77794	83000	80397	83889	85372	84631	352.0	403.0	407.3	438.8	7.8	2.9	5.3	15.7	8.9
S09	77794	83000	80397	44942	134574	89758	352.0	403.0	384.1	407.3	42.2	62.1	11.6	9.1	1.1
S10	82877	84054	83465	120672	113821	117247	379.0	420.0	429.1	459.5	45.6	35.4	40.5	13.2	9.4
S11	1897	3882	2889	1896	4027	2962	62.8	66.5	71.5	73.4	0.0	3.7	2.5	13.9	10.4

5.3. Parametric Analysis

The developed three dimensional analytical models were utilized for a parametric investigation to understand the effect of the connection design variables on the rotational stiffness and moment capacity. For this reason three web-depth (12 inch, 18 inch, 22 inch) column base-plate connections that are representative of real base-plate connections in low-rise buildings were selected as base models. Sixty five to sixty eight different column base-plate connection combinations then were created for each web depth in order to examine the effect of eleven different parameters on the rotational stiffness and moment capacity of the connections. The base-plate connection models are shown in Figure 5.9 and the model combinations for the 12 inch, 18 inch and 26 inch web depth connections are shown in Table 5.6, Table 5.7 and Table 5.8, respectively.

The parameters under investigation were the flange width, web thickness, flange thickness, base-plate width, base-plate thickness, anchor rod diameter, number of anchor rods, gage, setback and pitch distances of the anchor rods and the applied axial load. In parallel, the combination of different base-plate thickness with different anchor rod diameters and applied axial loads was examined. It should be noted that the minimum requirements for 1.0 inch anchor rod diameter is 4 inch setback and 10 inch base-plate width, and for 1 1/4 inch diameter anchor rod is 4 inch setback, 5 inch pitch and 5 inch gage and 10 inch base-plate width. These requirements needed to be violated in the sake of the parametric study. The rotational stiffness presented in the parametric analysis was calculated at 0.0025-0.0035 radians. Moment-rotation behaviors plotted from several models of the three web-depths estimated that this rotation range is a good estimation of the rotation in the elastic region. The moment capacity and rotational stiffness of each connection combination was normalized by the base model connections P01, P02, P03 (see Figure 5.9). In the case that there were two or three parameters altering while investigating the effect of the base-plate thickness, anchor rod diameter and the applied axial load (Sections 5.3.6, 5.3.7 and 5.3.12 to 5.3.15), the different model combinations were normalized by the combination indicated in red color.

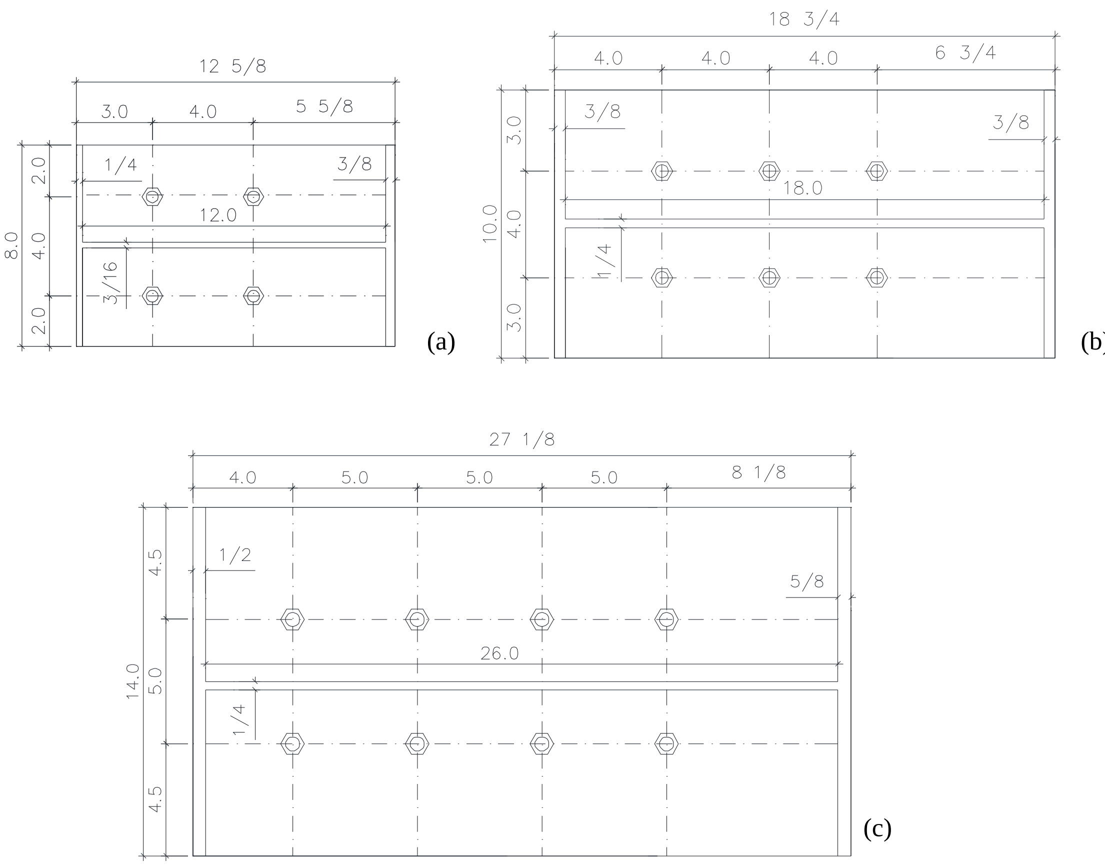

Figure 5.9. Base column base-plate connections for (a) 12 inch web depth connections (P01), (b) 18 inch web depth connections (P02), (c) 26 inch web depth connections (P03).

The results of the parametric study are presented in Sections 5.3.1-5.3.15. Each parameter under investigation is presented in a separate section for the three different web depths. At the beginning of each section, a table with the details of the connections and the model numbers referred in Table 5.6, Table 5.7 and Table 5.8 are presented. Then, the influence of the parameter under investigation for different web depths is discussed and the normalized results of the rotational stiffness and moment capacity are given. At the end of each section, a summary of the most important results is provided. The values for the rotational stiffness and moment capacity of all the combinations are given in Appendix D.

Table 5.6. Parametric Analysis Matrix for the 12 inch Web Depth Column Base-Plate Connections.

Model ID	Parameter	Web Depth	Flange Width	Web Thickness	Outside Flange Thickness	Inside Flange Thickness	Base-Plate Width	Base-Plate Thickness	Anchor Rod Diameter	Number of Anchor Rods	Pitch	Gage	Setback	Setback	Base Plate Depth	Axial Load
		d_w	b_f	t_w	t_{fo}	t_{fi}	b_{bp}	t_p	d_b	-	S_1	g	S_0	S	d	
		(inch)	(inch)	(inch)	(inch)	(inch)	(inch)	(inch)	(inch)		(inch)	(inch)	(inch)	(inch)	(inch)	(kips)
P01	-	12	8	3/16	1/4	3/8	8	3/8	3/4	4	4	4	3	5 5/8	12 5/8	50 C*
P01-01	**Flange Width**	12	6	3/16	1/4	3/8	8	3/8	3/4	4	4	4	3	5 5/8	12 5/8	50 C*
P01-02		12	10	3/16	1/4	3/8	10	3/8	3/4	4	4	4	3	5 5/8	12 5/8	50 C*
P01-03		12	12	3/16	1/4	3/8	12	3/8	3/4	4	4	4	3	5 5/8	12 5/8	50 C*
P01-04	**Web Thickness**	12	8	1/4	1/4	3/8	8	3/8	3/4	4	4	4	3	5 5/8	12 5/8	50 C*
P01-05		12	8	5/16	1/4	3/8	8	3/8	3/4	4	4	4	3	5 5/8	12 5/8	50 C*
P01-06		12	8	7/16	1/4	3/8	8	3/8	3/4	4	4	4	3	5 5/8	12 5/8	50 C*
P01-07	**Flanges Thicknesses**	12	8	3/16	3/16	5/16	8	3/8	3/4	4	4	4	3	5 1/2	12 1/2	50 C*
P01-08		12	8	3/16	5/16	7/16	8	3/8	3/4	4	4	4	3	5 3/4	12 3/4	50 C*
P01-09		12	8	3/16	5/16	5/16	8	3/8	3/4	4	4	4	3	5 5/8	12 5/8	50 C*
P01-10		12	8	3/16	7/16	7/16	8	3/8	3/4	4	4	4	3	5 7/8	12 7/8	50 C*
P01-11	**Base-Plate Width**	12	8	3/16	1/4	3/8	10	3/8	3/4	4	4	4	3	5 5/8	12 5/8	50 C*
P01-12		12	8	3/16	1/4	3/8	12	3/8	3/4	4	4	4	3	5 5/8	12 5/8	50 C*
P01-13		12	8	3/16	1/4	3/8	14	3/8	3/4	4	4	4	3	5 5/8	12 5/8	50 C*
P01-14	**Base-Plate Thickness**	12	8	3/16	1/4	3/8	8	1/2	3/4	4	4	4	3	5 5/8	12 5/8	50 C*
P01-15		12	8	3/16	1/4	3/8	8	5/8	3/4	4	4	4	3	5 5/8	12 5/8	50 C*
P01-16		12	8	3/16	1/4	3/8	8	3/4	3/4	4	4	4	3	5 5/8	12 5/8	50 C*
P01-17	**Anchor Rod Diameter**	12	8	3/16	1/4	3/8	8	3/8	1	4	4	4	**3	5 5/8	12 5/8	50 C*
P01-18		12	8	3/16	1/4	3/8	8**	3/8	1 1/4	4	**4	**4	**3	5 5/8	12 5/8	50 C*
P01-19	**Base-Plate Thickness and Anchor Rod Diameter**	12	8	3/16	1/4	3/8	8	1/2	1	4	4	4	**3	5 5/8	12 5/8	50 C*
P01-20		12	8	3/16	1/4	3/8	8	5/8	1	4	4	4	**3	5 5/8	12 5/8	50 C*
P01-21		12	8	3/16	1/4	3/8	8	3/4	1	4	4	4	**3	5 5/8	12 5/8	50 C*
P01-22		12	8	3/16	1/4	3/8	8**	1/2	1 1/4	4	**4	**4	**3	5 5/8	12 5/8	50 C*
P01-23		12	8	3/16	1/4	3/8	8**	5/8	1 1/4	4	**4	**4	**3	5 5/8	12 5/8	50 C*
P01-24		12	8	3/16	1/4	3/8	8**	3/4	1 1/4	4	**4	**4	**3	5 5/8	12 5/8	50 C*
P01-25	**Number of Anchor Rods**	12	8	3/16	1/4	3/8	8	3/8	3/4	6	4	4	3	1 5/8	12 5/8	50 C*
P01-26	**Pitch**	12	8	3/16	1/4	3/8	8	3/8	3/4	4	5	4	3	4 5/8	12 5/8	50 C*
P01-27		12	8	3/16	1/4	3/8	8	3/8	3/4	4	6	4	3	3 5/8	12 5/8	50 C*
P01-28	**Setback**	12	8	3/16	1/4	3/8	8	3/8	3/4	4	4	4	4	4 5/8	12 5/8	50 C*
P01-29		12	8	3/16	1/4	3/8	8	3/8	3/4	4	4	4	5	3 5/8	12 5/8	50 C*

*C stands for compression and T for Tension.

**Minimum requirements for 1 inch anchor rod diameter is 4 inch setback and 10 inch base-plate width, and for 1 1/4 inch diameter anchor rod is 4 inch setback, 5 inch pitch and 5 inch gage and 10 inch base-plate width.

Table 5.6. (Continued) Parametric Analysis Matrix for the 12 inch Web Depth Column Base-Plate Connections.

Model ID	Parameter	Web Depth	Flange Width	Web Thickness	Outside Flange Thickness	Inside Flange Thickness	Base-Plate Width	Base-Plate Thickness	Anchor Rod Diameter	Number of Anchor Rods	Pitch	Gage	Setback	Setback	Base Plate Depth	Axial Load
		d_w	b_f	t_w	t_{fo}	t_{fi}	b_{bp}	t_p	d_b	-	S_1	g	S_0	S	d	
		(inch)	(inch)	(inch)	(inch)	(inch)	(inch)	(inch)	(inch)		(inch)	(inch)	(inch)	(inch)	(inch)	(kips)
P01-30	**Axial Load**	12	8	3/16	1/4	3/8	8	3/8	3/4	4	4	4	3	5 5/8	12 5/8	0
P01-31		12	8	3/16	1/4	3/8	8	1/2	3/4	4	4	4	3	5 5/8	12 5/8	0
P01-32		12	8	3/16	1/4	3/8	8	5/8	3/4	4	4	4	3	5 5/8	12 5/8	0
P01-33		12	8	3/16	1/4	3/8	8	3/4	3/4	4	4	4	3	5 5/8	12 5/8	0
P01-34		12	8	3/16	1/4	3/8	8	3/8	1	4	4	4	**3	5 5/8	12 5/8	0
P01-35		12	8	3/16	1/4	3/8	8**	3/8	1 1/4	4	**4	**4	**3	5 5/8	12 5/8	0
P01-36		12	8	3/16	1/4	3/8	8	1/2	1	4	4	4	**3	5 5/8	12 5/8	0
P01-37		12	8	3/16	1/4	3/8	8	5/8	1	4	4	4	**3	5 5/8	12 5/8	0
P01-38		12	8	3/16	1/4	3/8	8	3/4	1	4	4	4	**3	5 5/8	12 5/8	0
P01-39		12	8	3/16	1/4	3/8	8**	1/2	1 1/4	4	**4	**4	**3	5 5/8	12 5/8	0
P01-40		12	8	3/16	1/4	3/8	8**	5/8	1 1/4	4	**4	**4	**3	5 5/8	12 5/8	0
P01-41		12	8	3/16	1/4	3/8	8**	3/4	1 1/4	4	**4	**4	**3	5 5/8	12 5/8	0
P01-42		12	8	3/16	1/4	3/8	8	3/8	3/4	4	4	4	3	5 5/8	12 5/8	25 C*
P01-43		12	8	3/16	1/4	3/8	8	1/2	3/4	4	4	4	3	5 5/8	12 5/8	25 C*
P01-44		12	8	3/16	1/4	3/8	8	5/8	3/4	4	4	4	3	5 5/8	12 5/8	25 C*
P01-45		12	8	3/16	1/4	3/8	8	3/4	3/4	4	4	4	3	5 5/8	12 5/8	25 C*
P01-46		12	8	3/16	1/4	3/8	8	3/8	1	4	4	4	**3	5 5/8	12 5/8	25 C*
P01-47		12	8	3/16	1/4	3/8	8**	3/8	1 1/4	4	**4	**4	**3	5 5/8	12 5/8	25 C*
P01-48		12	8	3/16	1/4	3/8	8	1/2	1	4	4	4	**3	5 5/8	12 5/8	25 C*
P01-49		12	8	3/16	1/4	3/8	8	5/8	1	4	4	4	**3	5 5/8	12 5/8	25 C*
P01-50		12	8	3/16	1/4	3/8	8	3/4	1	4	4	4	**3	5 5/8	12 5/8	25 C*
P01-51		12	8	3/16	1/4	3/8	8**	1/2	1 1/4	4	**4	**4	**3	5 5/8	12 5/8	25 C*
P01-52		12	8	3/16	1/4	3/8	8**	5/8	1 1/4	4	**4	**4	**3	5 5/8	12 5/8	25 C*
P01-53		12	8	3/16	1/4	3/8	8**	3/4	1 1/4	4	**4	**4	**3	5 5/8	12 5/8	25 C*
P01-54		12	8	3/16	1/4	3/8	8	3/8	3/4	4	4	4	3	5 5/8	12 5/8	25 T*
P01-55		12	8	3/16	1/4	3/8	8	1/2	3/4	4	4	4	3	5 5/8	12 5/8	25 T*
P01-56		12	8	3/16	1/4	3/8	8	5/8	3/4	4	4	4	3	5 5/8	12 5/8	25 T*
P01-57		12	8	3/16	1/4	3/8	8	3/4	3/4	4	4	4	3	5 5/8	12 5/8	25 T*
P01-58		12	8	3/16	1/4	3/8	8	3/8	1	4	4	4	**3	5 5/8	12 5/8	25 T*
P01-59		12	8	3/16	1/4	3/8	8**	3/8	1 1/4	4	**4	**4	**3	5 5/8	12 5/8	25 T*
P01-60		12	8	3/16	1/4	3/8	8	1/2	1	4	4	4	**3	5 5/8	12 5/8	25 T*
P01-61		12	8	3/16	1/4	3/8	8	5/8	1	4	4	4	**3	5 5/8	12 5/8	25 T*
P01-62		12	8	3/16	1/4	3/8	8	3/4	1	4	4	4	**3	5 5/8	12 5/8	25 T*
P01-63		12	8	3/16	1/4	3/8	8**	1/2	1 1/4	4	**4	**4	**3	5 5/8	12 5/8	25 T*
P01-64		12	8	3/16	1/4	3/8	8**	5/8	1 1/4	4	**4	**4	**3	5 5/8	12 5/8	25 T*
P01-65		12	8	3/16	1/4	3/8	8**	3/4	1 1/4	4	**4	**4	**3	5 5/8	12 5/8	25 T*

*C stands for compression and T for Tension.

**Minimum requirements for 1 inch anchor rod diameter is 4 inch setback and 10 inch base-plate width, and for 1 1/4 inch diameter anchor rod is 4 inch setback, 5 inch pitch and 5 inch gage and 10 inch base-plate width.

Table 5.7. Parametric Analysis Matrix for the 18 inch Web Depth Column Base-Plate Connections.

Model ID	Parameter	Web Depth	Flange Width	Web Thickness	Outside Flange Thickness	Inside Flange Thickness	Base-Plate Width	Base-Plate Thickness	Anchor Rod Diameter	Number of Anchor Rods	Pitch	Gage	Setback	Setback	Base Plate Depth	Axial Load
		d_w	b_f	t_w	t_{fo}	t_{fi}	b_{bp}	t_p	d_b	-	S_1	g	S_0	S	d	
		(inch)	(inch)	(inch)	(inch)	(inch)	(inch)	(inch)	(inch)		(inch)	(inch)	(inch)	(inch)	(inch)	(kips)
P02	-	18	10	4/16	3/8	3/8	10	1/2	1	6	4	4	4	6 3/4	18 3/4	50 C*
P02-01	**Flange Width**	18	8	4/16	3/8	3/8	10	1/2	1	6	4	4	4	6 3/4	18 3/4	50 C*
P02-02		18	12	4/16	3/8	3/8	12	1/2	1	6	4	4	4	6 3/4	18 3/4	50 C*
P02-03		18	14	4/16	3/8	3/8	14	1/2	1	6	4	4	4	6 3/4	18 3/4	50 C*
P02-04	**Web Thickness**	18	10	1/5	3/8	3/8	10	1/2	1	6	4	4	4	6 3/4	18 3/4	50 C*
P02-05		18	10	5/16	3/8	3/8	10	1/2	1	6	4	4	4	6 3/4	18 3/4	50 C*
P02-06		18	10	7/16	3/8	3/8	10	1/2	1	6	4	4	4	6 3/4	18 3/4	50 C*
P02-07	**Flanges Thicknesses**	18	10	4/16	4/16	4/16	10	1/2	1	6	4	4	4	6 1/2	18 1/2	50 C*
P02-08		18	10	4/16	4/16	6/16	10	1/2	1	6	4	4	4	6 5/8	18 5/8	50 C*
P02-09		18	10	4/16	6/16	4/16	10	1/2	1	6	4	4	4	6 5/8	18 5/8	50 C*
P02-10		18	10	4/16	8/16	10/16	10	1/2	1	6	4	4	4	7 1/8	19 1/8	50 C*
P02-11	**Base-Plate Width**	18	10	4/16	3/8	3/8	12	1/2	1	6	4	4	4	6 3/4	18 3/4	50 C*
P02-12		18	10	4/16	3/8	3/8	14	1/2	1	6	4	4	4	6 3/4	18 3/4	50 C*
P02-13		18	10	4/16	3/8	3/8	16	1/2	1	6	4	4	4	6 3/4	18 3/4	50 C*
P02-14	**Base-Plate Thickness**	18	10	4/16	3/8	3/8	10	3/8	1	6	4	4	4	6 3/4	18 3/4	50 C*
P02-15		18	10	4/16	3/8	3/8	10	5/8	1	6	4	4	4	6 3/4	18 3/4	50 C*
P02-16		18	10	4/16	3/8	3/8	10	3/4	1	6	4	4	4	6 3/4	18 3/4	50 C*
P02-17	**Anchor Rod Diameter**	18	10	4/16	3/8	3/8	10	1/2	3/4	6	4	4	4	6 3/4	18 3/4	50 C*
P02-18		18	10	4/16	3/8	3/8	10	1/2	1 1/4	6	**4	**4	4	6 3/4	18 3/4	50 C*
P02-19	**Base-Plate Thickness and Anchor Rod Diameter**	18	10	4/16	3/8	3/8	10	3/8	3/4	6	4	4	4	6 3/4	18 3/4	50 C*
P02-20		18	10	4/16	3/8	3/8	10	5/8	3/4	6	4	4	4	6 3/4	18 3/4	50 C*
P02-21		18	10	4/16	3/8	3/8	10	3/4	3/4	6	4	4	4	6 3/4	18 3/4	50 C*
P02-22		18	10	4/16	3/8	3/8	10	3/8	1 1/4	6	**4	**4	4	6 3/4	18 3/4	50 C*
P02-23		18	10	4/16	3/8	3/8	10	5/8	1 1/4	6	**4	**4	4	6 3/4	18 3/4	50 C*
P02-24		18	10	4/16	3/8	3/8	10	3/4	1 1/4	6	**4	**4	4	6 3/4	18 3/4	50 C*
P02-25	**Number of Anchor Rods**	18	10	4/16	3/8	3/8	10	1/2	1	4	4	4	4	10 3/4	18 3/4	50 C*
P02-26		18	10	4/16	3/8	3/8	10	1/2	1	8	4	4	4	2 3/4	18 3/4	50 C*
P02-27	**Pitch**	18	10	4/16	3/8	3/8	10	1/2	1	6	5	4	4	4 3/4	18 3/4	50 C*
P02-28		18	10	4/16	3/8	3/8	10	1/2	1	6	6	4	4	2 3/4	18 3/4	50 C*
P02-29	**Setback**	18	10	4/16	3/8	3/8	10	1/2	1	6	4	4	5	5 3/4	18 3/4	50 C*
P02-30		18	10	0.25	0.375	0.375	10	0.5	1	6	4	4	6	4.75	18.75	50 C*
P02-31	**Gage**	18	10	0.25	0.375	0.375	10	0.5	1	6	4	5	4	6.75	18.75	50 C*
P02-32		18	10	0.25	0.375	0.375	10	0.5	1	6	4	6	4	6.75	18.75	50 C*

*C stands for compression and T for Tension.
**Minimum requirements for 1 inch anchor rod diameter is 4 inch setback and 10 inch base-plate width, and for 1 1/4 inch diameter anchor rod is 4 inch setback, 5 inch pitch and 5 inch gage and 10 inch base-plate width.

Table 5.7. (Continued) Parametric Analysis Matrix for the 18 inch Web Depth Column Base-Plate Connections.

Model ID	Parameter	Web Depth	Flange Width	Web Thickness	Outside Flange Thickness	Inside Flange Thickness	Base-Plate Width	Base-Plate Thickness	Anchor Rod Diameter	Number of Anchor Rods	Pitch	Gage	Setback	Setback	Base Plate Depth	Axial Load
		d_w	b_f	t_w	t_{fo}	t_{fi}	b_{bp}	t_p	d_b	-	S_1	g	S_0	S	d	
		(inch)	(inch)	(inch)	(inch)	(inch)	(inch)	(inch)	(inch)		(inch)	(inch)	(inch)	(inch)	(inch)	(kips)
P02-33		18	10	4/16	3/8	3/8	10	1/2	1	6	4	4	4	6 3/4	18 3/4	0
P02-34		18	10	4/16	3/8	3/8	10	3/8	1	6	4	4	4	6 3/4	18 3/4	0
P02-35		18	10	4/16	3/8	3/8	10	5/8	1	6	4	4	4	6 3/4	18 3/4	0
P02-36		18	10	4/16	3/8	3/8	10	3/4	1	6	4	4	4	6 3/4	18 3/4	0
P02-37		18	10	1/4	3/8	3/8	10	1/2	3/4	6	4	4	4	6 3/4	18 3/4	0
P02-38		18	10	1/4	3/8	3/8	10	1/2	1 1/4	6	**4	**4	4	6 3/4	18 3/4	0
P02-39		18	10	4/16	3/8	3/8	10	3/8	3/4	6	4	4	4	6 3/4	18 3/4	0
P02-40		18	10	4/16	3/8	3/8	10	5/8	3/4	6	4	4	4	6 3/4	18 3/4	0
P02-41		18	10	4/16	3/8	3/8	10	3/4	3/4	6	4	4	4	6 3/4	18 3/4	0
P02-42		18	10	4/16	3/8	3/8	10	3/8	1 1/4	6	**4	**4	4	6 3/4	18 3/4	0
P02-43		18	10	4/16	3/8	3/8	10	5/8	1 1/4	6	**4	**4	4	6 3/4	18 3/4	0
P02-44		18	10	4/16	3/8	3/8	10	3/4	1 1/4	6	**4	**4	4	6 3/4	18 3/4	0
P02-45		18	10	4/16	3/8	3/8	10	1/2	1	6	4	4	4	6 3/4	18 3/4	25 C*
P02-46		18	10	4/16	3/8	3/8	10	3/8	1	6	4	4	4	6 3/4	18 3/4	25 C*
P02-47		18	10	4/16	3/8	3/8	10	5/8	1	6	4	4	4	6 3/4	18 3/4	25 C*
P02-48		18	10	4/16	3/8	3/8	10	3/4	1	6	4	4	4	6 3/4	18 3/4	25 C*
P02-49		18	10	1/4	3/8	3/8	10	1/2	3/4	6	4	4	4	6 3/4	18 3/4	25 C*
P02-50	Axial Load	18	10	1/4	3/8	3/8	10	1/2	1 1/4	6	**4	**4	4	6 3/4	18 3/4	25 C*
P02-51		18	10	4/16	3/8	3/8	10	3/8	3/4	6	4	4	4	6 3/4	18 3/4	25 C*
P02-52		18	10	4/16	3/8	3/8	10	5/8	3/4	6	4	4	4	6 3/4	18 3/4	25 C*
P02-53		18	10	4/16	3/8	3/8	10	3/4	3/4	6	4	4	4	6 3/4	18 3/4	25 C*
P02-54		18	10	4/16	3/8	3/8	10	3/8	1 1/4	6	**4	**4	4	6 3/4	18 3/4	25 C*
P02-55		18	10	4/16	3/8	3/8	10	5/8	1 1/4	6	**4	**4	4	6 3/4	18 3/4	25 C*
P02-56		18	10	4/16	3/8	3/8	10	3/4	1 1/4	6	**4	**4	4	6 3/4	18 3/4	25 C*
P02-57		18	10	4/16	3/8	3/8	10	1/2	1	6	4	4	4	6 3/4	18 3/4	25 T*
P02-58		18	10	4/16	3/8	3/8	10	3/8	1	6	4	4	4	6 3/4	18 3/4	25 T*
P02-59		18	10	4/16	3/8	3/8	10	5/8	1	6	4	4	4	6 3/4	18 3/4	25 T*
P02-60		18	10	4/16	3/8	3/8	10	3/4	1	6	4	4	4	6 3/4	18 3/4	25 T*
P02-61		18	10	1/4	3/8	3/8	10	1/2	3/4	6	4	4	4	6 3/4	18 3/4	25 T*
P02-62		18	10	1/4	3/8	3/8	10	1/2	1 1/4	6	**4	**4	4	6 3/4	18 3/4	25 T*
P02-63		18	10	4/16	3/8	3/8	10	3/8	3/4	6	4	4	4	6 3/4	18 3/4	25 T*
P02-64		18	10	4/16	3/8	3/8	10	5/8	3/4	6	4	4	4	6 3/4	18 3/4	25 T*
P02-65		18	10	4/16	3/8	3/8	10	3/4	3/4	6	4	4	4	6 3/4	18 3/4	25 T*
P02-66		18	10	4/16	3/8	3/8	10	3/8	1 1/4	6	**4	**4	4	6 3/4	18 3/4	25 T*
P02-67		18	10	4/16	3/8	3/8	10	5/8	1 1/4	6	**4	**4	4	6 3/4	18 3/4	25 T*
P02-68		18	10	4/16	3/8	3/8	10	3/4	1 1/4	6	**4	**4	4	6 3/4	18 3/4	25 T*

*C stands for compression and T for Tension.

**Minimum requirements for 1 inch anchor rod diameter is 4 inch setback and 10 inch base-plate width, and for 1 1/4 inch diameter anchor rod is 4 inch setback, 5 inch pitch and 5 inch gage and 10 inch base-plate width.

Table 5.8. Parametric Analysis Matrix for the 26 inch Web Depth Column Base-Plate Connections.

Model ID	Parameter	Web Depth	Flange Width	Web Thickness	Outside Flange Thickness	Inside Flange Thickness	Base-Plate Width	Base-Plate Thickness	Anchor Rod Diameter	Number of Anchor Rods	Pitch	Gage	Setback	Setback	Base Plate Depth	Axial Load
		d_w	b_f	t_w	t_{fo}	t_{fi}	b_{bp}	t_p	d_b	-	S_1	g	S_0	S	d	
		(inch)	(inch)	(inch)	(inch)	(inch)	(inch)	(inch)	(inch)		(inch)	(inch)	(inch)	(inch)	(inch)	(kips)
P03	-	26	14	1/4	1/2	5/8	14	5/8	1 1/4	8	5	5	4	8 1/8	27 1/8	100 C*
P03-01	Flange Width	26	10	1/4	1/2	5/8	14	5/8	1 1/4	8	5	5	4	8 1/8	27 1/8	100 C*
P03-02		26	12	1/4	1/2	5/8	14	5/8	1 1/4	8	5	5	4	8 1/8	27 1/8	100 C*
P03-03		26	16	1/4	1/2	5/8	16	5/8	1 1/4	8	5	5	4	8 1/8	27 1/8	100 C*
P03-04	Web Thickness	26	14	3/16	1/2	5/8	14	5/8	1 1/4	8	5	5	4	8 1/8	27 1/8	100 C*
P03-05		26	14	5/16	1/2	5/8	14	5/8	1 1/4	8	5	5	4	8 1/8	27 1/8	100 C*
P03-06		26	14	7/16	1/2	5/8	14	5/8	1 1/4	8	5	5	4	8 1/8	27 1/8	100 C*
P03-07	Flanges Thicknesses	26	14	1/4	3/16	5/16	14	5/8	1 1/4	8	5	5	4	7 1/2	26 1/2	100 C*
P03-08		26	14	1/4	5/16	7/16	14	5/8	1 1/4	8	5	5	4	7 3/4	26 3/4	100 C*
P03-09		26	14	1/4	5/8	3/4	14	5/8	1 1/4	8	5	5	4	8 3/8	27 3/8	100 C*
P03-10		26	14	1/4	1/2	1/2	14	5/8	1 1/4	8	5	5	4	8	27	100 C*
P03-11	Base-Plate Width	26	14	1/4	1/2	5/8	16	5/8	1 1/4	8	5	5	4	8 1/8	27 1/8	100 C*
P03-12		26	14	1/4	1/2	5/8	18	5/8	1 1/4	8	5	5	4	8 1/8	27 1/8	100 C*
P03-13		26	14	1/4	1/2	5/8	20	5/8	1 1/4	8	5	5	4	8 1/8	27 1/8	100 C*
P03-14	Base-Plate Thickness	26	14	1/4	1/2	5/8	14	3/8	1 1/4	8	5	5	4	8 1/8	27 1/8	100 C*
P03-15		26	14	1/4	1/2	5/8	14	1/2	1 1/4	8	5	5	4	8 1/8	27 1/8	100 C*
P03-16		26	14	1/4	1/2	5/8	14	3/4	1 1/4	8	5	5	4	8 1/8	27 1/8	100 C*
P03-17	Anchor Rod Diameter	26	14	1/4	1/2	5/8	14	5/8	3/4	8	5**	5**	4**	8 1/8	27 1/8	100 C*
P03-18		26	14	1/4	1/2	5/8	14	5/8	1	8	**5	**5	4	8 1/8	27 1/8	100 C*
P03-19	Base-Plate Thickness and Anchor Rod Diameter	26	14	1/4	1/2	5/8	14	3/8	3/4	8	5**	5**	4**	8 1/8	27 1/8	100 C*
P03-20		26	14	1/4	1/2	5/8	14	1/2	3/4	8	5**	5**	4**	8 1/8	27 1/8	100 C*
P03-21		26	14	1/4	1/2	5/8	14	3/4	3/4	8	5**	5**	4**	8 1/8	27 1/8	100 C*
P03-22		26	14	1/4	1/2	5/8	14	3/8	1	8	**5	**5	4	8 1/8	27 1/8	100 C*
P03-23		26	14	1/4	1/2	5/8	14	1/2	1	8	**5	**5	4	8 1/8	27 1/8	100 C*
P03-24		26	14	1/4	1/2	5/8	14	3/4	1	8	**5	**5	4	8 1/8	27 1/8	100 C*
P03-25	Number of Anchor Rods	26	14	1/4	1/2	5/8	14	5/8	1 1/4	6	5	5	4	13 1/8	27 1/8	100 C*
P03-26		26	14	1/4	1/2	5/8	14	5/8	1 1/4	10	5	5	4	3 1/8	27 1/8	100 C*
P03-27	Pitch	26	14	1/4	1/2	5/8	14	5/8	1 1/4	8	6	5	4	5 1/8	27 1/8	100 C*
P03-28		26	14	1/4	1/2	5/8	14	5/8	1 1/4	8	7	5	4	2 1/8	27 1/8	100 C*
P03-29	Setback	26	14	1/4	1/2	5/8	14	5/8	1 1/4	8	5	5	5	7 1/8	27 1/8	100 C*
P03-30		26	14	1/4	1/2	5/8	14	5/8	1 1/4	8	5	5	6	6 1/8	27 1/8	100 C*
P03-31	Gage	26	14	1/4	1/2	5/8	14	5/8	1 1/4	8	5	6	4	8 1/8	27 1/8	100 C*
P03-32		26	14	1/4	1/2	5/8	14	5/8	1 1/4	8	5	8	4	8 1/8	27 1/8	100 C*

*C stands for compression and T for Tension.

**Minimum requirements for 1 inch anchor rod diameter is 4 inch setback and 10 inch base-plate width, and for 1 1/4 inch diameter anchor rod is 4 inch setback, 5 inch pitch and 5 inch gage and 10 inch base-plate width.

Table 5.8. (Continued) Parametric Analysis Matrix for the 26 inch Web Depth Column Base-Plate Connections.

Model ID	Parameter	Web Depth	Flange Width	Web Thickness	Outside Flange Thickness	Inside Flange Thickness	Base-Plate Width	Base-Plate Thickness	Anchor Rod Diameter	Number of Anchor Rods	Pitch	Gage	Setback	Setback	Base Plate Depth	Axial Load
		d_w	b_f	t_w	t_{fo}	t_{fi}	b_{bp}	t_p	d_b	-	S_1	g	S_0	S	d	
		(inch)	(inch)	(inch)	(inch)	(inch)	(inch)	(inch)	(inch)		(inch)	(inch)	(inch)	(inch)	(inch)	(kips)
P03-33		26	14	1/4	1/2	5/8	14	5/8	1 1/4	8	5	5	4	8 1/8	27 1/8	0
P03-34		26	14	1/4	1/2	5/8	14	3/8	1 1/4	8	5	5	4	8 1/8	27 1/8	0
P03-35		26	14	1/4	1/2	5/8	14	1/2	1 1/4	8	5	5	4	8 1/8	27 1/8	0
P03-36		26	14	1/4	1/2	5/8	14	3/4	1 1/4	8	5	5	4	8 1/8	27 1/8	0
P03-37		26	14	1/4	1/2	5/8	14	5/8	3/4	8	5**	5**	4**	8 1/8	27 1/8	0
P03-38		26	14	1/4	1/2	5/8	14	5/8	1	8	**5	**5	4	8 1/8	27 1/8	0
P03-39		26	14	1/4	1/2	5/8	14	3/8	3/4	8	5**	5**	4**	8 1/8	27 1/8	0
P03-40		26	14	1/4	1/2	5/8	14	1/2	3/4	8	5**	5**	4**	8 1/8	27 1/8	0
P03-41		26	14	1/4	1/2	5/8	14	3/4	3/4	8	5**	5**	4**	8 1/8	27 1/8	0
P03-42		26	14	1/4	1/2	5/8	14	3/8	1	8	**5	**5	4	8 1/8	27 1/8	0
P03-43		26	14	1/4	1/2	5/8	14	1/2	1	8	**5	**5	4	8 1/8	27 1/8	0
P03-44		26	14	1/4	1/2	5/8	14	3/4	1	8	**5	**5	4	8 1/8	27 1/8	0
P03-45		26	14	1/4	1/2	5/8	14	5/8	1 1/4	8	5	5	4	8 1/8	27 1/8	50 C*
P03-46		26	14	1/4	1/2	5/8	14	3/8	1 1/4	8	5	5	4	8 1/8	27 1/8	50 C*
P03-47		26	14	1/4	1/2	5/8	14	1/2	1 1/4	8	5	5	4	8 1/8	27 1/8	50 C*
P03-48		26	14	1/4	1/2	5/8	14	3/4	1 1/4	8	5	5	4	8 1/8	27 1/8	50 C*
P03-49		26	14	1/4	1/2	5/8	14	5/8	3/4	8	5**	5**	4**	8 1/8	27 1/8	50 C*
P03-50	Axial Load	26	14	1/4	1/2	5/8	14	5/8	1	8	**5	**5	4	8 1/8	27 1/8	50 C*
P03-51		26	14	1/4	1/2	5/8	14	3/8	3/4	8	5**	5**	4**	8 1/8	27 1/8	50 C*
P03-52		26	14	1/4	1/2	5/8	14	1/2	3/4	8	5**	5**	4**	8 1/8	27 1/8	50 C*
P03-53		26	14	1/4	1/2	5/8	14	3/4	3/4	8	5**	5**	4**	8 1/8	27 1/8	50 C*
P03-54		26	14	1/4	1/2	5/8	14	3/8	1	8	**5	**5	4	8 1/8	27 1/8	50 C*
P03-55		26	14	1/4	1/2	5/8	14	1/2	1	8	**5	**5	4	8 1/8	27 1/8	50 C*
P03-56		26	14	1/4	1/2	5/8	14	3/4	1	8	**5	**5	4	8 1/8	27 1/8	50 C*
P03-57		26	14	1/4	1/2	5/8	14	5/8	1 1/4	8	5	5	4	8 1/8	27 1/8	50 T*
P03-58		26	14	1/4	1/2	5/8	14	3/8	1 1/4	8	5	5	4	8 1/8	27 1/8	50 T*
P03-59		26	14	1/4	1/2	5/8	14	1/2	1 1/4	8	5	5	4	8 1/8	27 1/8	50 T*
P03-60		26	14	1/4	1/2	5/8	14	3/4	1 1/4	8	5	5	4	8 1/8	27 1/8	50 T*
P03-61		26	14	1/4	1/2	5/8	14	5/8	3/4	8	5**	5**	4**	8 1/8	27 1/8	50 T*
P03-62		26	14	1/4	1/2	5/8	14	5/8	1	8	**5	**5	4	8 1/8	27 1/8	50 T*
P03-63		26	14	1/4	1/2	5/8	14	3/8	3/4	8	5**	5**	4**	8 1/8	27 1/8	50 T*
P03-64		26	14	1/4	1/2	5/8	14	1/2	3/4	8	5**	5**	4**	8 1/8	27 1/8	50 T*
P03-65		26	14	1/4	1/2	5/8	14	3/4	3/4	8	5**	5**	4**	8 1/8	27 1/8	50 T*
P03-66		26	14	1/4	1/2	5/8	14	3/8	1	8	**5	**5	4	8 1/8	27 1/8	50 T*
P03-67		26	14	1/4	1/2	5/8	14	1/2	1	8	**5	**5	4	8 1/8	27 1/8	50 T*
P03-68		26	14	1/4	1/2	5/8	14	3/4	1	8	**5	**5	4	8 1/8	27 1/8	50 T*

*C stands for compression and T for Tension

**Minimum requirements for 1 inch anchor rod diameter is 4 inch setback and 10 inch base-plate width, and for 1 1/4 inch diameter anchor rod is 4 inch setback, 5 inch pitch and 5 inch gage and 10 inch base-plate width.

5.3.1. Flange width

In this section the effect of the flange width on the moment capacity and rotational stiffness of the connections is investigated. Column base-plate connections with different flange widths, which is related to the base-plate width (Table 5.9) are presented for each of the three different web depths. The elastic rotational stiffness and moment capacity of the connections were normalized by those of P01, P02, P03 indicated in red color in Table 5.9. The normalized rotational stiffness and moment capacity for the 12 inch, 18 inch and 26 inch web depth connections are shown in Figure 5.10, Figure 5.11 and Figure 5.12, respectively.

Table 5.9. Parametric Study Models Investigating the Influence of the Flange Width on the Rotational Stiffness and Moment Capacity of the Connection (refer to Table 5.6, Table 5.7 and Table 5.8).

Model ID	Parameter Altering	Web Depth (inch)	Increment (inch)	Flange Width (inch)	Base-Plate Width (inch)
P01	Flange Width	12	-	8	8
P01-01			-2	6	8
P01-02			+2	10	10
P01-03			+4	12	12
P02		18	-	10	10
P02-01			-2	8	10
P02-02			+2	12	12
P02-03			+4	14	14
P03		26	-	14	14
P03-01			-4	10	14
P03-02			-2	12	14
P03-03			+2	16	16

It was observed that a decrease of the column flange width (baseline) resulted in a decrease of the moment capacity and elastic rotational stiffness of the 12 inch and 26 inch web depth connections. It is also seen that a decrease of the column flange width (baseline) had almost no effect on the rotational stiffness and moment capacity of the 18 inch web depth connections. This was due to the fact that the base-plate and anchor rod system is more rigid than the contribution of the flange stiffness, and thus decreasing the flange width (i.e., the flange area) did not change the behavior of the base-plate. In other words, for a given base-plate rotation, the applied moment did not change significantly by decreasing the flange width of the 18 inch web depth connections. On the other hand, the increase of the column flange by 2 inch increased the rotational stiffness of the 12 inch web depth connection, as well as the rotational stiffness and moment capacity of the 18 inch and 26 inch web depth connections. This was observed because the base-plate thickness of the column base-plate connections resulted in a balanced behavior, and thus an increase of the flange width increased the rigidity of base-plate connection. When the flange width was increased by 4 inch in the case of the case of the 18 inch web depth connections, then the base-plate tended to have predominantly flexural behavior and resulted in a decrease of the moment capacity and rotational stiffness.

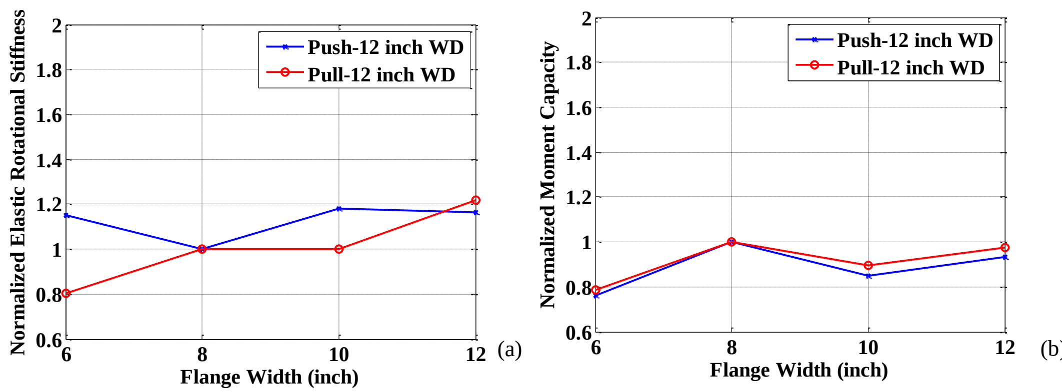

Figure 5.10. (a) Normalized elastic rotational stiffness and (b) normalized moment capacity for different flange widths of the 12 inch web depth connections.

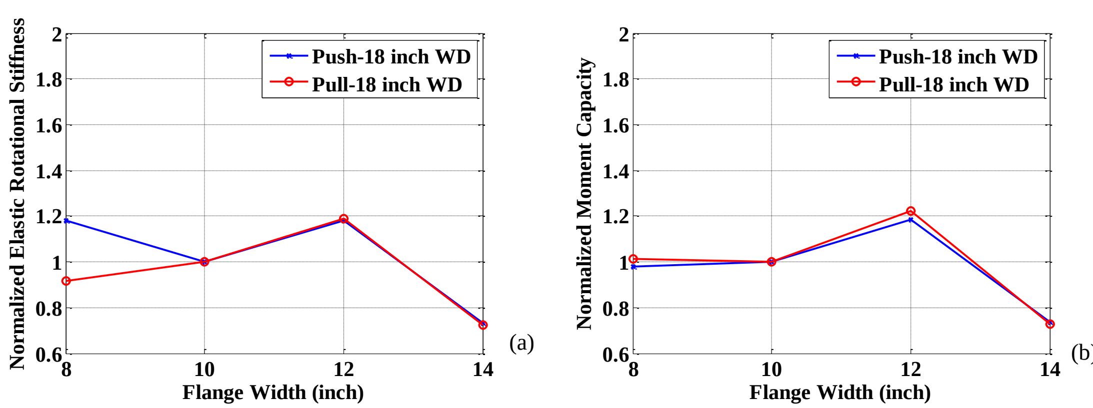

Figure 5.11. (a) Normalized elastic rotational stiffness and (b) normalized moment capacity for different flange widths of the 18 inch web depth connections.

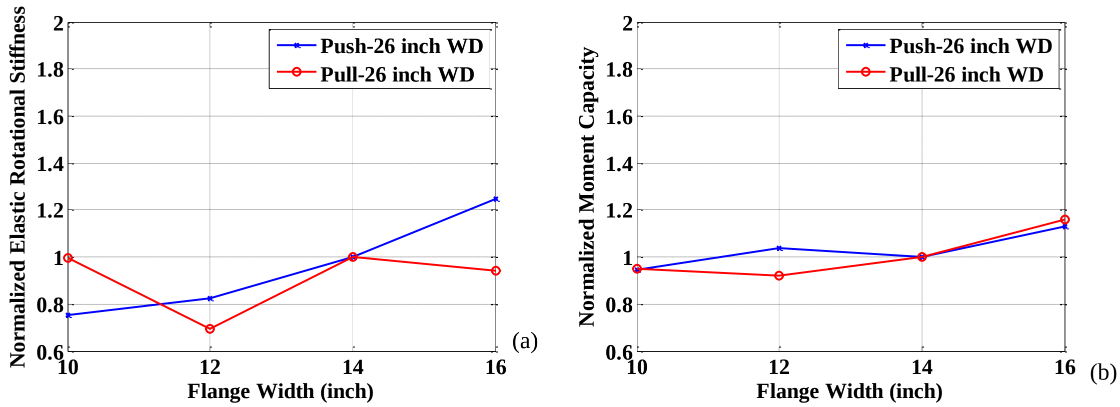

Figure 5.12. (a) Normalized elastic rotational stiffness and (b) normalized moment capacity for different flange widths of the 26 inch web depth connections.

5.3.2. Web thickness

The second parameter under investigation was the web thickness. The web thickness was varied as shown in Table 5.10 for each of the three different web depth connections. The elastic rotational stiffness and moment capacity of the connection combinations were normalized by the ones of S01, S02, S03 indicated in red color in Table 5.10. The normalized rotational stiffness and moment capacity for the 12 inch, 18 inch and 26 inch web depth connections are shown in Figure 5.13, Figure 5.14 and Figure 5.15, respectively.

Table 5.10. Parametric Study Models Investigating the Influence of the Web Thickness on the Rotational Stiffness and Moment Capacity of the Connection (refer to Table 5.6, Table 5.7 and Table 5.8).

Model ID	Parameter Altering	Web Depth (inch)	Increment (inch)	Flange Width (inch)
P01	Web Thickness	12	-	3/16
P01-04			+1/16	1/4
P01-05			+1/8	5/16
P01-06			+1/4	7/16
P02		18	-	1/4
P02-04			-1/16	3/16
P02-05			+1/16	5/16
P02-06			+3/16	7/16
P03		26	-	1/4
P03-04			-1/16	3/16
P03-05			+1/16	5/16
P03-06			+3/16	7/16

It was observed that the increase of the web thickness (baseline) resulted in the increase of the rotational stiffness and moment capacity of the 12 inch web depth connections. An increasing trend with the increase of the web thickness was also observed for the elastic rotational stiffness and moment capacity in the case of the 18 inch web depth connections. In the case of the 26 inch web depth connections, the elastic rotational stiffness decreased with increasing web thickness by 28% (Figure 5.15). For a thin web thickness (P03-04), a shear deformation of the web occurred [Figure 5.16(a)], which resulted in tension field action. Due to the shear deformation, the base-plate of P03-04 did not lift significantly compared to the model with thicker web (P03-06), in which shear deformation of the web was not observed [Figure 5.16(b)]. Therefore, the calculated rotational stiffness of the model with thinner web (P03-04) was higher than the one with thicker web (P03-06) because for the same moment, the base-plate of P03-04 lifted less than the one of P03-06. The moment capacity of the 26 inch web depth connections increased by 40% in the push loading direction and by 30% in the pull direction (see Figure 5.15) with web thickness increase. As shown in Figure 5.16(a), a shear deformation of the web limited the moment capacity of the model with the thinner web thickness (P03-04). In the contrary, the model having thicker web (P03-06) did not experience shear deformation of the web [Figure 5.16(a)], and this led in an increased moment capacity compared to model P03-04.

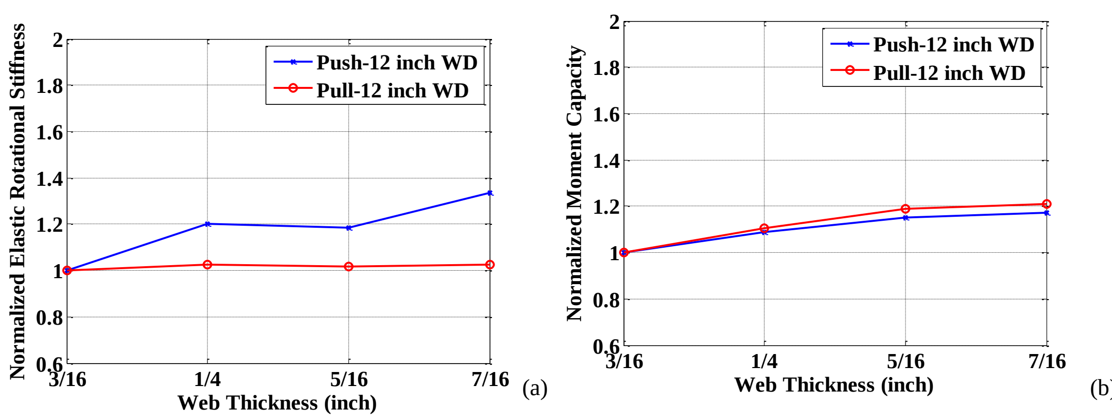

Figure 5.13. (a) Normalized elastic rotational stiffness and (b) normalized moment capacity for different web thicknesses of the 12 inch web depth connections.

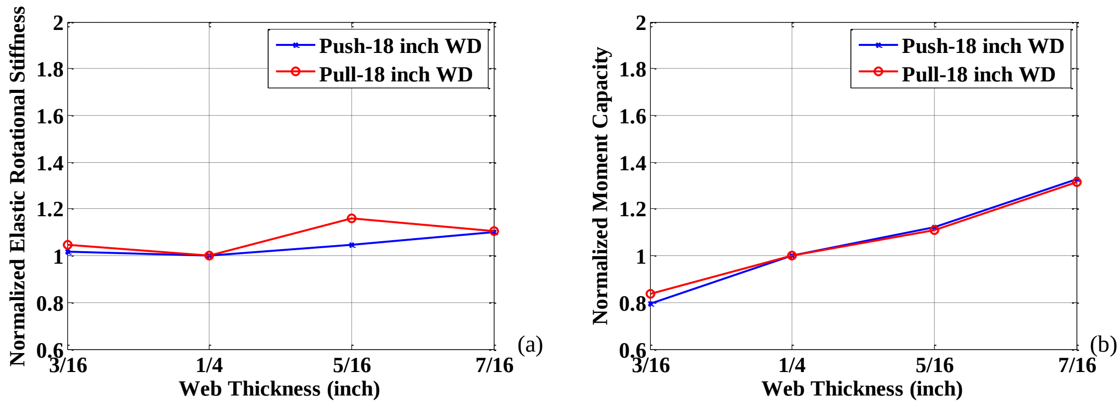

Figure 5.14. (a) Normalized elastic rotational stiffness and (b) normalized moment capacity for different web thicknesses of the 18 inch web depth connections.

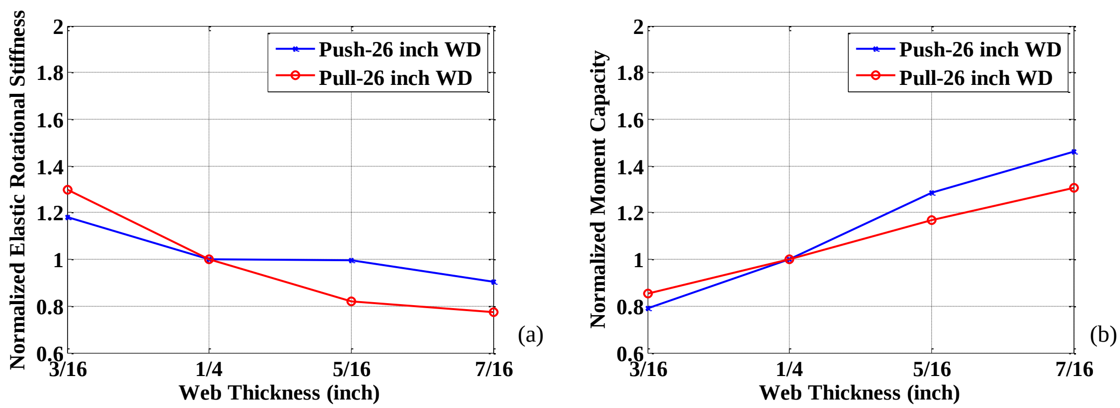

Figure 5.15. (a) Normalized elastic rotational stiffness and (b) normalized moment capacity for different web thicknesses of the 26 inch web depth connections.

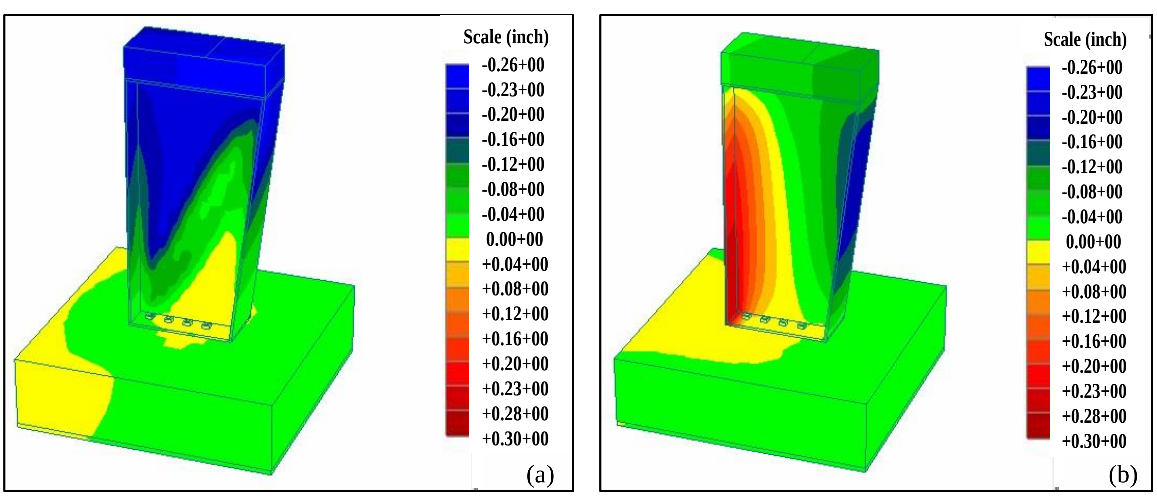

Figure 5.16. 26 inch web depth connections – Deformation contour of (a) P03-04 and (b) P03-06.

5.3.3. Flange thicknesses

The base-plate connection configurations investigating the effect of flange thickness are shown in Table 5.11. The elastic rotational stiffness and moment capacity of the connection combinations were normalized by those of S01, S02, S03 indicated in red color in Table 5.11. The normalized rotational stiffness and moment capacity for the 12 inch, 18 inch and 26 inch web depth connections are shown in Figure 5.17, Figure 5.18 and Figure 5.19, respectively.

Table 5.11. Parametric Study Models Investigating the Influence of the Flange Thicknesses on the Rotational Stiffness and Moment Capacity of the Connection (refer to Table 5.6, Table 5.7 and Table 5.8).

Model ID	Parameter Altering	Web Depth (inch)	Increment (inch)	Outside Flange Thickness (inch)	Inside Flange Thickness (inch)
P01	Flange Thicknesses	12	-	1/4	3/8
P01-07			-1/16,-1/16	3/16	5/16
P01-08			+1/16,	5/16	7/16
P01-09			5/16, 5/16	5/16	5/16
P01-10			7/16, 7/16	7/16	7/16
P02		18	-	3/8	3/8
P02-07			-1/8,-1/8	1/4	1/4
P02-08			-1/8,-	1/4	3/8
P02-09			-,-1/8	3/8	1/4
P02-10			+1/8,+1/4	1/2	5/8
P03		26	-	1/2	5/8
P03-07			-5/16,-5/16	3/16	5/16
P03-08			-3/16,-3/16	5/16	7/16
P03-09			+1/8,+1/8	5/8	3/4
P03-10			-,-1/8	1/2	1/2

It was observed that the decrease of the flange thicknesses increased the rotational stiffness of the 12 inch wed depth connections while it decreased the moment capacity of the connections. It should be noted here that the decrease of the flange thicknesses may led to the increase of the rotational stiffness due to the fact that the relative rigidity of the base-plate and anchor rod system to flange component is greater for thinner flange thickness. It was also observed that an increase of the flange thickness increased the rotational stiffness and moment capacity of the 12 inch web depth connections. The decrease of the flange thicknesses for the 18 inch web depth connections had almost no effect on the rotational stiffness while it decreased the moment capacity of the connections. This was explained based on the relative rigidity of the base-plate and anchor rod system compared to the flange component. The behavior of the base-plates of models P02 and P02-07 was predominantly rigid, and thus decreasing the flange thickness had no effect on the rotational stiffness. On the other hand, the increase of the rotational stiffness and moment capacity of the connections with the increase of the flange thicknesses ranging from 4 to 30% was observed. In the case of the 26 inch web depth connections the decrease of the flange thickness resulted in a decrease of the rotational stiffness and moment capacity of the connections by 32%. It was also observed that the increase of the flange thicknesses led to an increase of both the rotational stiffness and the moment capacity by 22%.

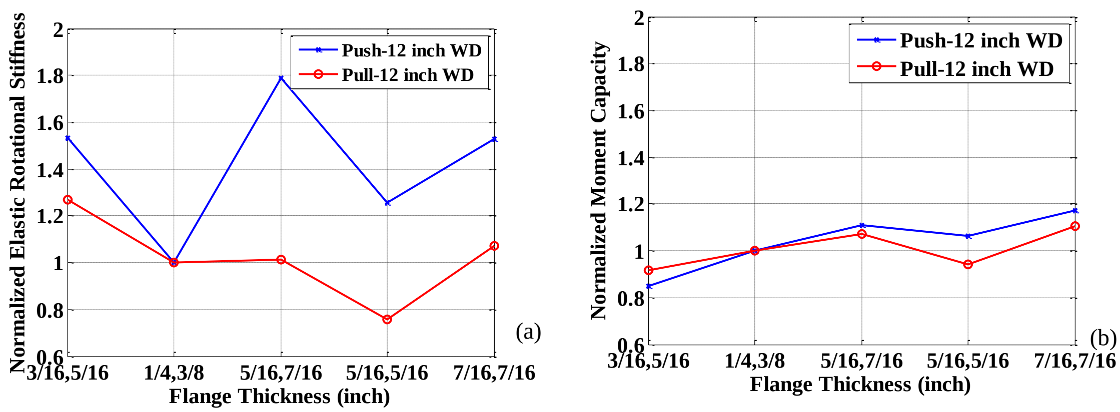

Figure 5.17. (a) Normalized elastic rotational stiffness and (b) normalized moment capacity for different flange thicknesses of the 12 inch web depth connections.

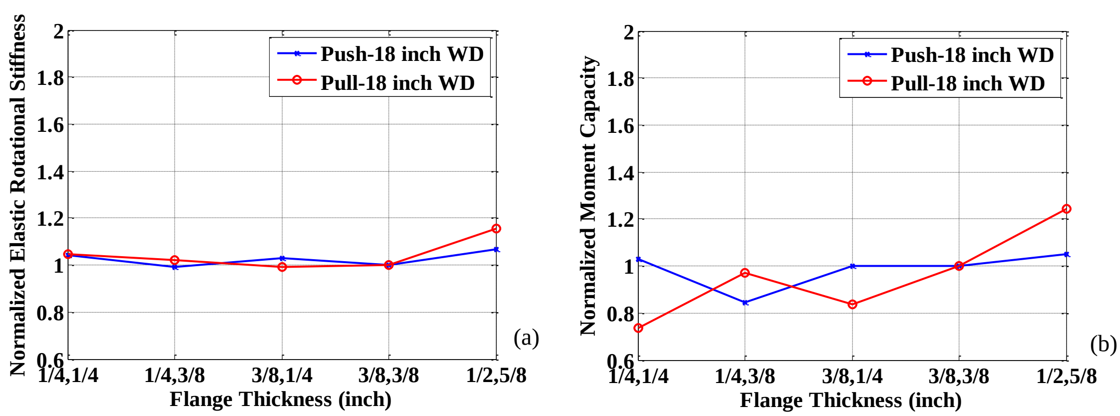

Figure 5.18. (a) Normalized elastic rotational stiffness and (b) normalized moment capacity for different flange thicknesses of the 18 inch web depth connections.

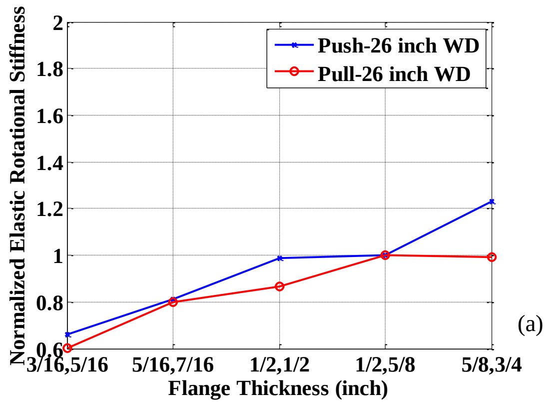

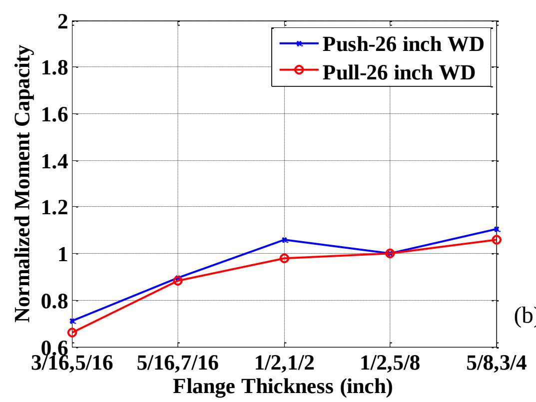

Figure 5.19. (a) Normalized elastic rotational stiffness and (b) normalized moment capacity for different flange thicknesses of the 26 inch web depth connections.

5.3.4. Base-Plate Width

The base-plate connection configurations investigating the effect of base-plate width are shown in Table 5.12. The rotational stiffness and moment capacity of the connection combinations are normalized by those of P01, P02, P03 indicated in red color in Table 5.12. The normalized rotational stiffness and moment capacity for the 12 inch, 18 inch and 26 inch web depth connections are shown in Figure 5.20, Figure 5.21 and Figure 5.22 respectively.

Table 5.12. Parametric Study Models Investigating the Influence of the Base-Plate Width on the Rotational Stiffness and Moment Capacity of the Connection (refer to Table 5.6, Table 5.7, Table 5.8).

Model ID	Parameter Altering	Web Depth (inch)	Increment (inch)	Base-Plate Width (inch)	Column Flange Width (inch)
P01	Base-Plate Width	12	-	8	8
P01-11			+2	10	8
P01-12			+4	12	8
P01-13			+6	14	8
P02		18	-	10	10
P02-11			+2	12	10
P02-12			+4	14	10
P02-13			+6	16	10
P03		26	-	14	14
P03-11			+2	16	14
P03-12			+4	18	14
P03-13			+6	20	14

The increase of the base-plate width resulted in the slight increase of the elastic rotational stiffness in the push loading direction for the 12 inch and 26 inch web depth connections. It was also observed that the increase of the base-plate width by 4 inch slightly decreased the rotational stiffness of the 18 inch web depth connections while there was almost no effect on the moment capacity of the connections for any of the web depth cases considered here.

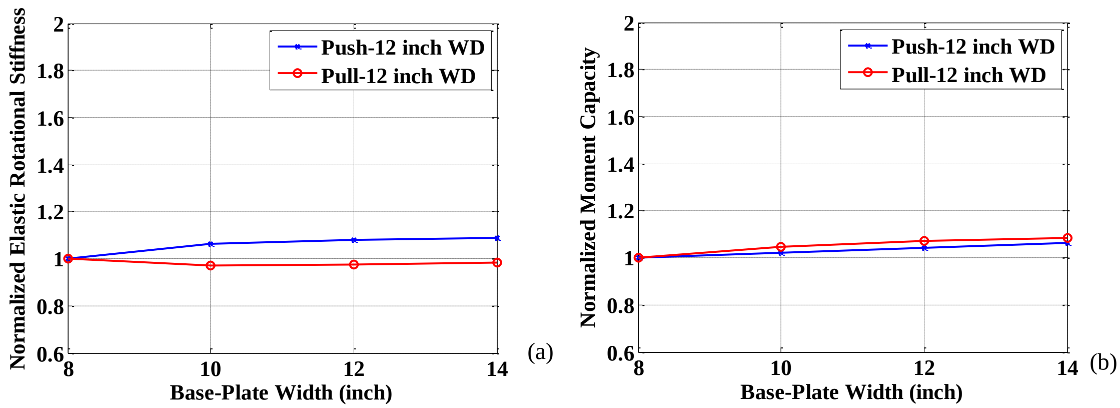

Figure 5.20. (a) Normalized elastic rotational stiffness and (b) normalized moment capacity for different base-plate widths of the 12 inch web depth connections.

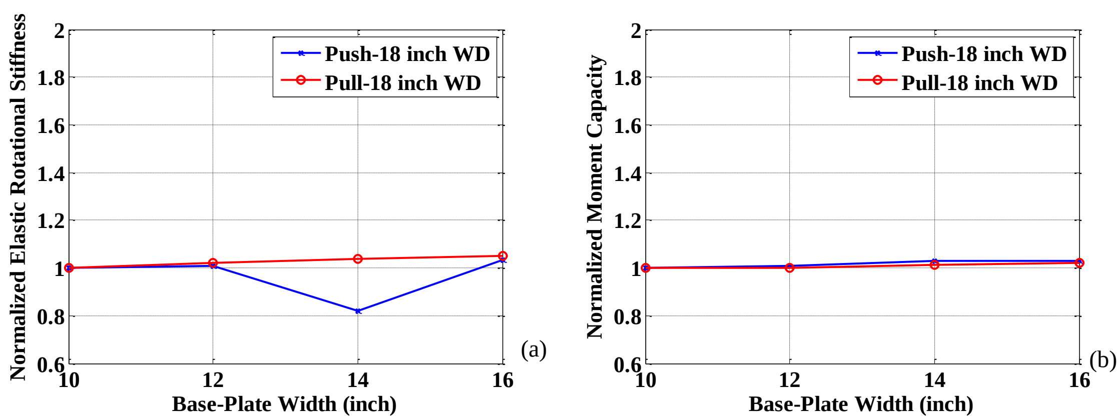

Figure 5.21. (a) Normalized elastic rotational stiffness and (b) normalized moment capacity for different base-plate widths of the 18 inch web depth connections.

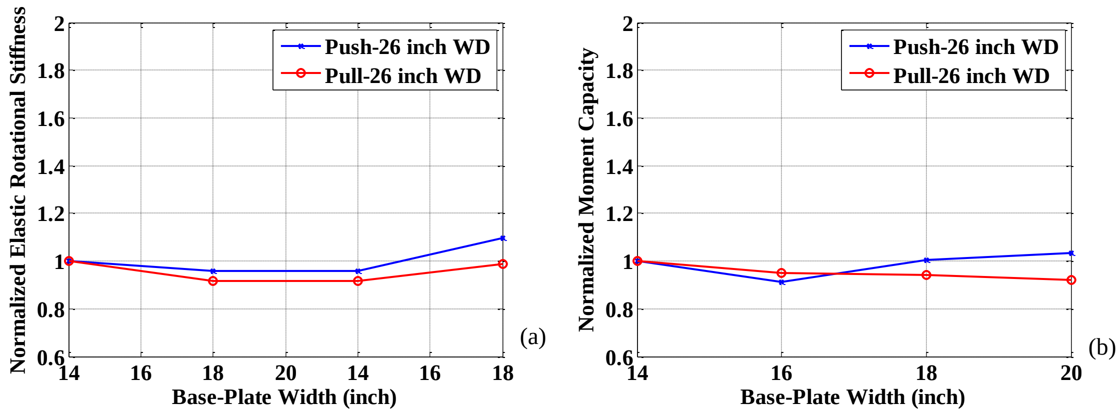

Figure 5.22. (a) Normalized elastic rotational stiffness and (b) normalized moment capacity for different base-plate widths of the 26 inch web depth connections.

5.3.5. Base-plate thickness

The base-plate connection configurations investigating the effect of base-plate thickness are shown in Table 5.13. The rotational stiffness and moment capacity of the connection combinations were normalized by those of P01, P02, P03 indicated in red color in Table 5.13. The normalized rotational stiffness and moment capacity for the 12 inch, 18 inch and 26 inch web depth connections are shown in Figure 5.23, Figure 5.24 and Figure 5.25 respectively.

Table 5.13. Parametric Study Models Investigating the Influence of the Base-Plate Thickness on the Rotational Stiffness and Moment Capacity of the Connection (refer to Table 5.6, Table 5.7, Table 5.8).

Model ID	**Parameter Altering**	**Web Depth (inch)**	**Increment (inch)**	**Base-Plate Thickness (inch)**	**Anchor Rod Diameter (inch)**
P01	Base-Plate Thickness	12	-	3/8	3/4
P01-14			+1/8	1/2	3/4
P01-15			+1/4	5/8	3/4
P01-16			+3/8	3/4	3/4
P02		18	-	1/2	3/4
P02-14			-1/8	3/8	3/4
P02-15			+1/8	5/8	3/4
P02-16			+1/4	3/4	3/4
P03		26	-	5/8	3/4
P03-14			-2/8	3/8	3/4
P03-15			-1/8	1/2	3/4
P03-16			+1/8	3/4	3/4

Despite exceptions, the general trend for the 12 inch and 18 inch web depth connections was that the rotational stiffness and moment capacity of the connections increased with an increase in the base-plate thickness. This is mainly because an increase of the base-plate thickness resulted in a more rigid base-plate behavior. The only exception is in the case of the 12 inch web depth connections where an increase of the base-plate thickness resulted in the decrease of the rotational stiffness of the connection in the pull loading direction. It should be noted that the results presented in Figure 5.23 are the combination of the base-plate thicknesses with 3/4 inch anchor rod diameter. As it was also observed from the experiments, the tensile forced from the rods are the ones which are dominating the connection's behavior.

In the case of the 26 inch web depth connections, it was observed that the rotational stiffness decreased when the base-plate thickness changed from 1/2 inch (P03-15) to 3/8 inch (P03-14) and from 5/8 inch (P03) to 3/4 inch (P03-16). This occurred because, as described in Section 5.3.2, the shear deformation of the web [Figure 5.16(a)] of P03 and P03-15 models limited the base-plate uplift compared to the base-plate uplift of models P03-14 and P03-16, in which shear deformation of the web [Figure 5.16(b)] did not occur. Therefore, for a given moment and for smaller base-plate uplift led to a higher rotational stiffness.

In the case of the 26 inch web depth connections, the moment capacity increased as the base-plate thickness increased from 3/8 inch to 3/4 inch. This was expected because the base-plate thickness increment led to a more rigid behavior of the base-plate. It should be noted that the shear deformation of the web of models P03 and P03-15 did not affect the moment capacity because the tension field action in the web assisted to transfer the applied load to the foundation and thus to maintain the ability of resisting the applied loads. Further investigation of the effect of the base-plate thickness combined with different anchor rod diameters on the rotational stiffness and moment capacity of the connections is presented in the Sections 5.3.7 and Sections 5.3.13to 5.3.15.

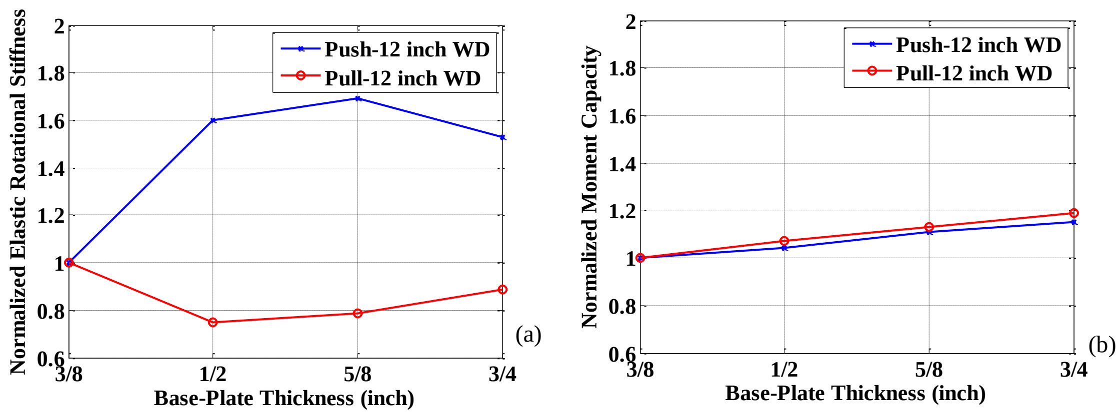

Figure 5.23. (a) Normalized elastic rotational stiffness and (b) normalized moment capacity for different base-plate thicknesses of the 12 inch web depth connections.

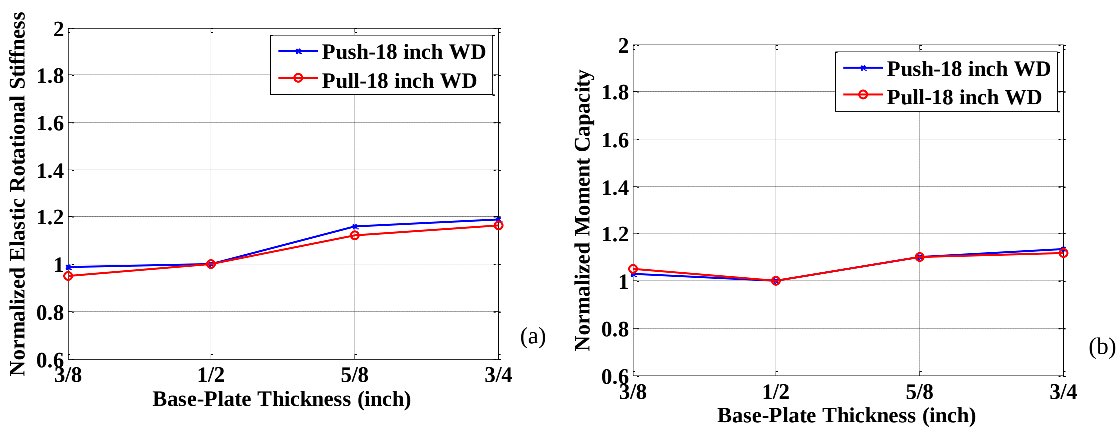

Figure 5.24. (a) Normalized elastic rotational stiffness and (b) normalized moment capacity for different base-plate thicknesses of the 18 inch web depth connections.

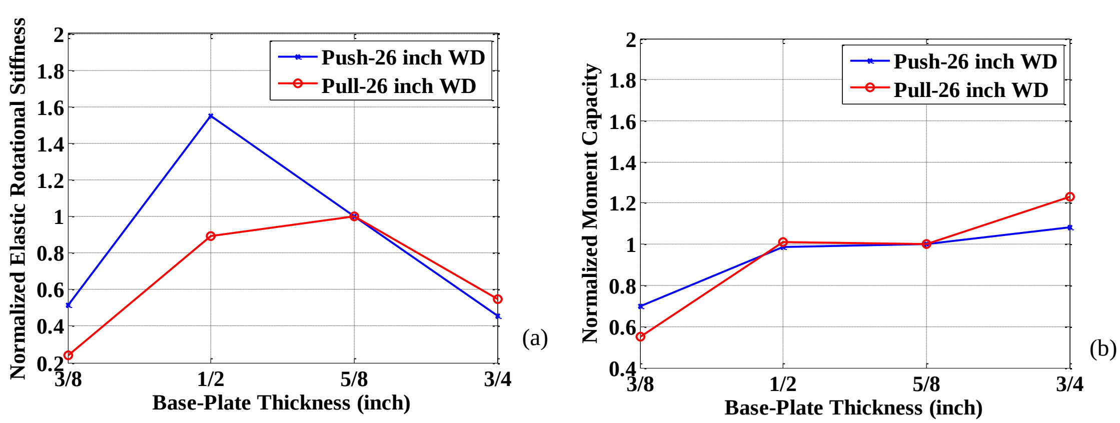

Figure 5.25. (a) Normalized elastic rotational stiffness and (b) normalized moment capacity for different base-plate thicknesses of the 26 inch web depth connections.

5.3.6. Anchor rod diameter

The base-plate connection configurations investigating the effect of base-plate thickness are shown in Table 5.14. The rotational stiffness and moment capacity of the connection combinations were normalized by those of P01, P02, P03 indicated in red color in Table 5.14. The normalized rotational stiffness and moment capacity for the 12 inch, 18 inch and 26 inch web depth connections are shown in Figure 5.26, Figure 5.27 and Figure 5.28, respectively.

Table 5.14. Parametric Study Models Investigating the Influence of the Anchor Rod Diameter on the Rotational Stiffness and Moment Capacity of the Connection (refer to Table 5.6, Table 5.7, Table 5.8).

Model ID	Parameter Altering	Web Depth (inch)	Increment (inch)	Anchor Rod Diameter (inch)	Base-Plate Thickness (inch)
P01	Anchor Rod Diameter	12	-	3/4	3/8
P01-17			+1/4	1.0	3/8
P01-18			+1/2	1 1/4	3/8
P02		18	-	1.0	3/8
P02-17			-1/4	3/4	3/8
P02-18			+1/4	1 1/4	3/8
P03		26	-	1 1/4	3/8
P03-17			-1/4	1.0	3/8
P03-18			-1/2	3/4	3/8

In the case of the 12 inch web depth connections, the general trend is that an increase of the anchor rod diameter resulted in the increase of the elastic rotational stiffness. The rotational stiffness was increased approximately 170% when the anchor rod diameter increases from 3/4 inch to 1 1/4 inch. For the same anchor rod diameter increment, the moment capacity of the connection increased approximately 23%. Note that in this case, a relatively thin base-plate (3/8 inch) was combined with large anchor rods (1 1/4 inch). It was observed from the experiments that this base-plate connection combination leads to a flexurally dominated, but having an increased rotational stiffness compared to base-plate connections with smaller anchor rods diameters. In the case of the 18 inch web depth connections, it was shown that an increase of the anchor rod diameter slightly increased the rotational stiffness of the connection. Similarly, an increase of the anchor rod diameter resulted in a decrease of the moment capacity. For the models under investigation, an anchor rod diameter increment resulted in a more flexible behavior of the base-plate, and as it was previously explained, base-plates having a predominantly flexural behavior led to a lower moment capacity. Finally, in the case of the 26 inch web depth connections, an increase of the anchor rod diameter led to a slight increase of the elastic rotational stiffness and moment capacity of the column base-plate connection. The base-plate of these 26 inch web depth connections was classified as balanced. Therefore, increasing the anchor rod diameter benefited the overall rigidity of the base-plate connection.

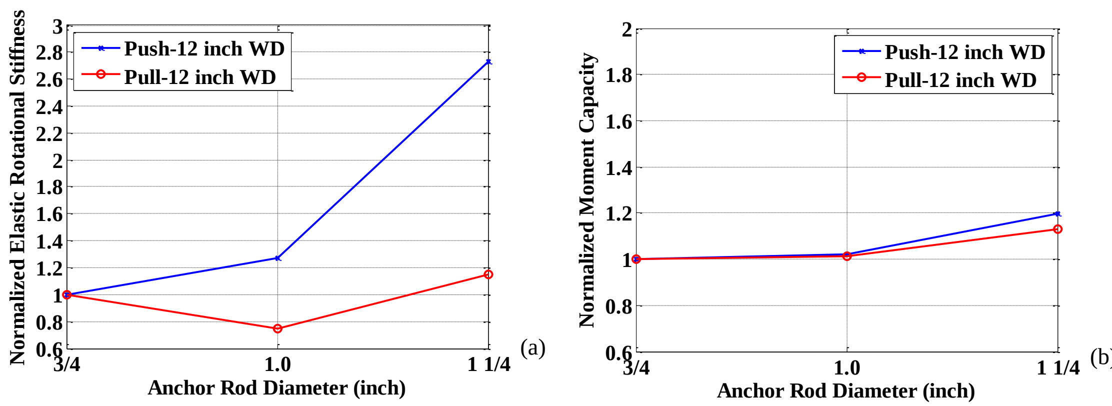

Figure 5.26. (a) Normalized elastic rotational stiffness and (b) normalized moment capacity for different anchor rod diameters of the 12 inch web depth connections.

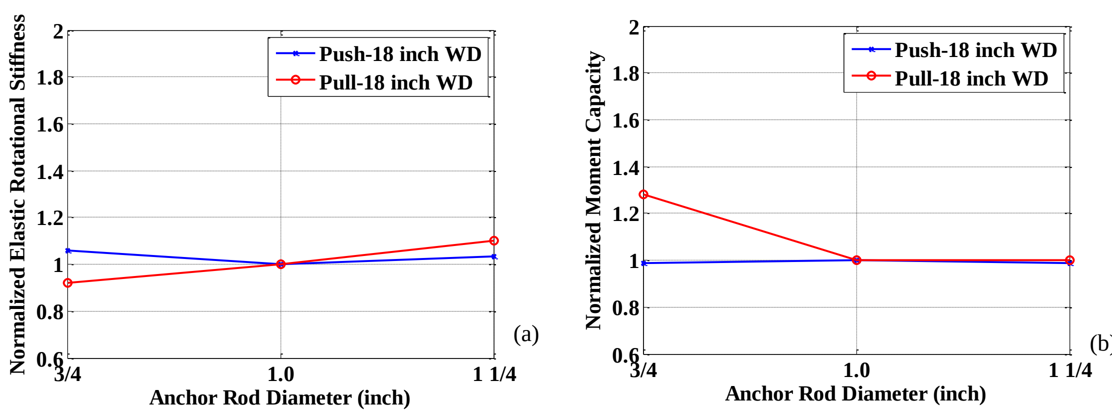

Figure 5.27. (a) Normalized elastic rotational stiffness and (b) normalized moment capacity for different anchor rod diameters of the 18 inch web depth connections.

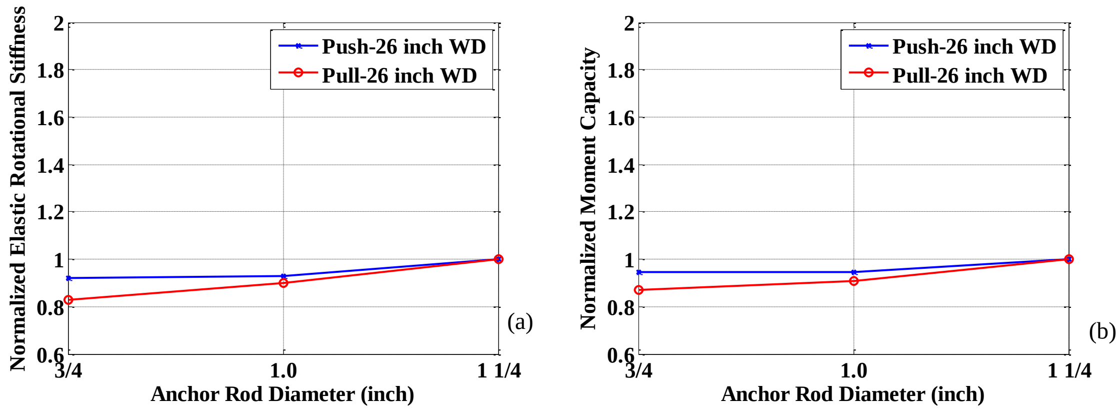

Figure 5.28. (a) Normalized elastic rotational stiffness and (b) normalized moment capacity for different anchor rod diameters of the 26 inch web depth connections.

5.3.7. Base-plate thickness-Anchor rod diameter

It has been shown from the experiments that the interaction of the anchor rod diameter with the base-plate thickness need to be studied in more detail to better understand the impact of these parameters on the rotational stiffness and moment capacity of the column base-plate connections. The interaction of the four different base-plate thicknesses (3/8 inch, 1/2 inch, 5/8 inch, 3/4 inch) with the three different anchor rod diameters (3/4 inch, 1 inch and 1 1/4 inch) were considered in the parametric analysis The base-plate connection configurations investigating the effect of base-plate thickness and anchor rod diameter are shown in Table 5.15. The rotational stiffness and moment capacity of the connection combinations were normalized by those of P01, P02 and P03 indicated in red color in Table 5.15. The normalized rotational stiffness and moment capacity for the 12 inch, 18 inch and 26 inch web depth connections are shown in Figure 5.29, Figure 5.30 and Figure 5.31, respectively.

Table 5.15. Parametric Study Models Investigating the Influence of the Base-Plate Thickness and Anchor Rod Diameter in the Rotational Stiffness and Moment Capacity of the Connection (refer to Table 5.6, Table 5.7, Table 5.8).

Model ID	Parameter Altering	Web Depth (inch)	Increment (inch)	Base-Plate Thickness (inch)	Anchor Rod Diameter (inch)
P01-17	Base-Plate Diameter and Anchor Rod Diameter	12	-	3/8	1.0
P01-19			+1/8,+1/4	1/2	1.0
P01-20			+1/4,+1/4	5/8	1.0
P01-21			+3/8,+1/4	3/4	1.0
P01-18			-	3/8	1 1/4
P01-22			+1/8,+1/2	1/2	1 1/4
P01-23			+1/4,+1/2	5/8	1 1/4
P01-24			+3/8,+1/2	3/4	1 1/4
P02-17		18	-	1/2	3/4
P02-19			-1/8,-1/4	3/8	3/4
P02-20			+1/8,-1/4	5/8	3/4
P02-21			+1/4,-1/4	3/4	3/4
P02-18			-	1/2	1 1/4
P02-22			-1/8,+1/4	3/8	1 1/4
P02-23			+1/8,+1/4	5/8	1 1/4
P02-24			+1/4,+1/4	3/4	1 1/4
P03-17		26	-	5/8	3/4
P03-19			-2/8,-1/2	3/8	3/4
P03-20			-1/8,-1/2	1/2	3/4
P03-21			+1/8,-1/2	3/4	3/4
P03-18			-	5/8	1.0
P03-22			-2/8,-1/4	3/8	1.0
P03-23			-1/8,-1/4	1/2	1.0
P03-24			+1/8,-1/4	3/4	1.0

In the case of the 12 inch web depth connections, the rotational stiffness [Figure 5.29(a)] fluctuated for different combinations of base-plate thicknesses and anchor rod diameters. This happened because the relative rigidity of anchor rod and base-plate changed for every combination. Additionally, increasing the anchor rod diameter at a given base-plate thickness gradually changed the base-plate behavior from rigid to more flexible. Regarding the moment capacity of the 12 inch web depth connections, the general trend, with few exceptions, was that the moment capacity increased as the base-plate thickness increased In addition, Figure 5.29 shows that for base-plates with thickness higher than 5/8 inch, the anchor rod diameter did not have any influence. This is due to the fact that in12 inch web depth connections when the base-plate thickness was greater than 5/8 inch, then the base-plate behaved predominantly rigidly and an increase of the anchor rod diameter did not influence the overall rigidity of the base-plate connection.

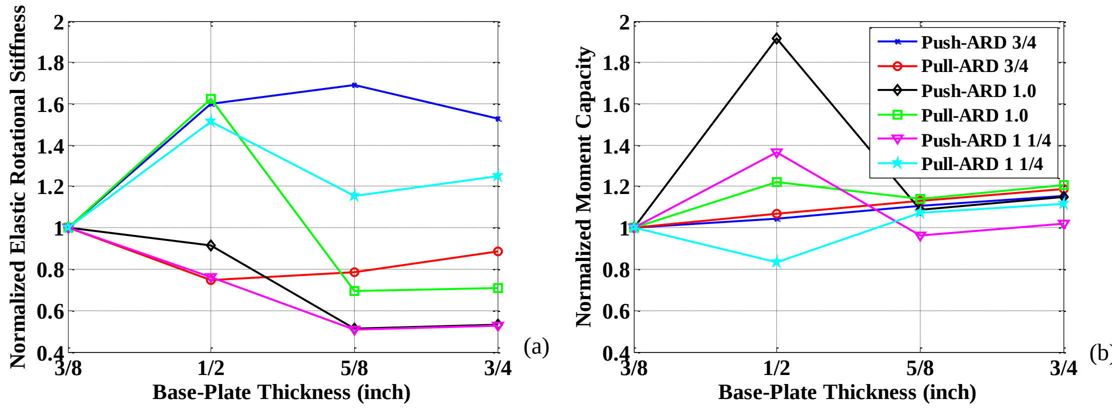

Figure 5.29. (a) Normalized elastic rotational stiffness and (b) normalized moment capacity for different anchor rod diameters (ARD) and base-plate thicknesses of the 12 inch web depth connections.

In the 18 inch web depth connections (see Figure 5.30), it was observed that the general trend is that the rotational stiffness and the moment capacity of the connections increase with increasing base-plate thickness despite the anchor rod diameter. An exception to this observation was combination of the 3/8 inch base-plate thickness with the 3/4 inch anchor rod diameter. The combination of 5/8 inch and 3/4 inch base-plate thicknesses with the 1.0 anchor rod diameter led to the highest elastic rotational stiffness and moment capacity of the connections.

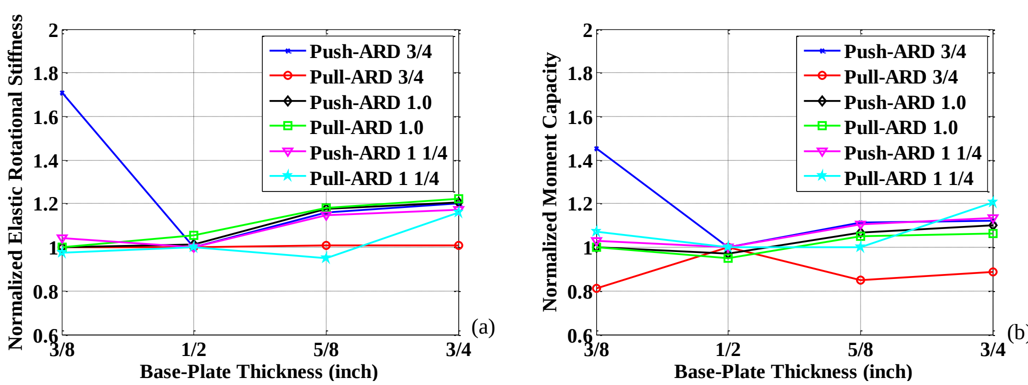

Figure 5.30. (a) Normalized elastic rotational stiffness and (b) normalized moment capacity for different anchor rod diameters (ARD) and base-plate thicknesses of the 18 inch web depth connections.

In the case of the 26 inch web depth connections (Figure 5.31), the elastic rotational stiffness decreased when the base-plate thickness changes from 1/2 inch (P03-20 and P03-23) to 3/8 inch (P03-19 and P03-22) and from 5/8 inch (P03-17 and P03-18) to 3/4 inch (P03-21 and P03-24). The decrease ranged from 60 to 75% for these base-plate connections. As explained in Section 5.3.5, and shown in Figure 5.25, the models with base-plate thickness of 3/8 inch (P03-19 and P03-22) and 5/8 inch (P03-17 and P03-18) experienced a shear deformation of their web [see Figure 5.16(a)], causing the base-plate to have a limited uplift. This resulted in a higher rotational stiffness than the models with a base-plate thickness of 1/2 inch (P03-20 and P03-23) and 3/4 inch (P03-21 and P03-24), where a shear deformation of the web was not observed [Figure 5.16(b)] and the base-plate uplift was higher than in models P03-17 to P03-19 and P03-22. On the other hand, the moment capacity of the 26 inch web depth connections followed an increasing trend with increasing base-plate thickness. Similar findings to the one shown in Figure 5.31 are previously explained in Section 5.3.5.

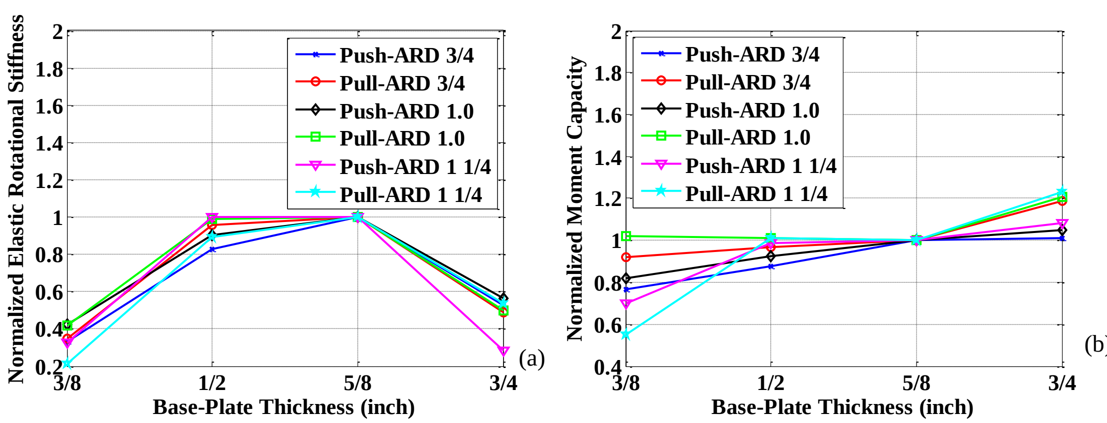

Figure 5.31. (a) Normalized elastic rotational stiffness and (b) normalized moment capacity for different anchor rod diameters (ARD) and base-plate thicknesses of the 26 inch web depth connections.

5.3.8. Number of anchor rods

The base-plate connection configurations investigating the effect of number of anchor rods are shown in Table 5.16. The rotational stiffness and moment capacity of the connection combinations were normalized by those of P01, P02, P03 indicated in red color in Table 5.16. The normalized rotational stiffness and moment capacity for the 12 inch, 18 inch and 26 inch web depth connections are shown in Figure 5.32, Figure 5.33 and Figure 5.34, respectively.

Table 5.16. Parametric Study Models Investigating the Influence of the Number of Anchor Rods on the Rotational Stiffness and Moment Capacity of the Connection (refer to Table 5.6, Table 5.7, Table 5.8).

Model ID	**Parameter Altering**	**Web Depth (inch)**	**Increment (inch)**	**Number of Anchor Rods**
P01	Anchor Rod Diameter	12	-	4
P01-25			+2	6
P02		18	-	6
P02-25			-2	4
P02-26			+2	8
P03		26	-	8
P03-25			-2	6
P03-26			+2	10

In the 12 inch web depth connections, an increase of the number of anchor rods in the push direction resulted in an increase of the rotational stiffness and moment capacity by 120% and 75%, respectively. This increase was observed because two more anchor rods in tension were added in the push direction. In the case of the 18 inch web depth connections the elastic rotational stiffness was increased in the push loading direction by 82% and the moment capacity by 42%. In parallel, a decrease of the number of anchor rods decreased the rotational stiffness in the push loading direction by 40% and the moment capacity by 35%. In the case of the 26 inch web depth connections there was less effect on the elastic rotational stiffness and moment capacity of the connections when the number of anchor rods changed in comparison with the 12 inch and 18 inch web depth connections.

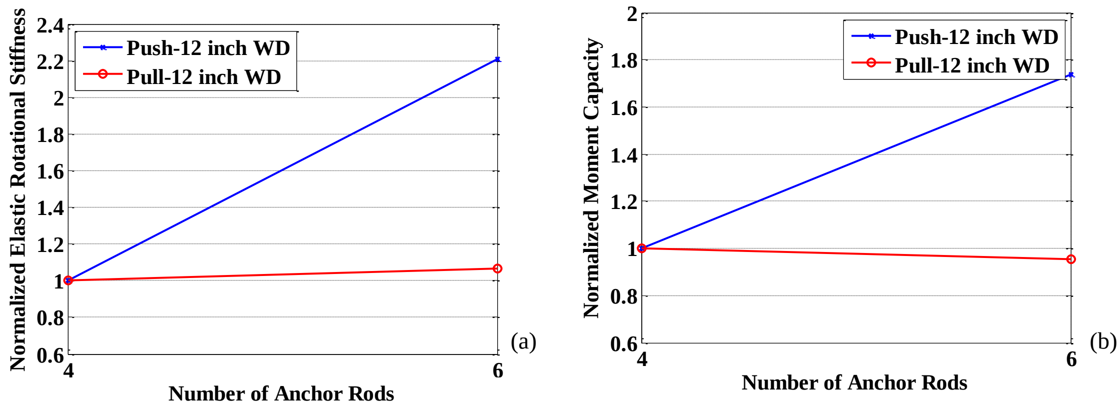

Figure 5.32. (a) Normalized elastic rotational stiffness and (b) normalized moment capacity for different number of anchor rods of the 12 inch web depth connections.

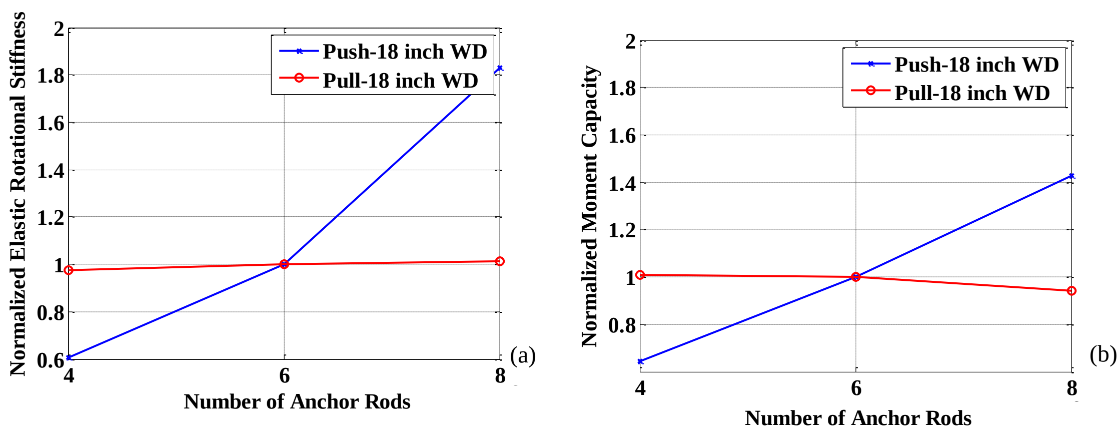

Figure 5.33. (a) Normalized elastic rotational stiffness and (b) normalized moment capacity for different number of anchor rods of the 18 inch web depth connections.

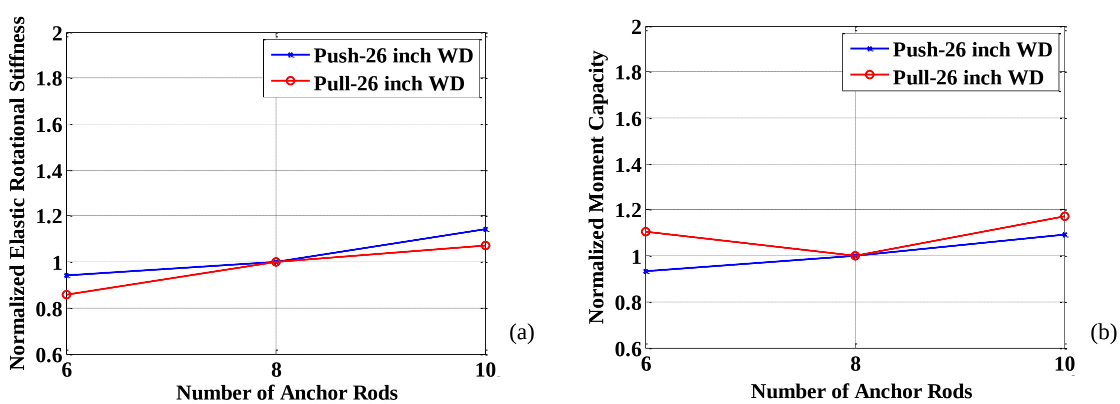

Figure 5.34. (a) Normalized elastic rotational stiffness and (b) normalized moment capacity for different number of anchor rods of the 26 inch web depth connections.

5.3.9. Pitch

The base-plate connection configurations investigating the effect of pitch are shown in Table 5.17. The rotational stiffness and moment capacity of the connection combinations were normalized by those of P01, P02, P03 indicated in red color in Table 5.17. The normalized rotational stiffness and moment capacity for the 12 inch, 18 inch and 26 inch web depth connections are shown in Figure 5.35 Figure 5.36 and Figure 5.37, respectively.

Table 5.17. Parametric Study Models Investigating the Influence of the Pitch on the Rotational Stiffness and Moment Capacity of the Connection (refer to Table 5.6, Table 5.7, Table 5.8).

Model ID	Parameter Altering	Web Depth (inch)	Increment (inch)	Pitch (inch)
P01	Pitch	12	-	4
P01-26			+1	5
P01-27			+2	6
P02		18	-	4
P02-26			+1	5
P02-27			+2	6
P03		26	-	5
P03-26			+1	6
P03-27			+2	7

In the case of the 12 inch and 18 inch web depth connections, an increase of the pitch resulted in an increase of the elastic rotational stiffness and moment capacity of the connections in a range from 28% to 60% in the push direction. This happened because by increasing the pitch, the anchor rods in tension were moved farther away from the concrete bearing area, and thus the moment arm between the resultant of concrete bearing force and the outer anchor rod in tension increased. For the same reason, in the pull direction the inner anchor (i.e., outer anchor rod in push direction) had moved closer to the concrete bearing area and thus the contribution of this anchor rod row to the rotational stiffness was decreased. As a result, the rotational stiffness in the pull direction decreased by 30%.

On the other hand, the elastic rotational stiffness and moment capacity of the 26 inch web depth connections was not affected by the pitch in the push direction. However, in the pull direction, it was observed that an increase of the pitch led to an increase of the elastic rotational stiffness by 58% and the moment capacity by 20%

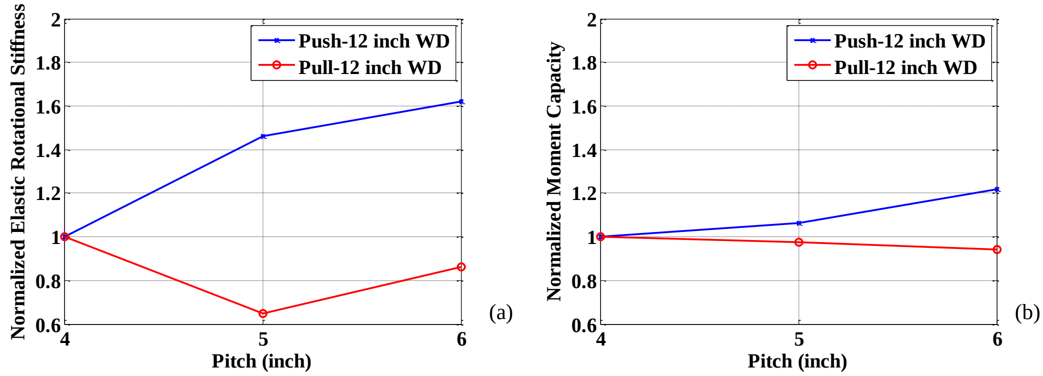

Figure 5.35. (a) Normalized elastic rotational stiffness and (b) normalized moment capacity for different pitch distances of the 12 inch web depth connections.

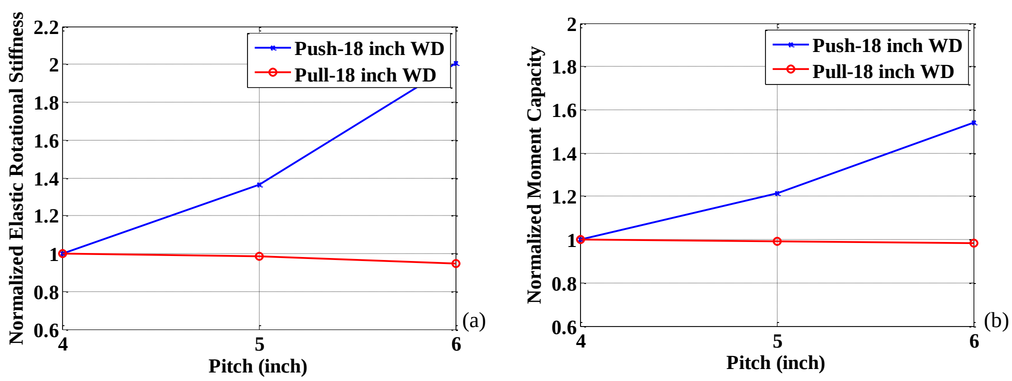

Figure 5.36. (a) Normalized elastic rotational stiffness and (b) normalized moment capacity for different pitch distances of the 18 inch web depth connections.

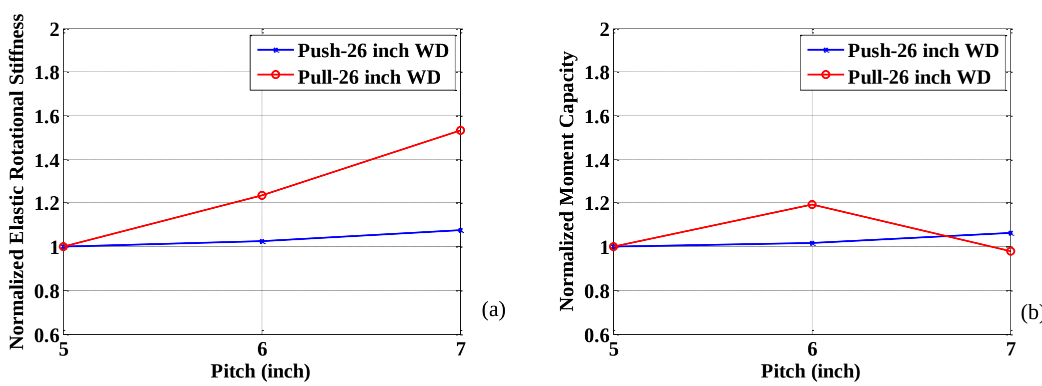

Figure 5.37. (a) Normalized elastic rotational stiffness and (b) normalized moment capacity for different pitch distances of the 26 inch web depth connections.

5.3.10. Setback

The base-plate connection configurations investigating the effect of the setback are shown in Table 5.18. The rotational stiffness and moment capacity of the connection combinations were normalized by those of P01, P02, P03 indicated in red color in Table 5.18. The normalized rotational stiffness and moment capacity for 12 inch, 18 inch and 26 inch web depth connections are shown in Figure 5.38, Figure 5.39 and Figure 5.40, respectively.

Table 5.18. Parametric Study Models Investigating the Influence of the Setback on the Rotational Stiffness and Moment Capacity of the Connection (refer to Table 5.6, Table 5.7, Table 5.8).

Model ID	Parameter Altering	Web Depth (inch)	Increment (inch)	Setback (inch)
P01	Setback	12	-	3
P01-29			+1	4
P01-30			+2	5
P02		18	-	4
P02-29			+1	5
P02-30			+2	6
P03		26	-	4
P03-29			+1	5
P03-30			+2	6

The 12 inch and 18 inch web depth connections followed the same increasing trend in the push direction and decreasing trend in the pull direction for the elastic rotational stiffness and moment capacity with increasing setback. As previously explained in Section 5.3.9, an increase of the setback resulted in greater moment arm between the concrete bearing force and tension load of the outer anchor rod. However, in the pull direction the effect of the inner rod (the outer anchor rod in push direction, is the inner rod in pull direction) decreased because the inner rod was closer in the concrete bearing area. It was observed that an increase of the setback of the 12 inch and 18 inch web depth connections resulted in an increase of the rotational stiffness in the range from 28% to 60 % in the push direction. Similarly, an increase of the setback led to the reduction of the elastic rotational stiffness in the pull loading direction from 28% to 30 % and of the moment capacity in the range from 15% to 30%. In the case of the 26 inch web depth connection, the rotational stiffness and moment capacity of the connections increased when the setback was increased by 3 inch. The 26 inch web depth connections involved four rows of anchor rods and therefore an increase of the setback would not greatly affect the rotational stiffness and moment capacity.

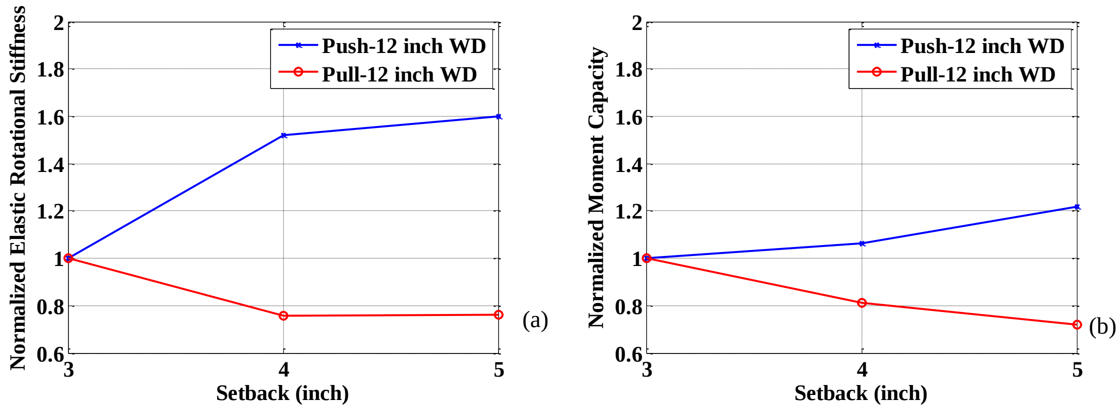

Figure 5.38. (a) Normalized elastic rotational stiffness and (b) normalized moment capacity for different setback distances of the 12 inch web depth connections.

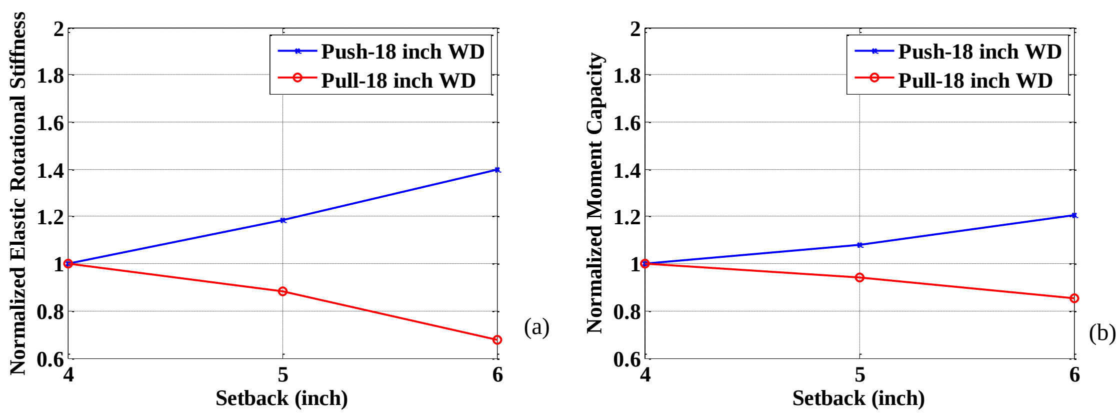

Figure 5.39. (a) Normalized elastic rotational stiffness and (b) normalized moment capacity for different setback distances of the 18 inch web depth connections.

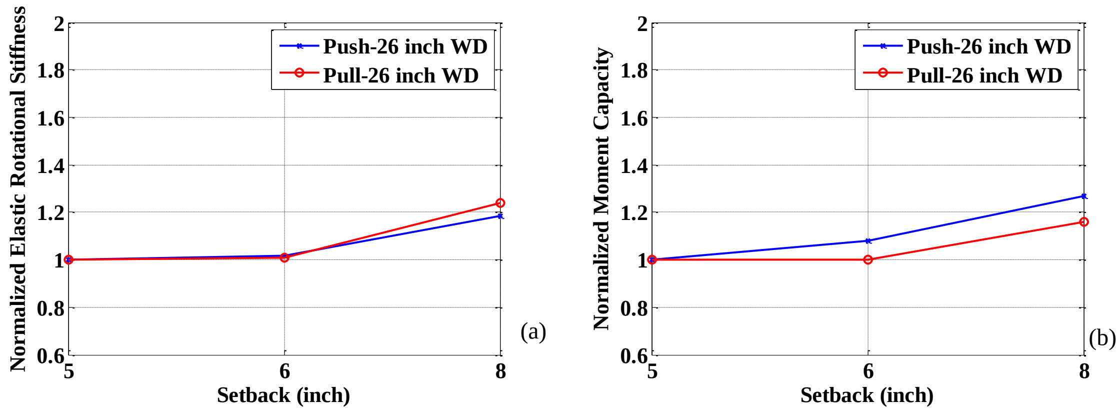

Figure 5.40. (a) Normalized elastic rotational stiffness and (b) normalized moment capacity for different setback distances of the 26 inch web depth connections.

5.3.11. Gage

The base-plate connection configurations investigating the effect of the gage are shown in Table 5.19. The rotational stiffness and moment capacity of the connection combinations were normalized by those of P02, P03 indicated in red color in Table 5.19. The normalized rotational stiffness and moment capacity for the 12 inch, 18 inch and 26 inch web depth connections are shown in Figure 5.41 and Figure 5.42, respectively.

Table 5.19. Parametric Study Models Investigating the Influence of the Gage on the Rotational Stiffness and Moment Capacity of the Connection (refer to Table 5.6, Table 5.7, Table 5.8).

Model ID	Parameter Altering	Web Depth (inch)	Increment (inch)	Pitch (inch)
P02	Gage	18	-	4
P02-31			+1	5
P02-32			+2	6
P03		26	-	5
P03-31			+1	6
P03-32			+3	8

It was observed that there is a limited effect of the anchor rod gage distance on the rotational stiffness and moment capacity of the 18 inch and 26 inch web depth connections. Specifically, in the case of the 18 inch web depth connections which were 10 inch wide, the rotational stiffness decreased by 17% while there was almost no effect on the moment capacity of the connections. On the other hand in the case of the 26 inch web depth connections, which were 14 inch wide, an increase of the gage distance led to an increase of the rotational stiffness and moment capacity by 20 % in the pull direction while there was almost no effect in the push direction. These observations could be explained by the fact that the gage distance was perpendicular to the column strong axis and the effect of the gage distance is minimum because the base-plate bended in the perpendicular direction.

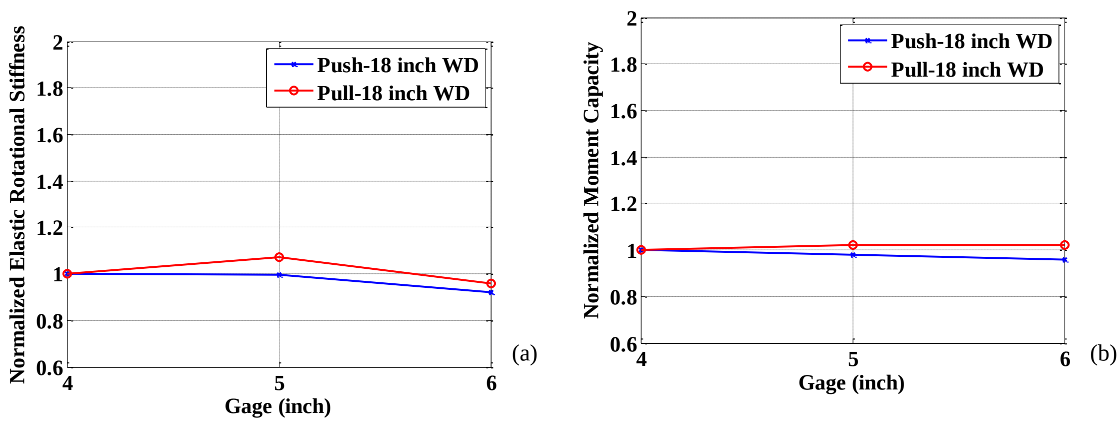

Figure 5.41. (a) Normalized elastic rotational stiffness and (b) normalized moment capacity for different gage distances of the 18 inch web depth connections.

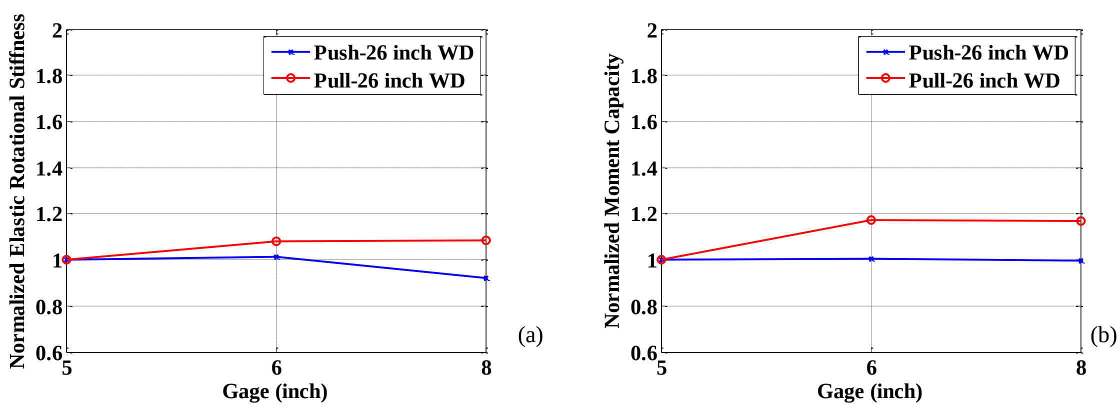

Figure 5.42. (a) Normalized elastic rotational stiffness and (b) normalized moment capacity for different gage distances of the 26 inch web depth connections.

5.3.12. Anchor rod diameter-Applied axial load

The base-plate connection configurations investigating the effect of the anchor rod diameter under different axial load levels are shown in Table 5.20, Table 5.21 and Table 5.22. The rotational stiffness and moment capacity of the connection combinations are normalized by those of P01, P02, P03 indicated in red color in Table 5.20, Table 5.21 and Table 5.22. The normalized rotational stiffness and moment capacity for the 12 inch, 18 inch and 26 inch web depth connections are shown in Figure 5.43, Figure 5.44 and Figure 5.45 respectively.

Table 5.20. Parametric Study Models Investigating the Influence of the Anchor Rod Diameter and Axial Load on the Rotational Stiffness and Moment Capacity of the Connection (refer to Table 5.6, Table 5.7 and Table 5.8).

Model ID	**Parameter Altering**	**Web Depth (inch)**	**Increment (inch)**	**Anchor Rod Diameter (inch)**	**Axial Load (kips)**	**Base-Plate Thickness (inch)**
P01	Anchor Rod Diameter-Axial Load	12	-	3/4	50k C	3/8
P01-42			-	3/4	25k C	3/8
P01-30			-	3/4	0k	3/8
P01-54			-	3/4	25k T	3/8
P01-17			+1/4	1.0	50k C	3/8
P01-46			+1/4	1.0	25k C	3/8
P01-34			+1/4	1.0	0k	3/8
P01-57			+1/4	1.0	25k T	3/8
P01-18			+1/2	1 1/4	50k C	3/8
P01-47			+1/2	1 1/4	25k C	3/8
P01-35			+1/2	1 1/4	0k	3/8
P01-57			+1/2	1 1/4	25k T	3/8

*C stands for compression, T for Tension and k for kips.

Table 5.21. Parametric Study Models Investigating the Influence of the Anchor Rod Diameter and Axial Load on the Rotational Stiffness and Moment Capacity of the Connection (refer to Table 5.6, Table 5.7 and Table 5.8).

Model ID	Parameter Altering	Web Depth (inch)	Increment (inch)	Anchor Rod Diameter (inch)	Axial Load (kips)	Base-Plate Thickness (inch)
P02	Anchor Rod Diameter-Axial Load	18	-	1.0	50k C	1/2
P02-45			-	1.0	25k C	1/2
P02-33			-	1.0	0k	1/2
P02-57			-	1.0	25k T	1/2
P02-17			-1/4	3/4	50k C	1/2
P02-49			-1/4	3/4	25k C	1/2
P02-37			-1/4	3/4	0k	1/2
P02-61			-1/4	3/4	25k T	1/2
P02-18			+1/4	1 1/4	50k C	1/2
P02-50			+1/4	1 1/4	25k C	1/2
P02-38			+1/4	1 1/4	0k	1/2
P02-62			+1/4	1 1/4	25k T	1/2

*C stands for compression, T for Tension and k for kips.

Table 5.22. Parametric Study Models Investigating the Influence of the Anchor Rod Diameter and Axial Load on the Rotational Stiffness and Moment Capacity of the Connection (refer to Table 5.6, Table 5.7 and Table 5.8).

Model ID	Parameter Altering	Web Depth (inch)	Increment (inch)	Anchor Rod Diameter (inch)	Axial Load (kips)	Base-Plate Thickness (inch)
P03	Anchor Rod Diameter-Axial Load	26	-	1 1/4	100k C	5/8
P03-45			-	1 1/4	50k C	5/8
P03-33			-	1 1/4	0k	5/8
P03-57			-	1 1/4	50k T	5/8
P03-17			-1/2	3/4	100k C	5/8
P03-49			-1/2	3/4	50k C	5/8
P03-37			-1/2	3/4	0k	5/8
P03-61			-1/2	3/4	50k T	5/8
P03-18			-1/4	1.0	100k C	5/8
P03-50			-1/4	1.0	50k C	5/8
P03-38			-1/4	1.0	0k	5/8
P03-62			-1/4	1.0	50k T	5/8

Despite exceptions, the general trend for the 12, 18 and 26 inch web depths connections (see Figure 5.43, Figure 5.44 and Figure 5.45) was that the rotational stiffness was reduced with reducing axial compressive load for the different anchor rod diameter connections. This was due to the fact that the less axial load applied to the column the easier it was to overturn the column.

Therefore, for the same moment but for less axial load, the base-plate uplift was greater than the base-plate uplift for more axial load, leading to a decreased rotational stiffness. It was also observed that a decrease of the compressive axial load has limited effect on the moment capacity of the connections. There was an exception in the case of the 18 inch web depth connection with the 3/4 inch anchor rod diameter. It was also seen that the rotational stiffness of the connections could decrease from 5% to 58% when tensile load was applied. It should be noted that the service axial tensile load was taken as 25 kips for the 12 inch and 18 inch web depth connections and 50 kips in the case of the 26 inch web depth connections. Typical tensile loads in base-plate connections under service loads were examined and these values were characterized as the most common for the tensile axial loads.

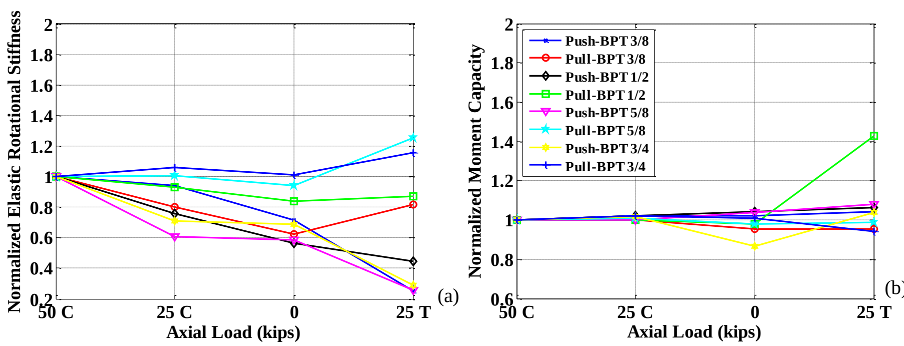

Figure 5.43. (a) Normalized elastic rotational stiffness and (b) normalized moment capacity for different axial load levels and anchor rod diameter of the 12 inch web depth connections.

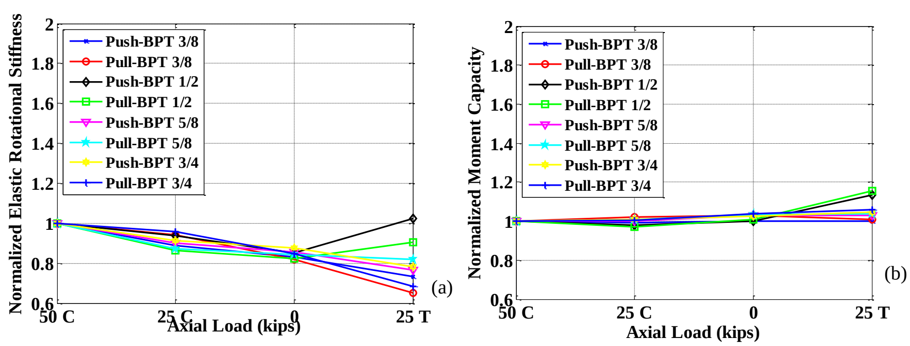

Figure 5.44. (a) Normalized elastic rotational stiffness and (b) normalized moment capacity for different axial load levels and anchor rod diameter of the 18 inch web depth connections.

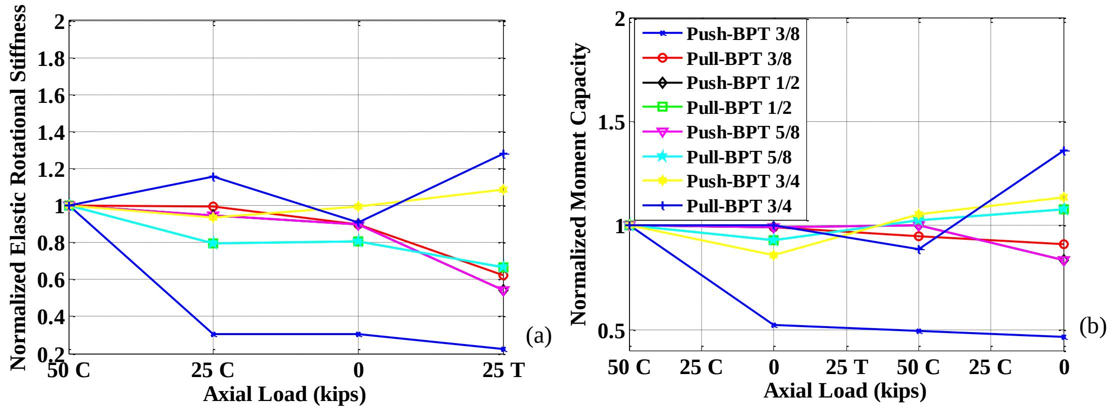

Figure 5.45. (a) Normalized elastic rotational stiffness and (b) normalized moment capacity for different axial load levels and anchor rod diameter of the 26 inch web depth connections.

5.3.13. Base-plate thickness-Anchor rod diameter-Applied axial load (12 inch web depth connections)

The base-plate connection configurations investigating the effect of the anchor rod diameter and base-plate thickness under different axial load levels are shown in Table 5.23, Table 5.24 and Table 5.25. The rotational stiffness and moment capacity of the connection combinations were normalized by those of P01 indicated in red color in Table 5.23, Table 5.24 and Table 5.25. The normalized rotational stiffness and moment capacity for the 12 inch web depth connections are shown in Figure 5.46, Figure 5.47 and Figure 5.48 respectively.

Table 5.23. Parametric Study Models Investigating the Influence of the Base-Plate Thickness and Axial Load on the Rotational Stiffness and Moment Capacity of the Connection (refer to Table 5.6, Table 5.7 and Table 5.8).

Model ID	Parameter Altering	Web Depth (inch)	Increment (inch)	Base-Plate Thickness (inch)	Axial Load (kips)	Anchor Rod Diameter (inch)
P01	Base-Plate Thickness-Axial Load	12	-	3/8	50k C*	3/4
P01-42			-	3/8	25k C*	3/4
P01-30			-	3/8	0k	3/4
P01-54			-	3/8	25k T	3/4
P01-14			+1/8	1/2	50k C	3/4
P01-43			+1/8	1/2	25k C	3/4
P01-31			+1/8	1/2	0k	3/4
P01-55			+1/8	1/2	25k T	3/4
P01-15			+1/4	5/8	50k C	3/4
P01-44			+1/4	5/8	25k C	3/4
P01-32			+1/4	5/8	0k	3/4
P01-56			+1/4	5/8	25k T	3/4
P01-16			+3/8	3/4	50k C	3/4
P01-45			+3/8	3/4	25k C	3/4
P01-33			+3/8	3/4	0k	3/4
P01-57			+3/8	3/4	25k T	3/4

*C stands for compression, T for Tension and k for kips.

Table 5.24. Parametric Study Models Investigating the Influence of the Base-Plate Thickness and Axial Load on the Rotational Stiffness and Moment Capacity of the Connection (refer to Table 5.6, Table 5.7 and Table 5.8).

Model ID	Parameter Altering	Web Depth (inch)	Increment (inch)	Base-Plate Thickness (inch)	Axial Load (kips)	Anchor Rod Diameter (inch)
P01-17	Base-Plate Thickness-Anchor Rod Diameter-Axial Load	12	-,+1/4	3/8	50k C	1.0
P01-46			-	3/8	25k C	1.0
P01-34			-	3/8	0k	1.0
P01-58			-	3/8	25k T	1.0
P01-19			+1/8	1/2	50k C	1.0
P01-48			+1/8	1/2	25k C	1.0
P01-36			+1/8	1/2	0k	1.0
P01-60			+1/8	1/2	25k T	1.0
P01-20			+1/4	5/8	50k C	1.0
P01-49			+1/4	5/8	25k C	1.0
P01-37			+1/4	5/8	0k	1.0
P01-61			+1/4	5/8	25k T	1.0
P01-21			+3/8	3/4	50k C	1.0
P01-50			+3/8	3/4	25k C	1.0
P01-38			+3/8	3/4	0k	1.0
P01-62			+3/8	3/4	25k T	1.0

*C stands for compression, T for Tension and k for kips.

Table 5.25. Parametric Study Models Investigating the Influence of the Base-Plate Thickness and Axial Load on the Rotational Stiffness and Moment Capacity of the Connection (refer to Table 5.6, Table 5.7 and Table 5.8).

Model ID	Parameter Altering	Web Depth (inch)	Increment (inch)	Base-Plate Thickness (inch)	Axial Load (kips)	Anchor Rod Diameter (inch)
P01-18	Base-Plate Thickness-Anchor Rod Diameter-Axial Load	12	-,+1/2	3/8	50k C	1 1/4
P01-47			-	3/8	25k C	1 1/4
P01-35			-	3/8	0k	1 1/4
P01-59			-	3/8	25k T	1 1/4
P01-22			+1/8	1/2	50k C	1 1/4
P01-51			+1/8	1/2	25k C	1 1/4
P01-39			+1/8	1/2	0k	1 1/4
P01-63			+1/8	1/2	25k T	1 1/4
P01-23			+1/4	5/8	50k C	1 1/4
P01-52			+1/4	5/8	25k C	1 1/4
P01-40			+1/4	5/8	0k	1 1/4
P01-64			+1/4	5/8	25k T	1 1/4
P01-24			+3/8	3/4	50k C	1 1/4
P01-53			+3/8	3/4	25k C	1 1/4
P01-41			+3/8	3/4	0k	1 1/4
P01-65			+3/8	3/4	25k T	1 1/4

*C stands for compression, T for Tension and k for kips.

It was observed that a decrease of the applied axial load in the 12 inch web depth connections resulted in a decrease of the elastic rotational stiffness of the connections. It was seen that the rotational stiffness of the connections consisting from 3/4 inch base-plate thickness combined with 1 inch and 1 1/4 inch anchor rod diameter decreased by 30% for no axial load. It was observed that the rotational stiffness of the connections with 5/8 inch base-plate thickness and 3/4 inch anchor rod diameter decreased by 38% for the 50% service axial load and by 41% for the no axial load case. It was also seen that the moment capacity of the connections was minimally affected by the change in the axial load. It was also observed that the base-plate thickness did not greatly influence the moment capacity of the connections. This can be explained by the fact that typically the base-plate moment capacity was governed by the anchor rod rupture, weld rupture, column flange buckling or concrete crashing. In all these cases the contribution of the base-plate thickness was minimal and only in yield line failure the base-plate thickness played a significant role. However according to the results the yield line failure did not dominate the behavior of the connections of this category.

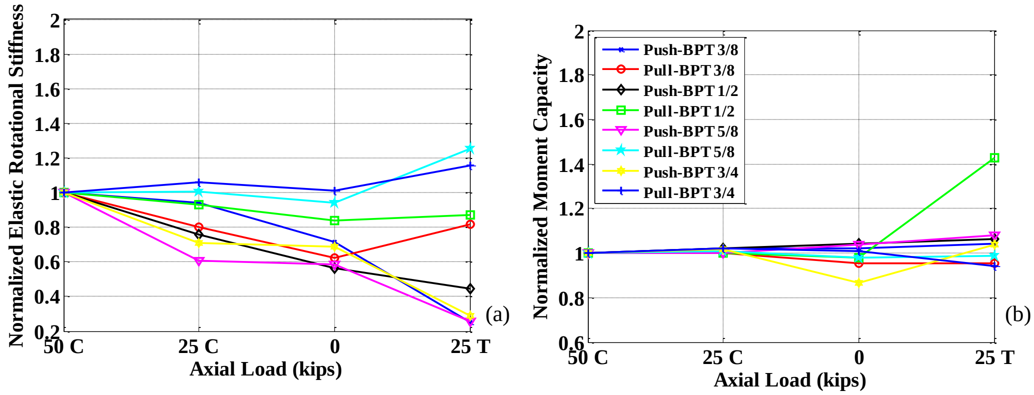

Figure 5.46. (a) Normalized elastic rotational stiffness and (b) normalized moment capacity for different axial load levels and base-plate thicknesses with 3/4 inch anchor rod diameter of the 12 inch web depth connections.

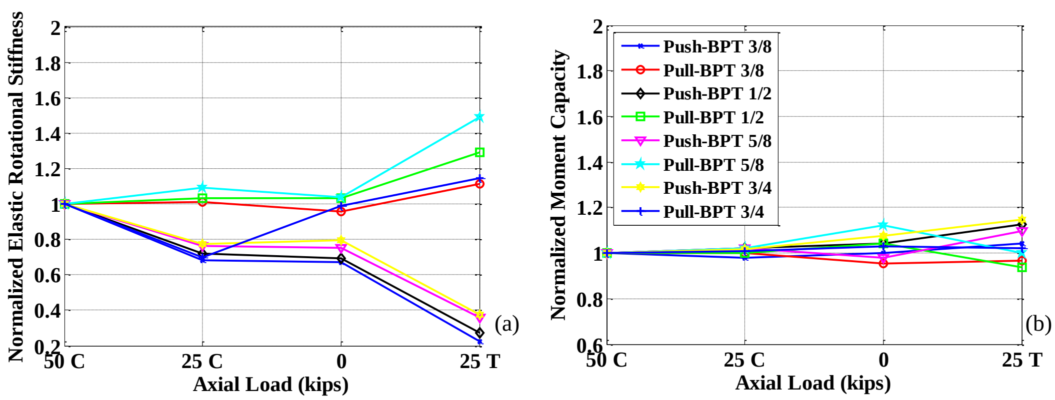

Figure 5.47. (a) Normalized elastic rotational stiffness and (b) normalized moment capacity for different axial load levels and base-plate thickness with 1.0 inch anchor rod diameter of the 12 inch web depth connections.

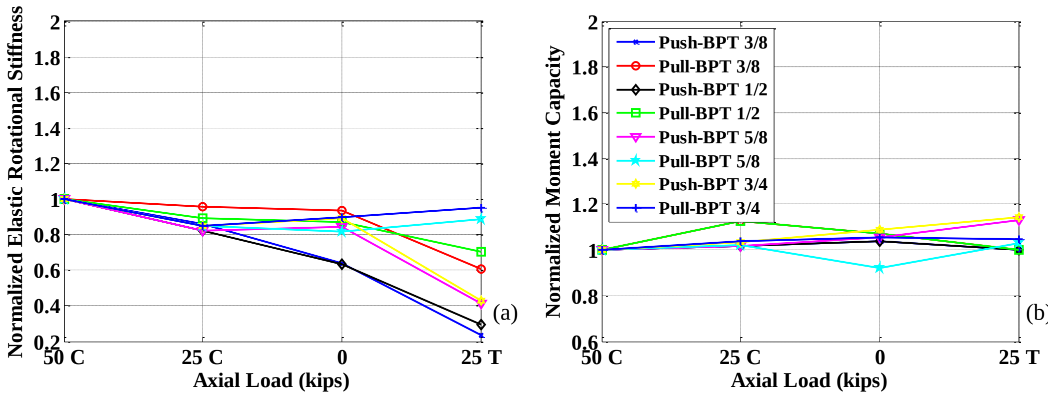

Figure 5.48. (a) Normalized elastic rotational stiffness and (b) normalized moment capacity for different axial load levels and base-plate thickness with 1 1/4 inch anchor rod diameter of the 12 inch web depth connections.

5.3.14. Base-plate thickness-Anchor rod diameter-Applied axial load (18 inch web depth)

The base-plate connection configurations investigating the effect of the anchor rod diameter and base-plate thickness under different axial load levels are shown in Table 5.26, Table 5.27and Table 5.28. The rotational stiffness and moment capacity of the connection combinations were normalized by those of P02 indicated in red color in Table 5.26, Table 5.27and Table 5.28. The normalized rotational stiffness and moment capacity for the 18 inch web depth connections are shown in Figure 5.49, Figure 5.50 and Figure 5.51 respectively.

Table 5.26. Parametric Study Models Investigating the Influence of the Base-Plate Thickness and Axial Load on the Rotational Stiffness and Moment Capacity of the Connection (refer to Table 5.6, Table 5.7 and Table 5.8).

Model ID	Parameter Altering	Web Depth (inch)	Increment (inch)	Base-Plate Thickness (inch)	Axial Load (kips)	Anchor Rod Diameter (inch)
P02-17	Base-Plate Thickness-Anchor Rod Diameter-Axial Load	18	-,-1/4	1/2	50k C	3/4
P02-49			-	1/2	25k C	3/4
P02-37			-	1/2	0k	3/4
P02-61			-	1/2	25k T	3/4
P02-19			-1/8	3/8	50k C	3/4
P02-51			-1/8	3/8	25k C	3/4
P02-39			-1/8	3/8	0k	3/4
P02-63			-1/8	3/8	25k T	3/4
P02-20			+1/8	5/8	50k C	3/4
P02-52			+1/8	5/8	25k C	3/4
P02-40			+1/8	5/8	0k	3/4
P02-64			+1/8	5/8	25k T	3/4
P02-21			+2/8	3/4	50k C	3/4
P02-53			+2/8	3/4	25k C	3/4
P02-41			+2/8	3/4	0k	3/4
P02-65			+2/8	3/4	25k T	3/4

*C stands for compression, T for Tension and k for kips.

Table 5.27. Parametric Study Models Investigating the Influence of the Base-Plate Thickness and Axial Load on the Rotational Stiffness and Moment Capacity of the Connection (refer to Table 5.6, Table 5.7 and Table 5.8).

Model ID	Parameter Altering	Web Depth (inch)	Increment (inch)	Base-Plate Thickness (inch)	Axial Load (kips)	Anchor Rod Diameter (inch)
P02	Base-Plate Thickness-Anchor Rod Diameter-Axial Load	18	-	1/2	50k C	1.0
P02-45			-	1/2	25k C	1.0
P02-33			-	1/2	0k	1.0
P02-57			-	1/2	25k T	1.0
P02-14			-1/8	3/8	50k C	1.0
P02-46			-1/8	3/8	25k C	1.0
P02-34			-1/8	3/8	0k	1.0
P02-58			-1/8	3/8	25k T	1.0
P02-15			+1/8	5/8	50k C	1.0
P02-47			+1/8	5/8	25k C	1.0
P02-35			+1/8	5/8	0k	1.0
P02-59			+1/8	5/8	25k T	1.0
P02-16			+2/8	3/4	50k C	1.0
P02-48			+2/8	3/4	25k C	1.0
P02-36			+2/8	3/4	0k	1.0
P02-60			+2/8	3/4	25k T	1.0

*C stands for compression, T for Tension and k for kips.

Table 5.28. Parametric Study Models Investigating the Influence of the Base-Plate Thickness and Axial Load on the Rotational Stiffness and Moment Capacity of the Connection (refer to Table 5.6, Table 5.7 and Table 5.8).

Model ID	Parameter Altering	Web Depth (inch)	Increment (inch)	Base-Plate Thickness (inch)	Axial Load (kips)	Anchor Rod Diameter (inch)
P02-18	Base-Plate Thickness-Anchor Rod Diameter-Axial Load	18	-,+1/4	1/2	50k C	1 1/4
P02-50			-	1/2	25k C	1 1/4
P02-38			-	1/2	0k	1 1/4
P02-62			-	1/2	25k T	1 1/4
P02-22			-1/8	3/8	50k C	1 1/4
P02-54			-1/8	3/8	25k C	1 1/4
P02-42			-1/8	3/8	0k	1 1/4
P02-66			-1/8	3/8	25k T	1 1/4
P02-23			+1/8	5/8	50k C	1 1/4
P02-55			+1/8	5/8	25k C	1 1/4
P02-43			+1/8	5/8	0k	1 1/4
P02-67			+1/8	5/8	25k T	1 1/4
P02-24			+2/8	3/4	50k C	1 1/4
P02-56			+2/8	3/4	25k C	1 1/4
P02-44			+2/8	3/4	0k	1 1/4
P02-68			+2/8	3/4	25k T	1 1/4

*C stands for compression, T for Tension and k for kips.

It was observed that a decrease of the applied axial load in the 12 inch and 18 inch web depth connections resulted in a decrease of the elastic rotational stiffness. The general trend of the 18 inch web depth connections showed that when the applied axial load decreased, then the decrease rate of the rotational stiffness and moment capacity was less compared to the ones of the 12 inch web depth connections. The decrease of the rotational stiffness ranged from 25 % for the connections consisting of a 3/8 inch thick base-plate and 3/4 inch anchor rod diameter to 55 % or the connections consisting of a 5/8 inch thick base-plate and 1 1/4 inch anchor rod diameter. As described in Section 5.3.12, a lower axial load provided a lower resistance to overturning moments and, for the same moment, the base-plate uplift was greater for less axial load than the base-plate uplift for more axial load. This led to a decreased rotational stiffness. Last, despite exceptions there was almost no effect of the axial load to the moment capacity of the connections. It was also observed that the base-plate thickness did not greatly influence the moment capacity of the connections. This can be explained by the fact that in all these cases the contribution of the base-plate thickness was minimal and only in yield line failure the base-plate thickness played a significant role. However according to the results the yield line failure did not dominate the behavior of the connections of this category.

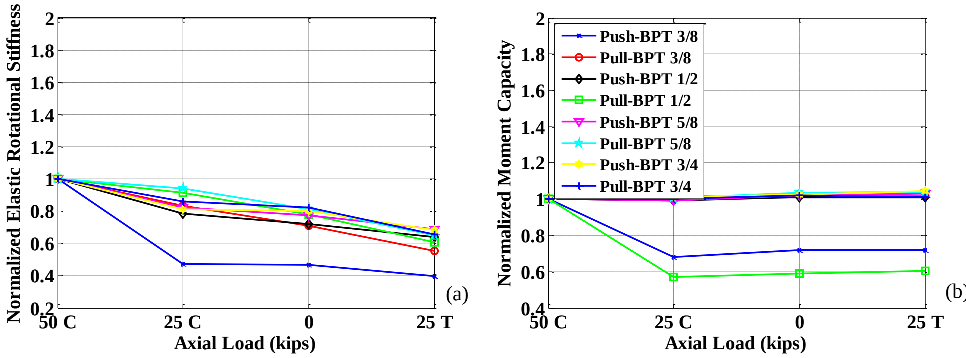

Figure 5.49 (a) Normalized elastic rotational stiffness and (b) normalized moment capacity for different axial load levels and base-plate thicknesses with 3/4 anchor rod diameter of the 18 inch web depth connections.

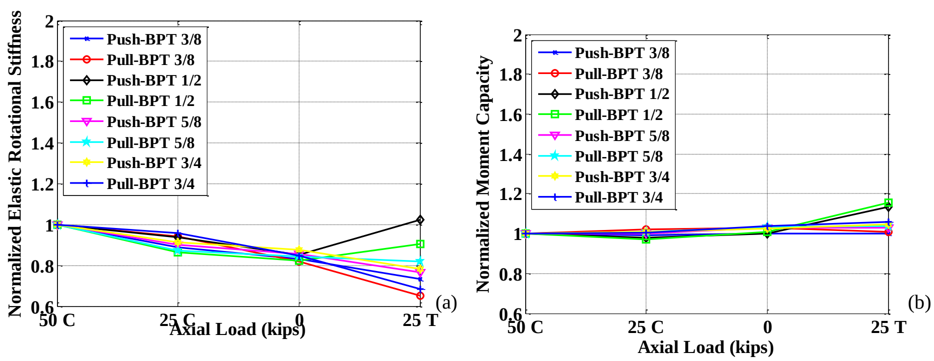

Figure 5.50. (a) Normalized elastic rotational stiffness and (b) normalized moment capacity for different axial load levels and base-plate thicknesses with 1.0 anchor rod diameter of the 18 inch web depth connections.

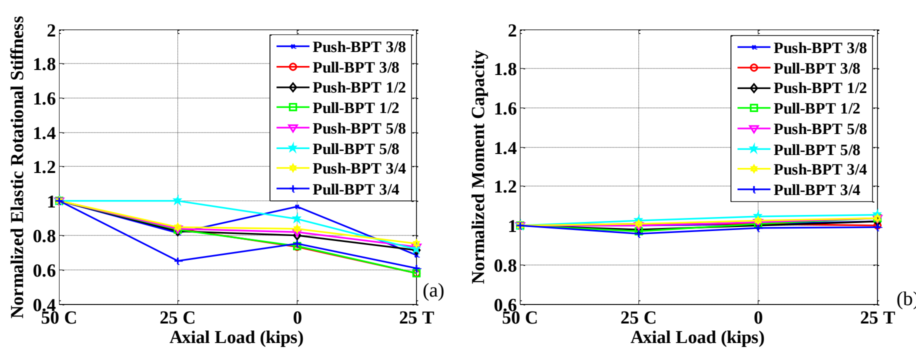

Figure 5.51. (a) Normalized elastic rotational stiffness and (b) normalized moment capacity for different axial load levels and base-plate thicknesses with 1 1/4 anchor rod diameter of the 18 inch web depth connections.

5.3.15. Base-plate thickness-Anchor rod diameter-Applied axial load (26 inch web depth)

The base-plate connection configurations investigating the effect of the anchor rod diameter and base-plate thickness under different axial load levels are shown in Table 5.29, Table 5.30 and Table 5.31. The rotational stiffness and moment capacity of the connection combinations were normalized by those of P03 indicated in red color in Table 5.29, Table 5.30 and Table 5.31. The normalized rotational stiffness and moment capacity for the 26 inch web depth connections are shown in Figure 5.52, Figure 5.53 and Figure 5.54 respectively.

Table 5.29. Parametric Study Models Investigating the Influence of the Base-Plate Thickness and Axial Load on the Rotational Stiffness and Moment Capacity of the Connection (refer to Table 5.6, Table 5.7 and Table 5.8).

Model ID	Parameter Altering	Web Depth (inch)	Increment (inch)	Base-Plate Thickness (inch)	Axial Load (kips)	Anchor Rod Diameter (inch)
P03-17	Base-Plate Thickness-Anchor Rod Diameter-Axial Load	26	-	5/8	100k C	3/4
P03-49			-	5/8	50k C	3/4
P03-37			-	5/8	0k	3/4
P03-61			-	5/8	50k T	3/4
P03-19			-2/8	3/8	100k C	3/4
P03-51			-2/8	3/8	50k C	3/4
P03-39			-2/8	3/8	0k	3/4
P03-63			-2/8	3/8	50k T	3/4
P03-20			-1/8	1/2	100k C	3/4
P03-52			-1/8	1/2	50k C	3/4
P03-40			-1/8	1/2	0k	3/4
P03-64			-1/8	1/2	50k T	3/4
P03-21			+1/8	3/4	100k C	3/4
P03-53			+1/8	3/4	50k C	3/4
P03-41			+1/8	3/4	0k	3/4
P03-65			+1/8	3/4	50k T	3/4

*C stands for compression, T for Tension and k for kips.

Table 5.30. Parametric Study Models Investigating the Influence of the Base-Plate Thickness and Axial Load on the Rotational Stiffness and Moment Capacity of the Connection (refer to Table 5.6, Table 5.7 and Table 5.8).

Model ID	**Parameter Altering**	**Web Depth (inch)**	**Increment (inch)**	**Base-Plate Thickness (inch)**	**Axial Load (kips)**	**Anchor Rod Diameter (inch)**
P03-18	Base-Plate Thickness-Anchor Rod Diameter-Axial Load	26	-	5/8	100k C	1.0
P03-50			-	5/8	50k C	1.0
P03-38			-	5/8	0k	1.0
P03-62			-	5/8	50k T	1.0
P03-22			-2/8	3/8	100k C	1.0
P03-54			-2/8	3/8	50k C	1.0
P03-42			-2/8	3/8	0k	1.0
P03-66			-2/8	3/8	50k T	1.0
P03-23			-1/8	1/2	100k C	1.0
P03-55			-1/8	1/2	50k C	1.0
P03-43			-1/8	1/2	0k	1.0
P03-67			-1/8	1/2	50k T	1.0
P03-24			+1/8	3/4	100k C	1.0
P03-56			+1/8	3/4	50k C	1.0
P03-44			+1/8	3/4	0k	1.0
P03-68			+1/8	3/4	50k T	1.0

*C stands for compression, T for Tension and k for kips.

Table 5.31. Parametric Study Models Investigating the Influence of the Base-Plate Thickness and Axial Load on the Rotational Stiffness and Moment Capacity of the Connection (refer to Table 5.6, Table 5.7 and Table 5.8).

Model ID	**Parameter Altering**	**Web Depth (inch)**	**Increment (inch)**	**Base-Plate Thickness (inch)**	**Axial Load (kips)**	**Anchor Rod Diameter (inch)**
P03	Base-Plate Thickness-Axial Load	26	-	5/8	100k C	1 1/4
P03-45			-	5/8	50k C	1 1/4
P03-33			-	5/8	0k	1 1/4
P03-57			-	5/8	50k T	1 1/4
P03-14			-2/8	3/8	100k C	1 1/4
P03-46			-2/8	3/8	50k C	1 1/4
P03-34			-2/8	3/8	0k	1 1/4
P03-58			-2/8	3/8	50k T	1 1/4
P03-15			-1/8	1/2	100k C	1 1/4
P03-47			-1/8	1/2	50k C	1 1/4
P03-35			-1/8	1/2	0k	1 1/4
P03-59			-1/8	1/2	50k T	1 1/4
P03-16			+1/8	3/4	100k C	1 1/4
P03-48			+1/8	3/4	50k C	1 1/4
P03-36			+1/8	3/4	0k	1 1/4
P03-60			+1/8	3/4	50k T	1 1/4

*C stands for compression, T for Tension and k for kips.

It was observed that the decrease of the applied axial load in the 26 inch web depth connections resulted in the decrease of the elastic rotational stiffness and moment capacity of the 26 inch web depth connections. It was seen that the rotational stiffness and moment capacity of the connections with 3/4 inch base-plate thickness combined with the three different anchor rod diameters (3/4 inch, 1.0 inch and 1 1/4 inch) was higher when 100% service tensile axial load was applied on the connection in comparison to 50% or 100% axial compressive service load. The shear failure of the column web it was typically observed at the 26 inch web depth connections and the application of the axial tensile force prevented this failure resulting in a higher rotational stiffness and moment capacity. The reduction of the rotational stiffness of the connections ranged from 0% to 35% depending on the base-plate thickness and anchor rod combination case. It is rather difficult to interpret the results in Figure 5.52 to Figure 5.54 because several of the models' response was governed by web shear deformation similar to [Figure 5.16(a)]. In the future, it is recommended to evaluate the base-plate behavior of 26 inch web depth connections by utilizing taller columns to prevent shear failure of the web.

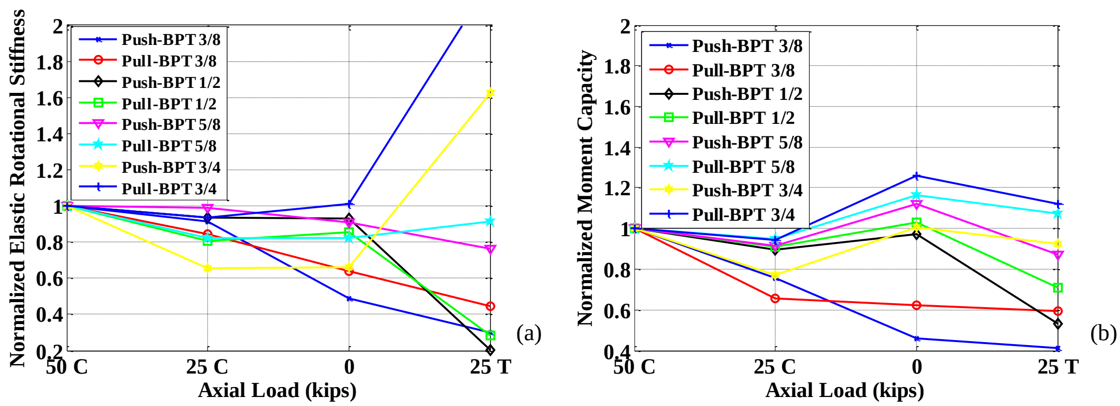

Figure 5.52. (a) Normalized elastic rotational stiffness and (b) normalized moment capacity for different axial load levels and base-plate thicknesses with 3/4 anchor rod diameter of the 26 inch web depth connections.

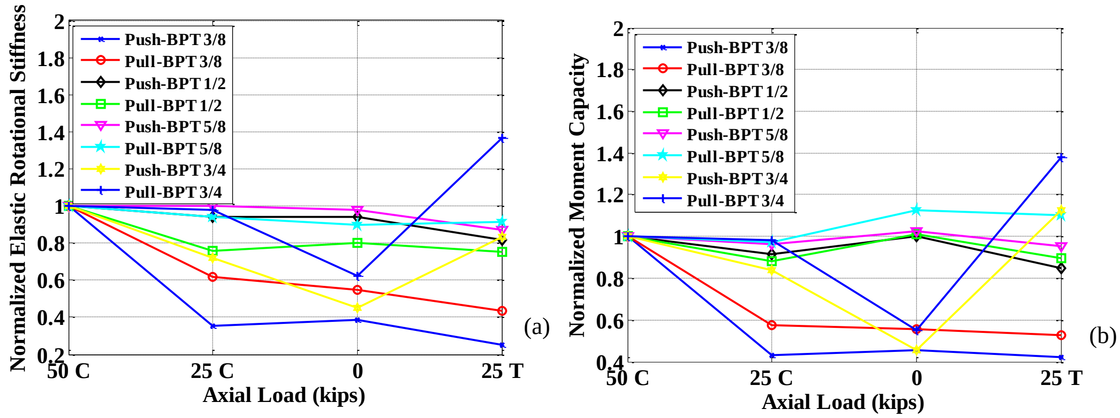

Figure 5.53. (a) Normalized elastic rotational stiffness and (b) normalized moment capacity for different axial load levels and base-plate thicknesses with 1.0 anchor rod diameter of the 26 inch web depth connections.

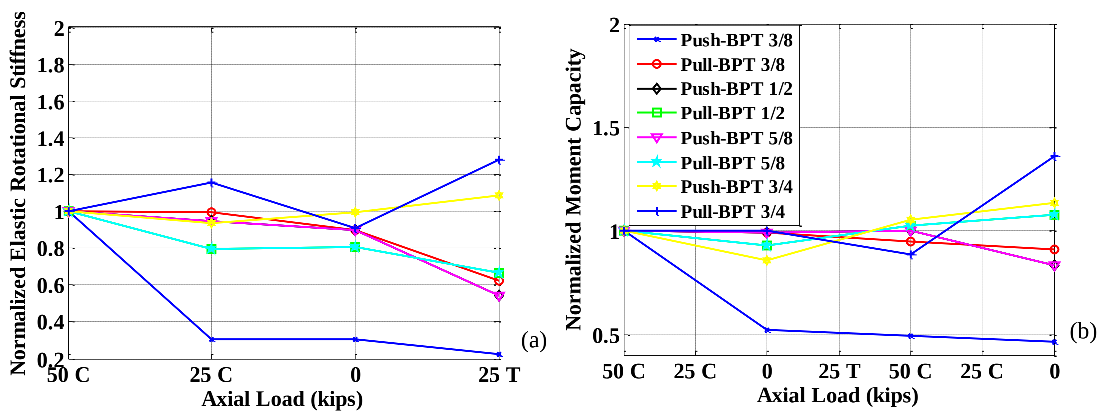

Figure 5.54. (a) Normalized elastic rotational stiffness and (b) normalized moment capacity for different axial load levels and base-plate thicknesses with 1 1/4 anchor rod diameter of the 26 inch web depth connections.

5.4. Methods for Estimating the Moment Capacity of Pinned Base-Plate Connections

In order to calculate the moment capacity of the connections, an extensive review of the available design guides was performed. Since there are no design provisions for the base-plate connections considered in his research, several assumptions had to be made that are presented in this section. This section presents the calculations to estimate the base-plate moment capacity based on the design codes [i.e., AISC Steel Construction Manual, 2011 and ACI 318, 2014, as well as Eurocode 3 (prEN1993-1-8) and Eurocode 2 (prEN1992-1-1)]. The limit states of anchor rod rupture, concrete crushing, flange yielding, and web yielding are included in the base-plate moment capacity calculation. AISC Design Guide 1 (Fisher and Kloiber, 2006) provides the design procedures to adequately size the base-plate connections. AISC Design Guide 1 (Fisher and Kloiber, 2006) along with AISC Steel Construction Manual (2011) are the basis to calculate the moment capacity of base-plate connections. Following the procedures outlined in AISC Design Guide 1 (Fisher and Kloiber, 2006), the moment capacity of the base-plate connection can be calculated according to Eurocodes. According to both AISC and Eurocodes provisions, the moment capacity of a base-plate is determined as the minimum moment capacity due to the failure of one component of the base-plate connection (i.e., anchor rods, base-plate, column flanges etc.). In other words, several base-plate moment capacities are calculated based on the strength of each component, and the lower bound of all solutions is the base-plate moment capacity.

5.4.1. Moment capacity due to anchor rod rupture

The first step is to assume that the base-plate and the column components (e.g., flanges) have adequate strength to resist the forces developed, and the ultimate moment capacity is governed by anchor rod rupture. Then the moment capacity of the base-plate connection is calculated based on the equilibrium of forces. At the ultimate level, the equivalent eccentricity, which is defined as the ratio of the moment (M) divided by the column axial force (P), is large enough to produce tension in the anchor rods. Assuming that the base-plate under consideration has length "N" and width "B" and based on the force diagram shown in Figure 5.55, then from the vertical force equilibrium the bearing force ($F_B = f_p \cdot B \cdot Y$) is equal to the summation of the applied axial force (P) and the tensile forces of the anchor rods (F_{nt_1}, F_{nt_2}).

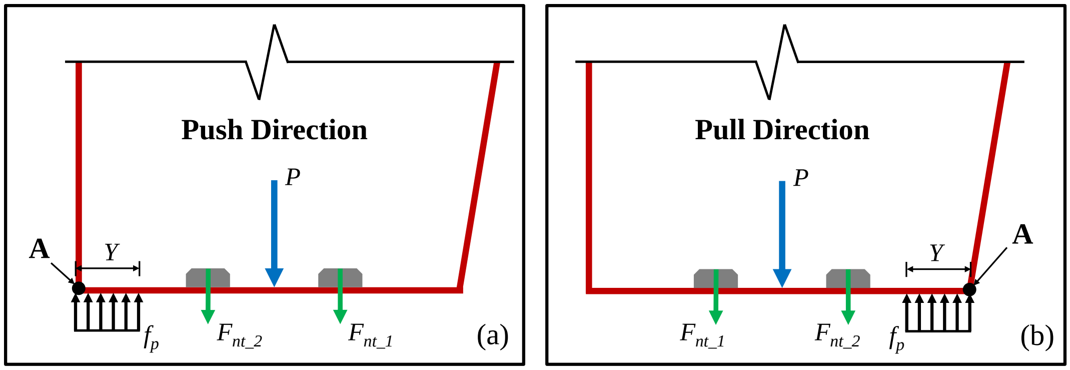

Figure 5.55. Base-plate forces in (a) push direction and (b) pull direction.

As proposed by Drake and Elkin (1999), a uniform distribution of the bearing stress is used to simulate the compressive force below the base-plate. The nominal bearing stress between the plate and concrete is determined in accordance with Table 14.5.6.1 of ACI 318 (2014). The same expression for the nominal bearing strength is provided in AISC Steel Construction Manual (2011), Section J8. In case the supporting surface (i.e., pedestal) is wider on all sides than the loaded area (i.e., base-plate), then the nominal bearing stress is given by Equation (5-1) as

$$f_p = \min\left\{\begin{matrix}\sqrt{A_2/A_1}\cdot(0.85\cdot f_c') \\ 2\cdot(0.85\cdot f_c')\end{matrix}\right\}, \tag{5-1}$$

where, A_1 is loaded area for consideration of bearing strength (inch^2), A_2 is projected bearing area of column base-plate load (inch^2), and f_c' is specified compressive strength of concrete (ksi). Similarly to Equation (5-1), the nominal bearing stress between the plate and concrete can be determined based on Equation 6.63 of Eurocode 2 (prEN1992-1-1).

The nominal bearing force (F_B) is given in Equation (5-2) as

$$F_B = f_p \cdot B \cdot Y, \tag{5-2}$$

where, f_p is maximum bearing stress between the plate and concrete (ksi), B is base-plate width (inch), and Y is length of bearing area (inch).

According to AISC Steel Construction Manual (2011), the design bearing force ($\varphi_c \cdot F_B$) is equal to the nominal bearing force (F_B) multiplied by a resistance factor (φ_c) of 0.65. Based on Eurocode 2 (prEN1992-1-1), the design bearing force (F_{Rdu}) is equal to the nominal bearing force (F_B) divided by a partial factor for concrete (γ_c) of 1.5.

The tensile forces on the anchor rods are estimated based on AISC Steel Construction Manual (2011). The nominal tensile stress of the extreme anchor rod (f_{nt_1}) can be computed based on AISC Steel Construction Manual (2011), Table J3.2 as given in Equation (5-3) as

$$\mathrm{f_{nt\_1}} = 0.75 \cdot \mathrm{f_u}, \tag{5-3}$$

where, f_u is specified minimum tensile strength (ksi). The nominal tensile stress of the extreme anchor rod (f_{nt_1}) can also be calculated based on Table 3.4 of Eurocode 3 (prEN1993-1-8).

The nominal tensile strength of the extreme anchor bolt (F_{nt_1}) is determined according to the limit states of tension rupture based on Equation J3-1 of AISC Steel Construction Manual (2011) as given in Equation (5-4) as

$$\mathrm{F_{nt\_1}} = \mathrm{f_{nt}} \cdot \mathrm{A_b}, \tag{5-4}$$

where, A_b is nominal unthreaded body area of anchor rod based on AISC Steel Construction Manual (2011), Table 7-17 (inch^2). The design tensile strength of the extreme anchor bolt ($\varphi_t \cdot F_{nt\_1}$) is equal to the nominal tensile strength of the extreme anchor bolt (F_{nt_1}) multiplied by a resistance factor (φ_t) of 0.75. Equivalently, the design tensile strength of the extreme anchor bolt ($F_{t,Rd}$) can be determined based on Table 3.4 of Eurocode 3 (prEN1993-1-8).

Based on material test results, the strain (ε_{nt_u}) at the peak stress of 3/4 inch diameter anchor rods is 0.063 inch/inch and for anchor rods with diameters of 1 inch and 1 1/2 inch, the strain (ε_{nt_u}) at the peak stress is 0.05 inch/inch From the strain gradient show in Figure 5.56, one can determine the strain (ε_{nt_2}) of the inner anchor rods, which are located between the extreme pair of anchor rods and the compression zone. Based on the inner anchor rod strain (ε_{nt_2}), the nominal tensile force of the inner anchor rod (F_{nt_2}) can be easily calculated in accordance with Equation (5-5) or (5-6) as

If $\varepsilon_{nt\_2} < f_y/E$:

$$F_{nt\_2} = E \cdot \varepsilon_{nt_2} \cdot A_b \text{ and} \tag{5-5}$$

If $\varepsilon_{nt\_2} > f_y/E$:

$$F_{nt\_2} = f_y \cdot A_b, \tag{5-6}$$

where, ε_{nt_2} is strain of the inner anchor rods (inch/inch), f_y is specified minimum yield strength (ksi), E is modulus of elasticity of steel (ksi), and A_b is nominal unthreaded body area of anchor rod based on AISC Steel Construction Manual (2011), Table 7-17 ($inch^2$).

The design force of the inner anchor bolt ($\varphi_t \cdot F_{nt\_2}$) is equal to the nominal tensile force of the inner anchor rod multiplied by a resistance factor (φ_t) of 0.75.

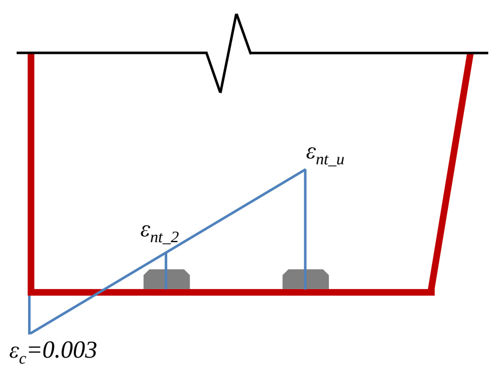

Figure 5.56. Strain gradient in push direction.

After calculating all the anchor rod forces shown in Figure 5.55, the length of bearing area (Y) is determined by applying the vertical force equilibrium. Last, the moment capacity of the base-plate connection is computed based on the summation of moments taken about the point A (Figure 5.55). The nominal moment capacity of the base-plate connection is computed based on the nominal forces (i.e., F_B, F_{nt_1}, F_{nt_2}), whereas, the design moment capacity of the base-plate configuration is calculated based on the design forces calculated either based on AISC Steel Construction Manual (2011) (i.e., $\varphi_c \cdot F_B$, $\varphi_t \cdot F_{nt\_1}$, $\varphi_t \cdot F_{nt\_2}$), or Eurocode 3 (prEN1993-1-8) (i.e., F_{Rdu}, $F_{t,Rd}$). In the case of flexible base-plate, only the extreme anchor rod row shall be included in the calculation of base-plate moment capacity. One can determine the base-plate behavior and whether the base-plate will show rigid or flexible behavior based on methodologies presented in Section 5.4.5 below.

5.4.2. Moment capacity based on yield line of base-plate

Another failure mechanism that can govern the moment capacity of the pinned base-plate connection is the yield failure of the base-plate. The moment capacity of the base-plate connection due to base-plate yielding is calculated utilizing the yield line method. AISC Design Guide 4 (Murray and Sumner, 2003) and AISC Design Guide 16 (Murray and Shoemaker, 2002) provide methods for yield line mechanisms of end plates of beam-to-column moment connections. Tables 3-4 and 3-5 of AISC Design Guide 4 (Murray and Sumner, 2003) present the nominal moments of end plates with four bolts and eight bolts, respectively, contributing to the yield line pattern. Similarly, Table 3-2 of AISC Design Guide 16 (Murray and Shoemaker, 2002) summarizes the nominal moments of end plates with two bolts contributing to the yield line pattern. Alternatively, the moment capacity of the base-plate connection due to base-plate yielding can be computed based on the yield line method presented in Tables 6.2 and 6.6 and Eurocode 3 (prEN1993-1-8).

It should be noted that based on the results, which are presented in Section 0, the yield line pattern of four bolts [Table 3-4 of AISC Design Guide 4 (Murray and Sumner, 2003)] underestimates the moment capacity of base-plate connection for S05 and S06. Even though the moment capacity of base-plate connections of S05 and S06 based on the yield line does not match the experimental results, the estimated moment capacity is conservative. In addition, Eurocode 3 (prEN1993-1-8) greatly underestimates the base-plate moment capacity due to yield line compared to AISC Steel Construction Manual (2011). This is due to the fact that the summation of the yield lines lengths ($0.25 \cdot \Sigma l_{eff,1}$) calculated based on Tables 6.2 and 6.6 of Eurocode 3 (prEN1993-1-8) is smaller than the ones calculated according to AISC Design Guide 4 (Murray and Sumner, 2003) or AISC Design Guide 16 (Murray and Shoemaker, 2002). Further research should be conducted to better estimate the yield line mechanism of base-plate connections with different geometries.

5.4.3. Moment capacity due to rupture of welds between column and base-plate

The next check to calculate the moment capacity of the pinned base-plate connection is to estimate the rupture strength of the welds that connect the column tension flange to the base-plate. The maximum bending stress at the tension flange (σ_{tf}) is computed based on engineering mechanics formula as

$$\mathrm{\sigma_{tf}} = \frac{\mathrm{M} \cdot (\mathrm{d_{bp}} - \mathrm{Y})}{\mathrm{I_w}}, \tag{5-7}$$

where, M is applied moment (kips-inch), d_{pb} is depth of base-plate (inch), Y is length of bearing area (inch) (see Figure 5.55), and I_w is moment of inertial of the welds about the axis of bending (inch^4).

The available strength of a welded joint that is given by Equation 8-1 of AISC Steel Construction Manual (2011) and presented in Equation (5-8) as

$$\mathrm{R_n} = 0.60 \cdot \mathrm{F_{EXX}} \cdot \frac{\sqrt{2}}{2} \cdot \mathrm{t_{w_{tf}}} \cdot \mathrm{b_f}, \tag{5-8}$$

where, R_n is available strength of the fillet weld (ksi), F_{EXX} is filler metal classification strength (ksi), t_{w_tf} is fillet weld size of the column flange in tension (inch), and b_f is base-plate width (inch). Equivalently, the fillet weld design resistance can be determined based on Section 4.5 of Eurocode 3 (prEN1993-1-8).

The force (F_{w_tf}) on the welds of the column flange in tension is calculated similarly to the available strength of a welded joint given by Equation (5-8) by substituting the term $0.60 \cdot F_{EXX}$ with the maximum bending stress (σ_{tf}). The force (F_{w_tf}) on the welds of the column flange in tension is given in Equation (5-9) as

$$\mathrm{F_{w\_tf}} = \sigma_{\mathrm{tf}} \cdot \frac{\sqrt{2}}{2} \cdot \mathrm{t_{w_{tf}}} \cdot \mathrm{b_f}, \tag{5-9}$$

where, σ_{tf} is maximum bending stress on the column flange in tension (ksi), t_{w_tf} is fillet weld size of the column flange in tension (inch), and b_f is base-plate width (inch).

Based on Equation J2-4 of AISC Steel Construction Manual (2011), the nominal strength (R_n) of the fillet welds is given by Equation (5-10) as

$$\mathrm{R_n} = \mathrm{F_{nw}} \cdot \mathrm{A_{we}} \text{ and} \tag{5-10}$$

$$\mathrm{F_{nw}} = 0.60 \cdot \mathrm{F_{EXX}} \cdot (1.0 + 0.50 \cdot \sin^{1.5}\theta), \tag{5-11}$$

where, F_{nw} is nominal stress of the weld metal (ksi), A_{we} is effective area of the weld of the column flange in tension (inch^2), F_{EXX} is filler metal classification strength (ksi), and θ is angle of loading measured from the weld longitudinal axis (degrees). The design strength ($\varphi_w \cdot R_n$) of the fillet welds is equal to the nominal weld strength multiplied by a resistance factor (φ_w) of 0.75. Similarly, the design resistance of the fillet weld can be computed according to Equation 4.1 of Eurocode 3 (prEN1993-1-8).

Hence, the nominal moment capacity of the pinned base-plate connection due to the rupture of the welds at the column flange in tension is determined by equilibrating Equation (5-9) and (5-10). The nominal (M_n) and design (M_d) moment capacity of the base-plate connection is given by Equations (5-12) and (5-13), respectively, as

$$\mathrm{M_n} = \frac{\mathrm{F_{nw}} \cdot \mathrm{I_w}}{(\mathrm{d_{bp}} - \mathrm{Y})} \text{ and} \tag{5-12}$$

$$M_d = \frac{\varphi_w \cdot F_{nw} \cdot I_w}{(d_{bp} - Y)}. \tag{5-13}$$

5.4.4. Moment capacity due to local buckling of the column flange

Based on observations during the experimental program, the moment capacity of the base-plate connection can be limited by the yielding or local buckling of the column flange. Sections F3, F4 and F5 of AISC Steel Construction Manual (2011) provide methodologies to estimate the nominal flexural strength of the column base due to yielding or local buckling of compression flange. Utilizing Table B4.1b of AISC Steel Construction Manual (2011), one can calculate the limiting width-to-thickness ratios of compact/noncompact (λ_p) and noncompact/slender (λ_r) webs. Based on the limiting width-to-thickness ratios, the part of web under compression can be classified as compact, noncompact, or slender. Depending on the classification, the nominal flexural strength of the column section at the base can be estimate based on the following sections of AISC Steel Construction Manual (2011):

- Section F3 for doubly-symmetric I-shaped members with compact webs and noncompact or slender flanges.
- Section F4 for other I-shaped members (including singly-symmetric I-shaped members) with compact or noncompact webs.
- Section F5 for doubly- and singly-symmetric I-shaped members with slender webs.

Similarly, the nominal and design flexural strengths of the column base due to yielding or local buckling of compression flange can be computed based on Eurocode 3 (prEN1993-1-1). First, the cross section shall be classified as Class 1, 2, 3, or 4 based on Section 5.5 of Eurocode 3 (prEN1993-1-1).Then, depending on cross section class, the nominal and design flexural strengths of the column base due to yielding or local buckling of compression flange can be calculated in accordance with Section 6.2.5 of Eurocode 3 (prEN1993-1-1).

In the case that the nominal flexural strength of the column base-plate is lower than the moment capacities of base-plate connection estimated by the abovementioned methods, then the moment capacity of the base-plate connection is equal to the nominal flexural strength of the column base.

5.4.5. Classification of the base-plate behavior

AISC Design Guide 1 (Fisher and Kloiber, 2006), Section 3.3.2 presents a procedure to compute the flexural strength of the cantilever portion of the base-plate in order to determine the required base-plate thickness. The required bending moment per unit width is computed based on the fixed end moment of a cantilever loaded with a uniform load equal to the bearing pressure. Equivalently, for the base-plate configurations presented in this study, the required bending moment per unit width is computed by idealizing the base-plate as a propped cantilever (Figure 5.57). The fixed end of the propped cantilever is located at the connection of the flange to the base-plate, and the pin connection at the location of the outer anchor rod (i.e., extreme anchor rod in tension). The propped cantilever is loaded with a uniform distributed load to represent the bearing pressure between the concrete and the base-plate and the tensile forces of the anchor rods are modeled as point loads (Figure 5.57).

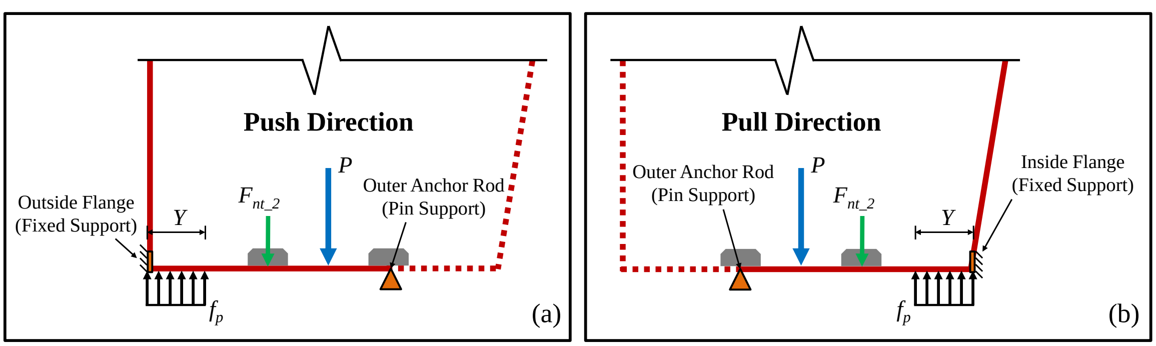

Figure 5.57. Idealization of the base-plate to evaluate the base-plate behavior (a) in the push direction and (b) in the pull direction.

The bending moment at the fixed end of the propped cantilever (M_A) is determined as the summation of the moments given in Equations (5-14) and (5-15) based on in Figure 5.58 and Figure

5.59. It should be mentioned that Equation (5-15) may be used multiple times in order to compute the fixed end moment due to multiple point loads (e.g., axial load "P", anchor rod forces "F_{nt_2}", "F_{nt_3}", etc. when more than three pairs of anchor rods are employed).

The fixed end moment due to a uniformly distributed load is (see Figure 5.58)

$$M_{A\_uniform} = \frac{f_p \cdot Y^2}{2} - \frac{f_p}{8 \cdot l^2} \cdot (4 \cdot l \cdot Y^3 - Y^4). \tag{5-14}$$

The fixed end moment due to a point load (Figure 5.59) is given by

$$M_{A\_point\_load} = \frac{F_{nt\_2} \cdot s_1 \cdot s}{2 \cdot l^2} \cdot (s_1 + l). \tag{5-15}$$

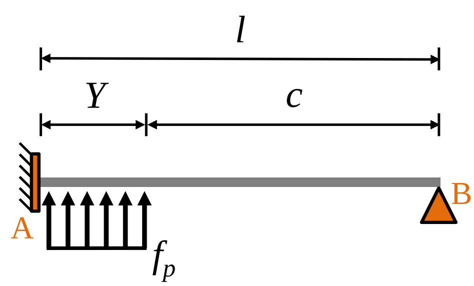

Figure 5.58. Propped cantilever loaded with a uniform distributed load.

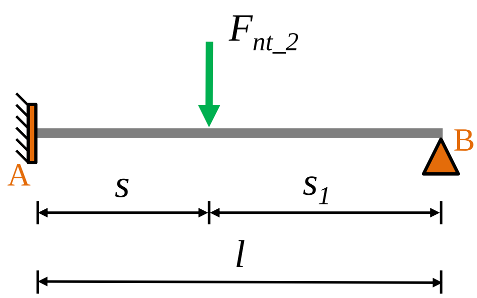

Figure 5.59. Propped cantilever loaded with a point load.

Based on AISC Design Guide 1 (Fisher and Kloiber, 2006), the nominal bending resistance (M_{n_bp}) per unit width of the plate is given by Equation (5-16) as

$$M_{n\_bp} = {f_y \cdot t_p^2}/{4}, \tag{5-16}$$

where, f_y is nominal stress of the weld metal (ksi), and t_p is base-plate thickness (inch).

The design bending resistance ($\varphi_b \cdot M_{n\_bp}$) per unit width of the plate is equal to the nominal bending resistance multiplied by a resistance factor (φ_b) of 0.90.

The base-plate behavior can be classified by comparing the required fixed end moment per unit width of the base-plate propped cantilever and the base-plate bending resistance per unit width. Table 5.32 and Table 5.33 compare the required fixed end moment per unit width of the base-plate propped cantilever and the base-plate bending resistance per unit width for push and pull directions. Based on observations made during the experimental program, the base-plate behaviors of specimens S01 to S11 are categorized as rigid, balanced, and flexural. This study has defined limits to correlate the difference between the required fixed end moment per unit width and the bending resistance per unit width with the observed base-plate behaviors during the tests as described in Table 4.11. It is concluded that in the case that the difference between the required fixed end moment per unit width (Figure 5.57) and the bending resistance per unit width is less than 20%, then the base-plate behavior would be predominantly rigid. When the required fixed end moment per unit width is more than 20% but less than 80% of the bending resistance per unit width, then the base-plate behavior would be balanced. For all other cases that the required fixed end moment per unit width is more than 80% of the bending resistance, the behavior of the base-plate would be predominantly flexurally dominated.

The proposed limits to classify a base-plate as rigid, balanced or flexural and the results shown in Table 5.32 and Table 5.33 are in a good agreement with the test observations listed in Table 4.11. For example, according to test results a rigid behavior of the base-plate connection is observed for S01, S02 and S11 (Figure 4.44) and based on Table 4.11 the observed base-plate damage is minor. This behavior is predicted by the results in Table 5.32 and Table 5.33 because the difference between the required fixed end moment per unit width and the bending resistance per unit width is less than 20%. In the contrary, the base-plate connection of S05 has a predominantly flexurally dominated behavior (Figure 4.48) and as per Table 4.11 the damage of the base-plate damage is excessive. The test observation for S05 is consistent with the estimated behavior in Table 5.32 and Table 5.33. The difference between the required fixed end moment per unit width and the bending resistance per unit width is calculated to be more than 80% indicating that the base-plate behavior of S05 is flexural. In the case of balanced base-plate behavior, the experiments showed that the behavior of S03, S04, and S06 to S10 base-plates (Figure 4.47) are balanced. A balanced base-plate behavior of these specimens was estimated as shown in Table 5.32 and Table 5.33 since the difference between the required fixed end moment per unit width and the bending resistance per unit width was more than 20% but less than 80%.

Table 5.32. Summary of the Base-Plate Required Fixed End Moment per Unit Width (M_A^+), the Base-Plate Bending Resistance per Unit Width ($M_{n\_bp}^+$), and their Difference for Push Direction.

Specimen ID	M_A^+	$\varphi \cdot M_A^+$	$M_{n\_bp}^+$	$\varphi \cdot M_{n\_bp}^+$	Difference	
	(kips-inch/inch)		(kips-inch/inch)		(%)	
S01	6.34	6.35	5.37	4.83	15.3	23.8
S02	5.86	6.43	5.37	4.83	8.4	24.8
S03	19.02	13.80	5.37	4.83	71.8	65.0
S04	23.64	15.76	5.37	4.83	77.3	69.3
S05	23.64	15.76	1.93	1.74	91.8	89.0
S06	23.64	15.76	5.37	4.83	77.3	69.3
S07	21.83	17.31	5.37	4.83	75.4	72.1
S08	18.65	16.06	5.37	4.83	71.2	69.9
S09	18.65	16.06	5.37	4.83	71.2	69.9
S10	18.65	16.06	7.73	6.96	58.5	56.7
S11	3.44	3.97	3.44	3.09	0.0	22.1

Table 5.33. Summary of the Base-Plate Required Fixed End Moment per Unit Width (M_A^-), the Base-Plate Bending Resistance per Unit Width ($M_{n\_bp}^-$), and their Difference for Pull Direction.

Specimen ID	M_A^-	$\varphi \cdot M_A^-$	$M_{n\_bp}^-$	$\varphi \cdot M_{n\_bp}^-$	Difference	
	(kips-inch/inch)		(kips-inch/inch)		(%)	
S01	6.17	6.69	5.37	4.83	13.0	27.7
S02	5.30	6.20	5.37	4.83	-1.3	22.0
S03	20.08	14.55	5.37	4.83	73.3	66.8
S04	23.06	15.41	5.37	4.83	76.7	68.6
S05	23.06	15.41	1.93	1.74	91.6	88.7
S06	23.84	15.88	5.37	4.83	77.5	69.6
S07	24.32	19.25	5.37	4.83	77.9	74.9
S08	18.61	16.05	5.37	4.83	71.1	69.9
S09	18.61	16.05	5.37	4.83	71.1	69.9
S10	18.61	16.05	7.73	6.96	58.4	56.6
S11	3.31	3.93	3.44	3.09	-3.7	21.2

5.4.6. Results of the calculations for estimating the moment capacity of pinned base-plate connections

Table 5.34 and Table 5.36 present the base-plate moment capacity from the experiments and the results of the base-plate nominal moment capacity based on the calculations. Similarly, Table 5.35 and Table 5.37 provide the results of the design (factored) moment capacity of each base-plate connection as calculated according to design codes.

In the push direction (Table 5.34), the dominant failure mode in most cases is the anchor rod rupture (S01 to S03, S07, and S11). This finding is consistent with most of the experimental results (S01, S02, and S11). The test results for S03 indicate that the failure mechanism is governed by a combination of limit states including anchor rod yielding, concrete cracking and base-plate yielding (Figure 4.46). The experimental observations for S03 are in a good agreement with the calculated failure mode. In the calculations described above, the anchor rod rupture is assumed to occur with concrete crushing. Based on Table 5.34, the governing failure mechanism of S03 is the anchor rod rupture, but the moment capacity of the base-plate based on the yield line failure mode is very close to the governing case (i.e., $Mn_{\_anchor\_rod}$ = 86.7 kip-ft and $Mn_{\_yield\_line}$ = 90.9 kip-ft). Therefore, the estimated base-plate moment capacity predicts a failure mode closely to the one observed during the test. In the case of S07 to S10, the magnitude of the estimated moment capacity of base-plate connection is close to the one measured during the tests, however, the calculations do not accurately predict the failure mechanism. During the experiments of S07 to S10, the failure mode observed is global concrete cracking of the entire foundation (Figure 4.50 to Figure 4.53). This is explained based on the fact that the concrete foundations of S07 to S10 could not be designed as larger elements due to test setup limitations. The calculations predict that the moment capacity of S04 in push direction is govern by the column flange local buckling, which is exactly what is observed in the test results. In addition, based on test results the moment capacities of S05 and S06 are limited to yield line capacity and weld rupture (Figure 4.48 and Figure 4.49), which is consistent with the yield line failure estimated based on the calculations (Table 5.34). Last, it should be noted that the design (factored) moment capacities (Table 5.35) calculated based on the codes are very conservative compared to the experimental values. This is due to the fact that the strength reduction factors decrease the strength of the different base-plate connection components.

In the pull direction (Table 5.36), the most common failure mode, similarly to the push direction, is the anchor rod rupture (S01 to S04 and S11). The estimated moment capacities and failure mechanisms for S01 to S04 and S11 are in a good agreement with the experimental result. The predicted failure mode for S04 in the pull direction is anchor rod rupture, which is inconsistent with the S04 test results where the flange local buckling governed. However, the local buckling of the flange (outside flange) occurred in the push direction and it would have not occurred if the column had been tested only in the pull direction because the outside flange would had been in tension. Similarly to the push direction, the global concrete cracking of the entire foundation of S07 to S10 is the governing failure mode. If the concrete foundation had adequate strength, then the dominant failure mechanism may had been weld rupture or yield line failure of the base-plate as predicted based on the calculations (Table 5.36). As previously mentioned, the design (factored) moment capacities (Table 5.37) calculated based on the provisions of the design codes are more conservative than the experimental values. This can be explain because the strength reduction factors decrease the estimated strength of the base-plate connection components.

The moment capacity for each base-plate under investigation was also calculated according to Eurocodes. The results of the nominal and design base-plate moment capacities for push and pull directions based on Eurocodes are presented in Table 5.38, Table 5.39, Table 5.40 and Table 5.41. It should be noted that in all cases the governing failure mechanism based on the calculations is due to yield line failure of the base-plate. This is explained by the fact that Eurocode 3 (prEN1993-1-8) greatly underestimates the base-plate yield line capacity.

Table 5.34. Summary of Base-Plate Nominal Moment Capacity from Tests and Based on Calculations for Push Direction According to AISC.

Specimen ID	**Moment Capacity**							**Governing Failure Mechanism based on Experiments**	**Governing Failure Mechanism based on Calculations**
	Experimental	**Anchor Rod Rupture**	**Base Plate Yield Line**	**Column Welds Rupture**	**Column Flange Local Buckling**	**Minimum**	**Difference from Experiment**		
	(kip-ft)	**(kip-ft)**	**(kip-ft)**	**(kip-ft)**	**(kip-ft)**	**(kip-ft)**	**(%)**		
S01	46.9	44.2	70.9	98.1	109.4	44.2	5.8	Anchor Rod Rupture	Anchor Rod Rupture
S02	49.4	55.7	91.2	98.1	109.4	55.7	-12.8	Anchor Rod Rupture	Anchor Rod Rupture
S03	87.4	86.7	90.9	120.9	109.4	86.7	0.8	Combination*	Anchor Rod Rupture
S04	147.9	133.9	117.6	132.9	109.4	109.4	26.0	Flange Local Buckling	Flange Local Buckling
S05	97.4	133.9	42.3	132.9	109.4	42.3	56.6	Yield Line & Weld Rupture	Yield Line
S06	123.8	133.9	117.6	147.3	274.4	117.6	5.0	Yield Line & Weld Rupture	Yield Line
S07	297.0	344.7	354.5	403.1	673.1	344.7	-16.1	Concrete Cracking	Anchor Rod Rupture
S08	407.3	533.0	482.7	403.1	673.1	403.1	1.0	Concrete Cracking	Weld Rupture
S09	384.1	533.0	482.7	403.1	673.1	403.1	-4.9	Concrete Cracking	Weld Rupture
S10	429.1	533.0	407.1	403.1	673.1	403.1	6.1	Concrete Cracking	Weld Rupture
S11	71.5	49.5	51.7	105.9	157.0	49.5	30.8	Anchor Rod Rupture	Anchor Rod Rupture

*Combination of anchor rod yielding, concrete cracking and base-plate yielding.

Table 5.35. Summary of Base-Plate Design Moment Capacity from Tests and Based on Calculations for Push Direction According to AISC.

Specimen ID	**Experimental**	**Anchor Rod Rupture**	**Base Plate Yield Line**	**Column Welds Rupture**	**Column Flange Local Buckling**	**Minimum**	**Difference from Experiment**	**Governing Failure Mechanism based on Experiments**	**Governing Failure Mechanism based on Calculations**
	(kip-ft)	**(kip-ft)**	**(kip-ft)**	**(kip-ft)**	**(kip-ft)**	**(kip-ft)**	**(%)**		
S01	46.9	31.0	63.8	75.4	98.4	31.0	33.9	Anchor Rod Rupture	Anchor Rod Rupture
S02	49.4	39.3	82.0	75.4	98.4	39.3	20.4	Anchor Rod Rupture	Anchor Rod Rupture
S03	87.4	56.0	81.8	90.6	98.4	56.0	35.9	Combination*	Anchor Rod Rupture
S04	147.9	84.8	105.8	96.9	98.4	84.8	42.7	Flange Local Buckling	Anchor Rod Rupture
S05	97.4	84.8	38.1	96.9	98.4	38.1	60.9	Yield Line & Weld Rupture	Yield Line
S06	123.8	84.8	105.8	107.4	246.9	84.8	31.5	Yield Line & Weld Rupture	Yield Line
S07	297.0	227.4	319.1	300.8	605.8	227.4	23.4	Concrete Cracking	Anchor Rod Rupture
S08	407.3	333.4	434.4	300.8	605.8	300.8	26.1	Concrete Cracking	Weld Rupture
S09	384.1	333.4	434.4	300.8	605.8	300.8	21.7	Concrete Cracking	Weld Rupture
S10	429.1	333.4	366.4	300.8	605.8	300.8	29.9	Concrete Cracking	Weld Rupture
S11	71.5	35.0	46.5	81.3	141.3	35.0	51.0	Anchor Rod Rupture	Anchor Rod Rupture

*Combination of anchor rod yielding, concrete cracking and base-plate yielding.

Table 5.36. Summary of Base-Plate Nominal Moment Capacity from Tests and Based on Calculations for Pull Direction According to AISC.

Specimen ID	Moment Capacity							Governing Failure Mechanism based on Experiments	Governing Failure Mechanism based on Calculations
	Experimental	Anchor Rod Rupture	Base Plate Yield Line	Column Welds Rupture	Column Flange Local Buckling	Minimum	Difference from Experiment		
	(kip-ft)	(kip-ft)	(kip-ft)	(kip-ft)	(kip-ft)	(kip-ft)	(%)		
S01	82.1	73.3	97.5	98.1	149.7	73.3	10.7	Anchor Rod Rupture	Anchor Rod Rupture
S02	75.2	62.7	97.5	98.1	149.7	62.7	16.6	Anchor Rod Rupture	Anchor Rod Rupture
S03	121.1	99.9	107.6	120.9	149.7	99.9	17.5	Combination*	Anchor Rod Rupture
S04	132.8	122.1	123.1	132.9	149.7	122.1	8.1	Flange Local Buckling	Anchor Rod Rupture
S05	79.4	122.1	40.7	132.9	149.7	40.7	48.7	Yield Line & Weld Rupture	Yield Line
S06	130.2	122.1	119.1	147.3	274.4	119.1	8.5	Yield Line & Weld Rupture	Yield Line
S07	432.7	538.9	471.9	403.1	811.9	403.1	6.8	Concrete Cracking	Weld Rupture
S08	438.8	538.9	485.7	403.1	811.9	403.1	8.1	Concrete Cracking	Weld Rupture
S09	407.3	538.9	485.7	403.1	811.9	403.1	1.0	Concrete Cracking	Weld Rupture
S10	459.5	538.9	411.3	403.1	811.9	403.1	12.3	Concrete Cracking	Weld Rupture
S11	73.4	52.3	57.2	105.9	157.0	52.3	28.7	Anchor Rod Rupture	Anchor Rod Rupture

*Combination of anchor rod yielding, concrete cracking and base-plate yielding.

Table 5.37. Summary of Base-Plate Design Moment Capacity from Tests and Based on Calculations for Pull Direction According to AISC.

Specimen ID	Moment Capacity							Governing Failure Mechanism based on Experiments	Governing Failure Mechanism based on Calculations
	Experimental	Anchor Rod Rupture	Base Plate Yield Line	Column Welds Rupture	Column Flange Local Buckling	Minimum	Difference from Experiment		
	(kip-ft)	(kip-ft)	(kip-ft)	(kip-ft)	(kip-ft)	(kip-ft)	(%)		
S01	82.1	52.1	87.7	75.4	134.7	52.1	36.5	Anchor Rod Rupture	Anchor Rod Rupture
S02	75.2	44.3	87.7	75.4	134.7	44.3	41.1	Anchor Rod Rupture	Anchor Rod Rupture
S03	121.1	64.5	96.8	90.6	134.7	64.5	46.7	Combination*	Anchor Rod Rupture
S04	132.8	77.5	110.8	96.9	134.7	77.5	41.6	Flange Local Buckling	Anchor Rod Rupture
S05	79.4	77.5	36.7	96.9	134.7	36.7	53.8	Yield Line & Weld Rupture	Yield Line
S06	130.2	77.5	107.2	107.4	246.9	77.5	40.5	Yield Line & Weld Rupture	Yield Line
S07	432.7	337.2	424.7	300.8	730.7	300.8	30.5	Concrete Cracking	Anchor Rod Rupture
S08	438.8	337.2	437.1	300.8	730.7	300.8	31.4	Concrete Cracking	Weld Rupture
S09	407.3	337.2	437.1	300.8	730.7	300.8	26.1	Concrete Cracking	Weld Rupture
S10	459.5	337.2	370.2	300.8	730.7	300.8	34.5	Concrete Cracking	Weld Rupture
S11	73.4	37.0	51.5	81.3	141.3	37.0	49.6	Anchor Rod Rupture	Anchor Rod Rupture

*Combination of anchor rod yielding, concrete cracking and base-plate yielding.

Table 5.38. Summary of Base-Plate Nominal Moment Capacity from Tests and Based on Calculations for Push Direction According to Eurocode3.

Specimen ID	Moment Capacity							Governing Failure Mechanism based on Experiments	Governing Failure Mechanism based on Calculations
	Experimental	Anchor Rod Rupture	Base Plate Yield Line	Column Welds Rupture	Column Flange Local Buckling	Minimum	Difference from Experiment		
	(kip-ft)	(kip-ft)	(kip-ft)	(kip-ft)	(kip-ft)	(kip-ft)	(%)		
S01	46.9	44.0	9.8	98.7	113.0	9.8	79.1	Anchor Rod Rupture	Yield Line
S02	49.4	54.8	11.3	98.7	113.0	11.3	77.2	Anchor Rod Rupture	Yield Line
S03	87.4	92.6	9.8	108.7	113.0	9.8	88.8	Combination*	Yield Line
S04	147.9	148.7	12.6	113.1	113.0	12.6	91.5	Flange Local Buckling	Yield Line
S05	97.4	148.7	4.5	113.1	113.0	4.5	95.3	Yield Line & Weld Rupture	Yield Line
S06	123.8	148.7	12.6	119.4	283.6	12.6	89.8	Yield Line & Weld Rupture	Yield Line
S07	297.0	346.2	17.3	375.8	717.6	17.3	94.2	Concrete Cracking	Yield Line
S08	407.3	474.3	21.3	375.8	717.6	21.3	94.8	Concrete Cracking	Yield Line
S09	384.1	474.3	21.3	375.8	717.6	21.3	94.5	Concrete Cracking	Yield Line
S10	429.1	474.3	30.7	375.8	717.6	30.7	92.9	Concrete Cracking	Yield Line
S11	71.5	56.4	7.8	107.2	167.0	7.8	89.1	Anchor Rod Rupture	Yield Line

*Combination of anchor rod yielding, concrete cracking and base-plate yielding.

Table 5.39. Summary of Base-Plate Design Moment Capacity from Tests and Based on Calculations for Push Direction According to Eurocode3.

Specimen ID	Moment Capacity							Governing Failure Mechanism based on Experiments	Governing Failure Mechanism based on Calculations
	Experimental	Anchor Rod Rupture	Base Plate Yield Line	Column Welds Rupture	Column Flange Local Buckling	Minimum	Difference from Experiment		
	(kip-ft)	(kip-ft)	(kip-ft)	(kip-ft)	(kip-ft)	(kip-ft)	(%)		
S01	46.9	39.3	9.8	81.6	113.0	9.8	79.1	Anchor Rod Rupture	Yield Line
S02	49.4	48.8	11.3	81.6	113.0	11.3	77.2	Anchor Rod Rupture	Yield Line
S03	87.4	79.1	9.8	92.2	113.0	9.8	88.8	Combination*	Yield Line
S04	147.9	124.4	12.6	96.7	113.0	12.6	91.5	Flange Local Buckling	Yield Line
S05	97.4	124.4	4.5	96.7	113.0	4.5	95.3	Yield Line & Weld Rupture	Yield Line
S06	123.8	124.4	12.6	101.7	283.6	12.6	89.8	Yield Line & Weld Rupture	Yield Line
S07	297.0	286.5	17.3	308.2	717.6	17.3	94.2	Concrete Cracking	Yield Line
S08	407.3	389.0	21.3	308.2	717.6	21.3	94.8	Concrete Cracking	Yield Line
S09	384.1	389.0	21.3	308.2	717.6	21.3	94.5	Concrete Cracking	Yield Line
S10	429.1	389.0	30.7	308.2	717.6	30.7	92.9	Concrete Cracking	Yield Line
S11	71.5	49.5	7.8	88.5	167.0	7.8	89.1	Anchor Rod Rupture	Yield Line

*Combination of anchor rod yielding, concrete cracking and base-plate yielding.

Table 5.40. of Base-Plate Nominal Moment Capacity from Tests and Based on Calculations for Pull Direction According to Eurocode3

Specimen ID	Moment Capacity							Governing Failure Mechanism based on Experiments	Governing Failure Mechanism based on Calculations
	Experimental	Anchor Rod Rupture	Base Plate Yield Line	Column Welds Rupture	Column Flange Local Buckling	Minimum	Difference from Experiment		
	(kip-ft)	(kip-ft)	(kip-ft)	(kip-ft)	(kip-ft)	(kip-ft)	(%)		
S01	82.1	81.8	9.9	98.7	135.8	9.9	87.9	Anchor Rod Rupture	Yield Line
S02	75.2	71.1	11.3	98.7	135.8	11.3	85.0	Anchor Rod Rupture	Yield Line
S03	121.1	100.5	9.9	108.7	135.8	9.9	91.9	Combination*	Yield Line
S04	132.8	142.1	12.5	113.1	135.8	12.5	90.6	Flange Local Buckling	Yield Line
S05	79.4	142.1	4.5	113.1	135.8	4.5	94.3	Yield Line & Weld Rupture	Yield Line
S06	130.2	150.9	12.5	119.4	283.6	12.5	90.4	Yield Line & Weld Rupture	Yield Line
S07	432.7	588.6	17.8	375.8	813.0	17.8	95.9	Concrete Cracking	Yield Line
S08	438.8	588.6	21.3	375.8	813.0	21.3	95.1	Concrete Cracking	Yield Line
S09	407.3	588.6	21.3	375.8	813.0	21.3	94.8	Concrete Cracking	Yield Line
S10	459.5	588.6	30.7	375.8	813.0	30.7	93.3	Concrete Cracking	Yield Line
S11	73.4	48.5	8.0	107.2	185.5	8.0	89.0	Anchor Rod Rupture	Yield Line

*Combination of anchor rod yielding, concrete cracking and base-plate yielding.

Table 5.41. Summary of Base-Plate Design Moment Capacity from Tests and Based on Calculations for Pull Direction According to Eurocode3.

Specimen ID	Moment Capacity							Governing Failure Mechanism based on Experiments	Governing Failure Mechanism based on Calculations
	Experimental	Anchor Rod Rupture	Base Plate Yield Line	Column Welds Rupture	Column Flange Local Buckling	Minimum	Difference from Experiment		
	(kip-ft)	(kip-ft)	(kip-ft)	(kip-ft)	(kip-ft)	(kip-ft)	(%)		
S01	82.1	71.8	9.9	81.6	135.8	9.9	87.9	Anchor Rod Rupture	Yield Line
S02	75.2	62.4	11.3	81.6	135.8	11.3	85.0	Anchor Rod Rupture	Yield Line
S03	121.1	85.9	9.9	92.2	135.8	9.9	91.9	Combination*	Yield Line
S04	132.8	118.8	12.5	96.7	135.8	12.5	90.6	Flange Local Buckling	Yield Line
S05	79.4	118.8	4.5	96.7	135.8	4.5	94.3	Yield Line & Weld Rupture	Yield Line
S06	130.2	126.3	12.5	101.7	283.6	12.5	90.4	Yield Line & Weld Rupture	Yield Line
S07	432.7	480.5	17.8	308.2	813.0	17.8	95.9	Concrete Cracking	Yield Line
S08	438.8	480.5	21.3	308.2	813.0	21.3	95.1	Concrete Cracking	Yield Line
S09	407.3	480.5	21.3	308.2	813.0	21.3	94.8	Concrete Cracking	Yield Line
S10	459.5	480.5	30.7	308.2	813.0	30.7	93.3	Concrete Cracking	Yield Line
S11	73.4	43.4	8.0	88.5	185.5	8.0	89.0	Anchor Rod Rupture	Yield Line

*Combination of anchor rod yielding, concrete cracking and base-plate yielding.

5.5. Method for Estimating the Rotational Stiffness of Base-plate Connections

An important aspect of the frame design optimization is to determine the stiffness of the rotational spring that should be used as boundary condition at the column base during the frame analysis. The experimental results indicate that the rotational stiffness of the base-plate is highly dependent on the geometric parameters of the base-plate (e.g., anchor rod diameter, base-plate thickness etc.). As presented in Section 2.3.5, Eurocode 3 (prEN1993-1-8), Section 6.3 provides a methodology to estimate the rotational stiffness of the base-plate connection based on the flexibilities of its main components (e.g., anchor rods, base-plate, and concrete pedestal). This section presents the comparison of rotational stiffness results from the experimental program and the calculations in accordance with Eurocode 3 (prEN1993-1-8).

Table 5.42 summarizes the results of the base-plate rotational stiffness from the experimental study and the calculations as per Eurocode 3 (prEN1993-1-8). For the base-plate connections with two rows of anchor rods (i.e., S01 to S06, and S11), in most cases better results were obtained when both rows of anchor rods are considered in the calculation or rotational stiffness. In general the rotational stiffness of base-plate connections with two rows of anchor rods is overestimated if one anchor rod row is used in the calculation. For example, the estimated rotational stiffness of S04 and S11 in the push direction is overestimated by 174% and 129% respectively when one anchor rod row is used in the calculation. Exception to this rule is S05 where both of the rotational stiffness computed using two and one anchor rod rows are highly underestimating the actual rotational stiffness measured during the test. This may be explained by the fact that the base-plate connection of S05 had a flexurally dominated behavior. Consequently, the base-plate flexural stiffness does not contribute substantially to the connection stiffness. From all the connection components, the anchor rods and the concrete are the components that contributed to the rotational stiffness of the connection. If the contribution of the base-plate flexural stiffness (i.e., equivalent T-stub) had been omitted from the Eurocode 3 (prEN1993-1-8), then the rotational stiffness for push (K_I^+) and pull

(K_1^-) directions would have been computed as 11313 kips-ft/rad and 10528 kips-ft/rad, respectively. These results are 8% and 35% higher than the experimental data of S05 shown in Table 5.42. For specimens with more than two anchor rod rows (i.e., S07 to S10), it is recommended to estimate the rotational stiffness of the base-plate connection utilizing one anchor rod row because the rotational stiffness based on one anchor rod row is close to the experimental results.

Table 5.42. Summary of Base-Plate Rotational Stiffness Results Based on Tests and Eurocode 3

Specimen ID	Experimental		Eurocode 3 (Two Rows of Anchor Rods)		Difference		Eurocode 3 (One Row of Anchor Rods)		Difference	
	K_1^+	K_1^-	K_1^+	K_1^-	K_1^+	K_1^-	K_1^+	K_1^-	K_1^+	K_1^-
	(kips-ft/rad)		(kips-ft/rad)		(%)		(kips-ft/rad)		(%)	
S01	3456	9722	3184	6044	7.9	37.8	5879	11196	-70.1	-15.2
S02	6091	8030	5264	6044	13.6	24.7	9718	11196	-59.5	-39.4
S03	6862	11994	5163	6030	24.8	49.7	9357	10975	-36.4	8.5
S04	4300	7226	6421	5922	-49.3	18.0	11770	10897	-173.7	-50.8
S05	10462	7762	2460	2266	76.5	70.8	4721	4360	54.9	43.8
S06	9882	15312	5773	5964	41.6	61.0	10657	11041	-7.8	27.9
S07	28171	58142	18484	34609	34.4	40.5	34127	64080	-21.1	-10.2
S08	83889	85372	34044	34609	59.4	59.5	62855	64080	25.1	24.9
S09	44942	134574	34044	34609	24.2	74.3	62855	64080	-39.9	52.4
S10	120672	113821	40067	40730	66.8	64.2	73376	74795	39.2	34.3
S11	1896	4027	2294	2669	-21.0	33.7	4348	5072	-129.3	-26.0

6. CONCLUSIONS AND RECOMMENDATIONS FOR FUTURE RESEARCH

6.1. Remarks from the Experimental Program - Phase 1

The first phase of the experimental program included the testing of eight column base-plate connections under combined axial and flexural loading. The experimental data was used to develop a global moment rotation relationship for the column base-plate connections used in frame analysis. The key research findings from the first phase of the experimental program are provided below:

- The rotational stiffness of base-plate connections varied substantially depending on the connection configuration. More than one test variable changed from specimen to specimen; therefore, a direct conclusion on the influence of different connection details (e.g., anchor rod diameter) on the elastic stiffness and moment capacity could not be made.
- It was observed that the rotational stiffness also showed a substantial difference in push and pull directions. The push-to-pull rotational stiffness ratio varied from 0.7 to 2.6.
- The damage to the base-plate connections occurred in the form of anchor rod elongation and rupture, yielding of the flanges and yielding of the base-plate. No yielding of the web or buckling was observed for any of the configurations.
- The specimens were grouped into three distinct categories according to the distribution of the observed damage: (1) energy absorption mainly achieved by yielding of the flanges and the base-plate while little elongation of the anchor rods was observed ($S04_{phase1}$ and $S05_{phase1}$), (2) energy absorption achieved through combined yielding of the flanges, base-plate and the anchor rods ($S01_{phase1}$, $S03_{phase1}$ and $S08_{phase1}$), (3) energy absorption achieved through yielding (and ultimately rupture in some cases) of the

anchor rods while the flanges and base-plate remained mostly elastic ($S02_{phase1}$, $S06_{phase1}$ and $S07_{phase1}$).

- The observed damage according to the above-mentioned categories was influenced by more than one parameter among which the base-plate thickness, the inside and outside flange thicknesses and the diameter and number of anchor rods were identified as the most influential ones.
- Degradation of lateral strength was not observed up to drift levels of 6%, i.e., the bases showed a stable load carrying capacity with increasing drift (or rotation), unless failure occurred due to anchor rod rupture (e.g., $S02_{phase1}$).

6.2. Remarks from the Experimental Program – Phase 2

The results from the second phase of the experimental research indicated that the base-plate connections provide significant stiffness and strength. Additionally, it was observed that various aspects of the connections under investigation (i.e., base-plate dimensions, number and dimension of the anchor rods, and flange thicknesses) affect the overall response. The key findings of the experimental research are summarized below:

- All the aspects of the connections under investigation (i.e., base-plate dimensions, number and dimension of the anchor rods, flange thicknesses, pitch and foundation) affect the overall response.
- An axial compressive load at 50% of the expected service load of the column, increased the average (of push and pull directions) lateral stiffness of the column base-plate connections from 6.0% to 46% in comparison to no axial load case. The 100% axial load compared with the 0% axial loading case increased the average lateral stiffness of the column base-plate connections from 19.8% to 89.5%.

- An axial compressive load at 50% of the expected service load of the column, increased the average rotational stiffness of the column base-plate connections from 10.2% to 80.7% in comparison to no axial load case. The 100% axial load compared with the 0% axial loading case increased the average lateral stiffness of the column base-plate connection from 33.2% to 145.6%.
- The specimens (S04, S06) with the thicker base-plates (5/8 inch) and larger anchor rods (1 1/4 inch diameter) showed the highest lateral strength and moment capacity amongst the 10-12 inch web depth specimens. Among all the 22 inch web depth specimens (S07-S10), the specimen with the thickest base-plate (S10) showed the highest lateral strength and moment capacity.
- The failure modes observed during the tests were yielding of the inside flange, yielding (and in one case buckling) of the outside flange, yielding (and in some cases rupture) of the base-plate, yielding of the web, yielding (and in some cases rupture) of the anchor rods, rupture of the welds connecting the base-plate to the web and the flanges and cracking of the concrete foundation. Accordingly, the specimens were grouped into four distinct categories based on the observed damage. All the parameters investigated here influenced the behavior of the column base-plate connections and resulted in a combination of failure mechanisms explained above.
- The specimens which experienced a failure mode consisting of a combination of yielding of different components of the connections, showed the highest displacement ductility. On the other hand the 22 inch web depth specimens experienced the lowest displacement ductility amongst all the specimens. Their failure was due to the excessive cracking of the concrete foundation; therefore, these specimens experienced a less ductile behavior.

- The specimen with the thinnest base-plate (3/8 inch base-plate thickness) showed the highest rotational ductility amongst all the specimens. On the other hand the specimens which had thicker base-plates (5/8 inch) with larger anchor rods (1 ¼ inch diameter) showed the lowest rotational ductility.
- A combination of thick flanges, thick base-plate, and large anchor rod diameter led to a less ductile behavior of the connections. The ultimate failure occurred in the form of weld rupture connecting the web and flanges with the base-plate.
- The failure of the connections with 3/4 inch diameter anchor rods was mainly due to the excessive anchor rod elongation (and rupture in some cases), accompanied by slight flange yielding and cracking of the concrete around the base-plate area.
- Specimens with larger diameter anchor rods (1.0 inch and 1 ¼ inch) experienced less elongation of the anchor rods accompanied by more extensive flange and base-plate yielding and ultimately by rupture of the welds in certain cases.
- For the 22 inch web-depth specimens, the concrete foundation experienced excessive cracking while the column was slightly damaged.

With regards to the parameters investigated, the following conclusions were reached:

- The specimens tested on concrete foundations in comparison to a rigid steel foundation showed lower elastic lateral and rotational stiffness, and moment capacity. The average elastic lateral and average rotational stiffness were 13.6% and 60.0% less for the specimens tested on concrete foundations. Similarly, the average (push and pull) moment capacity was 88.8% less.
- An increase of the pitch between the anchor rods for the tested base-plate connection configurations increased the average lateral stiffness of the connection by 5.8% and the average rotational stiffness by 6.7% when the specimens were tested under 100% of the service axial load. There was minimal difference in terms of moment capacity

due to changing setback distance with changing pitch as explained in the main body of the thesis.

- An increase of the anchor rod diameter for the tested base-plate connection configurations led to an increase of the average rotational stiffness and average moment capacity by 30.1% and 38.1%, respectively, when the connection was tested under 100% of the service axial load. There was minimal difference in terms of average lateral stiffness due to changing setback distance with changing anchor rod diameter as explained in the main body of the thesis.
- It was found that an increase of the base-plate thickness for the tested base-plate connection configurations could lead to a decrease in the average elastic lateral and average rotational stiffness of the connection by 38.3% and 58.1%, respectively, when the difference in the base-plate thickness is large and the stiffness of the connection is governed by that of the anchor rods. The average moment capacity on the other hand was higher for thicker base-plate configurations by 34.1% to 40.2%.
- An increase of the flange thicknesses for the tested base-plate connection configurations increased the average lateral stiffness of the connection by 32.2% and the average rotational stiffness by 54.3% when the specimens were tested under 100% of the service axial load. The average moment capacity, on the other hand, reduced by 10.5% due to changing failure mode from flange, web and base-plate yielding to weld and base-plate rupture.
- An increase of the number of anchor rods for the tested base-plate configurations increased the average lateral stiffness by 18.2% and the average rotational stiffness by 49.0% when the specimens were tested under 100% of the service axial load. Similarly, the average moment capacity increased for the higher number anchor rod base-plate configuration by 27.1% and 1.4% in push and pull directions, respectively.

- It was observed that the rocking versus bending behavior of the column base-plate connections was mostly influenced by the relative stiffness and strength of the anchor rods in comparison to those of the base-plate. The base-plate stiffness and strength was at the same time influenced by the thickness of the flanges and the web. Further research is needed to develop a parameter (or parameters) that will allow the design community predict the flexurally dominated versus rigid-body type rocking motion. Simplified design equations are also needed to predict the rotational stiffness and moment capacity of these connections.
- In the elastic region, the number and the axial stiffness of the anchor rods dominated the stiffness of the connections particularly for the connections with larger anchor rod diameters (1 ¼ inch).

6.3. Frame Analysis – Phase 1

Frame analyses demonstrated that accounting for this rotational stiffness in the frame design can result in moderate weight savings. In the first phase of the experimental part of this research, eight column base-plate connections were tested under combined axial and flexural loading. The experimental data were used to develop a global moment rotation relationship for the column base-plate connections. From these relationships the rotational stiffness of the column base-plate connections was calculated at the H/60 drift limit (where H is the building height). This rotational stiffness was used for the frame analysis and the response of the frames with and without the rotational stiffness of the column base-plate connections were compared in terms of weight and maximum deflection. The key findings of this research are summarized below.

- A decrease in the total weight (from 0 to 11.4% depending on the governing design limit-state) and the deflections (from 9 to 34%) was observed when the rotational stiffness of the column base-plate connections is considered in design of typical low-rise metal buildings. This is considered a non-negligible improvement by the low-rise metal building industry where cost is a primary consideration.

- An increase as much as 34% in the lateral stiffness and 30% of the strength of the frame models with the semi-rigid base-plate connections was observed compared to pinned connection assumption.
- The lateral stiffness and strength of the optimized semi-rigid frames exceeded those of the initial designs based on a pinned connection assumption by 22% and 15% on average, respectively.

6.4. Parametric Study – Phase 2

Having the developed analytical models as a basis, a parametric study was performed to evaluate the most influential parameters of the column base-plate connections on the rotational stiffness and moment capacity of the connections. Three different web depth connections were modeled in order to create a matrix with eleven parameters under investigation. The main purpose of the parametric analysis was to evaluate the influence of the geometric characteristics of the connections on the overall behavior of the column base-plate connections, as well to provide additional information to develop design guidelines. Moment-rotation behaviors plotted from several models of the three web-depths and a rotation equal to 0.003 radians approximately was considered for the calculation of the rotational stiffness in the elastic area.

- The parameters that less affected the rotational stiffness and moment capacity of the connections were the flange and base-plate width, and the gage distance of the anchor rods. All the other parameters considered in the parametric analysis were highly affected the rotational stiffness and moment capacity of 12 inch, 18 inch and 26 inch web depth connections.
- The increase of the web thickness resulted in the increase of the rotational stiffness and moment capacity of the 12 inch and 18 inch web depth connections. In the case of the

26 inch web depth connections, the elastic rotational stiffness decreased with increasing web thickness by 28%. For thin web thickness (P03-04), a shear deformation of the web occurred which resulted in tension field action. Due to the shear deformation, the base-plate of thinned web connections did not lift significantly compared to the model with thicker web (P03-06), in which shear deformation of the web was not observed. Therefore, the calculated rotational stiffness of the model with thinner web (P03-04) was higher than the one with thicker web

- It was observed that the decrease of the flange thicknesses increased the rotational stiffness of the 12 inch wed depth connections while it decreases the moment capacity of the connections. This can be explained by the fact that the decrease of the flange thicknesses led to the increase of the rotational stiffness due to the fact that the relative rigidity of the base-plate and anchor rod system to flange component was greater for thinner flange thickness. The decrease of the flange thicknesses for the 18 inch web depth connections had almost no effect on the rotational stiffness while it decreases the moment capacity of the connections. The behavior of the base-plates of models was predominantly rigid, and thus decreasing the flange thickness had no effect on the rotational stiffness. In the case of the 26 inch web depth connections the decrease of the flange thickness resulted in a decrease of the rotational stiffness and moment capacity of the connections
- An increase of the number of the anchor rods by 2 resulted in an increase of the rotational stiffness in the push loading direction of the 12 inch, 18 inch and 26 inch web depth connections by 120%, 82% and 42% respectively. In addition the increase of the anchor rods to the increased moment capacity of the 12 inch, 18 inch and 26 inch web depth connections by 75%, 35% and 16% respectively. So, it was observed that

the 26 inch web depth connections were less affected by the increase of the anchor rods in comparison with the 12 inch and 18 inch web depth connections.

- An increase of the pitch resulted in an increase of the elastic rotational stiffness and moment capacity of the 12 inch and 18 inch web depth connections in a range from 28% to 60% in the push direction. This happened because by increasing the pitch, the anchor rod in tension moved farther away from the concrete bearing area, and thus the moment arm between the resultant of concrete bearing force and the outer anchor rod in tension increased. For the same reason, in the pull direction the inner anchor (i.e., outer anchor rod in push direction) had moved closer to the concrete bearing area and thus the contribution of this anchor rod row to the rotational stiffness has decreased. As a result, the rotational stiffness in the pull direction decreased by 30. For the 26 inch web depth connections, an increase of the rotational stiffness and moment capacity was observed in the pull direction.
- In a similar manner as the pitch, the increase of the setback resulted in the increase of the rotational stiffness and moment capacity of the 12 inch and 18 inch web depth connections. However, in the pull direction the effect of the inner rod (the outer anchor rod in push direction, is the inner rod in pull direction) decreased because the inner rod was closer in the concrete bearing area. In the case of the 26 inch web depth connection, the rotational stiffness and moment capacity of the connections increased when the setback was increased by 3 inch.
- Despite the general trend for the 12, 18 and 26 inch web depths connections was that the rotational stiffness was reduced with reducing axial compressive load for the different anchor rod diameter connections. This was due to the fact that the less axial load applied to the column the easier it was to overturn the column. Therefore, for the

same moment but for less axial load, the base-plate uplift was greater than the base-plate uplift for more axial load, leading to a decreased rotational stiffness.

- In the case of the 12 inch web depth connections it was seen that the rotational stiffness of the connections consisting from 3/4 inch base-plate thickness combined with 1 inch and 1 1/4 inch anchor rod diameter decreased by 30% for no axial load. It was observed that the rotational stiffness of the connections with 5/8 inch base-plate thickness and 3/4 inch anchor rod diameter decreased by 38% for the 50% service axial load and no axial load case. In addition, in the case of the 18 inch web depth connections the decrease of the rotational stiffness ranged from 25 % for the connections consisting of a 3/8 inch thick base-plate and 3/4 inch anchor rod diameter to 55 % or the connections consisting of a 5/8 inch thick base-plate and 1 1/4 inch anchor rod diameter. Last, in the case of the 26 inch web depth connections the reduction of the rotational stiffness of the connections ranges from 0 to 35% depending on the base-plate thickness and anchor rod combination case

6.5. Provisions for the Design of the "Pinned" Column Base-Plate Connections

In order to calculate the moment capacity of the connections an extensive review of the available design guides was performed. Since there are no design provisions for the base-plate connections considered in his research, several assumptions had to be made in order to determine the connection capacities. Following the procedures of the design guides, simple methods to estimate the base-plate moment capacity were described and their validation and comparison with the findings from the experimental study were presented.

- A step by step procedure was presented for finding the nominal and design capacities of the "pinned" base-plate connection. The minimum moment capacity due to the failure of one components of the base-plate connection (i.e., anchor rods, base-plate, column flanges, etc.) was calculated. The findings from the design guides were consistent with most of the experimental results.

- The moment capacity calculated based on Eurocodes was smaller compared to the experimental results and the calculated moment capacity as per AISC Steel Construction Manual, 2011. This was due to the fact that in all cases the moment capacity calculated based on Eurocodes was dominated by yield line failure and Eurocodes greatly underestimates the base-plate moment capacity due to yield line.
- The base-plate behavior was classified as rigid, balanced or flexural by comparing the required fixed end moment per unit width of the base-plate propped cantilever and the base-plate bending resistance per unit width. In the case that the ratio is less than 20%, the base-plate behavior can be considered as rigid. In the case that the ratio is more than 20% but less than 80% then the base-plate is classified as balanced. Lastly, when the ratio is greater than 80% the connection is categorized as flexural.
- The experimental results indicated that the rotational stiffness of the base-plate is highly dependent on the geometric parameters of the base-plate (e.g., anchor rod diameter, base-plate thickness etc.). The rotational stiffness of the connections was calculated according to Eurocode 3 (prEN1993-1-8). For the base-plate connections with two rows of anchor rods (i.e., S01 to S06, and S11), better results were obtained when two anchor rod rows in tension configuration was used in the calculation of rotational stiffness based on Eurocode 3 (prEN1993-1-8). However the results had a discrepancy in the case of connections with flexural dominated behavior. Considering one anchor rod row provided a better estimate than considering two rows of anchor rods but still the rotational stiffness was greatly underestimated. It was found that omitting the stiffness of the base-plate component resulted in reasonable estimation of

the rotational stiffness. Therefore, it is recommended to develop models to better predict the base-plate flexural dominated behavior.

- For base-plates with more than two anchor rod rows (i.e., S07 to S10), it was recommended to estimate the rotational stiffness of the base-plate connection utilizing one row of anchor rods in tension. This recommendation is in a good agreement with the findings from the experimental and analytical studies.

6.6. Recommendations for Future Research

The following recommendations are made for future research.

- One key parameter that is anticipated to influence the connection behavior is the net tensile load. Additional tests should be performed to validate the numerical models under net tensile loading.
- It was observed that the different web depth connections considered in the parametric analysis showed a different overall behavior. Further parametric analysis and testing on other web depth connections is suggested, particularly those deeper than 26 inches.
- There is a lack of design guidelines and simplified predictive models to determine the rotational stiffness and moment capacity of these pinned base-plate connections. It is recommended that through more parametric studies of numerical models combined with analysis of the mechanics of the problem, simplified relationships are developed to predict the rotational stiffness and moment capacity.

REFERENCES

ACI Committee 318 (2014). "Building Code Requirements for Structural Concrete (ACI 318-14) and Commentary," *American Concrete Institute,* Farmington Hills, Michigan, USA.

Adany, S., Calado, L., and Dunai, L. (2000). "Experimental Studies on Cyclic Behavior Modes of Base-Plate Connections," *Proceedings of the Third International Conference on the Behavior of Steel Structures in Seismic Areas* (STESSA 2000), Montreal, Canada, 97-104.

American Institute of Steel Construction (AISC) (2011). "Steel Construction Manual," 14th Edition, *AISC*, Chicago, Illinois.

American Institute of Steel Construction (AISC) (2010). "Seismic Design Manual," 2nd Edition, *AISC*, Chicago, Illinois.

Architectural Institute of Japan (AIJ) (2001). "Recommendations for Design of Connections in Steel Structures", Tokyo (in Japanese).

ASCE. 2010. Minimum Design Loads for Buildings and Other Structures. ASCE/SEI Standard 7-10.

ASTM Standard C31/C31M-15a (2015). "Standard Practice for Making and Curing Concrete Test Specimens in the Field," *ASTM International*, West Conshohocken, PA, DOI: 10.1520/C0031_C0031M-15a.

ASTM Standard C39/C39M -16 (2016). "Standard Test Method for Compressive Strength of Cylindrical Concrete Specimens," *ASTM International,* West Conshohocken, PA, DOI: 10.1520/C0039_C0039M-16.

ASTM Standard C496/C496M-11 (2011). "Standard Test Method for Splitting Tensile Strength of Cylindrical Concrete Specimens," *ASTM International,* West Conshohocken, PA, DOI: 10.1520/C0496_C0496M-11.

ASTM Standard C78/C78M-15b (2015). "Standard Test Method for Flexural Strength of Concrete (Using Simple Beam with Third-Point Loading)," *ASTM International*, West Conshohocken, PA, DOI: 10.1520/C0078_C0078M-15b.

ASTM Standard C469/C469M-14 (2014). "Standard Test Method for Static Modulus of Elasticity and Poisson's ratio of Concrete in Compression," *ASTM International*, West Conshohocken, PA, DOI: 10.1520/C0469_C0469M-14.

ASTM Standard A370 -15 (2015). "Standard Test Methods and Definitions for Mechanical Testing of Steel Products," *ASTM International*, West Conshohocken, PA, DOI: 10.1520/A0370-15.

Astaneh, A., Bergsma, G., and Shen J. H. (1992). "Behavior and Design of Base-plates for Gravity, Wind and Seismic Loads," *Proceedings of the National Steel Construction Conference*, Las Vegas, Nevada, AISC, Chicago, Illinois.

ATENA 3D (2016). Program Documentation, ATENA 3D User's Manual, CERVENKA CONSULTING.

Bajwa, M. S., Charney, F. and Moen, C. (2010). "Assesement of Analytical Procedures for Designing Metal Buidlings for Wind Drift Serviceability," CE/VPI-ST 10/05, Virginia Polytechnic Institute and State University, Blacksburg, VA.

BEI Sensors: http://ecatalog.beisensors.com/viewitems/linear-position-sensors/linear-position-sensor-9600-series-compact-spri (Accessed on April 21, 2016)

Camacho J (2007). "Seismic Performance of Exposed Column Base-plates (Phase I)," Proceedings, Earthquake Engineering Symposium for Young Researchers, Seattle, Washington.

Celesco Measurement Specialties: http://www.celesco.com/_datasheets/sm1.pdf (Accessed on April 21, 2016)

Comité Européen de Normalisation (CEN) (1992). "EN1992 Eurocode 2; Design of Concrete Structures," Brussels, Belgium.

Comité Européen de Normalisation (CEN) (2003). "EN1993 Eurocode 3; Design of Steel Structures," Brussels, Belgium.

DeWolf, J. T. (1978). "Axially Loaded Column Base-plates," *Journal of the Structural Division*, ASCE, 104(ST5), 781-794.

DeWolf, J. T. (1978). "Axially Loaded Column Base-plates," *Journal of the Structural Division*, ASCE, Vol. 104, No. ST5, May, pp. 781-794.

DeWolf, J.T. and Sarisley, E. F. (1980). "Column Base-plates with Axial Loads and Moments," *Journal of the Structural Division*, ASCE, Vol. 106, No. ST11, November, pp. 2167-2184.

DeWolf, J. T. (1982). "Column Base-plates," *Structural Engineering Practice*, Vol. 1, No. 1, pp. 39-51.

Drake, R.M. and Elkin, S.J. (1999), "Beam-Column Base-plate Design—LRFD Method," *Engineering Journal,* Vol. 36, No. 1, First Quarter, AISC, Chicago, IL.

El-Khoraibie H. (1978). "Behavior of Simple Column Base Connections," *PhD Thesis,* Department of Civil Engineering and Applied Mechanics, McGill University, Montreal, Quebec, Canada.

Elnashai, A. S., Papanikolaou, V. K. and Lee, D. (2010).ZEUS NL - A System for Inelastic Analysis of Structures, User's Manual, Mid-America Earthquake (MAE) Center, Department of Civil and Environmental Engineering, University of Illinois at Urbana Champaign, Urbana, Illinois, USA.

Ermopoulos, J. and Stamatopoulos, G. (1996a). "Mathematical Modeling of Column Base-plate Connections," *Journal of Constructional Steel Research,* Vol. 36, No. 2, pp. 79-100.

Ermopoulos, J. and Stamatopoulos, G. (1996b). "Analytical Modeling of Column Base-plates under Cyclic Loading," *Journal of Constructional Steel Research*, Vol. 40, No. 3, pp. 225-238.

Eroz, M., White, D. and DesRoches, R. (2009). "Direct Analysis and Design of Steel Frames Accounting for Partially Restrained Column Base Conditions," *Journal of Structural Engineering,* Vol. 134, pp. 1508-1517.

Fahmy, M., Stojadinovic, B., and Goel, S. C. (1999), “Analytical and Experimental Studies on the Seismic Response of Steel Column Bases,” *Proceedings of the 8th Canadian Conference on Earthquake Engineering,* Vancouver, Canada.

Fisher, J. and West, M. A. (2004). “Serviceability Design Considerations for Steel Buildings, Steel Design Guide 3,” *American Institute of Steel Construction (AISC),* Chicago, IL.

Fisher, J.M. and Doyle, J.M. (2005). “Discussion: BeamColumn Base-plate Design—LRFD Method,” Engineering Journal, Vol. 36, No. 1, Fourth Quarter, AISC, Chicago, IL.

Fisher, J. and Kloiber, L. (2006). “Base-plate and Anchor Rod Design, Steel Design Guide 1,” *American Institute of Steel Construction (AISC)*, Chicago, IL.

Galambos, T. V. (1960). "Influence of partial base fixity on frame stability," Journal of the Structural Division, Vol. 86, No. 5, pp. 85-117.

Gomez, I.R., Kanvinde A.M., and Deierlein G.G. (2010). “Exposed Column Base Connections Subjected to Axial Compression and Flexure,” *American Institute of Steel Construction (AISC)*, Chicago, IL.

Hitaka, T., Suitaa K., and Kato M. (2003). “CFT Column Base Design and Practice in Japan,” *Proceedings of the International Workshop on Steel and Concrete Composite Construction* (IWSCCC-2003), Report No. NCREE-03-026, National Center for Research in Earthquake Engineering, Taipei, Taiwan, October 8-9, 2003, National Center for Research in Earthquake Engineering, Taipei, Taiwan, pp. 35-45.

Hon, K.K. and Melchers, R.E. (1988). “Experimental Behavior of Steel Column Bases,” *Journal of Constructional Steel Research*, Vol. 9, No. 143, pp. 35-50.

Hong, J. K. (2007). "Development of a Seismic Design Procedure for Metal Building Systems," *Ph.D. Thesis*, Department of Civil and Environmental Engineering, University of California, San Diego.

Jaspart, J. P. and Vandegans, D. (1998). "Application of Component Method to Column Bases," *Journal of Constructional Steel Research*, Vol. 48, pp. 89-106.

Kaehler, R., White, D. and Kim, Y. D. (2011). "Frame Design Using Web-Tapered Members, Steel Design Guide 25", *American Institute of Steel Construction (AISC)*, Chicago, IL.

Kanvinde, A. M., Grilli, D. A., and Zareian, F. (2012). "Rotational Stiffness of Exposed Column Base Connections – Experiments and Analytical Models", *ASCE Journal of Structural Engineering*, Vol. 138, pp. 549–560.

Kawano, A. and Matsui, C. (1998). "On the Effect of Restoring Force Characteristics of Column Base on Inelastic Response Behavior of Weak-Beam Steel Frame under Earthquake Ground Motion," *Journal of Structural and Construction Engineering*, No. 507, pp. 139-146.

Melchers, R. E. (1992). "Column-Base Response under Applied Moment," *Journal of Constructional Steel Research*, Vol. 23, pp. 127-143.

Metal Building Manufacturers Association. (2015). *MBMA 2015 Annual Report.* Retrieved from http:// http://www.mbma.com/Annual_Reports.asp, Accessed on 7/1/2016.

Melenciuc S. C., Budescu M., Munteanu V., Rosca V. E. (2015). "Behavior of Steel Column Base Connections under Cycling Loading Conditions", Buletinul Institutului Politehnic Din Iasi, LXI (LXV), 2, Constr. Arhit.

Murray, T. M. (1983). "Design of Lightly Loaded Steel Column Base-plates," *Engineering Journal*, AISC, Vol. 20, No. 4, Fourth Quarter, pp. 143-152.

Murray T., Shoemaker W.L. (2002) "Moment End-Plate Connections-Flush and Extended Multiple-Row-AISC Steel Design Guide 16," *American Institute of Steel Construction (AISC)*, Chicago, IL.

Murray T., Sumner E.A. (2003) "Extended End-Plate Moment Connections-Seismic and Wind Applications-AISC Steel Design Guide 4," *American Institute of Steel Construction (AISC)*, Chicago, IL.

Nakashima, S. (1992). "Mechanical Characteristics of Steel Column-Base Connections Repaired by Concrete Encasement," *Proceedings of the Tenth World Conference on Earthquake Engineering*, Madrid, Spain.

Occupational Safety and Health Administration (OSHA) (2001). "Safety Standards for Steel Erection," *29 CFR Part 1926 and Subpart R of 29 CFR Part 1926, RIN No. 1218-AA65*, OSHA, U.S. Department of Labor.

Penserini, P. and Colson, A. (1989). "Ultimate Limit Strength of Column-Base Connections," *Journal of Constructional Steel Research*, Vol. 14, pp. 301-320.

Picard, A. and Beaulieu, D. (1985). "Behavior of a Simple Column Base Connection," *Canadian Journal of Civil Engineering*, Vol. 12, pp. 126-136.

Picard, A., Beaulieu, D., and Perusse, B. (1987). "Rotational Restraint of a Simple Column Base Connection," *Canadian Journal of Civil Engineering*, Vol. 14, pp. 49-57.

Robertson, A. P. (1991). "A Study of Base Fixity Effects on Portal Frame Behavior," *The Structural Engineer,* Vol. 69, No. 2/22, pp. 17-24.

Sato, K. (1987). "A Research on the Aseismic Behavior of Steel Column Base for Evaluating Its Strength Capacity and Fixity," *Report No. 69*, Kajima Institute of Construction Technology, Tokyo, Japan.

Smith, M. D. (2013). "Seismic Testing and Analytical Studies for the Development of New Seismic Force Resisting Systems for Metal Buildings," *PhD Thesis*, Department of Structural Engineering University of California, San Diego, La Jolla, CA.

Stamatopoulos, G. and Ermopoulos, J. (2011). "Experimental and Analytical Investigation of Steel Column Bases," *Journal of Constructional Steel Research*, Vol. 67, pp. 1341-1357.

Targowski, R., Lamblin, D., and Guerlement, G. (1993). "Base-plate Column Connection under Bending: Experimental and Numerical Study," *Journal of Constructional Steel Research*, Vol. 27, pp. 37-54.

Thambiratnam, D. P. and Paramasivam, P. (1986). "Base-plates under Axial Loads and Moments," *Journal of Structural Engineering*, ASCE, Vol. 112, No. 5, pp. 1166-1181.

Thambiratnam, D. P. and Krishnamurthy N. (1989). "Computer Analysis of Column Base-plates," *Computers and Structures,* Vol. 33, No. 3, pp. 839-850.

Verma, A. (2012). "Influence of Column Base Fixity on Lateral Drift of Gable Frames," *MS Thesis*, Department of Civil and Environmental Engineering, Virginia Tech, Blacksburg, VA.

Vernon, B. and Watwood, M. (1985). "Gable Frame Design Considerations," *Journal of Structural Engineering*, Vol. 111, No. 7,pp. 1543-1558.

Wald F. (1995). "Column-Bases, 1st edition," EVUT, Praha, pp. 137, ISBN 80-01-01337-5.

Wong, M.F. and Chung, K.F. (2002). "Structural behavior of bolted moment connections in cold-formed steel beam-column sub-frames," *Journal of Constructional Steel Research.*, Vol. 58, No. 2, pp. 253-274.

Yamada, S. and Akiyama, H. (1997). "Influence of the Rigidity of Column Bases on the Ultimate Earthquake Resistance of Multi-Story Steel Moment Frames," *Journal of Structural and Construction Engineering*, No. 496, pp. 113.

APPENDIX A: EXPERIMENTAL DATA

Table A. 1 Explanatory table - Phase 1.

SPECIMEN AND TEST INFORMATION	
This figure shows the drift levels that the specimen was subjected to in the push and pull directions.	This figure shows the Force versus time response of the specimen.
This figure shows the rotations obtained from the linear potentiometers and string (rotary) potentiometer as explained in section 3.6.1 and explained graphically in Figure 3.9.	This figure shows the rotations obtained from the string (rotary) potentiometers placed along the height of the specimen as explained in section 3.6.1 and explained graphically in Figure 3.9 (a).
This figure shows the inelastic tests Force (kips) – Drift (%) graphs obtained from the experiments. The force and drift values were derived from the actuator load cell and actuator LVDT. The envelopes are plotted in red.	This figure shows the Moment (kips-ft) – Rotation (rad) graphs obtained from the inelastic experiments. The moment was calculated as explained in Section 3.6.24.6.2 and the rotation was derived from the instruments as explained in Section 3.6.1. The envelopes are plotted in red.

Specimen No.	Test	Type of Test	Axial Load (kips)	Base-Plate Thickness (in)	Anchor Rod Diameter (in)	Base-Plate Dimensions (in)	Flange Thickness (in) Out-In
$S01_{phase1}$	10% drift	Cyclic	20.9	0.5	0.75	10.7 x 6	0.3125-0.375

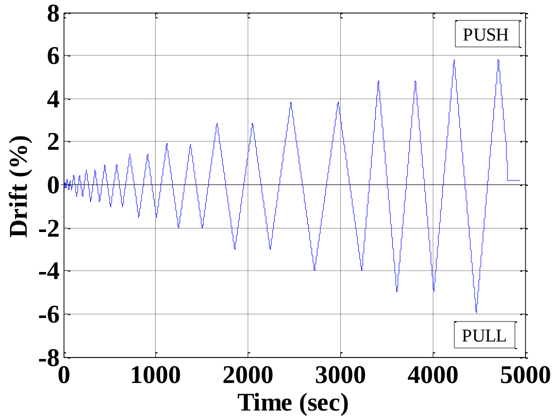

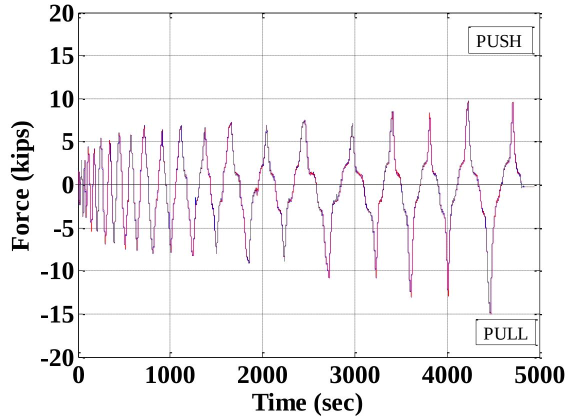

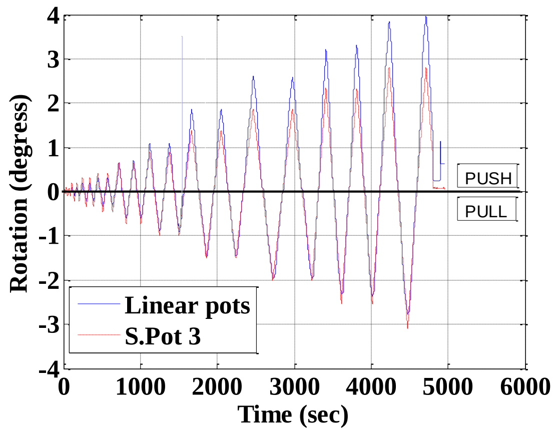

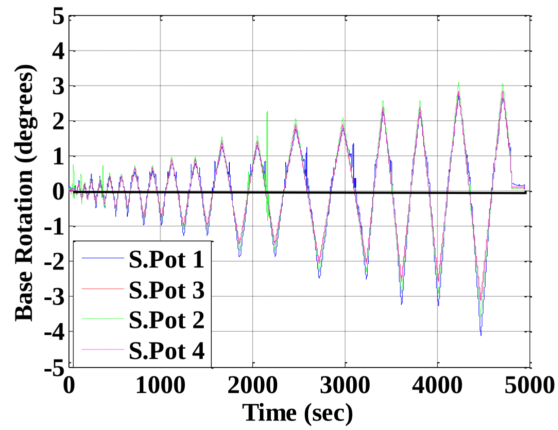

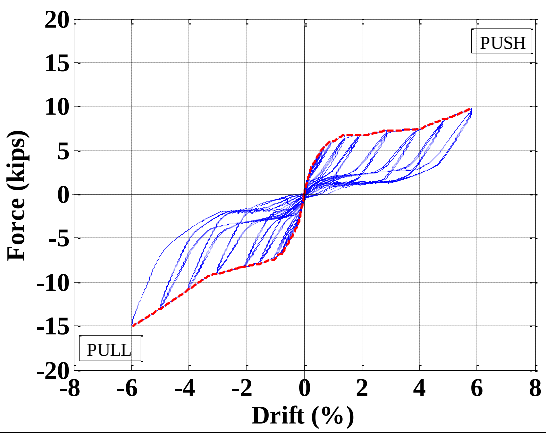

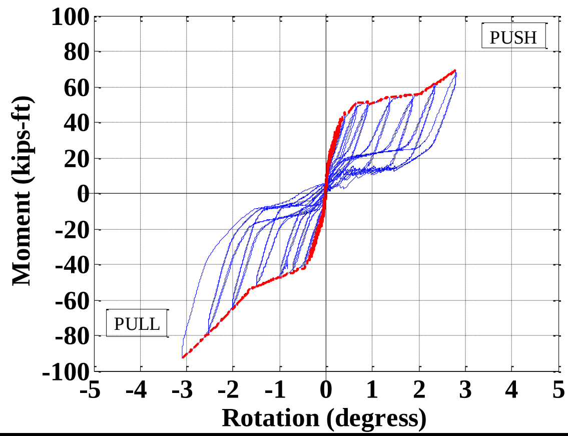

Specimen No.	Test	Type of Test	Axial Load (kips)	Base-Plate Thickness (in)	Anchor Rod Diameter (in)	Base-Plate Dimensions (in)	Flange Thickness (in) Out-In
$S02_{phase1}$	10% drift	Cyclic	26	0.625	0.75	12.7 x 8	0.375-0.3125

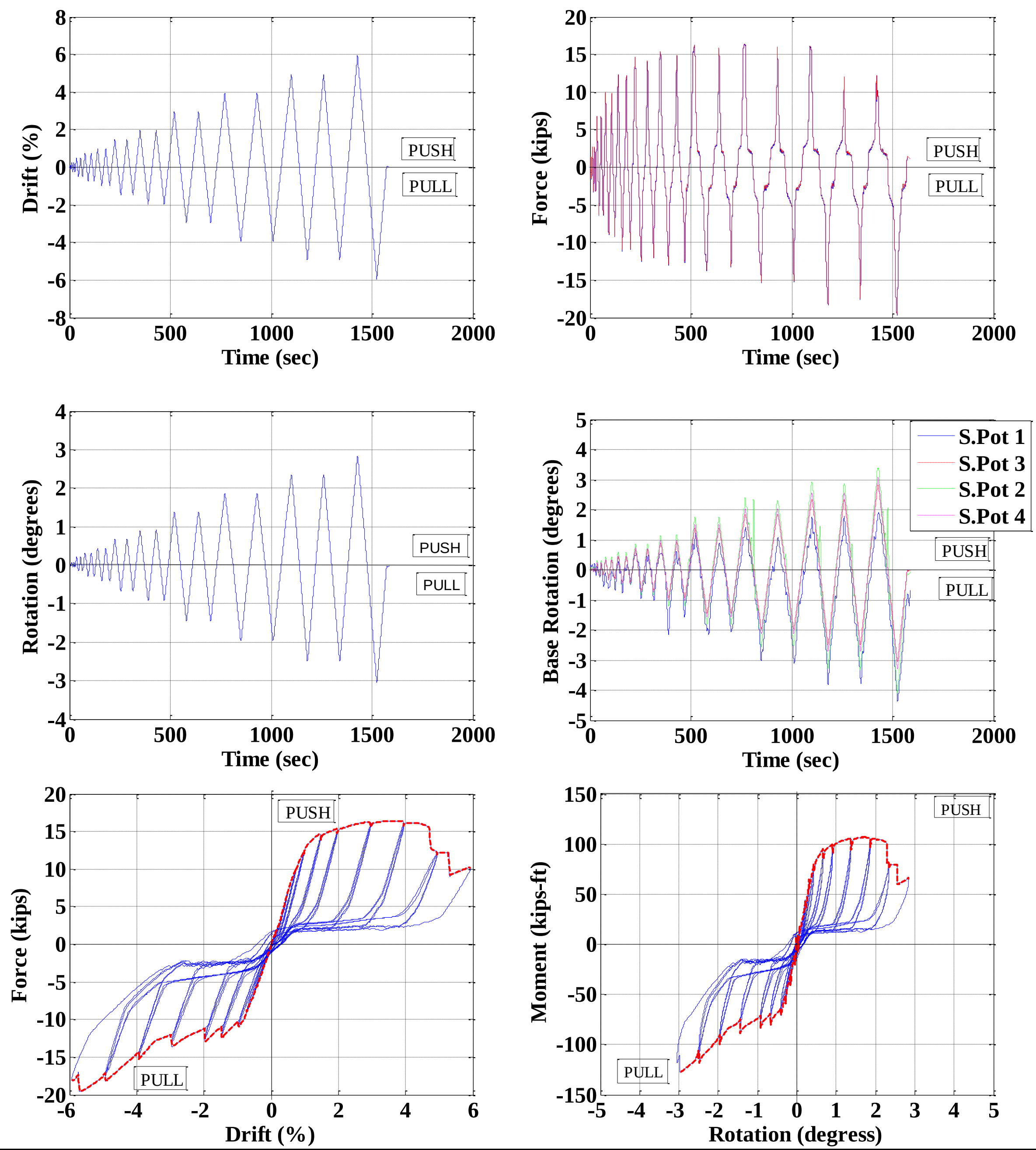

Specimen No.	Test	Type of Test	Axial Load (kips)	Base-Plate Thickness (in)	Anchor Rod Diameter (in)	Base-Plate Dimensions (in)	Flange Thickness (in) Out-In
$S03_{phase1}$	10% drift	Cyclic	51.4	0.625	0.75	12.7 x 8	0.25-0.375

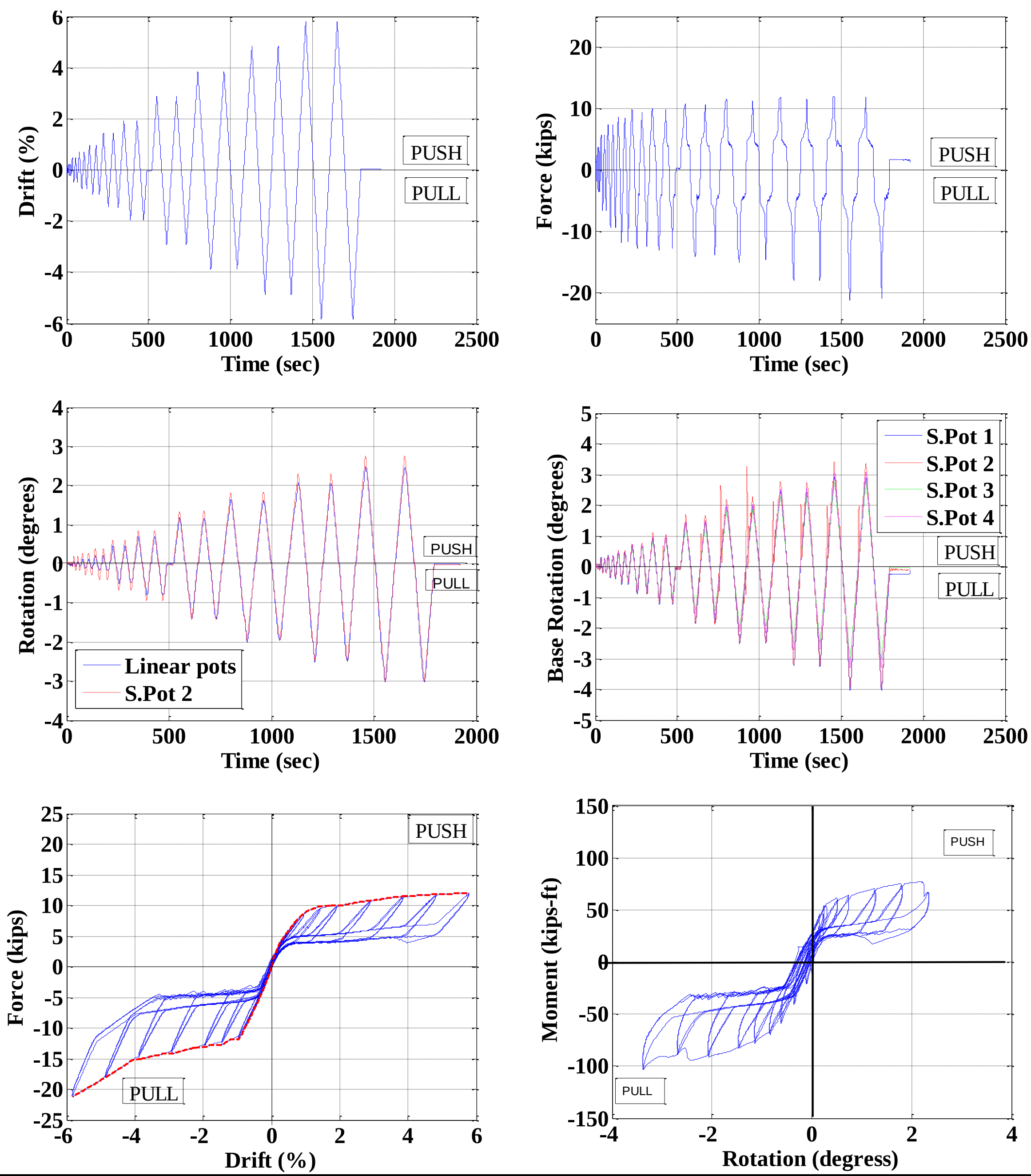

Specimen No.	Test	Type of Test	Axial Load (kips)	Base-Plate Thickness (in)	Anchor Rod Diameter (in)	Base-Plate Dimensions (in)	Flange Thickness (in) Out-In
S03phase1	Repeated	Cyclic	51.4	0.625	0.75	12.7 x 8	0.25-0.375

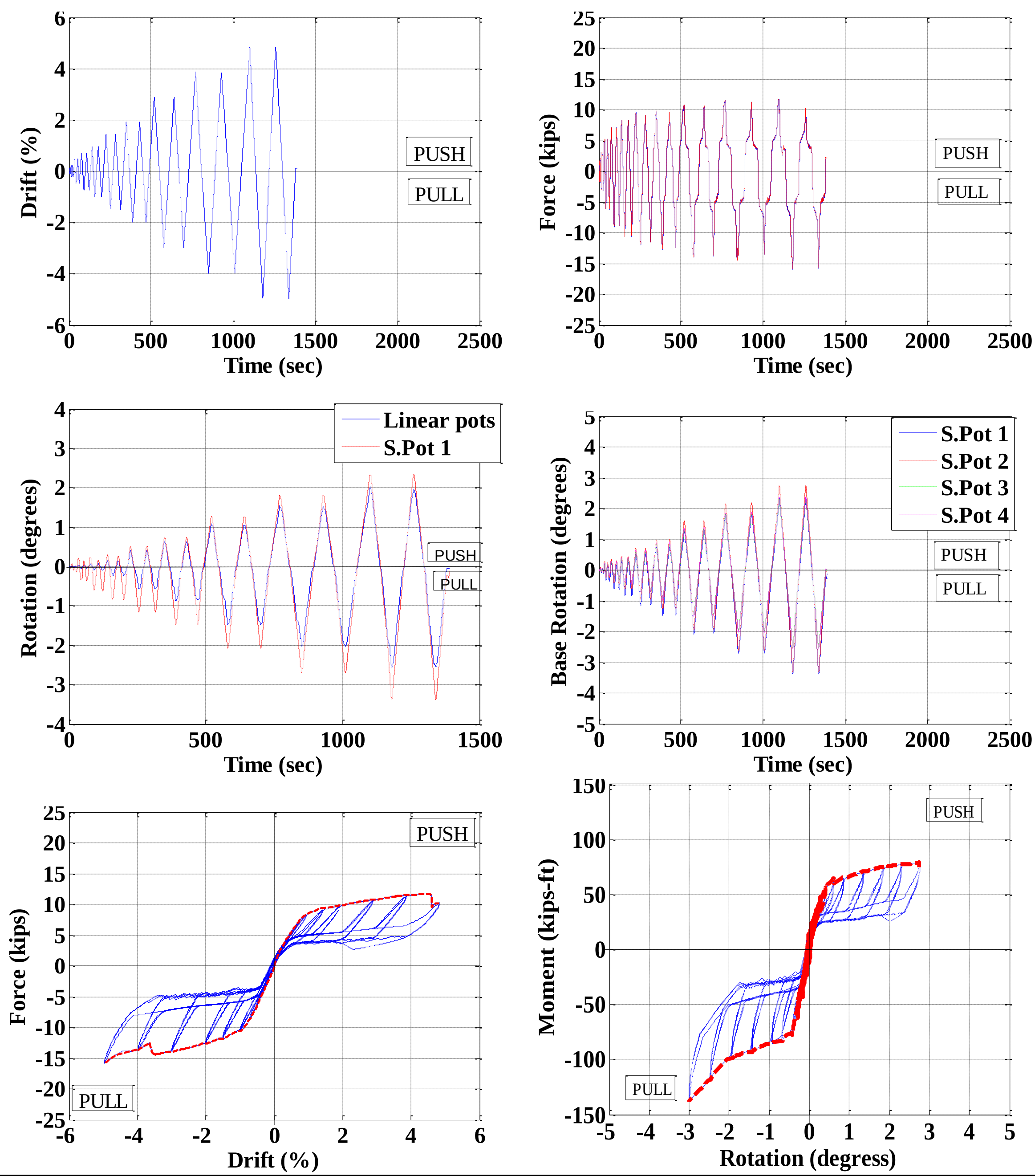

Specimen No.	Test	Type of Test	Axial Load (kips)	Base-Plate Thickness (in)	Anchor Rod Diameter (in)	Base-Plate Dimensions (in)	Flange Thickness (in) Out-In
$S04_{phase1}$	10% drift	Cyclic	64	0.625	1	11.1x 8	0.5-0.625

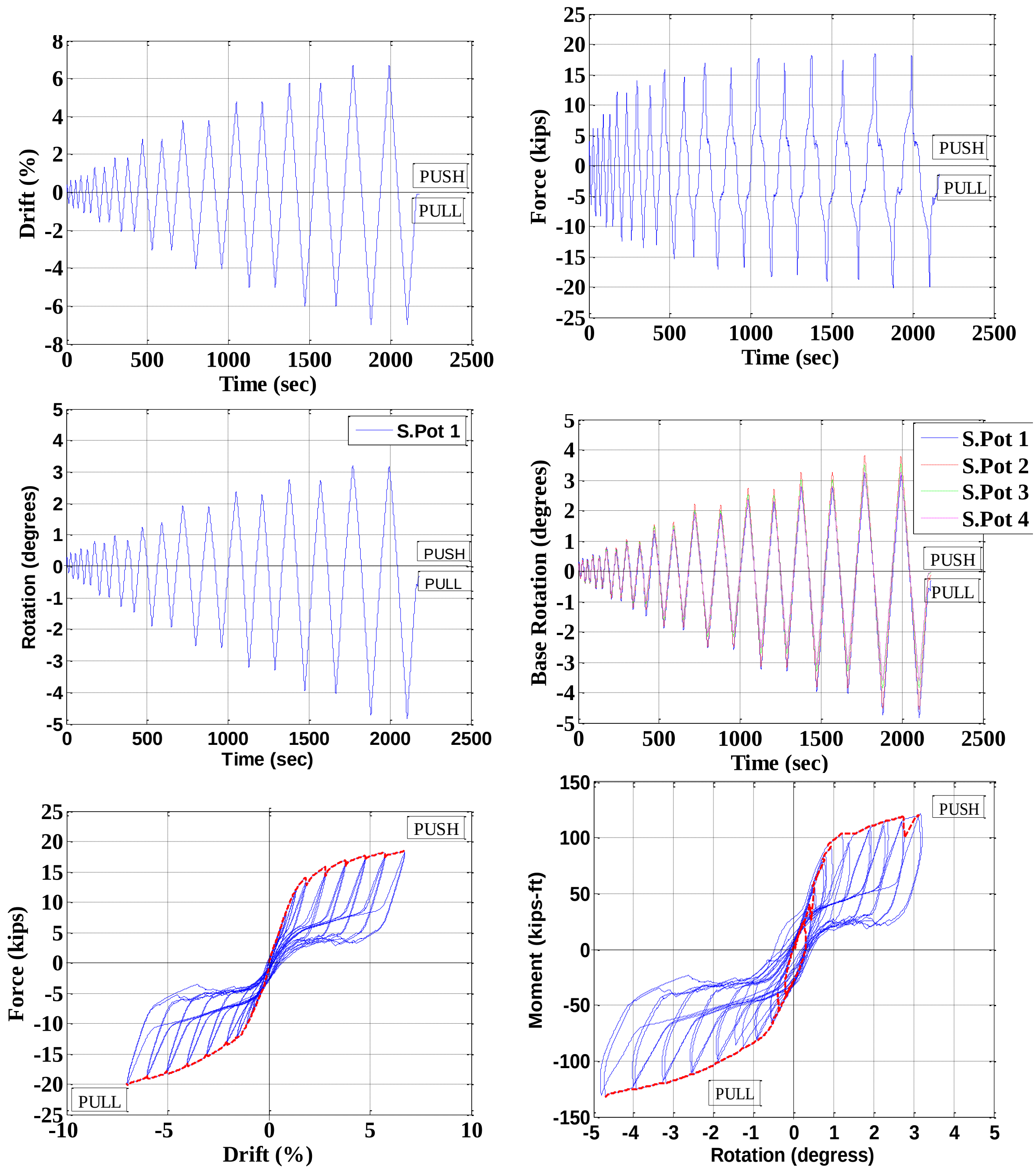

Specimen No.	Test	Type of Test	Axial Load (kips)	Base-Plate Thickness (in)	Anchor Rod Diameter (in)	Base-Plate Dimensions (in)	Flange Thickness (in) Out-In
$S05_{phase1}$	10% drift	Cyclic	10.8	0.375	0.75	12x6	0.25-0.25

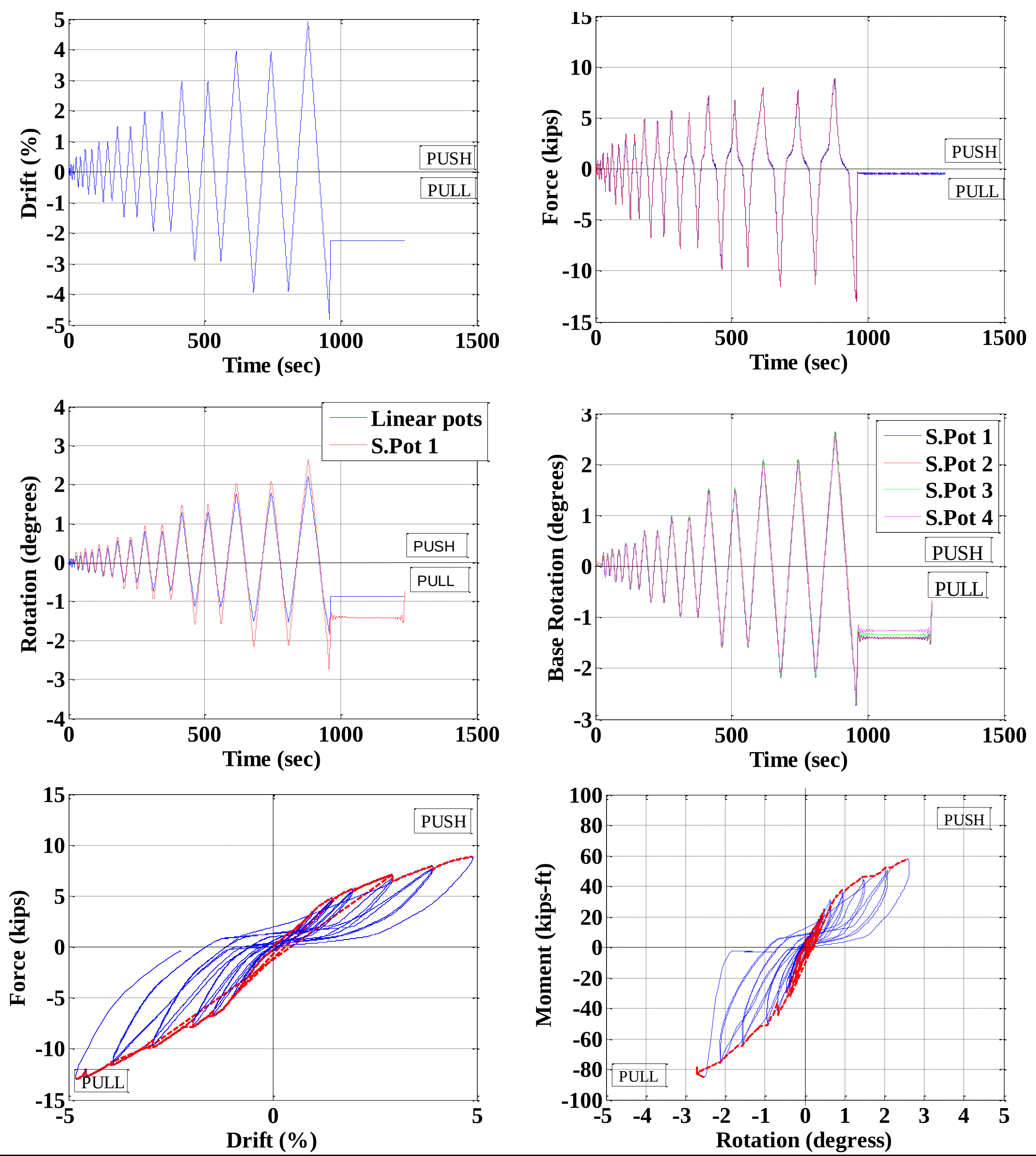

Specimen No.	Test	Type of Test	Axial Load (kips)	Base-Plate Thickness (in)	Anchor Rod Diameter (in)	Base-Plate Dimensions (in)	Flange Thickness (in) Out-In
$S06_{phase1}$	10% drift	Cyclic	67.4	0.625	0.75	12.6x8	0.25-0.375

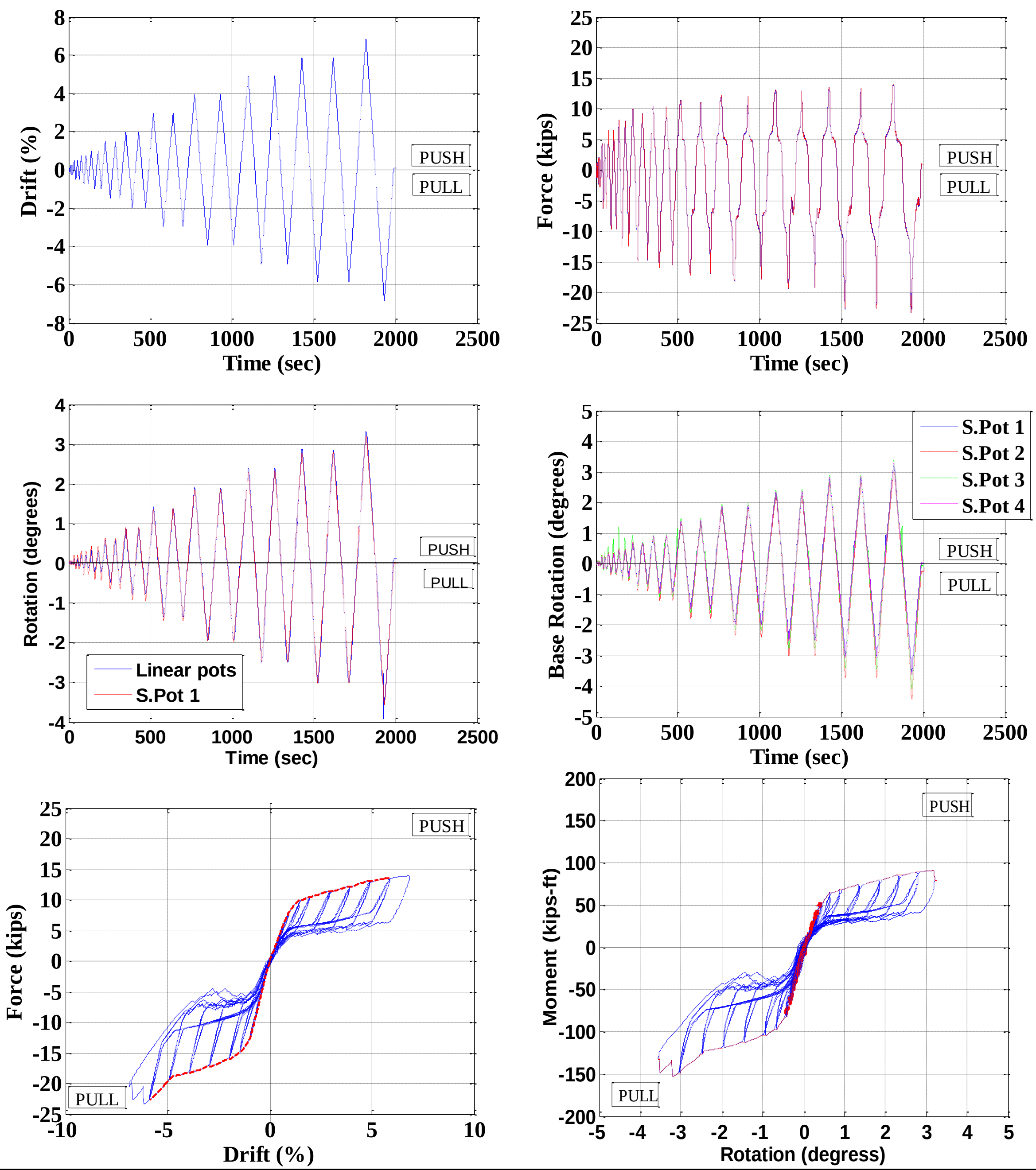

Specimen No.	Test	Type of Test	Axial Load (kips)	Base-Plate Thickness (in)	Anchor Rod Diameter (in)	Base-Plate Dimensions (in)	Flange Thickness (in) Out-In
$S07_{phase1}$	10% drift	Cyclic	39.2	0.5	0.75	10.75x10	0.375-0.375

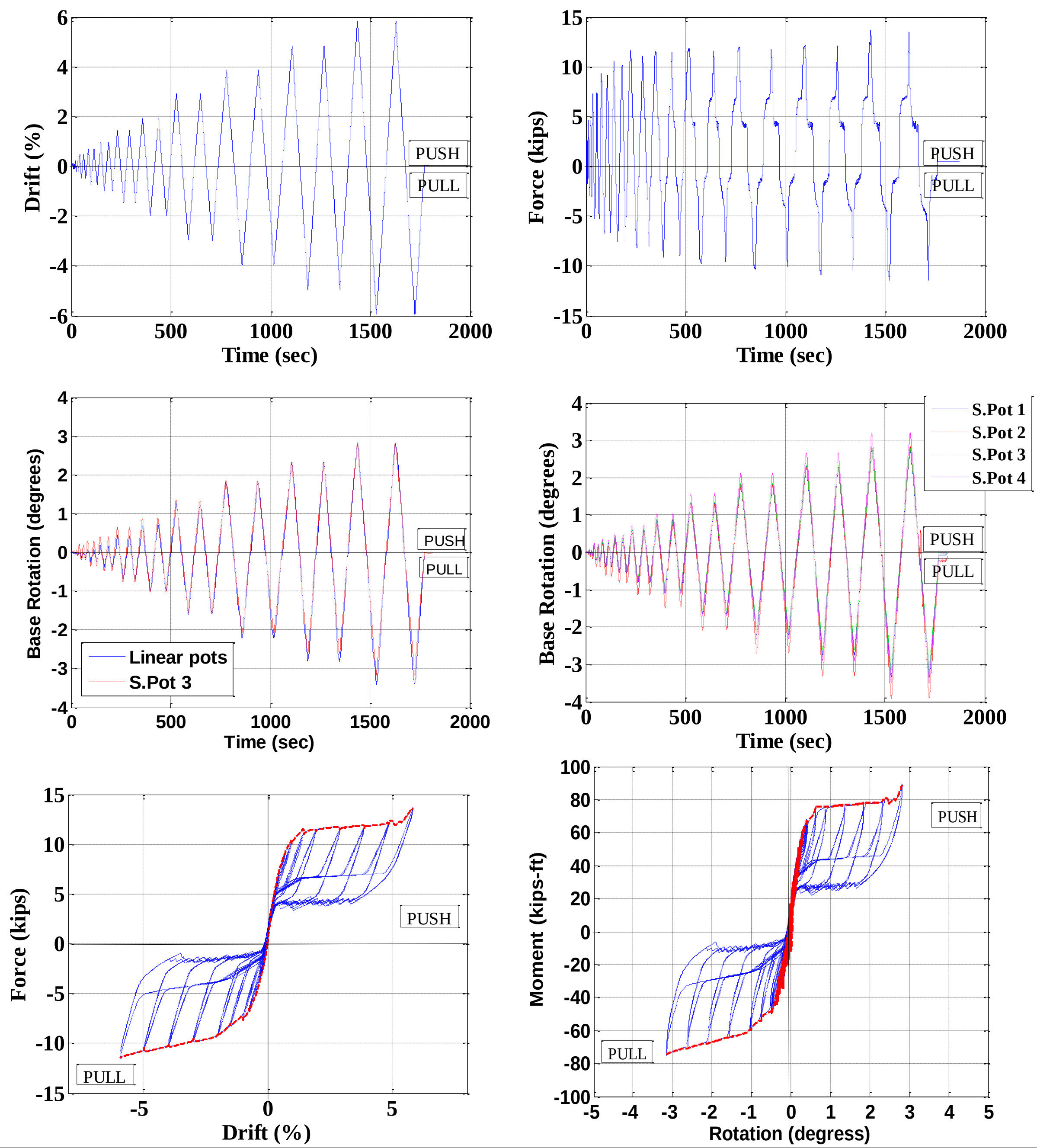

Specimen No.	Test	Type of Test	Axial Load (kips)	Base-Plate Thickness (in)	Anchor Rod Diameter (in)	Base-Plate Dimensions (in)	Flange Thickness (in) Out-In
S08$_{phase1}$	10% drift	Cyclic	43.6	0.75	1.25	14x10	0.375x0.625

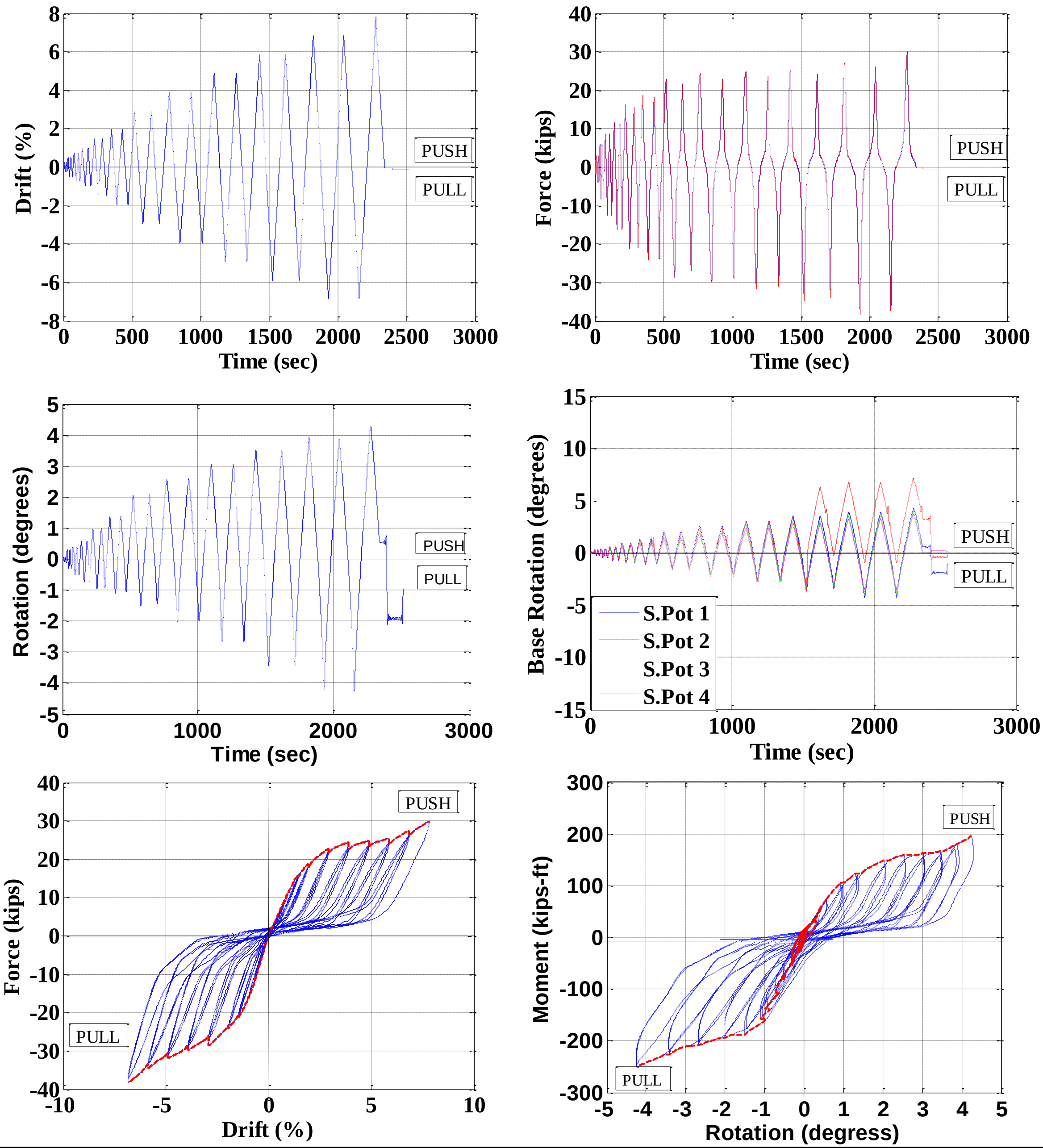

Table A. 2 Explanatory table - Phase 2.

SPECIMEN AND TEST INFORMATION	
This figure shows the Force (kips) – Drift (%) graphs obtained from the 10% inelastic tests. The force and drift values were derived from the actuator load cell and actuator LVDT. The envelopes are plotted in red.	This figure shows the Moment (kips-ft) – Rotation (rad) graphs obtained from the 10% inelastic tests. The moment was calculated as explained in Section 4.6.2 and the rotation was derived from the instruments as explained in Section 4.6.1. The envelopes are plotted in red.
This figure shows the First Moment (kips-ft) – Drift (%) graphs in x, y and z directions (the directions x, y, z are shown in Figure 3.14.). The moment was calculated as explained in Section 4.6.2, and the displacement values were taken from the actuator LVDT.	This figure shows the first- and second-order, and total (first plus second order) moments (kips-ft) versus drift (%) in x direction (shown in Figure 3.14.). The moment was calculated as explained in Section 4.6.2 and the displacement values were taken from the actuator LVDT.
This figure shows the five different rotations calculated from the rotary (string) potentiometers (String Potentiometer 1 – 5) along the height of the specimens as explained in Section 4.6.1, and shown in Figure 4.13(b) versus drift. Additionally, it compares these rotations against the rotation calculated from the rotary (string) potentiometers placed at the center of the flanges on either side of the specimen (String Potentiometer 6&7) as explained in Section 4.6.1 and shown in Figure 4.13(b).	

Specimen No.	Test	Number of Anchor Rods	Axial Load (kips)	Base-plate Thickness (inch)	Anchor Rod Diameter (inch)	Base-plate Dimensions (inch)	Flange Thickness Out-In (inch)
S01	10% Drift	Cyclic	50	5/8	3/4	12 5/8 x 8	1/4-3/8

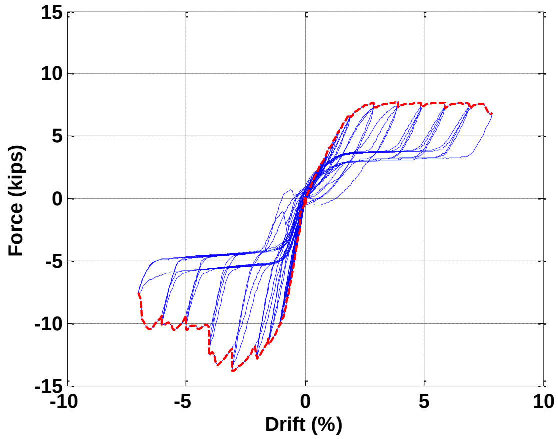

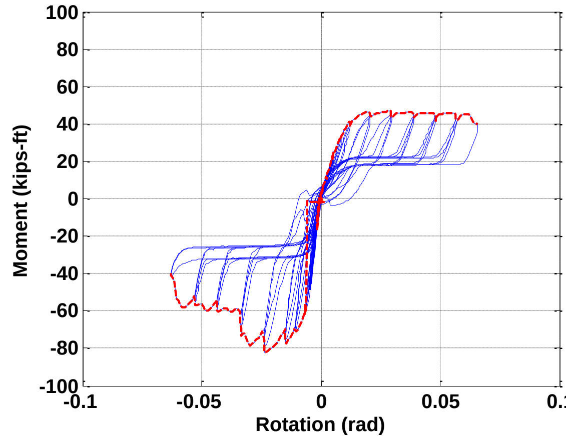

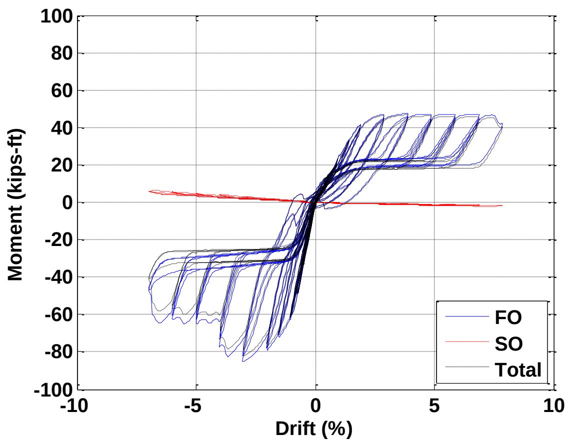

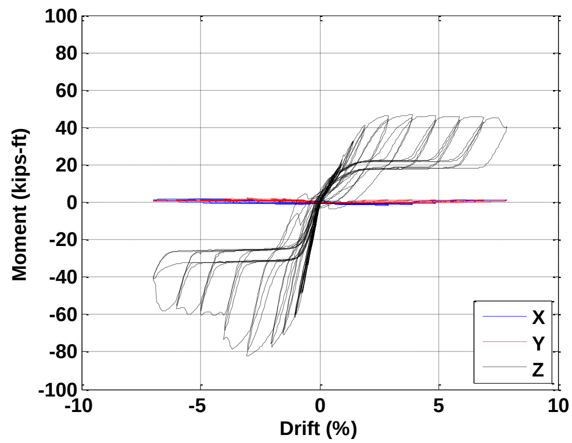

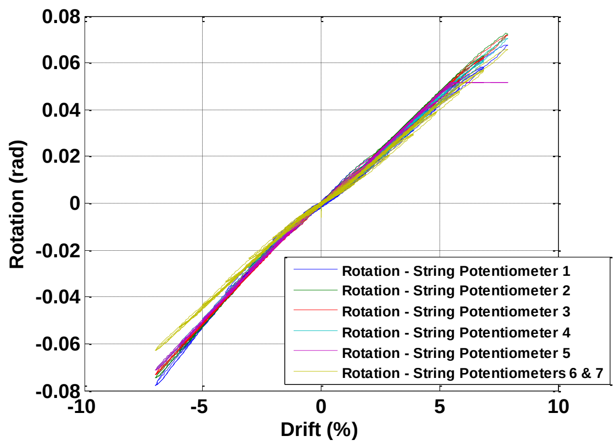

Specimen No.	Test	Number of Anchor Rods	Axial Load (kips)	Base-Plate Thickness (inch)	Anchor Rod Diameter (inch)	Base-Plate Dimensions (inch)	Flange Thickness Out-In (inch)
S02	10% Drift	4	50	5/8	3/4	12 5/8 x 8	1/4-3/8

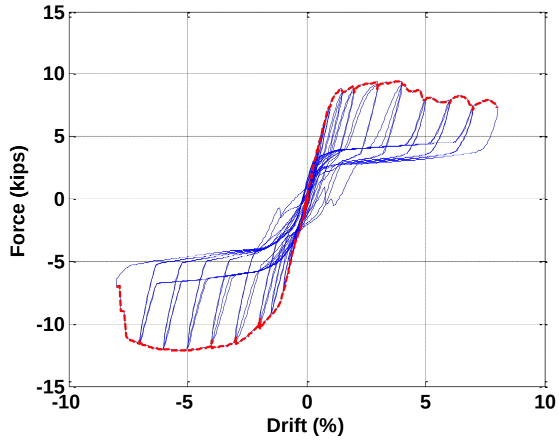

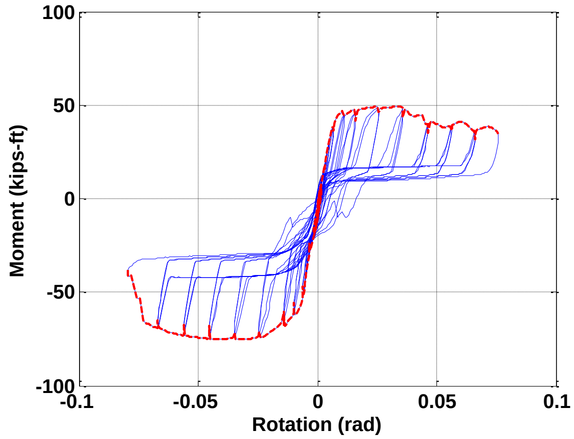

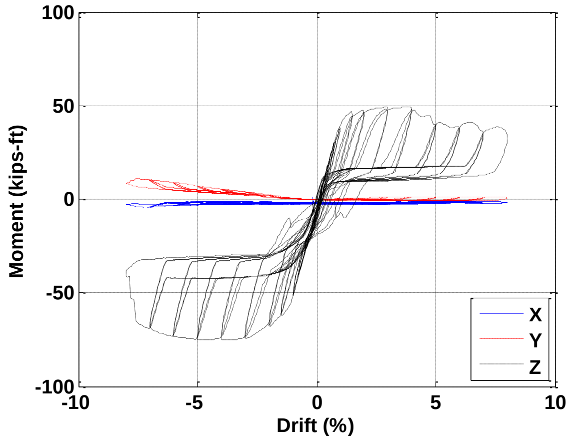

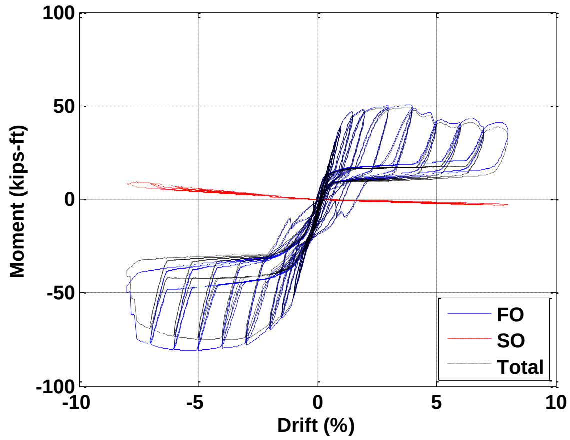

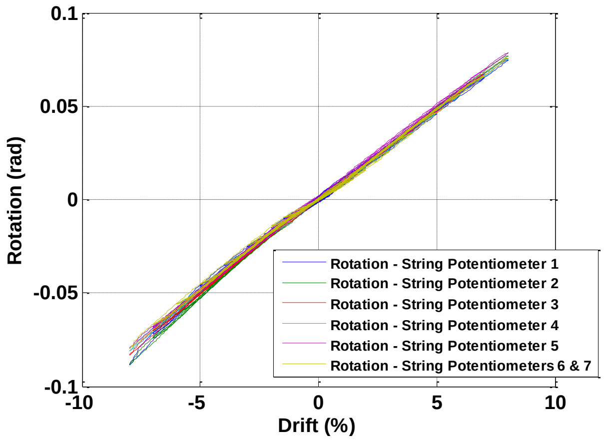

Specimen No.	Test	Number of Anchor Rods	Axial Load (kips)	Base-plate Thickness (inch)	Anchor Rod Diameter (inch)	Base-plate Dimensions (inch)	Flange Thickness Out-In (inch)
S03	10% Drift	4	50	5/8	1.0	12 5/8 x 8	1/4-3/8

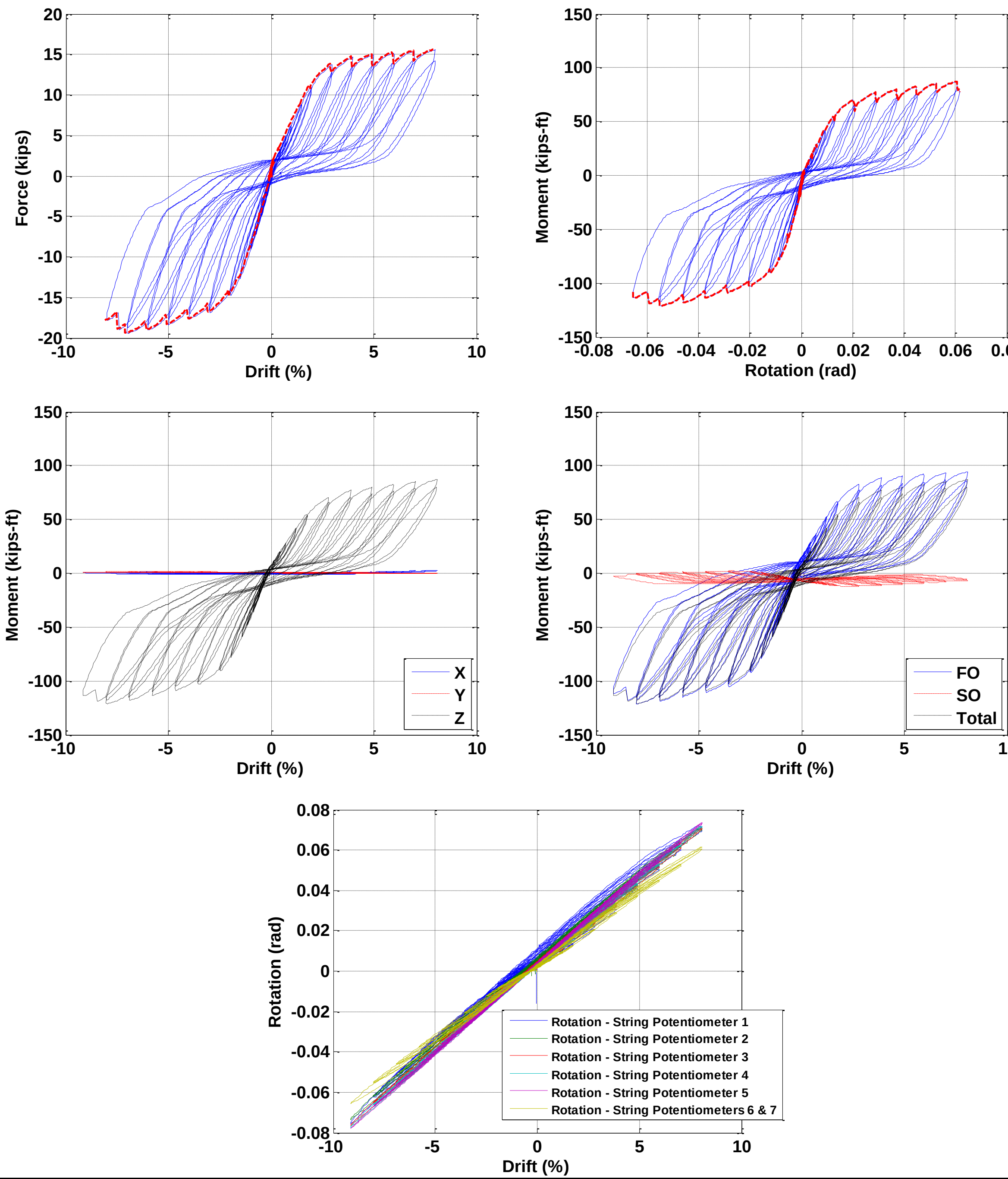

Specimen No.	Test	Number of Anchor Rods	Axial Load (kips)	Base-plate Thickness (inch)	Anchor Rod Diameter (inch)	Base-plate Dimensions (inch)	Flange Thickness Out-In (inch)
S04	10% Drift	Cyclic	50	5/8	1 1/4	12 5/8 x 10	1/4-3/8

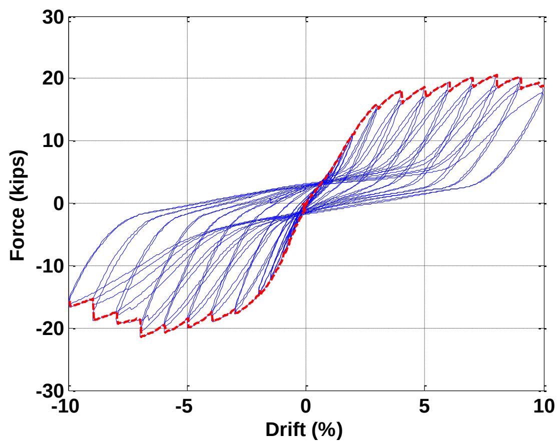

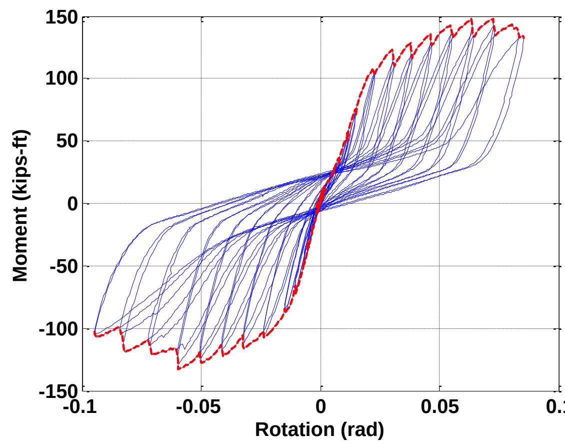

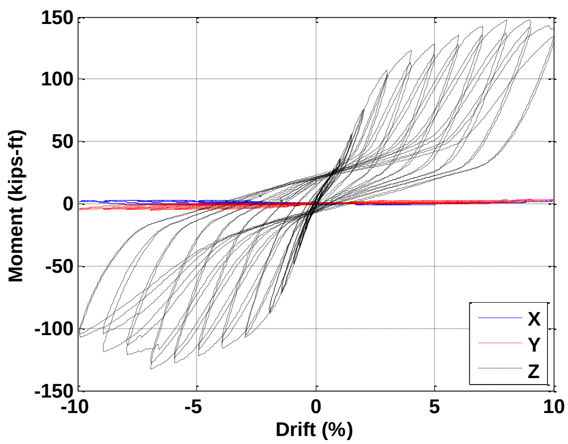

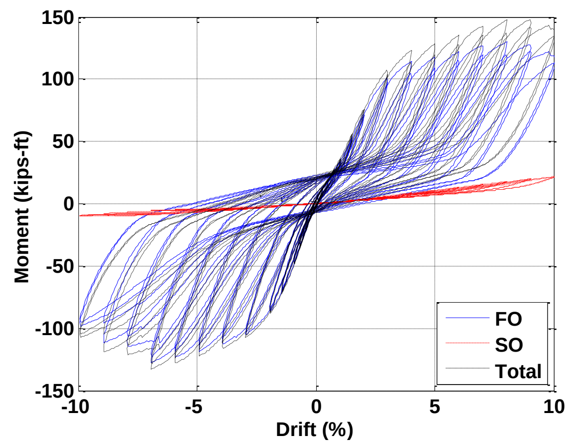

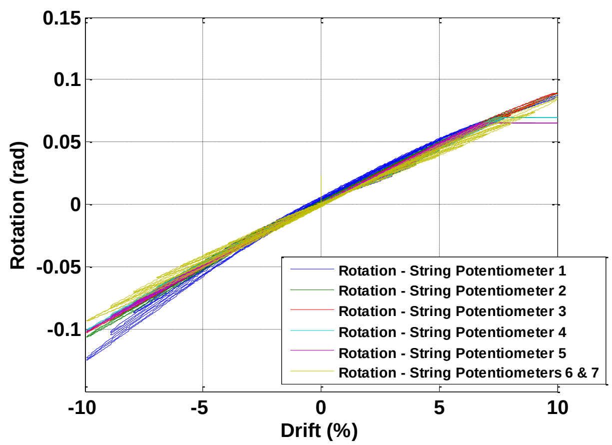

Specimen No.	Test	Number of Anchor Rods	Axial Load (kips)	Base-plate Thickness (inch)	Anchor Rod Diameter (inch)	Base-plate Dimensions (inch)	Flange Thickness Out-In (inch)
S05	10% Drift	4	50	3/8	1 1/4	12 5/8 x 10	1/4-3/8

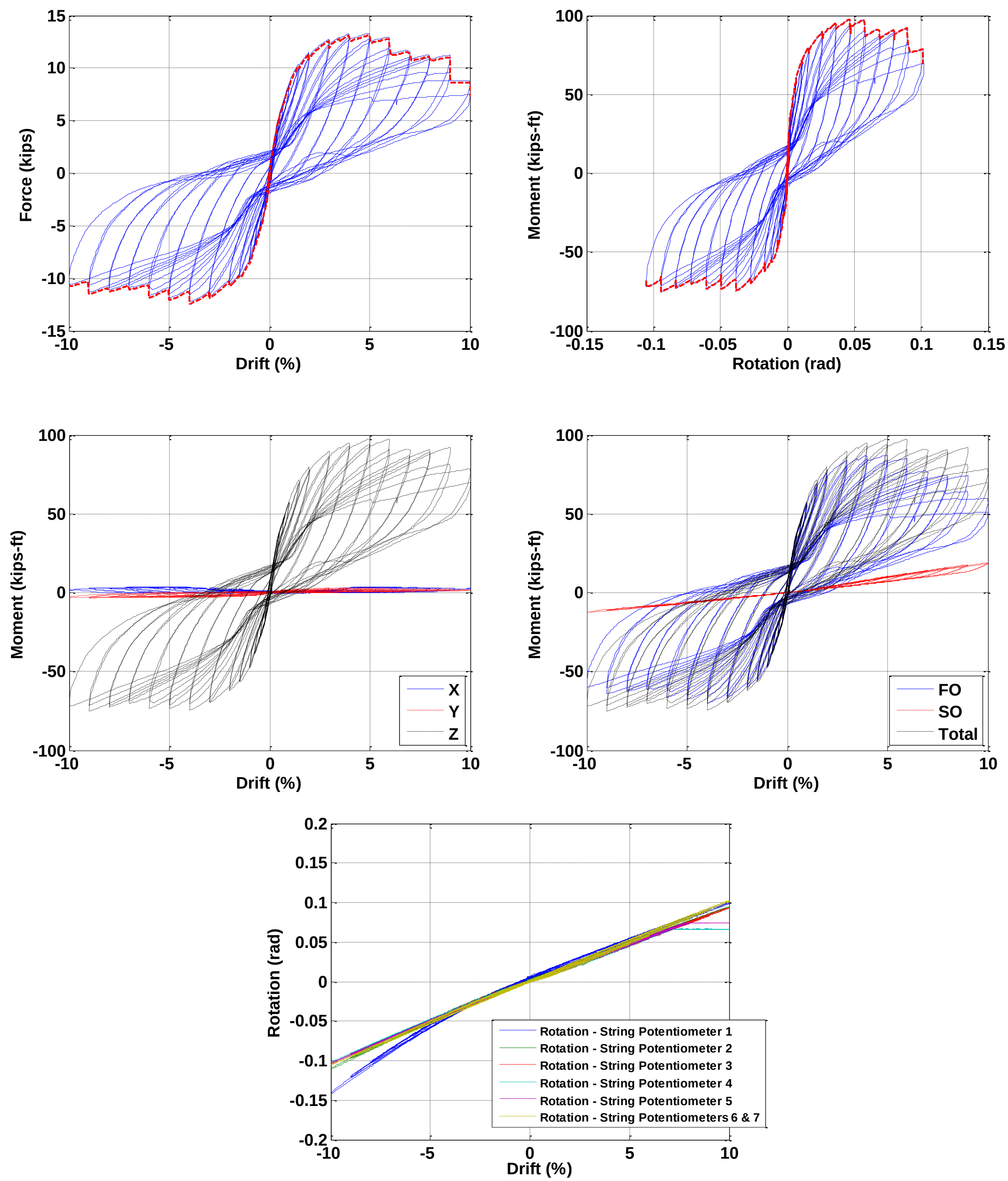

Specimen No.	Test	Number of Anchor Rods	Axial Load (kips)	Base-plate Thickness (inch)	Anchor Rod Diameter (inch)	Base-plate Dimensions (inch)	Flange Thickness Out-In (inch)
S06	10% Drift	4	50	5/8	1 1/4	13 5/8 x 10	1/2-5/8

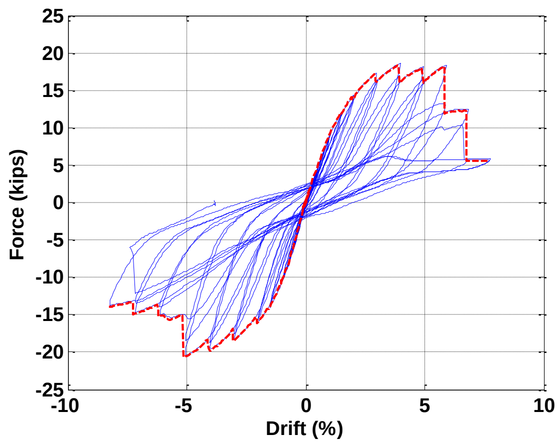

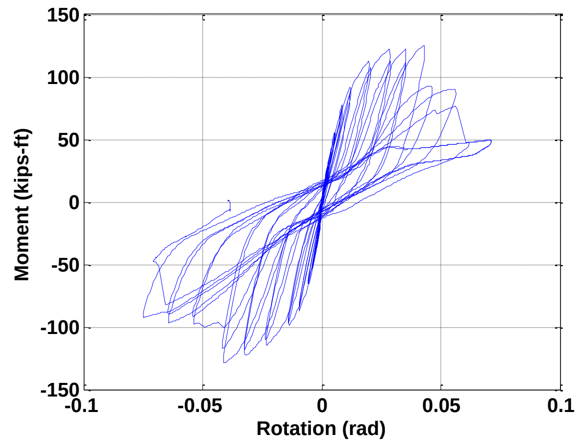

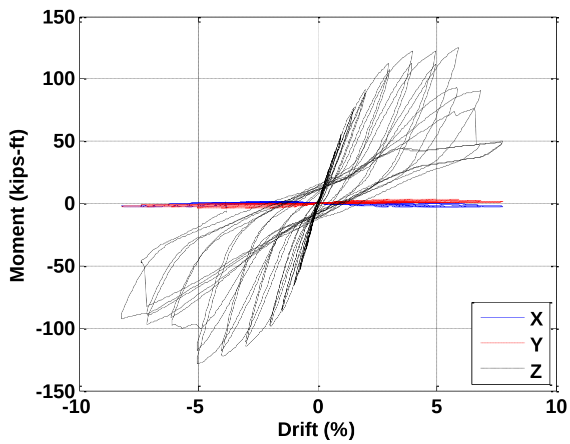

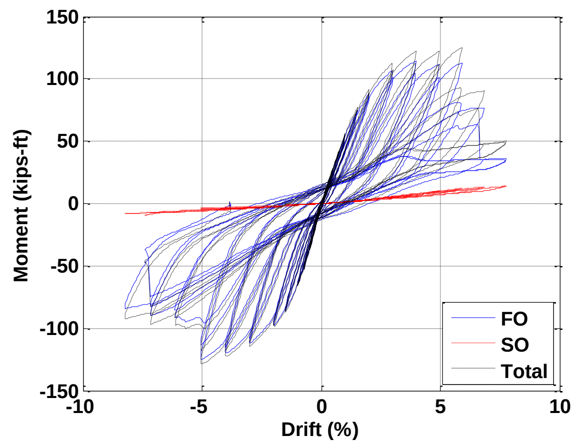

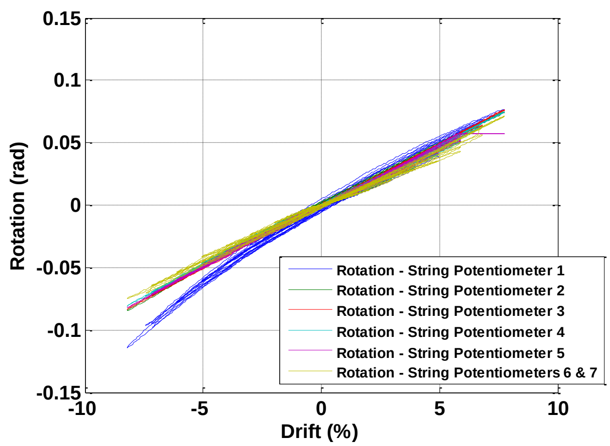

Specimen No.	Test	Number of Anchor Rods	Axial Load (kips)	Base-plate Thickness (inch)	Anchor Rod Diameter (inch)	Base-plate Dimensions (inch)	Flange Thickness Out-In (inch)
S07	10% Drift	6	50	5/8	1 1/4	23 1 /8 x 14	1/2-5/8

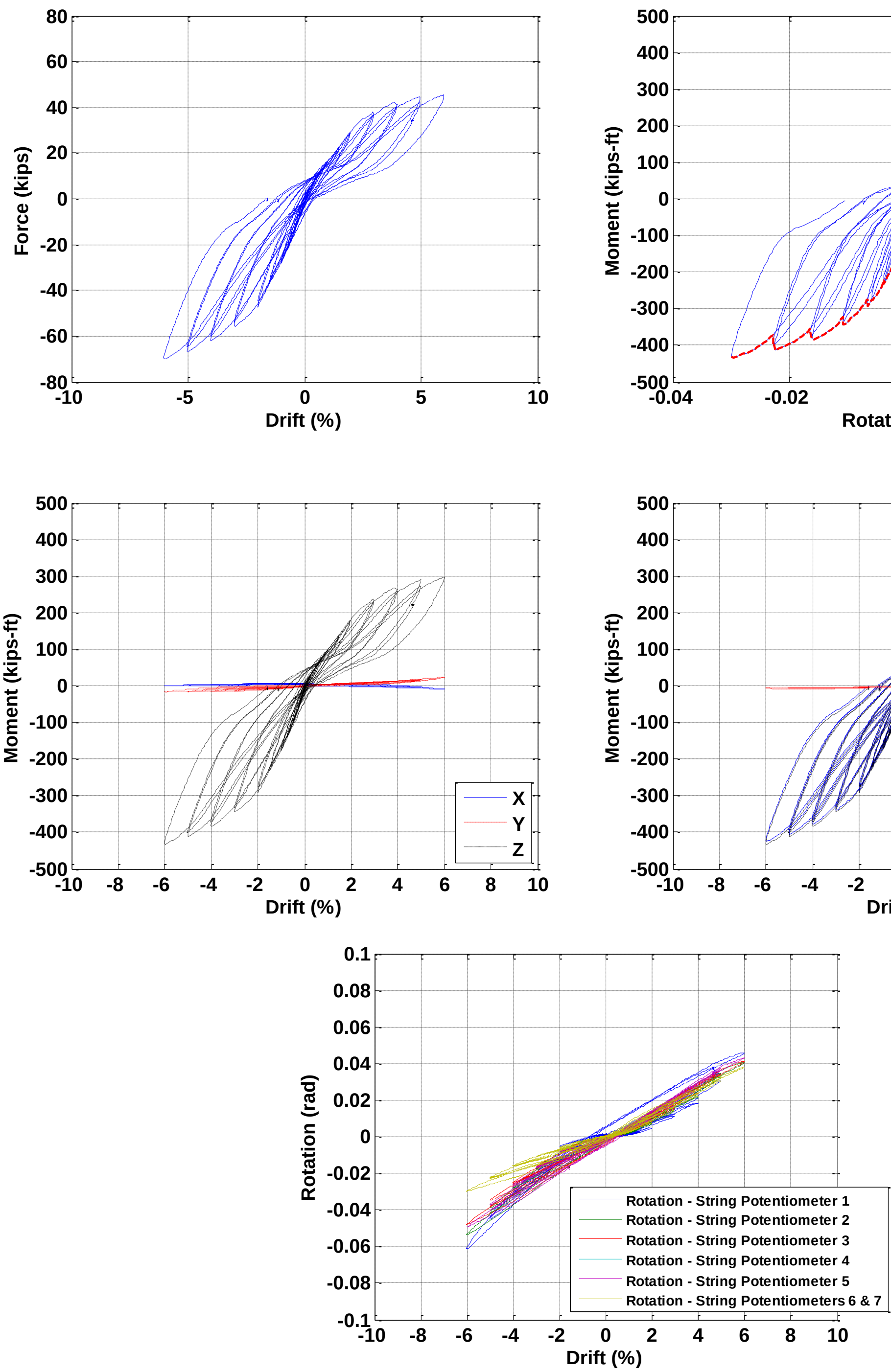

Specimen No.	Test	Number of Anchor Rods	Axial Load (kips)	Base-plate Thickness (inch)	Anchor Rod Diameter (inch)	Base-plate Dimensions (inch)	Flange Thickness Out-In (inch)
S08	10% Drift	8	50	5/8	1 1/4	23 1 /8 x 14	1/2-5/8

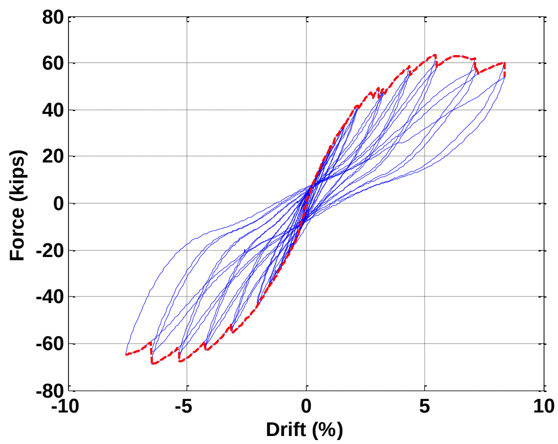

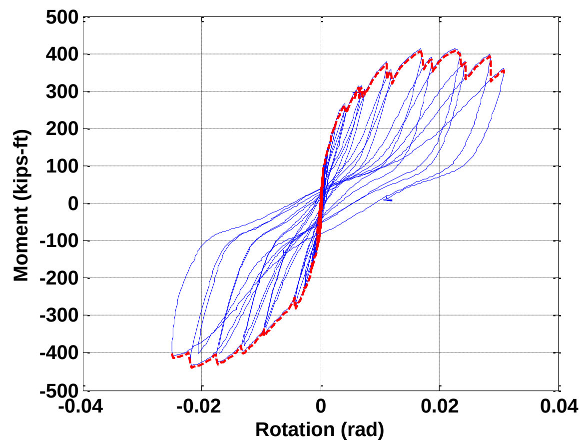

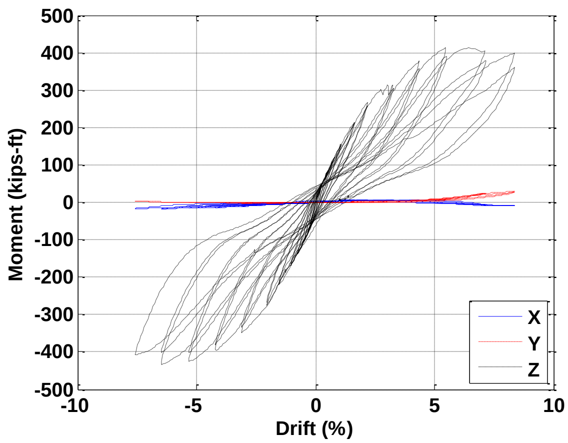

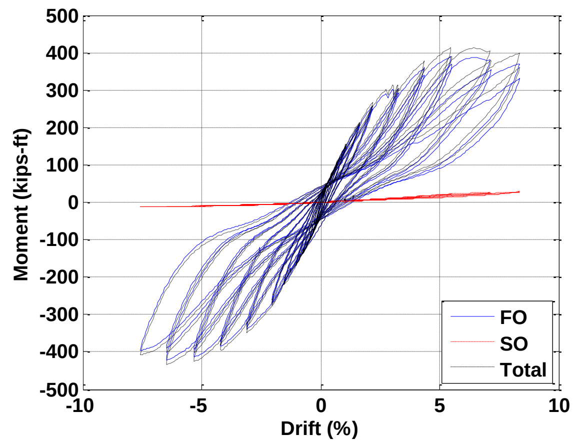

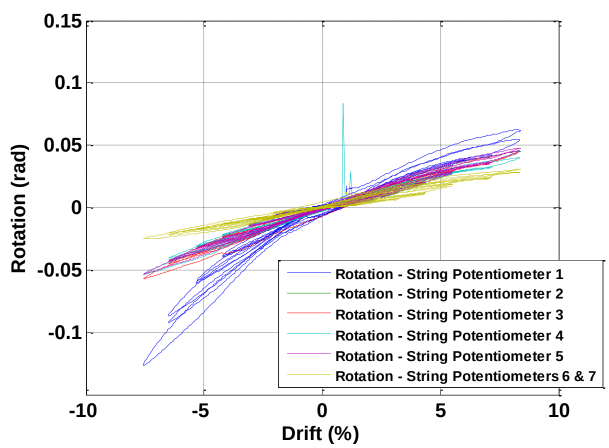

Specimen No.	Test	Number of Anchor Rods	Axial Load (kips)	Base-plate Thickness (inch)	Anchor Rod Diameter (inch)	Base-plate Dimensions (inch)	Flange Thickness Out-In (inch)
S09	10% Drift	8	50	5/8	1 1/4	23 1 /8 x 14	1/2-5/8

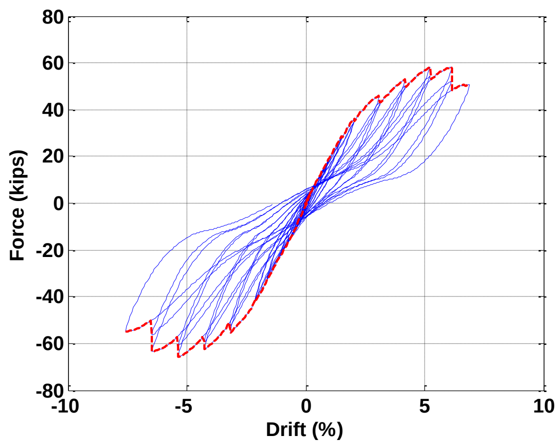

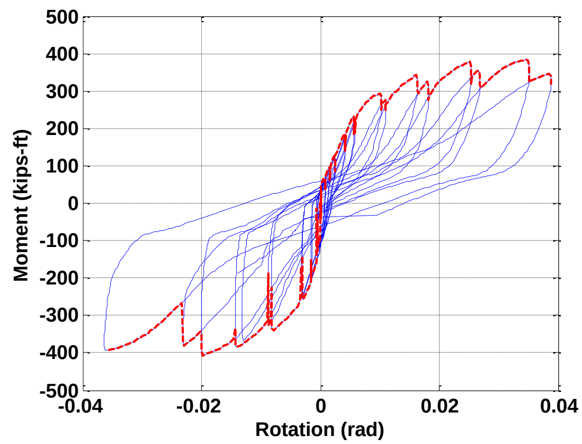

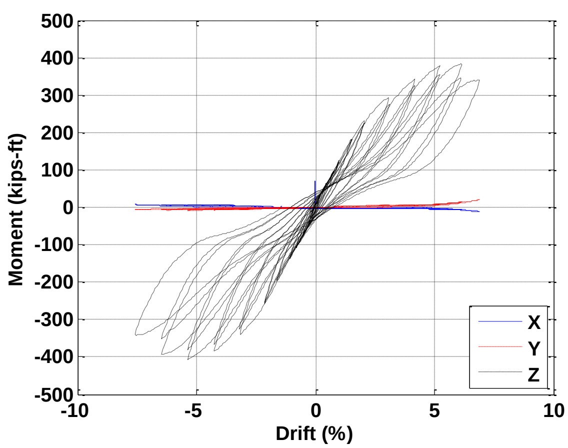

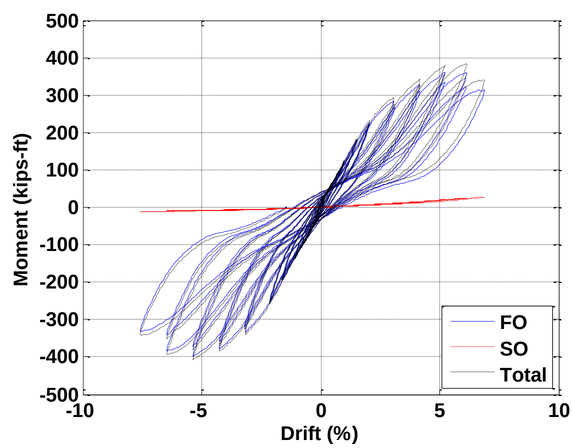

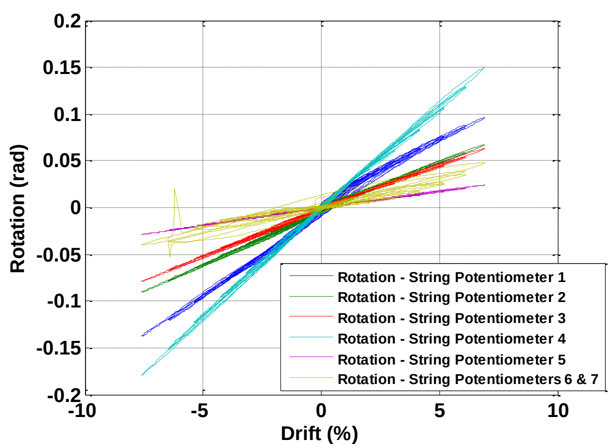

Specimen No.	Test	Number of Anchor Rods	Axial Load (kips)	Base-plate Thickness (inch)	Anchor Rod Diameter (inch)	Base-plate Dimensions (inch)	Flange Thickness Out-In (inch)
S10	10% Drift	8	50	3/4	1 1/4	23 1 /8 x 14	1/2-5/8

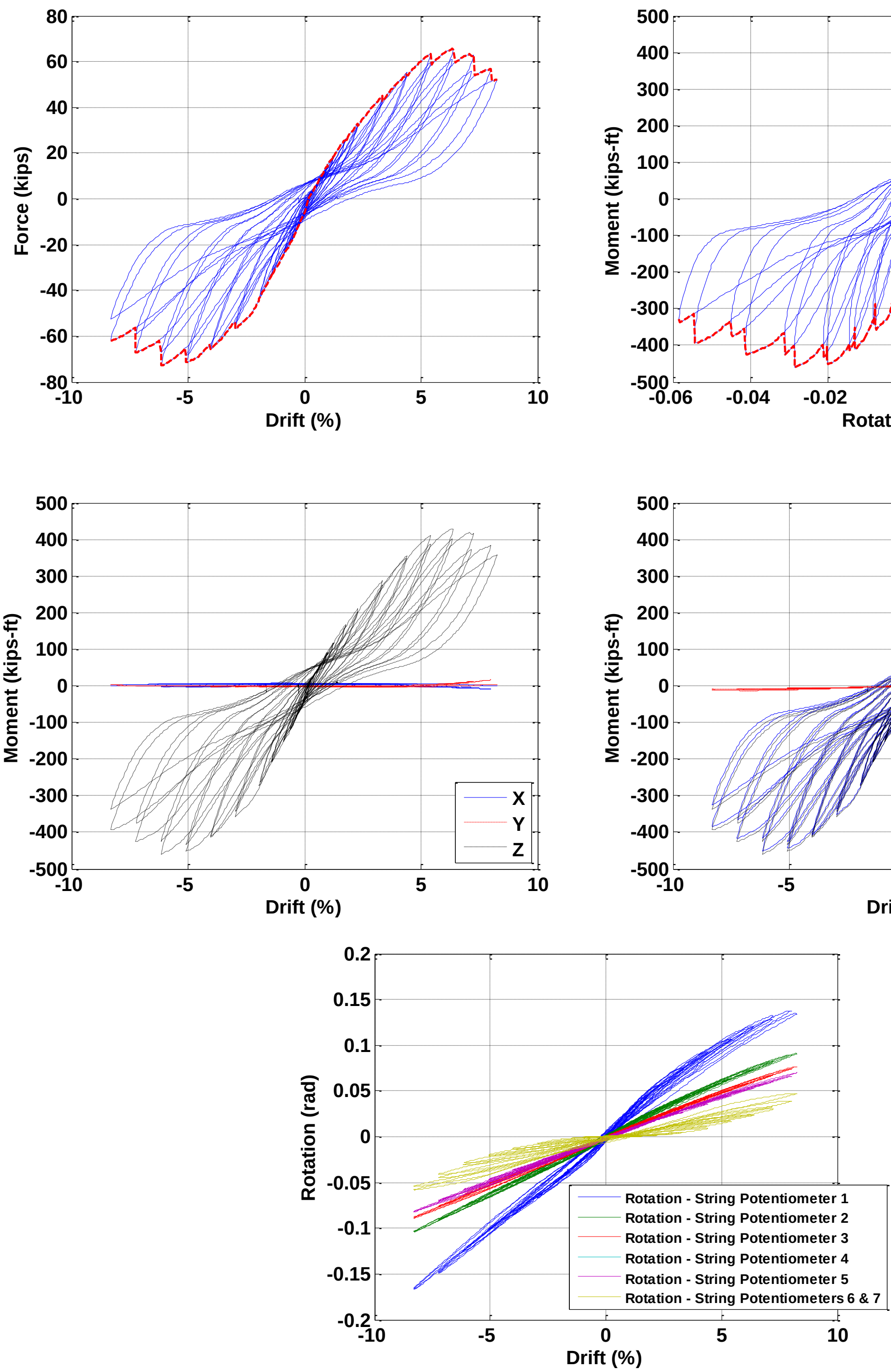

Specimen No.	Test	Number of Anchor Rods	Axial Load (kips)	Base-plate Thickness (inch)	Anchor Rod Diameter (inch)	Base-plate Dimensions (inch)	Flange Thickness Out-In (inch)
S11	10% Drift	4	50	3/4	3/4	10 3/4 x 10	3/8-3/8

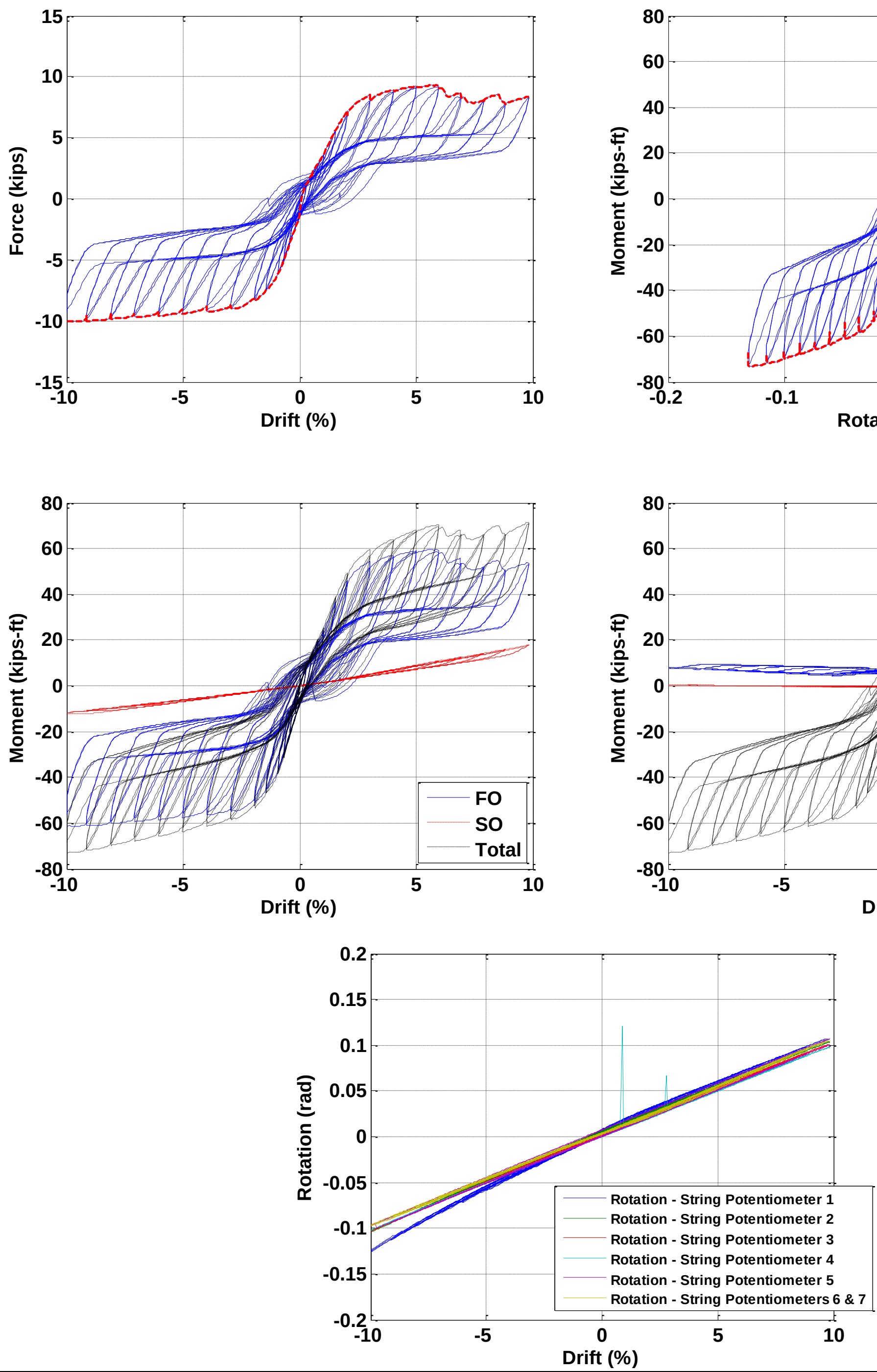

APPENDIX B: TEST CONFIGURATIONS AND CORRESPONDING FRAME DESIGNS-PHASE 1

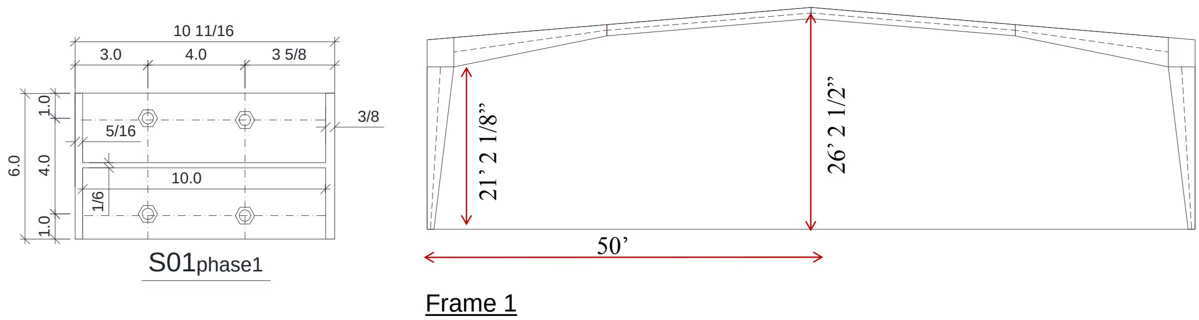

Figure B.1. Base-plate connection S01phase1 and corresponding frame dimensions.

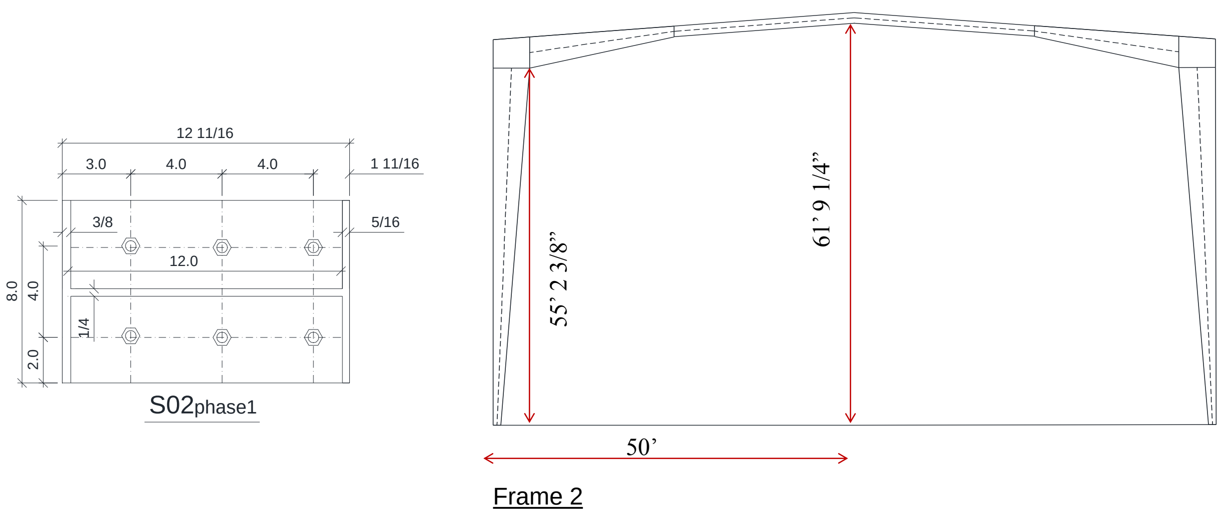

Figure B.2. Base-plate connection $S02_{phase1}$ and corresponding frame dimensions.

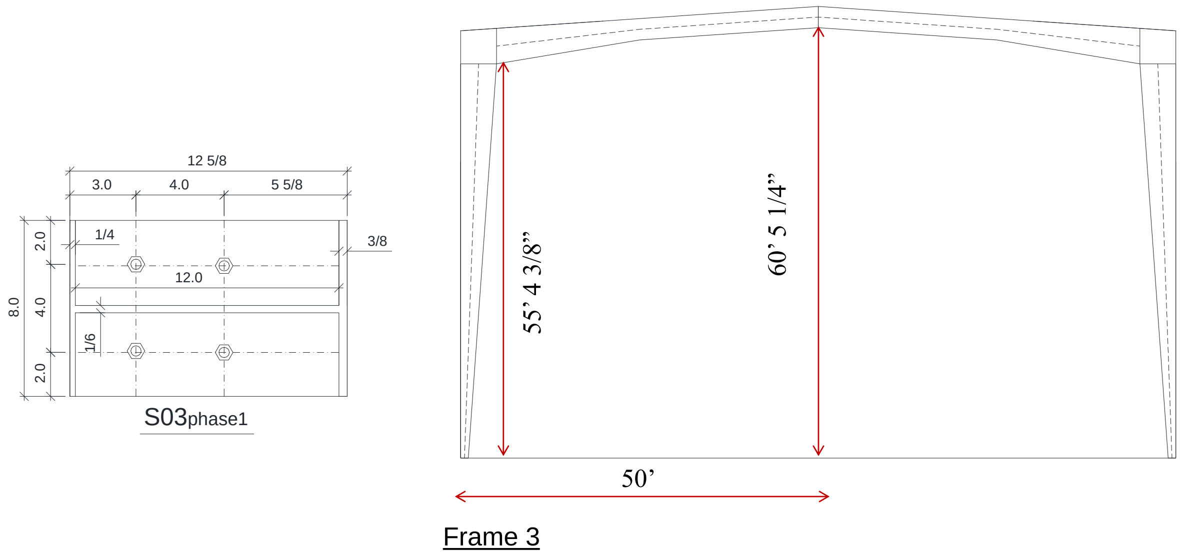

Figure B.3. Base-plate connection S03$_{phase1}$ and corresponding frame dimensions.

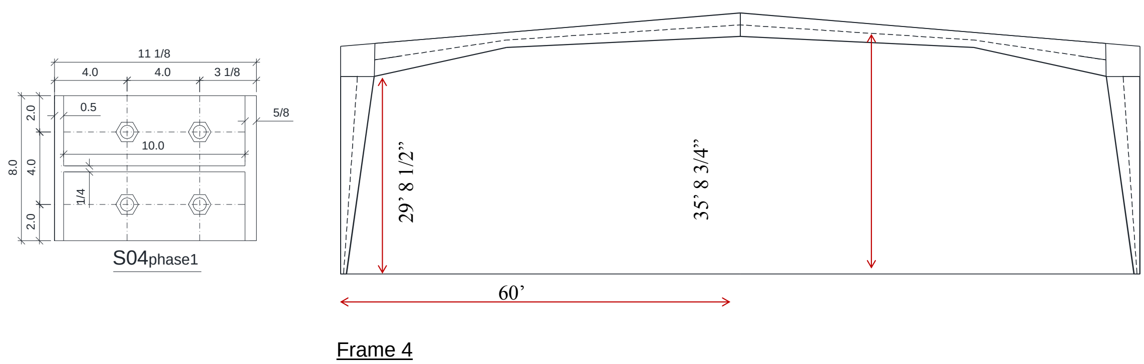

Figure B.4. Base-plate connection S04$_{phase1}$ and corresponding frame dimensions.

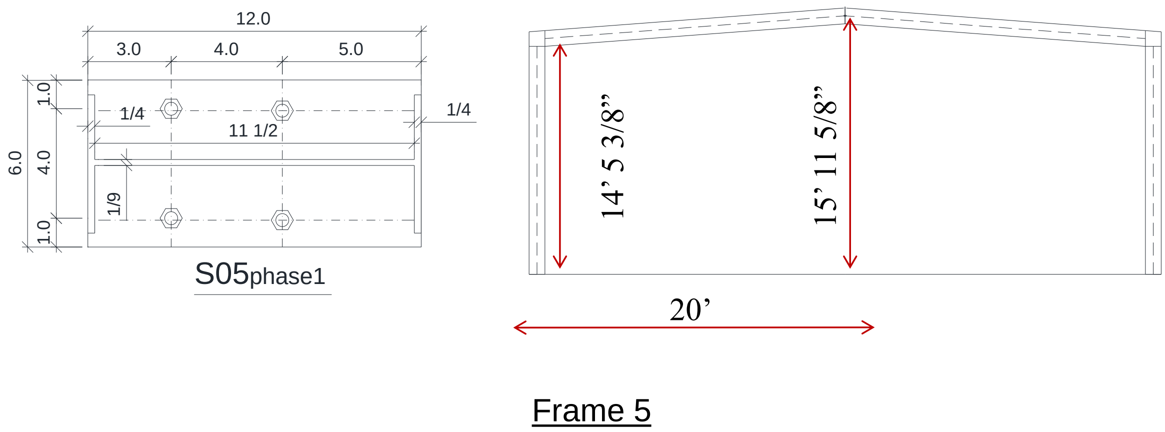

Figure B.5. Base-plate connection S05$_{phase1}$ and corresponding frame dimensions.

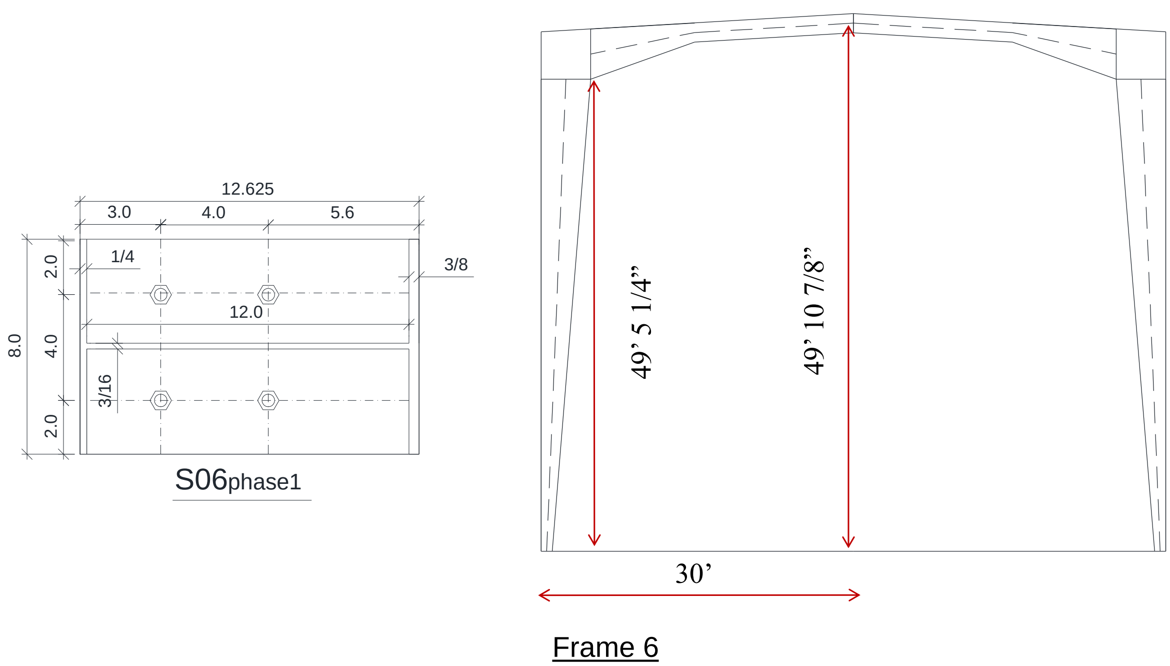

Figure B.6. Base-plate connection S06$_{phase1}$ and corresponding frame dimensions.

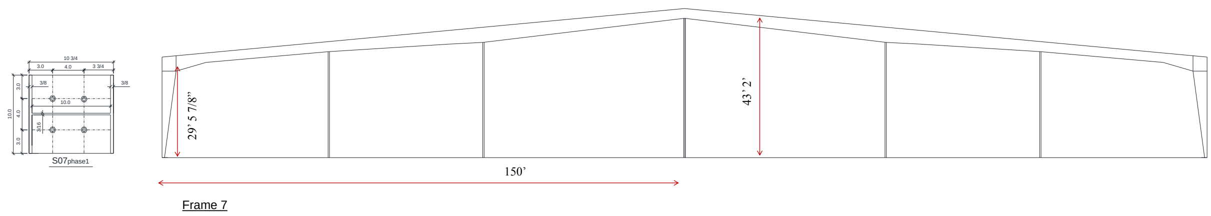

Figure B.7. Base-plate connection $S07_{phase1}$ and corresponding frame dimensions.

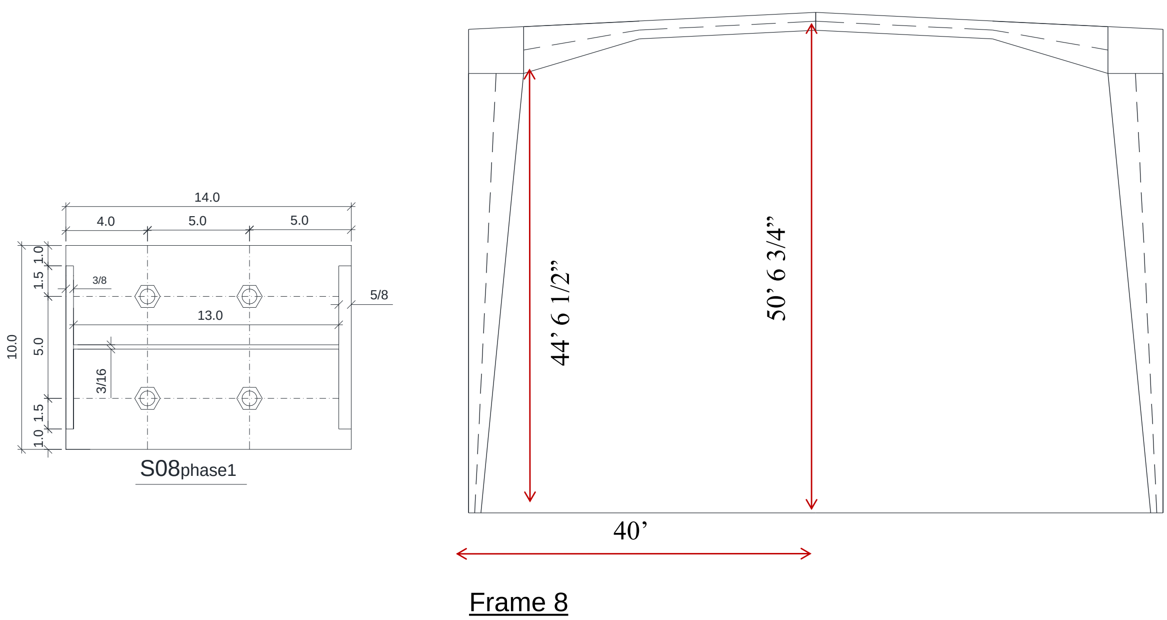

Figure B.8. Base-plate connection $S08_{phase1}$ and corresponding frame dimensions.

APPENDIX C: MATERIAL TESTS

Table C.1. Concrete Compressive Tests Results – Second Phase of the Experimental Program.

Days-Specimen	Cylinder No	Max Load (lb)	Stress (ksi)	Avearge (ksi)	Standard Deviation (ksi)	Age of concrete	Date
7 days	C1	40190	3.20	3.06	0.14	7 days	3/3/2015
	C2	38690	3.08				
	C3	36475	2.90				
	C4	40955	3.26				
	C5	37195	2.96				
	C6	37535	2.99				
28 days	C1	60000	4.77	4.34	0.39	28 days	3/27/2015
	C2	55375	4.41				
	C3	48036	3.82				
	C4	54756	4.36				
S01	C1	50371	4.01	4.08	0.14	127 days	7/2/2015
	C2	52611	4.19				
	C3	52805	4.20				
	C4	49050	3.90				
S02	C1	69395	5.52	5.70	0.23	139 days	7/15/2015
	C2	69050	5.49				
	C3	73190	5.82				
	C4	75100	5.98				
S03	C1	70050	5.57	5.32	0.17	161 days	8/7/2015
	C2	65260	5.19				
	C3	66640	5.30				
	C4	65620	5.22				
S04	C1	59485	4.73	4.75	0.13	161 days	8/7/2015
	C2	60166	4.79				
	C3	59366	4.72				
S05, S06	C1	61436	4.89	4.85	0.18	173 days	8/19/2015
	C2	60645	4.83				
	C3	61378	4.88				
	C4	59440	4.73				
	C5	62135	4.94				
S07, S08	C1	63340	5.04	5.06	0.17	189 days	9/5/2015
	C2	65030	5.17				
	C3	60610	4.82				
	C4	65445	5.21				
S09,S10,S11	C1	65025	5.17	4.86	0.23	249 days	11/4/2015
	C2	58640	4.67				
	C3	61375	4.88				
	C4	59295	4.72				
Additional*	C1	62830	5.00	4.92	0.15	279 days	12/4/2015
	C2	59275	4.72				
	C3	60975	4.85				
	C4	59530	4.74				
	C5	63730	5.07				
	C6	62770	5.00				
	C7	63280	5.04				

*Additional cylinders tested after the completion of the experiments

Table C.2. Concrete Split Tensile Tests Results – Second Phase of the Experimental Program.

Days-Specimen	Cylinder No	Max Load (lb)	Stress (ksi)	Avearge (ksi)	Standard Deviation (ksi)	Age of concrete	Date
7 days	C1	11805	0.23	0.27	0.03	7 days	3/3/2015
	C2	14295	0.28				
	C3	12590	0.25				
	C4	15485	0.31				
28 days	C1	27581	0.55	0.54	0.02	28 days	3/27/2015
	C2	27962	0.56				
	C3	25723	0.51				
S01	C1	32300	0.64	0.56	0.07	127 days	7/2/2015
	C2	26200	0.52				
	C3	26300	0.52				
S02	C1	32125	0.64	0.64	0.04	139 days	7/15/2015
	C2	34170	0.68				
	C3	30180	0.60				
S03	C1	29320	0.58	0.54	0.04	161 days	8/7/2015
	C2	26285	0.52				
	C3	25150	0.50				
S04	C1	33110	0.66	0.61	0.06	161 days	8/7/2015
	C2	27200	0.54				
	C3	31000	0.62				
S05, S06	C1	28330	0.56	0.55	0.02	173 days	8/19/2015
	C2	28275	0.56				
	C3	28360	0.56				
	C4	26975	0.54				
	C5	25515	0.51				
S07, S08	C1	26350	0.52	0.54	0.04	189 days	9/5/2015
	C2	25567	0.51				
	C3	30170	0.60				
	C4	26250	0.52				
S09,S10,S11	C1	29970	0.60	0.54	0.04	249 days	11/4/2015
	C2	26245	0.52				
	C3	26050	0.52				
	C4	26390	0.53				
Additional*	C1	27360	0.54	0.56	0.02	279 days	12/4/2015
	C2	28270	0.56				
	C3	27200	0.54				
	C4	28956	0.58				

*Additional cylinders tested after the completion of the experiments

Table C.3. Concrete Modulus of Rupture Tests Results – Second Phase of the Experimental Program.

Days/Specimen	Prism No	Stress (ksi)	Avearge (ksi)	Standard Deviation (ksi)	Aging of concrete	Date
28 days	P1	0.72	0.67	0.06	28 days	3/27/2015
	P2	0.70				
	P3	0.61				
S01	P1	0.75	0.66	0.08	127 days	7/2/2015
	P2	0.63				
	P3	0.60				
S05,S06	P1	0.60	0.75	0.14	173 days	19/8/2015
	P2	0.77				
	P3	0.87				
S09,S10,S11	P1	0.65	0.68	0.03	249 days	11/4/2015
	P2	0.72				
	P3	0.66				
	P4	0.71				
	P5	0.68				
Additional	P1	0.71	0.70	0.04	279 days	12/4/2015
	P2	0.74				
	P3	0.70				
	P4	0.75				
	P5	0.66				
	P6	0.64				
	P7	0.69				

*Additional cylinders tested after the completion of the experiments

APPENDIX D: PARAMETRIC STUDY RESULTS

Table D.1. Parametric Analysis Results for the 12 inch Web Depth Column Base-Plate Connections.

Model ID	Rotational stiffness-Push direction (kips-ft/rad)	Rotational stiffness-Pull direction (kips-ft/rad)	Moment capacity-Push direction (kips-ft)	Moment capacity-Pull direction (kips-ft)
P01	5362	12055	46.1	-85.3
P01-01	6167	9670	34.5	-66.8
P01-02	6327	12051	39.5	-76.1
P01-03	6235	14688	43.3	-83.3
P01-04	6433	12360	50.1	-94.0
P01-05	6351	12280	52.7	-101.0
P01-06	7160	12342	53.8	-102.8
P01-07	8219	15304	39.5	-78.3
P01-08	9595	12204	50.6	-90.5
P01-09	6741	9151	48.8	-80.1
P01-10	8201	12935	53.9	-93.9
P01-11	5706	11716	47.4	-88.7
P01-12	5799	11775	48.3	-91.1
P01-13	5837	11870	49.4	-92.2
P01-14	8574	9023	48.5	-90.8
P01-15	9067	9492	50.9	-95.6
P01-16	8192	10684	53.4	-101.4
P01-17	6803	9000	47.0	-85.7
P01-18	14641	13854	55.2	-95.8
P01-19	13400	22519	90.0	-105.5
P01-20	7505	9595	51.4	-97.9
P01-21	7806	9821	54.1	-104.1
P01-22	11183	20989	75.1	-80.4
P01-23	7406	15981	53.2	-102.9
P01-24	7732	17337	56.2	-107.2
P01-25	11853	24843	79.8	-81.1
P01-26	7834	7800	49.0	-82.7
P01-27	8701	10377	55.8	-80.1
P01-28	8156	9152	49.3	-69.0
P01-29	8578	9188	56.4	-60.9

Table D.1. (Continued) Parametric Analysis Results for the 12 inch Web Depth Column Base-Plate Connections.

Model ID	Rotational stiffness-Push direction (kips-ft/rad)	Rotational stiffness-Pull direction (kips-ft/rad)	Moment capacity-Push direction (kips-ft)	Moment capacity-Pull direction (kips-ft)
P01-30	3830	7480	46.8	-80.6
P01-31	4848	10544	49.9	-89.2
P01-32	5286	8947	53.0	-94.4
P01-33	5653	10803	46.1	-101.7
P01-34	4566	8593	47.4	-82.4
P01-35	9387	12954	57.1	-102.7
P01-36	7387	25812	80.3	-110.1
P01-37	5733	10469	54.3	-98.9
P01-38	6194	9723	58.5	-106.9
P01-39	6094	16805	66.5	-89.0
P01-40	6255	13041	56.0	-94.9
P01-41	6894	15576	60.5	-112.6
P01-42	5035	9629	46.5	-84.7
P01-43	5459	8410	48.9	-91.0
P01-44	5506	9541	51.3	-97.4
P01-45	5809	11320	53.7	-102.7
P01-46	4629	9112	46.4	-85.7
P01-47	4265	545074	54.1	-105.4
P01-48	3495	11786	49.1	-92.4
P01-49	5647	9942	52.0	-99.8
P01-50	6057	6866	55.4	-104.9
P01-51	7141	24889	52.0	-106.8
P01-52	6164	15151	56.3	-108.4
P01-53	6556	14771	57.6	-111.3
P01-54	1345	9828	47.9	-81.1
P01-55	3827	14884	51.3	-136.5
P01-56	2318	11916	55.0	-95.2
P01-57	2353	10442	55.0	-95.2
P01-58	1514	10005	49.1	-83.2
P01-59	3419	8441	55.4	-96.4
P01-60	4464	36669	52.7	-90.4
P01-61	2691	14308	56.4	-97.7
P01-62	2918	11297	61.5	-105.6
P01-63	2210	10441	61.5	-101.3
P01-64	3045	14212	60.2	-106.2
P01-65	3303	16494	64.5	-111.8

Table D.2. Parametric Analysis Results for the 18 inch Web Depth Column Base-Plate Connections.

Model ID	Rotational stiffness-Push direction (kips-ft/rad)	Rotational stiffness-Pull direction (kips-ft/rad)	Moment capacity-Push direction (kips-ft)	Moment capacity-Pull direction (kips-ft)
P02	15139	25812	98.2	-135.6
P02-01	17844	23666	134.2	-137.8
P02-02	17886	30706	116.3	-165.5
P02-03	11067	18647	72.3	-99.0
P02-04	15396	27025	78.3	-113.8
P02-05	15853	29981	110.4	-150.9
P02-06	16690	28523	129.7	-178.9
P02-07	24783	27052	100.8	-100.0
P02-08	15030	26355	82.9	-131.8
P02-09	15615	25606	97.9	-113.8
P02-10	16133	29825	103.1	-168.7
P02-11	15282	26334	98.6	-136.1
P02-12	12412	26801	100.5	-138.2
P02-13	15639	27091	101.4	-138.9
P02-14	14923	24513	100.9	-143.2
P02-15	17577	28946	108.1	-150.2
P02-16	18017	29995	111.1	-152.4
P02-17	16041	23799	97.1	-174.0
P02-18	15660	28372	97.1	-136.0
P02-19	25869	25869	141.0	-141.0
P02-20	17527	26058	107.6	-148.2
P02-21	18220	26066	108.9	-153.5
P02-22	16333	27684	100.2	-146.2
P02-23	17975	26918	106.8	-136.0
P02-24	18351	32869	109.6	-163.9
P02-25	19190	25117	63.3	-136.8
P02-26	27721	26120	139.8	-127.9
P02-27	20672	25392	118.7	-135.3
P02-28	30387	24454	151.5	-133.9
P02-29	17967	22757	106.3	-127.9
P02-30	21174	17536	118.2	-115.9
P02-31	15077	27645	96.2	-139.5
P02-32	13932	24780	94.4	-138.5

Table D.2. (Continued) Parametric Analysis Results for the 18 inch Web Depth Column Base-Plate Connections.

Model ID	Rotational stiffness-Push direction (kips-ft/rad)	Rotational stiffness-Pull direction (kips-ft/rad)	Moment capacity-Push direction (kips-ft)	Moment capacity-Pull direction (kips-ft)
P02-33	12875	21218	98.2	-136.6
P02-34	12400	20067	100.7	-147.1
P02-35	15074	24419	110.9	-155.3
P02-36	15761	25398	113.9	-158.2
P02-37	11536	18563	98.1	-132.4
P02-38	12534	20970	97.0	-137.2
P02-39	12043	18375	101.2	-143.1
P02-40	13583	21160	109.6	-152.8
P02-41	14592	21402	111.8	-156.6
P02-42	15834	20282	100.6	-147.2
P02-43	14702	24064	109.3	-156.7
P02-44	15409	24799	112.7	-162.5
P02-45	14226	22270	96.3	-131.9
P02-46	13247	23077	100.0	-146.0
P02-47	15833	25242	108.3	-151.3
P02-48	16451	28717	111.9	-153.0
P02-49	12565	21772	96.0	-128.2
P02-50	12910	23688	95.4	-131.8
P02-51	12258	21616	96.0	-143.3
P02-52	14439	24528	107.2	-149.4
P02-53	14818	22405	109.9	-154.4
P02-54	13329	23247	99.8	-147.5
P02-55	15072	26918	107.0	-153.7
P02-56	15594	21366	110.7	-157.2
P02-57	15490	23364	110.7	-157.2
P02-58	10955	15921	101.3	-143.9
P02-59	13442	23666	111.1	-156.4
P02-60	14088	20499	116.1	-160.6
P02-61	10221	14437	98.3	-135.1
P02-62	11215	16442	98.6	-140.9
P02-63	10203	14316	101.3	-142.7
P02-64	12087	16985	110.8	-154.1
P02-65	12420	17061	114.0	-156.1
P02-66	11169	16067	101.6	-145.8
P02-67	13177	19334	111.1	-157.5
P02-68	13793	19920	114.4	-162.6

Table D.3. Parametric Analysis Results for the 26 inch Web Depth Column Base-Plate Connections.

Model ID	Rotational stiffness-Push direction (kips-ft/rad)	Rotational stiffness-Pull direction (kips-ft/rad)	Moment capacity-Push direction (kips-ft)	Moment capacity-Pull direction (kips-ft)
P03	175105	186487	498.3	-516.5
P03-01	132198	185826	472.3	-489.6
P03-02	144423	129810	517.3	-475.6
P03-03	218414	175936	561.8	-597.7
P03-04	206816	242102	393.1	-440.4
P03-05	174759	153257	640.3	-601.7
P03-06	158020	144129	726.7	-673.9
P03-07	115858	112509	354.7	-341.8
P03-08	141924	148972	445.6	-454.7
P03-09	215331	185369	551.3	-545.8
P03-10	173027	161387	527.9	-504.9
P03-11	167883	171043	455.2	-714.9
P03-12	167883	171043	455.2	-485.0
P03-13	192359	184554	513.9	-474.8
P03-14	90030	45038	349.0	-284.5
P03-15	271133	166241	491.0	-522.3
P03-16	80168	102108	540.0	-636.2
P03-17	161484	154697	471.2	-448.6
P03-18	162898	167522	471.2	-469.3
P03-19	53860	53988	359.7	-413.3
P03-20	133545	147901	412.1	-435.2
P03-21	85293	75820	476.7	-532.7
P03-22	68986	70385	385.5	-477.5
P03-23	146738	165912	436.1	-473.5
P03-24	91811	83783	495.3	-566.8
P03-25	164931	160235	464.8	-570.3
P03-26	200458	199505	544.2	-604.6
P03-27	179390	230509	506.3	-614.8
P03-28	188093	286042	530.2	-506.0
P03-29	178320	187981	538.0	-516.1
P03-30	207299	231146	632.3	-598.0
P03-31	177633	201334	500.9	-604.2
P03-32	161321	202390	496.9	-601.7

Table D.3. (Contimued) Parametric Analysis Results for the 26 inch Web Depth Column Base-Plate Connections.

Model ID	Rotational stiffness-Push direction (kips-ft/rad)	Rotational stiffness-Pull direction (kips-ft/rad)	Moment capacity-Push direction (kips-ft)	Moment capacity-Pull direction (kips-ft)
P03-33	157430	148848	498.3	-529.3
P02-34	27336	40321	171.8	-269.3
P02-35	155567	147791	477.4	-525.0
P02-36	79698	92840	568.5	-565.1
P02-37	146589	126998	528.8	-522.8
P02-38	159128	150196	481.7	-528.8
P02-39	261870	34457	165.0	-256.9
P02-40	124135	126400	400.2	-448.7
P02-41	56374	76556	479.5	-671.8
P02-42	26606	38354	176.1	-264.5
P02-43	138412	132948	436.7	-479.8
P02-44	41469	52014	224.9	-313.3
P02-45	165634	148402	492.5	-480.0
P02-46	27465	44899	181.6	-280.9
P02-47	169383	125539	492.3	-456.0
P02-48	74843	117906	461.8	-637.5
P02-49	160210	127140	432.1	-425.4
P02-50	163167	157610	452.6	-454.5
P02-51	49125	45671	272.0	-272.2
P02-52	125124	119515	369.8	-395.5
P02-53	55695	70852	369.5	-503.6
P02-54	24399	43660	167.2	-275.0
P02-55	138372	125851	398.6	-417.4
P02-56	66329	82174	414.2	-556.4
P02-57	94861	124724	414.7	-556.4
P02-58	20080	28044	161.7	-258.0
P02-59	129285	185826	383.2	-535.8
P02-60	87000	130997	611.9	-864.8
P02-61	122888	141138	411.4	-481.4
P02-62	142092	153134	449.2	-515.7
P02-63	16103	23920	149.3	-245.8
P02-64	27384	41909	220.0	-309.0
P02-65	138435	170236	441.3	-597.5
P02-66	17156	30547	163.0	-250.6
P02-67	119969	124636	368.9	-423.8
P02-68	76631	114294	557.5	-783.4